Engineering Library

AUG 22 1936

UNITED STATES DEPARTMENT OF COMMERCE

Journal of Research

of the

National Bureau of Standards

Vol. 17, No. 1 July 1936

CONTENTS

RP	TITLE AND AUTHOR	Page
899.	Distribution of the energy in the extreme ultraviolet of the solar spectrum. W. W. Coblentz and R. Stair..... [Price 5c]	1
900.	Measurements of flame velocity by a modified burner method. Francis A. Smith and S. F. Pickering..... [Price 5c]	7
901.	Intensity distribution in the line emission spectrum of cesium. Fred L. Mohler..... [Price 5c]	45
902.	Solubility of calcium 2-methylbutyrate in water. David F. Houston..... [Price 5c]	55
903.	Determination of the Brinell number of metals. Serge N. Petrenko, Walter Ramberg, and Bruce Wilson..... [Price 5c]	59
904.	Oxidation of wool: Photochemical oxidation. Arthur L. Smith and Milton Harris..... [Price 5c]	97
905.	Drop of potential in the metallic electrodes of certain electrolytic cells. Chester Snow..... [Price 5c]	101
906.	Term analysis of the first spectrum of vanadium (V I). William F. Meggers and Henry Norris Russell..... [Price 10c]	125

The articles listed above may be purchased separately (see cover page II) at the prices indicated in the table of contents

A monthly periodical of pure and applied science published by our National Government

Journal of Research

of the

National Bureau of Standards

The July 1936 issue of the Journal of Research of the National Bureau of Standards begins the seventeenth semiannual volume of this periodical. Fundamental researches in progress in the Bureau's laboratories are reported in this JOURNAL. If you are interested in new developments in science and technology, you should receive the JOURNAL. If you are not already a subscriber you are invited to send in your subscription.

Technical News Bulletin

This is a monthly publication containing short articles reporting progress of work in the Bureau laboratories, abstracts of papers which appear in the Journal of Research, accounts of scientific and technical meetings in which the Bureau has taken part, a list of all publications by members of the staff, and other items within the Bureau's field. The BULLETIN is designed primarily to give a general and timely review of the activities of the Bureau in brief form. It is a prompt and reliable source of official information. If you have not already subscribed for the BULLETIN, you are invited to do so.

ANNUAL SUBSCRIPTION	Prices	
	United States Canada, Cuba, Mexico, Newfoundland, Republic of Panama	Other countries
Journal of Research of the National Bureau of Standards:		
12 monthly issues (2 volumes), paper covers	$2.50	$3.25
Bound volume (½ year, 1 volume), blue buckram . . .	3.00	3.50
Technical News Bulletin, 12 monthly issues	.50	.70

Research Papers, reprinted individual articles appearing in the Journal of Research, are available from the Superintendent of Documents shortly after appearance of monthly issue of the JOURNAL

Address orders only to
Superintendent of Documents, U. S. Government Printing Office,
Washington, D. C.

UNITED STATES DEPARTMENT OF COMMERCE
DANIEL C. ROPER, Secretary
NATIONAL BUREAU OF STANDARDS
LYMAN J. BRIGGS, Director

✦

Journal of Research

of the

National Bureau of Standards

✦

Volume 17, Number 1
July 1936

UNITED STATES
GOVERNMENT PRINTING OFFICE
WASHINGTON : 1936

For sale by the Superintendent of Documents, Washington, D. C. - - - - Price 25 cents
$2.50 per year on subscription

The prices of the separate Research Papers appearing in this JOURNAL are given on the front cover page. If 100 or more copies of any separate are ordered, a discount of 25 percent is allowed. Those who desire copies of separate Research Papers should send their orders and remittances without delay to the Superintendent of Documents, U. S. Government Printing Office, Washington, D. C. This will aid him to determine the number of copies to be printed for sale. Research Papers are not printed from electrotypes, and usually no more reprints can be had when the first and only printing is exhausted.

U. S. Department of Commerce National Bureau of Standards

RESEARCH PAPER RP899

Part of Journal of Research of the National Bureau of Standards, Volume 17, July 1936

DISTRIBUTION OF THE ENERGY IN THE EXTREME ULTRAVIOLET OF THE SOLAR SPECTRUM

By W. W. Coblentz and R. Stair

ABSTRACT

Supplementing the data given in a previous publication (NBS Research Paper RP877), the present paper gives further calculations and graphs showing the distribution of energy in the extreme ultraviolet of the solar spectrum, for various air masses traversed by the rays, at a sea-level station (Washington); also the spectral-energy distribution of solar radiation outside the earth's atmosphere, showing that there is no similarity with the radiation of a black body at 6,000° K, which is sometimes used in calculating the ultraviolet solar spectral energy.

The second part of the paper describes progress made in assembling apparatus for measuring the spectral quality and total intensity of ultraviolet solar radiation by means of a photoelectric cell and filter radiometer transported aloft in sounding balloons.

CONTENTS

	Page
I. Introduction	1
II. Distribution of energy in the extreme ultraviolet of the solar spectrum, within and outside of the earth's atmosphere	2
1. Correlation of ultraviolet and total solar radiation	3
III. A meter for determining the ultraviolet solar spectral-energy distribution by means of sounding balloons	4
IV. References and notes	6

I. INTRODUCTION

In a previous communication [1] [1] a photoelectric cell and filter radiometer was described for determining the distribution of energy in the extreme ultraviolet of the solar spectrum. Data were given on the distribution of energy in the extreme ultraviolet for various solar altitudes, and the shape of the solar spectral-energy curve outside the earth's atmosphere was discussed. It was shown that the common procedure of calculating the spectral-energy distribution (in the ultraviolet), on the assumption that the radiation is similar to that of a black body at a temperature of 6,000° K, is untenable because spectroradiometric measurements indicate that there is an abrupt and continuous drop in the solar spectral-energy curve, of wave lengths shorter than 3000 A, outside the earth's atmosphere.

The need having arisen, in the meantime, for more specific information on this subject, in connection with questions on heliotherapy, the object of the present paper is (a) to present further data on the distribution of energy in the extreme ultraviolet of the solar spectrum

[1] Numbers in brackets refer to references and notes at the end of this paper.

within and outside the earth's atmosphere, and (b) to give an outline of a method for determining the ultraviolet solar spectral-energy distribution in the stratosphere by means of a photoelectric cell (of special design), filters and auxiliary apparatus, transported to the highest elevations attainable by means of sounding balloons.

This involves the problem of transmitting certain radio signals from the balloon to the ground. For this purpose the writers had the choice of two methods: (a) the newly designed, mechanically controlled, signaling mechanism of Curtiss and Astin [2], or (b) an adaptation of an early type of audion bulb which, when evacuated to a few millimeters gas pressure, transmits a pulsating current that changes in frequency with change in current in the input circuit [3].

As originally used with a photoelectric cell, the signal was received as a change in pitch of the sound in a telephone receiver [3]. For the present purpose this audio signal is used to modulate a transmitted radio wave. Hence, since the radio signals from the photoelectric apparatus, transported by a sounding balloon, are to be received by the Radio Section of the Bureau, the latter method of radio transmission was adopted.

Fortunately, commercial radio tubes are now available [2] that can be operated to transform feeble photoelectric currents into audio signals suitable to meet our needs. The general hookup of this apparatus is described in section III.

Calculations of intensities to be expected at high altitudes [1], and ground tests of assembled apparatus, indicate that important data on spectral quality (spectral-energy distribution) and total intensity of ultraviolet solar radiation are to be expected from measurements in the stratosphere.

The delay in making field tests is owing to our inability to secure photoelectric cells of special design to meet our requirements.

II. DISTRIBUTION OF ENERGY IN THE EXTREME ULTRAVIOLET OF THE SOLAR SPECTRUM, WITHIN AND OUTSIDE OF THE EARTH'S ATMOSPHERE

In a previous paper [1] data were given on the ultraviolet solar spectral-energy distribution in relative units, but no attempt was made to correlate the various spectral-energy curves for different air masses traversed by the solar rays.

From the average values of the total ultraviolet solar radiation observed through various air masses (solar altitudes) it is possible to obtain factors that give the heights of the various spectral-energy curves relative to each other. In figure 1 are depicted the spectral-energy curves based upon the data previously published [1].

Judged by the closeness with which the data fall upon the isochromatic curves (not published) in which the ordinates were plotted on the logarithmic scale, as commonly employed, the measurements are in good agreement.

As noted in the previous paper [1] the use of two photoelectric cells (differing greatly in spectral response) and four filters gives eight conditions for establishing the shape of the spectral-energy

[2] The writers are indebted to F. W. Dunmore for calling attention to this newly developed radio tube, which had escaped their notice, although a description of the device was published some time ago [4].

Cambridge

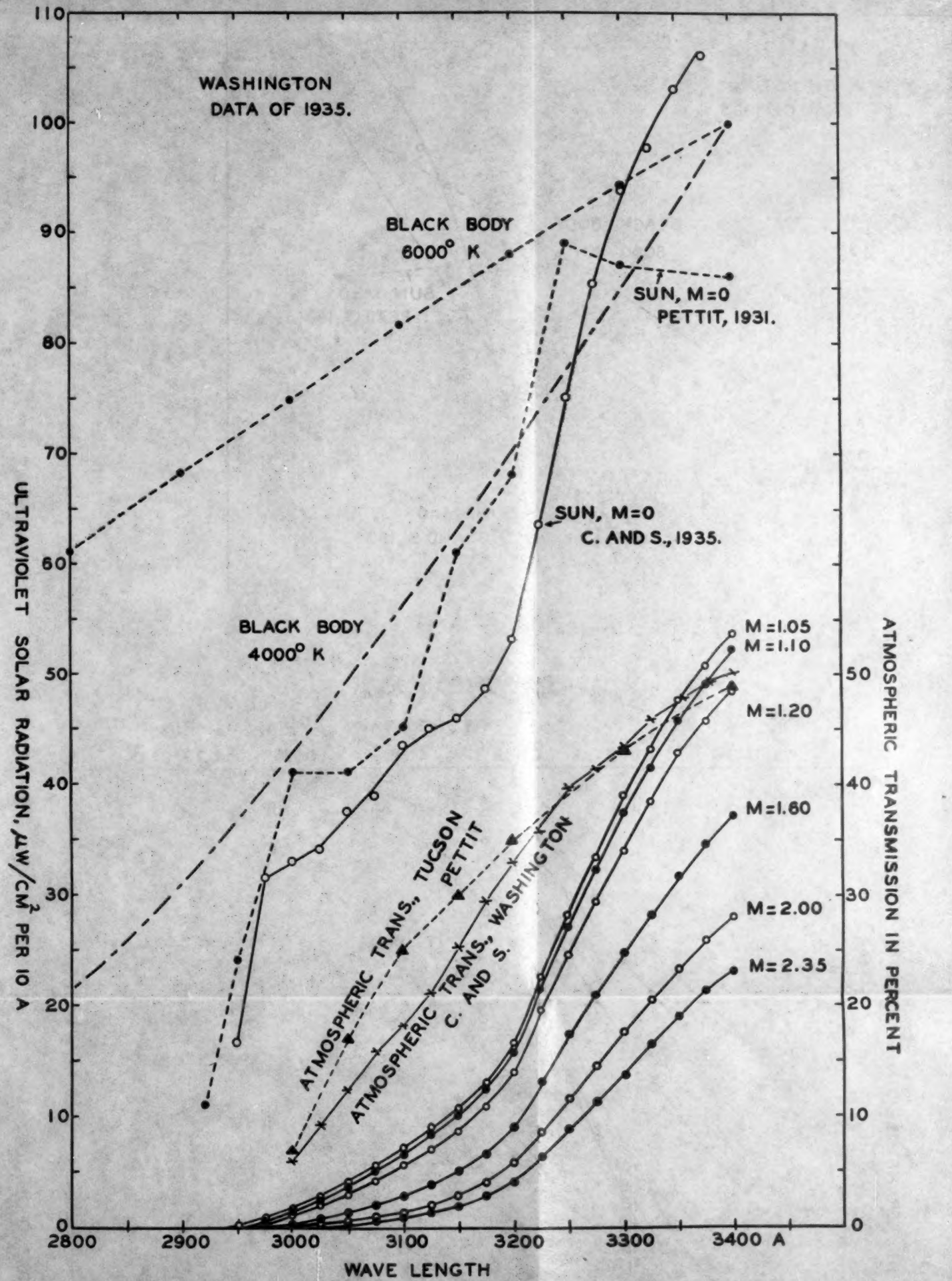

FIGURE 1.—*Distribution of energy in the extreme ultraviolet of the solar spectrum, within and outside the earth's atmosphere; also atmospheric transmission curves.*

73059—36. (Face p. 2)

UNIV. OF MICH.

WASHINGTON
DATA OF 1935.
BLACK BODY
6000° K
BLACK BODY
4000° K
ULTRAVIOLET SOLAR RADIATION, μW/CM² PER 10
110
100
90
80
70
60
50
40
30
20

curve for any given air mass traversed by the solar rays. From this it would appear that this good agreement is real and not the result of a fortuitous combination of factors including (a) the spectral responses of the photoelectric cells, (b) the spectral transmissions of the filters, and (c) the observations of the integrated ultraviolet transmissions through the various filters.

In figure 1 is given the ultraviolet solar spectral-energy distribution outside the earth's atmosphere as deduced by Pettit [5] and by the writers. As noted in the previous paper [1], in both cases the spectral intensities show a continuous drop with decrease in wave length.

In this same illustration is given also the ultraviolet spectral-energy distribution of a black body at 4,000° K and at 6,000° K, respectively. The spectral-energy distribution of a black body at 4,000° K represents most closely the observed (extrapolated) data. It, therefore, seems incorrect to compute the ultraviolet solar spectral-energy distribution on the assumption that the radiation is similar to that of a black body at 6,000° K [11, 12].

The atmospheric transmission curves as deduced from our spectral-energy curves are somewhat lower than observed by Pettit [5] as is to be expected, seeing that the data refer to two stations differing about 2,000 feet in elevation.

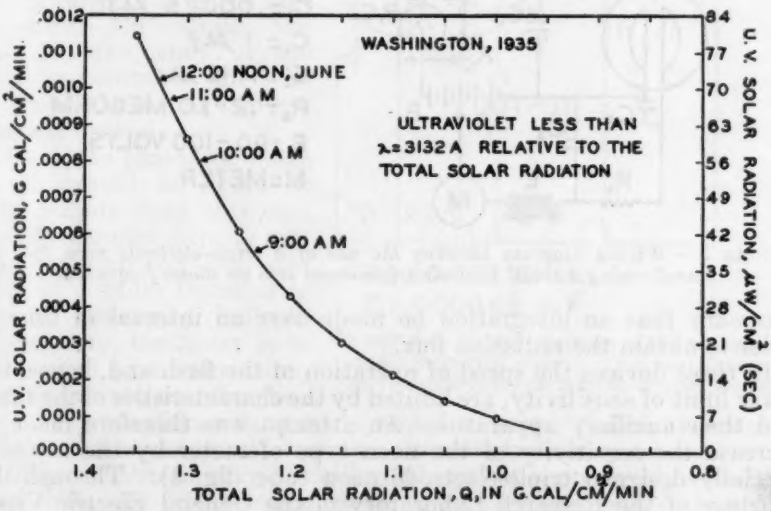

FIGURE 2.

1. CORRELATION OF ULTRAVIOLET AND TOTAL SOLAR RADIATION

In view of the fact that in heliotherapy the patient is usually exposed to the total (unfiltered) radiation from the sun, in figure 2 is shown the ultraviolet of wave lengths shorter than and including 3132 A, relative to the total incident solar radiation, in gram calories per square centimeter per minute. The total radiation data are average values, for Washington, taken from the Smithsonian Meteorological Tables.

For a low sun (a long air mass traversed) the spectral quality is different from, and the total intensity is much lower than, that observed at high solar elevations.

III. A METER FOR DETERMINING THE ULTRAVIOLET SOLAR SPECTRAL-ENERGY DISTRIBUTION BY MEANS OF SOUNDING BALLOONS

Various types of direct-current amplifiers have been designed and made to work quite satisfactorily [6, 7, 8] in the measurement of small currents, such as are produced by photoelectric cells used in the evaluation of short-wave-length ultraviolet solar radiation. In all cases, these devices require the attention of an expert operator to keep the voltage and zero of the scale reading properly adjusted. Hence, they are not suitable for operating automatic-recording instruments, or for the transmission of signals by radio from sounding balloons.

An ultraviolet meter which makes use of a glow relay tube has been described by Rentschler [9], and a somewhat similar meter which uses a neon-flash lamp has been described by Taylor [8]. While these instruments are very useful, they have their limitations in that for accurate reproduction their speed of operation is limited to a small number of impulses ("clicks" or "flashes") per minute. Hence it is

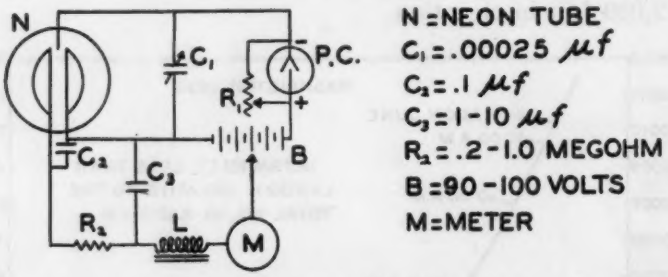

FIGURE 3.—*Wiring diagram showing the use of a triple-electrode neon tube for transforming a small photoelectric current into an audio frequency.*

necessary that an integration be made over an interval of time in order to obtain the radiation flux.

In these devices the speed of operation of the flash and, hence, the lower limit of sensitivity, are limited by the characteristics of the tubes and their auxiliary apparatus. An attempt was therefore made to increase the sensitivity of the neon type of meter by the use of a specially designed triple-electrode neon tube (fig. 3). Through the courtesy of the Research Laboratory of the General Electric Vapor Lamp Co., Hoboken, N. J., several triple-electrode neon tubes were constructed. While they are much superior to the ordinary neon tubes having two electrodes, they have several defects which prevent their use in ultraviolet meters for precision measurements. There is a leakage in these tubes that must be counterbalanced by a resistance in parallel with the photoelectric cell. Moreover, the breakdown and recovery voltages are not absolutely constant. Although much more sensitive than neon tubes having two electrodes, the sensitivity is insufficient to give the high audio frequency desired when activated by small photoelectric currents, and operated in connection with radio apparatus and frequency meters.

It is to be noted that the triple-electrode neon tube may find valuable applications in the operation of relays without the use of auxiliary radio amplifying apparatus.

Consideration was then given to other methods of producing an audio-frequency signal, including the use of a leaky triode previously used by one of the writers [3] for the production of a change in pitch of the sound in a telephone receiver, when used in connection with a photoelectric cell. In this connection our attention was called to the use, by Herold [4], of a standard radio tube (type 57) in place of a neon tube to produce an audio frequency.

For our work a similar type (1A6) tube was chosen because of its low filament current and voltage. This tube is a stable oscillator and has a high grid-circuit resistance (partly due to the location of the grid at the top of the tube), and, hence, provides an extremely sensitive means for measuring low photoelectric currents. The complete instrument (see fig. 4) is about one hundred times as sensitive as could be made by using the special neon tubes, and should be practical for measuring currents as low as about 10^{-12} or 10^{-13} ampere.

In operation, the condenser C is adjusted to the proper capacity to give a suitable audio signal when the photoelectric cell is illuminated. On covering the cell the frequency of the signal generated by the tube decreases to one or two cycles per second.

Only the generator stage is illustrated in figure 4. The output from this unit may be coupled directly into the transmitting oscillator tube of a radio transmitter on an unmanned balloon. If, however, the meter is to be used at a ground station, additional stages of audio-frequency amplification must be added to supply sufficient power to operate a frequency meter or an automatic frequency recorder.

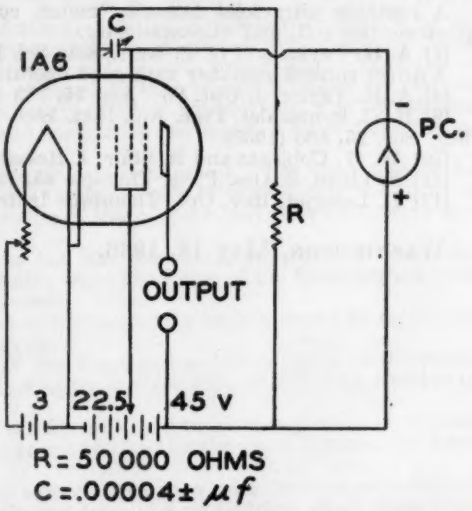

FIGURE 4.—*Wiring diagram of the photoelectric audio-frequency generator for modulating the carrier wave in the radio transmission of signals.*

This instrument may be calibrated against a previously standardized meter, or directly against an ultraviolet standard of radiation [10], as is done with the ordinary type of balanced amplifier photoelectric meter [6]. The calibration of the frequency scale is made in terms of microwatts per square centimeter, for example, for a certain band of radiation in sunlight. The radiation intensity may be read directly from a calibrated frequency meter or automatically recorded with suitable apparatus.

However, the primary purpose of this investigation was the development of means of transforming small photoelectric currents into suitable pulses for automatic transmission by radio from small sounding balloons released into the upper atmosphere. When coupled into the oscillator circuit of a small transmitter this method appears to be ideal for transmitting data on the intensity and spectral quality of the ultraviolet solar radiation in terms of an audio-frequency modulation of the carrier wave.

IV. REFERENCES AND NOTES

[Bracketed numbers are the designating literature reference numbers as cited in the text of this paper]

The following publications of the National Bureau of Standards are obtainable only through the Superintendent of Documents, Washington, D. C., prepaid, at the prices indicated.

[1] W. W. Coblentz and R. Stair, J. Research NBS **16**, 315 (1936) RP877 (10c).
[2] L. F. Curtiss and A. V. Astin, Aeronaut. Sci. **3**, 35 (1935).
[3] W. W. Coblentz, BS Sci. Papers **16**, 635 (1920) S398 (10c); Misc. Pub. NBS 46, p. 138 (1921).
Thermal-radiophonic devices for secret signaling.
[4] E. W. Herold, Proc. Inst. Radio Eng. **23**, 1200 (1935).
Negative resistance and devices for obtaining it.
[5] E. Pettit, Astrophys. J. **75**, 185 (1932); Pub. Astronom. Soc. Pacific **47**, No. 280 (December 1935).
[6] W. W. Coblentz and R. Stair, BS J. Research **12**, 231 (1934) RP647 (5c).
A portable ultraviolet intensity meter, consisting of a balanced amplifier, photoelectric cell, and microammeter.
[7] A. H. Taylor and G. P. Kerr, Rev. Sci. Instr. **4**, 28 (1933).
A direct current amplifier with good operating characteristics.
[8] A. H. Taylor, J. Opt. Soc. Am. **24**, 183 (1934).
[9] H. C. Rentschler, Proc. Am. Inst. Elec. Eng. **49**, 113 (1930); Trans. Illum. Eng. Soc. **25**, 406 (1930).
[10] W. W. Coblentz and R. Stair, J. Research NBS **16**, 83 (1936) RP858 (5c).
[11] F. Linke, Z. Ges. Phys. Therapie **45**, 169 (1933).
[12] R. Latarjet, Rev. Opt. Théorique Instr. **14**, 398 (1935).

WASHINGTON, May 18, 1936.

U. S. Department of Commerce National Bureau of Standards

RESEARCH PAPER RP900

Part of Journal of Research of the National Bureau of Standards, Volume 17, July 1936

MEASUREMENTS OF FLAME VELOCITY BY A MODIFIED BURNER METHOD

By Francis A. Smith and S. F. Pickering

ABSTRACT

This paper describes a study of the application of the burner method to the determination of the velocity of propagation of flame relative to mixtures with air of various combustible gases. Observations have been made on the effect of varying the size of the burner port, of changing the velocity of flow of the mixture from the burner, of changing the composition of the mixture, and of different methods of measuring the flame and computing the result. All of these factors relate to problems of gas utilization.

The apparatus and procedure are described in detail. The relationships developed between the size and shape of the flame surface as related to the diameter of the burner port and the composition of the mixture lead to the following conclusions:

1. The most consistent results by the burner method, regardless of variations in the above conditions, are obtainable when the shape of the flame surface most nearly approximates a geometrical cone.
2. Distortion at the tip and base of the flame may be minimized by using mixtures in nearly theoretical proportions.
3. Measurements of the slope of the flame surface (at a point on the radius 0.7 r from the axis) involve a portion of the surface little or not at all affected by the distortion at the tip and base.
4. The adequate separation of the tip and base to leave a portion of the surface unaffected by distortion may be accomplished by the use of burners over 4 mm in diameter.
5. Measurements of the entire surface area may yield results considerably more in error on account of departures from the geometrical shape than those computed from measurements of the angle between the axis and the side of the flame surface at 0.7 r from the axis.
6. The only points on the curves of two or more fuel gases which even approach suitability for a direct comparison between the different gases are the maxima.

An attempt has been made to derive the shape of the flame surface by the application consecutively of a series of facts and assumptions based on facts.

The flare at the base of the flame surface where it overhangs the burner port is explained in terms of the magnitude and direction of flow of the gas mixture rather than by a cooling effect of the port.

The gap between the flame and the metal port is considered to represent the distance required by the temperature gradient from the port to the flame front.

A gradient layer underlying the entire flame surface is postulated, with a thickness similar to that of the gap between the flame and the metal port.

The curvature of the upper part of the flame surface convex upward may be caused by a modification of the originally parabolic distribution of the velocity of flow of the combustible mixture, after leaving the burner tube, rather than by an increase in the flame speed caused by a higher initial temperature of the combustible mixture. The rounding off of the extreme tip, however, is doubtless caused by the overlapping of the thin gradient layers and may result in an actual increase in the flame speed to several times the speed in other parts of the flame surface.

CONTENTS

		Page
I.	Introduction	8
II.	Choice of method	9
III.	Description of the method	10
IV.	Apparatus and procedure	13
	1. Manipulation of gases	13
	2. Measurement of gases	15
	3. Mixing of gases	16
	4. By-pass cock	17
	5. Flash-back trap	17
	6. The burner	17
	7. The camera	18
	8. The goniometer	18
	9. Treatment of the results	19
V.	Dependence of numerical result upon experimental factors	20
	1. Effect of mixture velocity	21
	2. Effect of the size of the burner port and of the method of measurement of the photographs	22
	3. Effect of the overhanging flame	28
	4. A test of the applicability of the expression $D\overline{v}=0.707\ D$	30
VI.	The shape of the flame surface as a resultant of several variable components	34
VII.	Summary and conclusions	40
VIII.	References	43

I. INTRODUCTION

The velocity with which flame is propagated in the combustible mixture issuing from the ports of a gas burner is one of the important factors which must be taken into account in any study of the performance and design of gas burners.

It was thought that a knowledge of the flame velocity in mixtures of the single combustible gases in varying proportions with air and with oxygen would be required if a means of calculating the flame velocity in complex mixtures of these constituents with air and oxygen was to be found. It was also desired to correlate the flame-velocity data with the conditions under which the flame flashes back through the ports of the burner, or blows off from them. Therefore, the measurement of the flame velocity in simple mixtures of a number of the constituents encountered in the various fuel gases was undertaken.

The fact that many workers using different methods obtain different results, which cannot be readily correlated or even compared on a common basis, makes the problem of determining flame velocities and applying the results a rather difficult one. There are several reasons for this. One source of confusion is that flame velocity, like "flame temperature", "ignition temperature", "explosive and inflammable limits", etc., has been too often considered to be a characteristic of a gas itself. Actually all of them are properties of the system as a whole, including usually the apparatus. Each of these so-called properties depends to so great an extent upon other factors that the identity of the combustible gas can be considered as only one of the several factors which, taken together, determine the numerical values in a given case. Such data must be used with the knowledge that the numerical values given may or may not be applicable to conditions which differ from those under which the measurements were made.

Furthermore, a direct comparison between two individual combustible gases with respect to flame velocity is not the simple matter it

appears to be at first glance. For example, the data from the two gases may be obtained by the same method, with the same apparatus, and the comparison may be made (a) by substituting one combustible gas for the other in a gas-air mixture which is otherwise unchanged in composition and temperature. The two gases may be methane and propane, each constituting 7.5 percent of its mixture with air. An examination of the curves plotted in figure 5 shows that all that can be elicited from such a comparison is that the flame velocity in a very lean mixture containing 7.5 percent of methane is more than twice that in a very rich mixture containing 7.5 percent of propane. (b) The comparison may be made between mixtures, each of which contains the same percentage of the total air required for the complete combustion of the respective gases. The curves plotted in figure 4 show that such a comparison may be valid between methane and propane, but if either of these gases is compared with hydrogen in mixtures containing, for example, 80 percent of the air required for complete combustion, the same difficulties are encountered as before but not to such an extreme degree. Such comparisons are obviously invalid, and the alternative of choosing the maximum-speed mixtures as the only points on the curves which are much more than roughly comparable one with another must be accepted. Even with maximum-speed mixtures, the flame velocities obtained by different methods may be compared with validity only when each method yields the same result with a given mixture, the composition, temperature, and pressure being the same in each case.

In making use of data, care must be taken to select those which have been obtained by the method most nearly corresponding to the experimental or practical conditions with which the data are to be connected, until more is known than at present concerning the mechanism of each process. For example, if detonation is involved, data obtained with detonating mixtures should be used. If the interest is in the behavior of flames in closed vessels, use should be made of data so obtained. If the question concerns the velocity in space (relative to a stationary object) with which flame travels in tubes or tubular openings of various sizes in various materials, the results obtained by the use of corresponding (or similar) tubes may be applicable. If the velocity in space of flame in large tubes or in the open is in question, the data must come from work done in tubes of corresponding diameter.

II. CHOICE OF METHOD

A survey of the methods in use for determining flame velocities resulted in the selection of the bunsen-burner method for the present study, for a number of reasons.

The method of Bunsen [1],[1] modified successively by Gouy [2], Michelson [3], Ubbelohde [4], and by Stevens [5], was found by Stevens and by the present authors to yield results which, in the case of $CO–O_2$ mixtures, were in surprisingly good agreement with results obtained by the "constant-pressure bomb" or "soap-bubble" method of Stevens [6]. Both methods permit the evaluation of the velocity of the combustible mixture in space, and the determination of the velocity of propagation of the flame relative to the combustible mixture.

[1] The figures given in brackets here and throughout the text correspond to the numbered references at the end of this paper.

The use of the burner appeared to involve fewer difficulties in the construction of the apparatus, was more readily adapted to use in the related problems of burner performance, and permitted the collection of flame-velocity data under conditions which approximate those to which they were to be applied.

It is recognized by the authors that the burner method in general may not be a particularly accurate one for the determination of absolute values for the rate of propagation of flame relative to the mixture in which the flame travels. However, the method herein described, as will be shown later, is suited to direct comparisons between the maximum flame velocities shown by various fuel gases under a given set of conditions with a precision of about 2 percent or better.

It was hoped that the apparatus and technique described in this paper would eliminate most of the objectionable features of the general burner method. It developed, however, that the numerical result obtained for the flame speed was not entirely independent of the diameter of the burner tube, a circumstance reported by Ubbelohde and Hofsäss [7] in 1913, but which has been neglected by many workers who have made use of various modifications of the burner method.

III. DESCRIPTION OF THE METHOD

The method in principle is the same as that employed by Bunsen [1], Gouy [2], Michelson [3], Ubbelohde [4], Mache [8], and Stevens [5], but was modified further in certain respects by the authors.

These modifications were, in large measure, refinements to determine or to control conditions with a view to eliminating variables, the effects of which might obscure those under investigation. The numerical result depends to so great an extent on the conditions of operation and the methods of measurement and computation, that careful control and careful specification of experimental conditions are essential. It seems desirable, therefore, to describe in some detail the apparatus and technique employed in the present work.

A brief review of the essential points of difference in the methods of some of the investigators named above may serve to clarify references to various modifications which have been made since Bunsen's original attempt to measure flame velocity by means of a burner.

Bunsen [1] assumed that the velocity of the flame front downward just exceeded the velocity of the gas mixture upward at the moment when the flame flashed back down the burner tube. Obviously this could be true only if the velocity of the stream of gas mixture was the same at the center of the burner tube as it was at the walls.

Gouy [2] probably sensed something wrong with Bunsen's assumption, for he at first considered the flame velocity to be equal to the product of the velocity of the gas mixture with the sine of the angle which the side of the flame cone made with its axis. Then finding that the surface formed by the flame front did not approximate sufficiently to a true cone, and that the result obtained depended upon what part of the flame front he used when he measured the angle, he eliminated the angle from consideration by setting the velocity of the flame equal to the volume rate of flow of the mixture divided by the area of the flame surface. This involves the concept of flame velocity as simply the rate of transformation of the mixture, without the necessity of considering the velocity of the gas mixture and its

direction of flow. The two concepts would yield identical results if the flame surface were a geometrical cone with the burner port for a base.

Gouy determined the area of the flame surface from measurements of the image of the flame projected on a screen. Considering the figure as a surface of revolution, he obtained the area by integration.

Michelson [3] measured the volume rate of flow of the mixture and determined the actual area of the "cone" by treating measurements of enlarged photographs in the same way that Gouy had done.

Ubbelohde [4] concluded that the rounded tip and the curved base of the flame surface represented deviations from what he termed the "normal" flame velocity, so he measured the angle made by the "straight" portion of the flame surface with its axis, and computed the result as Gouy had done originally.

Stevens [5] was unable to obtain results with the burner which were in satisfactory agreement with the results he obtained with the "bubble" when he determined the area of a flame surface as Gouy and Michelson or Ubbelohde had done. He recognized, as did Ubbelohde, that the approximately conical flame surface was the resultant of several components, one of which was a mixture velocity which varied from practically zero at the walls of the burner tube to a maximum at the center. Stevens, therefore, decided to make use of only that part of the flame surface which resulted from gas mixture whose actual linear velocity was equal to the mean velocity over the cross section of the stream. He constructed on his photograph a triangle having as its base the cross section of the burner tip and sides parallel to the tangents to the flame surface at the part where the velocity of the mixture equalled the mean velocity. Considering this triangle as a section through the axis of a cone the area of the cone was easily calculated without integration from the measured altitude and base, and values obtained from it for the velocity of the flame front relative to CO-O_2 mixtures agreed with those obtained with the bubble so closely that the two methods, for many purposes, could be used interchangeably.

A number of other workers have adhered to Gouy's assumption, expressing flame velocity in terms of volume of combustible mixture per second divided by the area of the flame surface. Of these, some use the actual integrated area of the flame surface and others use the area of a geometrical cone having the burner port as a base. The area of this geometrical cone has been arrived at in various ways, among which are the following: (*a*) by using the actual measured height of the flame cone; (*b*) this cone height corrected by a factor designed to bring the numerical result into agreement with the results obtained by integrating the surface of revolution; (*c*) by using the angle between the straight portion of the side of the flame and the axis. Since the area of the burner port divided by the lateral area of a geometrical cone of which the burner port forms the base is equal to $\sin \alpha$ (where α is the angle between the side and the axis of the cone), the cone may also be defined by the burner port and the angle α. All of these expressions would lead to the same numerical result were the flame surface a geometrical cone.

Instead of measuring and computing the area of the cone as Stevens had done, the present authors have chosen to measure directly the angle α between the tangents and the axis, which, together with the burner port, is sufficient to define the cone. Instead of dividing

the volume rate of flow of the combustible mixture by the area of the cone to obtain the flame velocity, it has been divided by the area of the burner port, thus obtaining the average linear velocity of flow of the mixture. The angle is measured at that part of the flame surface where the local velocity of flow of the mixture is equal to the average velocity. The sine of the angle α, multiplied by the average velocity of the mixture, then gives the same numerical value for the flame velocity as does the other method. This is essentially a combination of the original method of Gouy [2] with those of Michelson [3], Ubbelohde [4], and Stevens [5].

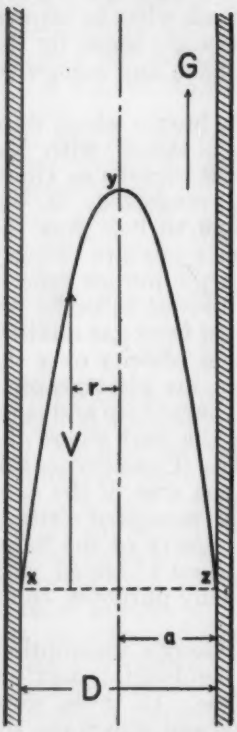

FIGURE 1.—*Velocity diagram of fluid in laminar flow through a tube.*

The distance, from the center of a tube, at which the velocity is the mean for the tube as a whole, is, theoretically, equal to 0.707 times the radius of the tube. Twice this distance will be called the "mean velocity diameter" and will be designated $D_{\bar{v}}$. This factor is constant for tubes of all sizes and for all fluids, as will be evident from the following relationship, which is familiar in hydraulics.[2] In a tube of radius a (fig. 1) the curve x, y, z represents the velocity V at a distance r from the axis of the stream of fluid of viscosity μ moving under a pressure gradient G. Then the velocity V of an annular ring of fluid of any radius r will be $V_r = \frac{G}{4\mu}(a^2-r^2)$; and the mean velocity $\bar{V}$ will be $\bar{V} = \frac{Ga^2}{8\mu}$. Placing $V_r = \bar{V}$ and solving for r; $\frac{G}{4\mu}(a^2-r^2) = \frac{Ga^2}{8\mu}$; $a^2-r^2 = \frac{a^2}{2}$; $r^2 = \frac{a^2}{2}$; $r = \frac{a}{\sqrt{2}} = \frac{a}{1.414} = 0.707\,a$. Therefore, $D_{\bar{v}} = 0.707\,D$.[3]

When measuring the photograph, $D_{\bar{v}}$ must be multiplied by a magnification factor. D is determined by measuring the diameter of the burner port with a micrometer, and the magnification factor is obtained from the photograph of a scale substituted in the place of the flame in the axis of the burner tube. A pair of dividers is adjusted to the computed $D_{\bar{v}}$ distance, and moved upon the negative image of the flame front on the photographic plate until an outside diameter equal to this distance has been located, when marks are made on the image by pressing the points of the dividers into the emulsion.

The marked plate is then mounted in a goniometer, illuminated from behind with a diffuse light, the intensity of which can be varied to give the best visibility of the image, and rotated until the cross hair of a reading telescope is judged to be tangent to the image of the flame surface at the mark, on first one side of the flame and then on the other. The angle through which the plate was rotated between settings is read on a vernier scale, and is equal to 2α.

[2] Derivation supplied by E. Buckingham, National Bureau of Standards.
[3] The validity of the application of the factor 0.707 to the measurement of the photographs of flames is treated in the section on the effects of experimental factors, page 30.

Angle measurements were made by two observers, one making settings and the other reading and recording the angles. After two settings on each side of the flame, the observers changed places and the observations were repeated, giving four values of 2α. The average of these observations was used in calculating the flame velocity, or rate of transformation of the mixture, which has been designated S_T.

The volume rate of the gas mixture was divided by the area of the burner port computed from D, giving the mean linear velocity of the gas mixture. This has been designated S_M. The velocity of propagation of the flame front, in a direction normal to its surface and relative to the combustible mixture in which it moves, is then given by the equation $S_T = S_M \sin \alpha$.[4]

IV. APPARATUS AND PROCEDURE

1. MANIPULATION OF GASES

A diagram of the apparatus used for obtaining photographs of the flames is shown in figure 2. Those combustible gases which could not be utilized directly from cylinders, such as manufactured gas, and acetylene, were stored in two water-sealed gas holders, H, having a combined capacity of about 70 cubic feet. The holders were equipped with piping which permitted mixing the gas in the holders by means of a small rotary compressor. The gas from the holders was delivered, saturated with water, to the measuring apparatus at a pressure of 5 to 6 inches of water above the barometric pressure. "Bottled gases" and others which could be obtained in and utilized directly from cylinders under pressure were delivered directly from the cylinder. The flow was in all cases accurately controlled by a good needle valve, V_1, placed far enough ahead of the capillary flowmeter, M_1, to avoid disturbing the flow through the capillary.

The air used was taken from the low-pressure laboratory supply, passed through a saturator S, the temperature of which was measured in order that the proportion of water in the air might be known, and, thence, through a diaphragm pressure-reducing valve, D, past a tee to which was attached a 12-inch rubber pilot-balloon bag, P, to equalize pressure fluctuations, past a similar tee to which was attached a bleeder valve, V_2, for the same purpose, and then through the needle valve, V_3, used to control the flow through a capillary flowmeter, M_2, similar to that used to measure the gas.

These precautions proved insufficient to eliminate all fluctuations in the rate of flow of the gas mixture through the burner port, the tip of the cone showing rapid and irregular pulsations which made a sharply defined photographic image impossible. Some of these pulsations were definitely traced to pressure fluctuations in the atmosphere of the room, caused by the ventilating fans. Others, which persisted with the fans shut down and the windows open, were imposed by the movements of the air outside the building.

A tile wall was built across one side of the laboratory, inclosing a space of about 700 cubic feet, which contained all the apparatus except the saturator and gas holders. The wall was plastered on both sides and all joints were sealed with bituminous cement. Openings in the wall connecting with the fume exhaust were covered with doors made tight with a seal of rubber tubing, as was the main door-

[4] The apparent assumptions that flame travel is in a direction normal to its surface, and that the velocity of travel is proportional to sin α, are justified by an application of Huyghens' principle to the geometrical derivation of the flame surface, which is treated later on p. 36.

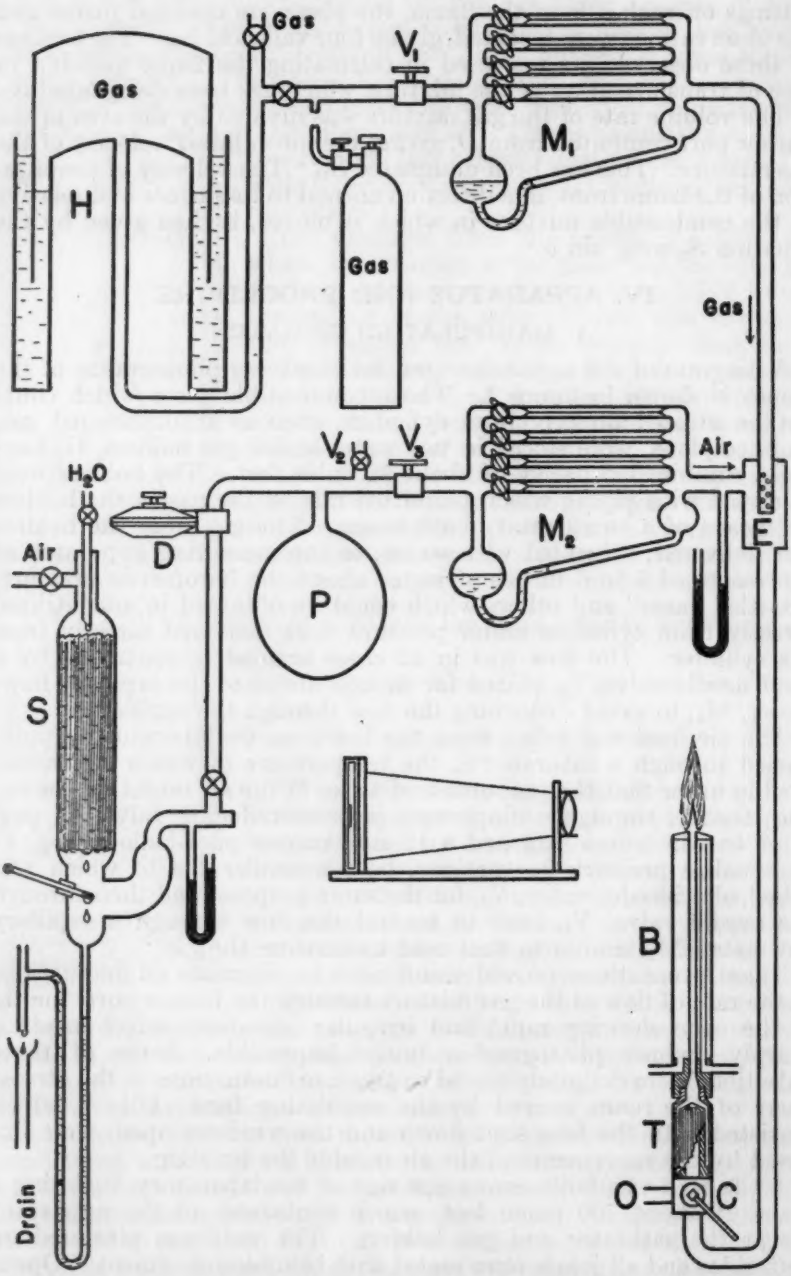

FIGURE 2.—*Diagram of the apparatus used to control and photograph flames.*

way. The entire inner surface of the room was given two coats of bituminous paint to seal the plaster and provide a black interior to minimize reflections. This treatment eliminated the pulsations of the flame to such an extent that perfectly sharp images resulted from exposures as long as 10 minutes.

The effectiveness of the air saturator, S, was checked by weighing the water absorbed by magnesium perchlorate trihydrate from a measured volume of air. The amount of water found in the air from the saturator agreed with the percentage calculated within 0.1 percent, assuming saturation at the observed temperature and pressure of the saturator.

2. MEASUREMENT OF GASES

The gases were measured by passage through glass capillary flowmeters, M_1 and M_2, equipped with slope gages. Each flowmeter consisted of a unit made up of four capillary tubes, 20 cm long and having different diameters, sealed together in parallel. Each capillary was preceded by a stopcock so that by a suitable selection of capillaries any desired rate of flow up to 205 ml per second could be obtained at a differential pressure within the range of the manometer.

The manometers were tubes about 4 mm in diameter and 1 m long. A meter stick firmly fixed to the tube served as a scale. The tubes were inclined with the upper end 10 cm higher than the lower end, to which was attached the reservoir for the manometer liquid.

A light liquid petrolatum was used because its low vapor pressure reduced to a minimum contamination of the gases measured, and because it was free from meniscus troubles. It was dyed red to facilitate reading the position of the meniscus.

Both flowmeters were calibrated with air against a 0.1-cubic-foot wet displacement meter, which in turn had been calibrated against a standard 0.1-cubic-foot bottle. During the calibration of the flowmeters the temperature of the room was maintained at $30 \pm 0.2°$ C, and all work was done with the room at $30 \pm 1°$ C, in order to avoid the introduction of a temperature-correction factor in the use of the calibration.

The resistance to the flow of the mixture from the outlet of the flowmeters to the tip of the burner was kept at a minimum, and this, with the low differential pressure across the capillaries, kept the average pressure of the gas in the capillary from exceeding atmospheric pressure by more than 1 percent at the maximum rate of flow and with the smallest burner. This made a pressure correction for the flowmeter calibration unnecessary. The differences in the temperature and pressure at which the air was saturated in the wet meter and the temperature and pressure at which it was saturated in the previously described air saturator were taken into account in computing the volume passed by the meter. In all cases, except those involving very low rates of flow, the meter was timed for an integral number of complete revolutions in order to avoid errors arising from variations in the volumes of the four compartments of the meter drum. The time was measured with a stop watch which had been checked against the standard second signal and found accurate to 1 part in 600.

73059—36——2

The capillary tubes were calibrated individually and with all connected in parallel. Smooth curves were drawn through the points, and the maximum deviation of the points from the curve on all curves but one for the individual tubes was 1 part in 460. The maximum deviation from the curves for the combined tubes was 1 part in 300. The smallest capillary of the group required an excessively long time to complete one revolution of the meter, so parts of a revolution were used, and only three points were obtained, which showed a maximum deviation of 1 part in 125.

By operating the air flowmeter and gas flowmeter simultaneously, with the wet meter connected at the common outlet, it was then determined that the rate of flow indicated by the air flowmeter, plus the rate indicated by the gas flowmeter, was equal to the total rate of flow as indicated by the wet meter. This relationship made possible the computation of the composition of the mixtures supplied to the burner from the flowmeter readings and a knowledge of the composition of the constituents. Mixtures prepared in this manner were analyzed chemically, and the computed composition agreed with that determined by the analysis. The average percentage deviation of the points from the calibration curves justifies the assumption that the composition of mixtures may be computed in this way with a precision of about ± 0.1 percent.

At the outset the authors desired to avoid the necessity of making a complete calibration of the flowmeter for each gas to be measured. Accordingly, it was decided to make use of a viscometer to obtain the ratio of the time required for the effiux of any gas to the time required for the efflux of the same volume of air under the same head and at the same temperature, 30° C. This time ratio for each gas was used as a correction factor applied to the air calibration.

Unfortunately, the composition of a mixture computed in this way differed by 3 or 4 percent from the results of the analysis. This led to the discovery that the correction factor was different for different tubes and varied with the rate of flow. It was necessary, therefore, to use some of each fuel gas to calibrate as many of the tubes as were required directly against the wet meter. This was done at a sufficient number of points to establish a curve for each tube showing the variation of the correction factor with the rate of flow.

With some gases the factor was small, differed but little with different tubes, and was practically constant at all rates of flow. With other gases the reverse was true.

3. MIXING THE GASES

The combustible gas leaving the gas flowmeter passed through a metal tube which extended downward into a metal box only slightly larger than the tube. The gas flowed from the tube through a number of holes in the sides. The air entered the box from the air flowmeter and flowed downward past the holes from which gas was issuing and thence out through a metal pipe which led to the burner. The front of the box was closed by a window of thin cellophane. The device, shown at E in figure 2, thus served the dual purpose of mixer and explosion head, protecting the flowmeters from the effects of explosions, which sometimes passed the flash-back trap.

The mixing of the gases was completed during the subsequent passage through 2 feet of iron pipe, two ells, a by-pass cock, C, and a

flash-back trap, T, on the outlet of which was screwed the burner, B. The volume of the fittings intervening between flowmeters and burner was kept small in order that when the composition of the mixture at the outlet of the flowmeters was changed by adjusting the needle valves, the new mixture would replace the old within a few seconds, even at a low rate of flow. At the same time the volume of the fittings was large enough and the flow sufficiently disturbed to insure a perfectly homogeneous mixture at the base of the burner.

4. BY-PASS COCK

A large-bore cock of the plug type, C in figure 2, was placed immediately below the flash-back trap, T. It was fitted up as a tee-cock so that a 90° turn of the plug would cut off the flow of mixture from the flash-back trap and burner, and permit unrestricted flow out of the side opening, O, through a tube to a ventilator flue. This made it possible to extinguish flames which had flashed down the burner tube, B, and were burning in the flash-back trap, without cutting off the supply of gas or air, and without disturbing the flowmeter readings.

5. FLASH-BACK TRAP

A flash-back trap, shown at T, consisted of a cylindrical cast-iron dome with walls about 5 mm thick. Slots about 0.3 to 0.4 mm wide were sawed through the sides of this dome lengthwise. A sufficient number of slots provided a combined area of opening as large as the cross section of the pipe, so that no significant impediment to the flow resulted. The dome was screwed to the outlet of the by-pass cock, and, in turn, was surrounded by a brass cylinder, slightly larger, which screwed on at the base of the slotted dome. This brass cylinder terminated at the top in a screw fitting to which various burners could be attached as desired.

The purpose of the trap was to prevent flames which flashed down the burner tube from traveling back to the flowmeters. Should this occur the supply of gas would have to be cut off until the flame was extinguished, which would necessitate readjusting the flow to the desired rate. The flames being unable to pass through the narrow slots against the high velocity, burned on the outside of the dome which, having thick walls, readily dissipated the heat evolved for a short time. The flame was then easily extinguished when the stream of mixture was diverted by means of the by-pass cock. The slotted dome was a part of a burner designed by the National Lighting Co., for use with acetylene.

6. THE BURNER

Several burners of different diameters were used, the construction of which is indicated at B. All were made of seamless brass tubing, the inside surface of which was cylindrical and polished smooth. The burner tubes were mounted on duplicate bases, so that they might be readily interchanged. They were inclosed in water jackets to prevent preheating the gas mixture to an unknown and variable temperature. Any uncertainty in the temperature of the mixture would cause a corresponding uncertainty in its volume rate and consequently in the velocity with which it issued from the burner tip.

The temperature of the mixture was maintained at 50° C during the studies on all except the first three gases. This was done to prevent the condensation of moisture from the flame around the rim of the port. In the case of the first three, hydrogen, carbon monoxide, and acetylene, the temperature was approximately 30° C. Subsequent investigation, to be reported in another paper, showed that the effect of changing the temperature by 20° C in this temperature range was not sufficient to justify repeating the work on these three gases.

The gas mixture was preheated on its way to the burner by a nichrome coil heated electrically and placed directly in the gas stream. Water at 50° C was circulated through the burner jacket, and the temperature of the unlighted mixture was measured at frequent intervals by means of a thermocouple swung into position just above the burner port. A detailed description of this equipment will constitute a part of the subsequent paper mentioned above.

The lengths of the burner tubes were, in all cases, more than 40 times their diameters. This was ample to permit eddies and turbulence introduced by the flow through the various fittings to die out and insure laminar or streamline flow of the mixture before it reached the tip of the burner. A permanent condition of turbulent flow would result only in case the value of the Reynolds number R is allowed to exceed 2,300.[5] The range of operation was kept below this limit.

7. THE CAMERA

The camera used to photograph flames for measurement in the determination of flame velocity was made in the woodworking shop of this Bureau from a sketch supplied by the authors. A few parts, bellows, plateholders, and lens with its mechanism, came from other sources. The lens was a U.S.4 rapid rectilinear of the Bausch and Lomb Optical Co. The bellows could be extended to 20 inches, which permitted focusing at short object distances, as well as magnification in the case of small flames. Ordinarily the magnification factor was kept at about 2.

Six pictures were made on each 5- by 7-inch plate by shifting the plateholder past a vertical 1-inch focal plane stop placed in the center of the field. The exposure time varied according to the intensity and actinic quality of the light from the various flames. Times as long as 4 minutes were required in the case of the hydrogen flame. In most cases the time was about 1 second.

The brightly illuminated scale used to determine the magnification factor was used as the object upon which to focus the camera, the image being formed on a fine-ground glass plate substituted for the plateholder.

8. THE GONIOMETER

The instrument with which the angle α was determined was designed to permit rapid measurement, with a minimum of fatigue to the eyes and nerves of the observers, maximum freedom from personal errors, and the highest practicable precision. The instrument shown in figure 3 was found to be very much better, in all respects, than any

---

$R=\frac{D\times V\times d}{\mu}$, and

D=diameter of burner tube, expressed in centimeters.
V=velocity of fluid, in centimeters per second.
d=density of fluid, in grams per cubic centimeter.
μ=viscosity of fluid, in cgs units.

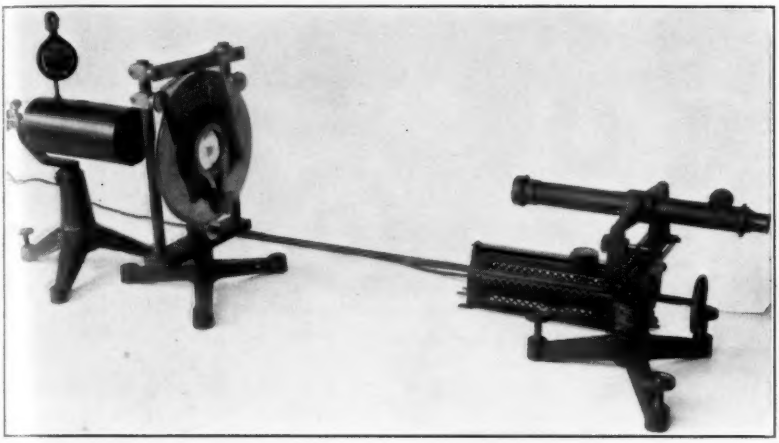

FIGURE 3.—*Goniometer and reading telescope for measuring the angle between the two sides of the flame surface.*

In making the photograph, a mirror was mounted over the illuminator in the hope of showing vernier and scale on the back of the goniometer.

UNIV. OF MICH.

of the four or five devices which had previously been used, improved upon, and discarded. The time required and the resulting fatigue were greatly reduced and the precision was improved by decreasing the number of operations and by simplifying those which remained. The personal element was eliminated from all of the operations except that in which the observer was required to set the cross hair of the reading telescope tangent to the curved flame surface at a marked point. The radius of curvature of the flame surface was not constant, the curve resembling a parabola, so the operation involved personal judgment trained by a study of the geometry of the figures, and some practice, before settings could be reproduced with desirable precision. In order to reduce the effect of this personal factor, two observers made settings alternately and their results were averaged. The precision attainable was a function of the character of the flame, the character of the negative, and of the curvature of the flame surface. The average deviation of all the angles measured from the means of their groups was 2.3 percent.

9. TREATMENT OF THE RESULTS

The numerical results obtained in this investigation add little to the mass of data already on record, and are presented here primarily to serve as a basis for the investigation and discussion of the effects upon them of changing several experimental variables.

The data are in approximate agreement with those of other workers with the burner method and, in the case of CO–O_2 mixtures, with the bubble method of Stevens. Flame speeds derived from measurements in 1-inch horizontal glass tubes are, however, very nearly twice those obtained with similar mixtures by the former two methods, probably because the combustible mixture in which the flame traveled was itself moving along the tube. Chapman and Wheeler [9] show that this occurs in the case of tubes open at both ends.

All the data have been plotted as shown in figure 4. Smooth curves have been drawn through the points so that the sum of the positive and negative deviations of the points from their curve is very small.

The composition of the mixtures has been expressed in terms of the air in the mixture, as compared to the total amount required for the complete combustion of the gas. The abscissas, therefore, represent primary air, expressed as percentages, of the total air required. (Primary air is that which is mixed with the gas before combustion. The remainder of the air required for complete combustion must come from the atmosphere surrounding the flame, and is called secondary air.)

This means of expressing the composition places all the gases as nearly as is possible upon the same basis, not only on the score of the air required for complete combustion, but on that of heat of combustion as well, for the heat evolved is at least roughly proportional to the oxygen consumed.

The data have also been plotted in figure 5, in which the composition is expressed in terms of the percentage of combustible gas in the mixture. This has been done only to facilitate comparison with the data of other investigators and to illustrate certain points under discussion.

V. DEPENDENCE OF NUMERICAL RESULT UPON EXPERIMENTAL FACTORS

In order to provide a basis for the investigation of the effects of changing experimental factors on the numerical result obtained, the following assumption has been made.

In any combustible mixture of gases, of given composition, temperature, and pressure, there is a definite fixed value for the velocity of propagation of flame relative to the gas mixture. Consequently, if different values are obtained by different means, it must be concluded either that one of the supposedly fixed experimental conditions was

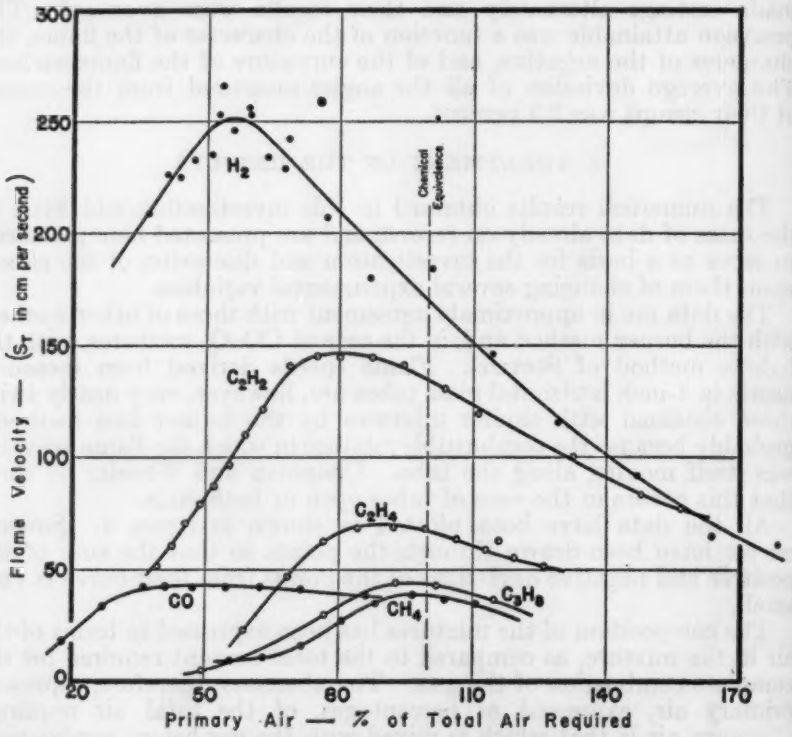

FIGURE 4.—*Flame-velocity curves for six fuel gases.*

The curves are plotted to place these gases on a common basis with respect to the air required for combustion, and nearly so with respect to heating value.

not what it was supposed to be, or that the differences in the numerical result have been imposed by differences in the methods of measurement and computation, or by the apparatus.

On this basis, the degree to which the numerical result is found to be independent of the method or apparatus used to obtain it may be used as a criterion of the extent to which that result approaches the supposedly correct definite fixed value assumed above to exist.

An attempt has been made to discover the cause of differences in the numerical result obtained when the flame velocity relative to comparable gas mixtures has been computed under varying conditions.

The variables were average velocity of mixture, composition, size of port, the angle α, and the method of measurement and computation. Insofar as it was practicable they were varied one at a time.

1. EFFECT OF MIXTURE VELOCITY

With a gas mixture of given flame velocity, the magnitude of the angle α depends upon the velocity with which the mixture flows from the burner port. Increasing S_M decreases α, and vice versa. It was desired to know whether the product $S_M \sin \alpha$, which is the flame velocity S_T, was dependent upon the magnitude of S_M.

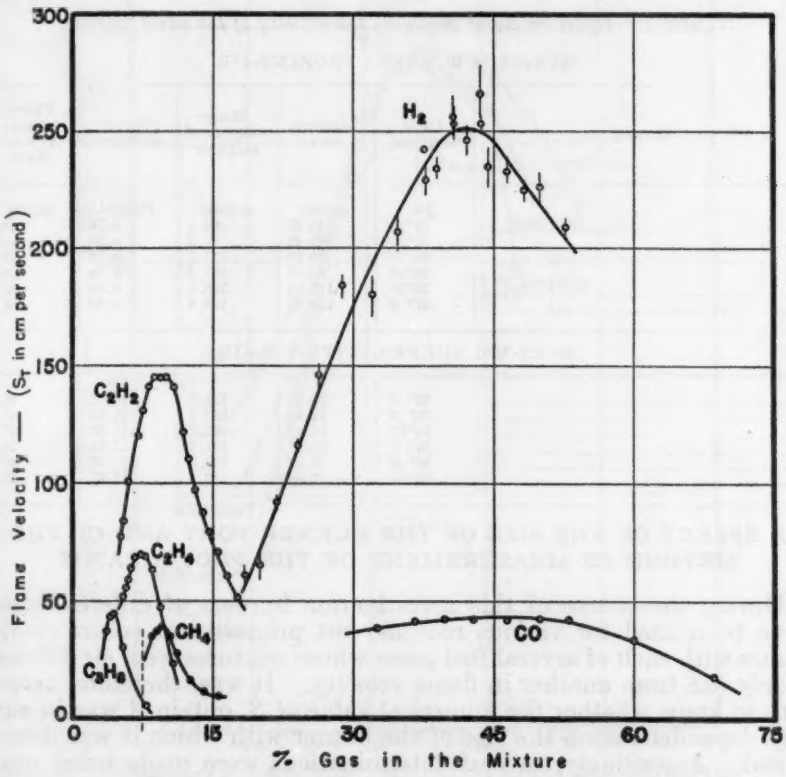

FIGURE 5.—*The flame-velocity curves of figure 4 plotted in the usual manner, with "percentage of gas in the mixture" as abscissa.*

Accordingly, the following test was applied to the largest and to the smallest of the burners used in this study, which were 9.60 mm and 2.75 mm in diameter, respectively. A gas was selected for each which would accommodate a large change in S_M between the limits at which the flame flashed back or lifted off when burning the mixture in which S_T was a maximum. The mixture of maximum S_T was chosen, because at or near the maximum small changes in composition have least effect upon S_T. The flowmeters were adjusted to give mixtures of very nearly the same composition at several different rates of flow, the highest rate being nearly three times the lowest

rate in the case of the large burner, and nearly twice the lowest rate in the case of the small burner. S_T was computed for each rate.

The results are shown in table 1. Regardless of allowable variations in S_T, because of variations in composition from the maximum-speed mixture, the average deviation from the mean value of S_T was 0.67 cm per second, or 2.0 percent, in the case of the large burner, and 0.70 cm per second, or 1.5 percent, in the case of the small burner. This variation corresponds approximately to the precision of the measurements. The conclusion is that the numerical result obtained is independent of the velocity of flow of the gas mixture within these limits.[6]

TABLE 1.—*Effect on S_T of changing the velocity of the same mixture*

(A) 9.60-MM BURNER. PROPANE-AIR.

Record	Angle measured	Mixture rate	Mean velocity of mixture	Gas in mixture	Flame velocity $S_T = S_M \sin \alpha$
	2α	ml/sec	cm/sec	*Percent*	cm/sec
1	63°38′	46.62	64.4	4.76	33.9
2	46°33′	62.43	87.2	4.69	34.5
3	35°23′	80.02	111.7	4.59	33.9
4	29°36′	94.51	131.2	4.54	33.5
5	25°27′	112.14	155.9	4.41	34.3
6	21° 6′	128.42	178.4	4.38	32.7

(B) 2.75-MM BURNER. CITY GAS-AIR.

1	24° 6′	13.16	221.7	17.55	46.3
2	26° 2′	12.44	209.4	17.56	47.2
3	28°16′	11.48	193.3	17.48	47.2
4	31° 6′	10.17	171.3	17.47	46.0
5	36° 6′	8.93	150.4	17.57	46.6
6	43°39′	7.65	128.8	17.53	47.9

2. EFFECT OF THE SIZE OF THE BURNER PORT AND OF THE METHOD OF MEASUREMENT OF THE PHOTOGRAPHS

During the course of this investigation burners of different sizes have been used for various reasons, but primarily to secure stable flames with each of several fuel gases whose mixtures with air differed widely one from another in flame velocity. It was, therefore, necessary to know whether the numerical value of S_T obtained was in any way dependent upon the size of the burner with which it was determined. Accordingly, several determinations were made using mixtures of air with the same fuel gas (city gas) on each of four burners having diameters of 9.60, 6.50, 4.45, and 2.75 mm, respectively, maintained at 50° C. The resulting curves are shown in figure 6.

In the course of a description of a method and apparatus which incorporates many of the features of the apparatus described in this paper, Corsiglia [10] states that direct comparisons between burners of different sizes showed them to be in agreement within the limits of experimental error. The method of measurement and computation by which the flame-velocity data were derived by him from the photographic negatives was essentially a combination of those of

[6] Ubbelohde and Koelliker [4] have determined the maximum flame velocities in H_2-air mixtures for different mixture velocities. The maxima were constant for the two points in which the flow in the burner tube remained laminar, $R<2{,}300$, but the velocity of the mixture measured next was 1,300 cm per second giving $R=>2{,}400$, and showing an increase in the value of the maximum flame velocity.

Michelson [3] and Gouy [2]. The enlarged image of the original negative projected upon a ground-glass surface was traced, and the necessary measurements were made from the tracing. The area of the surface of revolution was computed in a manner which probably differed somewhat from that of Gouy and Michelson, no integration being required except that performed by a planimeter in determining the area of the axial section delineated by the photograph.

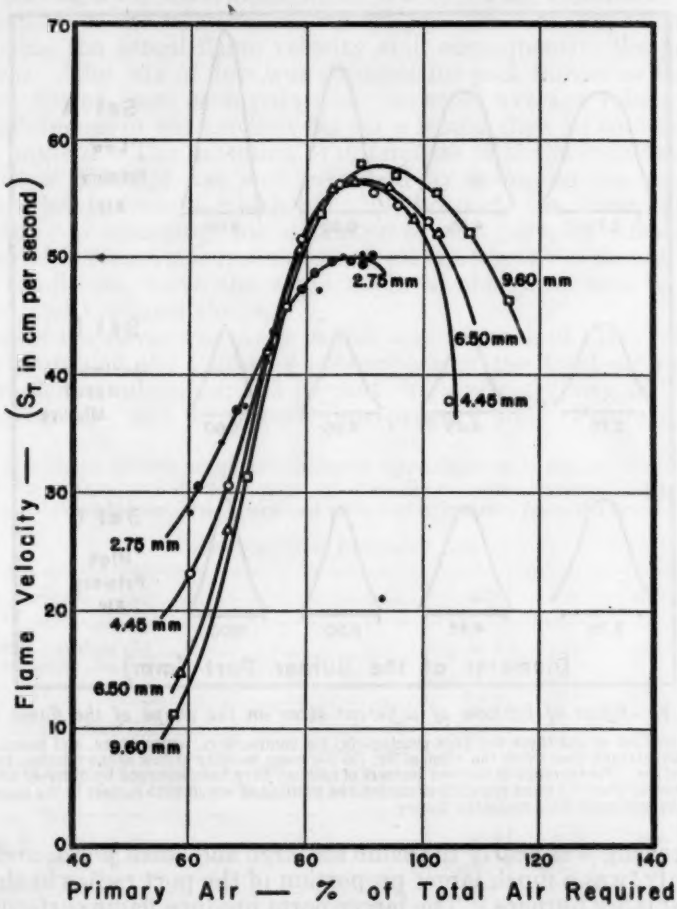

FIGURE 6.—*Flame-velocity curves obtained with burners of different sizes burning mixtures of the same gas with air.*

In view of the discrepancies which appear in figure 6 between the curves obtained with the four burners by the method in which the angle α is used as the basis of computation, it was considered desirable to make some comparative measurements to see whether the agreement between results from the different burners was improved by the use of the area of the flame surface in computing the flame

velocity.[7] Differences in the shape of the flame surface when the same mixture is burned on burners of different sizes immediately suggested themselves as a possible cause of such discrepancies. Such differences in shape have long been noted.[8]

For example, the base of the flame surface is somewhat larger in diameter than the port, and this "overhang" appeared to be greater with small ports. A few preliminary measurements indicated that

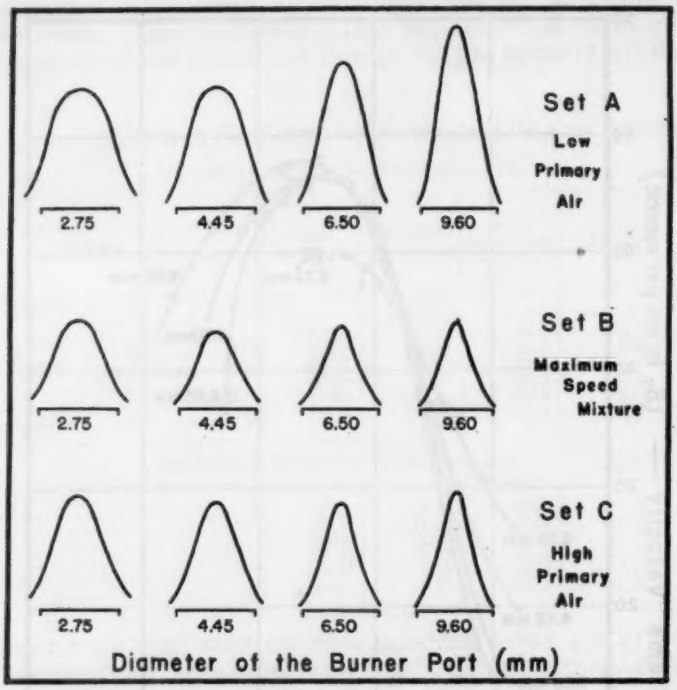

FIGURE 7.—*Effect of burners of different sizes on the shape of the flame surface*

Within each set of four there was kept constant (a) the composition, temperature, and pressure of the combustible mixture, thus fixing the value of S_T; (b) the mean velocity of flow of the mixture, thus fixing the value of S_M. Photographs of the four burners of each set have been enlarged by different amounts to give each burner port the same apparent diameter, the position of which with respect to the flame is indicated by the horizontal lines under the flames.

the overhang was nearly the same for large and small ports, and, consequently, was a much larger proportion of the port radius in the case of the smaller burners. The larger ports produce flame surfaces with relatively sharp tips and sides which are concave near the base.

[7] Computations based on measurements of the "cone height" involve, for the most part, determinations of the area of the flame surface made from time to time and the use of a correction factor which, with the cone height, will give this area. Such a procedure is, therefore, roughly equivalent to that of Corsiglia, provided such correction factors have been determined over a sufficient range of flame shapes to determine the variation of the factor with the shape of the flame.

[8] Ubbelohde and Koelliker [4] describe a method by which the form of the inner cone may be derived from the parabolic distribution of the mixture velocity across the diameter of the port. They conclude that burners of different sizes will yield different results, but that the differences become negligible with large burners and with mixtures of nearly theoretical proportions.

With the smaller ports the flame surface tends to become thimble shaped, the tip becoming broadened into a dome. Similar changes in the shape of the flame surface occur with the same port as the proportion of air in the mixture is reduced.

In order to facilitate direct comparison of the flame surfaces resulting from the use of ports of different sizes, and to compare the results obtained by the two methods of measurement and computation, a set of photographs were made under the following conditions. The composition of the mixture and its temperature were kept constant, thus fixing the actual flame velocity and, consequently, the product $S_M \sin \alpha$. The rate of flow was adjusted for each burner so that the mixture flowed from each port with the same average velocity, S_M. Any differences in the product $S_M \sin \alpha$ would then be concentrated in the angle α. The detection of differences in shape between flame surfaces of different size was simplified by enlarging the negatives by appropriate factors, which gave all the ports the same apparent diameter. If changing the diameter of the port by substituting burners of different size had no effect, all the negatives should, under these conditions, have the same angle α, the same area of flame surface, and the same shape.

A set of negatives was made in this way for each of three mixtures which contained the following proportions of the total air required for complete combustion: 103 percent (high primary air), 90 percent (maximum S_T), and 62 percent (low primary air). Figure 7 shows

TABLE 2.—*Effect of changes of port diameter upon the area of the flame surface and upon the angle α; and the consequent effect on the numerical value of flame velocity calculated from the angle as compared with that calculated from the area*

SET A. LOW PRIMARY AIR					
Port diameter (mm)			2.75	4.45	6.50	9.60
Composition of mixture (%)			62.3	62.3	62.0	61.9
Velocity of mixture (S_M, cm/sec)			85.4	85.2	85.1	85.2
Angle α			19°5′	16°32′	11°48′	9°43′
Enlarged area [1]			654.0	729.3	801.9	869.9
Flame velocity (cm/sec)	$S_M \sin \alpha$		27.9	24.2	17.4	14.4
	volume rate / actual area		18.5	16.8	15.1	13.8
SET B. MAXIMUM-SPEED MIXTURE					
Composition of mixture (%)			90.4	89.6	89.6	89.6
Velocity of mixture (S_M, cm/sec)			121.0	120.2	120.4	120.7
Angle α			22°58′	26°27′	26°19′	26°36′
Enlarged area [1]			589.6	455.3	390.1	356.1
Flame velocity (cm/sec)	$S_M \sin \alpha$		47.2	53.5	53.4	53.7
	volume rate / actual area		29.0	38.0	43.8	47.7
SET C. HIGH PRIMARY AIR					
Composition of mixture (%)			103.2	103.5	100.7	103.7
Velocity of mixture (S_M, cm/sec)			140.2	140.0	140.8	140.3
Angle α			19°4′	20°8′	20°13′	20°3′
Enlarged area [1]			644.4	560.9	483.7	453.8
Flame velocity (cm/sec)	$S_M \sin \alpha$		45.8	48.2	48.7	48.1
	volume rate / actual area		30.7	35.9	41.3	43.6

[1] The enlarged area is the area of the flame surface, in arbitary units, measured after the flames have been brought to a common basis for comparison, by enlargement of all ports to the same apparent diameter. If changing the size of the port had no effect upon the shape of the flame, and if the flame base was congruent with the port, all four areas within a given set would be equal, as well as the angles.

the outlines of the resulting flame surfaces. A line drawn beneath each flame represents the approximate position and apparent diameter of the port, and shows qualitatively the extent to which the base of the flame differs in radius and in elevation from the port on which it was formed. Table 2 shows the diameters of the ports, the composition and velocity of the mixture, the angle α, the area of the enlarged surface,[9] and the flame velocity as derived from the angle and also from the actual area of the flame surface in each case.

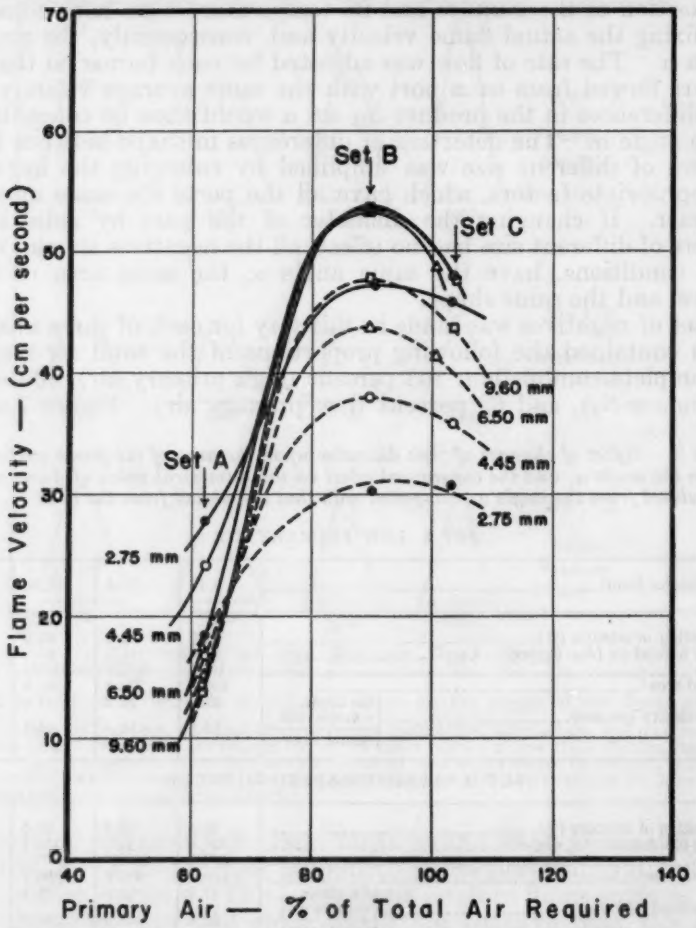

FIGURE 8.—*Flame-velocity curves derived from measurements of the flames of figure 7.*

The solid curves result from measurements of the angle. The dotted curves result from measurements of the area of the flame surface by the method of Corsiglia.

Figure 8 shows the flame-velocity curves resulting from the two methods of measurement and computation. The solid curves are the result of measurements of the angles, and the broken curves result from measurements of the surface area. By reference to table 2 it may be seen that within each set the composition of the mixture and its average velocity were kept substantially the same with each of the four burners. In sets B and C, the angle α is surprisingly constant

[9] See footnote to table 2, page 25.

for the three larger burners, but is somewhat smaller with the 2.75-mm burner in each case. In consequence, the flame velocity, as computed from the angle, also is nearly the same for each of the three larger burners in sets B and C, and with the smallest burner it is somewhat lower: Set A (low primary air) differs markedly from the other two sets in several respects. Not only is the angle not constant, but the smallest burner shows the largest instead of the smallest angle. The angle decreases progressively as the size of the burner is increased, and the numerical value for the flame velocity varies accordingly. This is illustrated graphically in figure 8 by the divergence of the solid curves below 75 percent of the total air required.

In none of the sets is the area of the surface the same for the various burners, but the area decreases progressively in sets B and C, and it causes a corresponding increase in the numerical value for flame velocity computed from the area, as the size of the burner is increased. This is illustrated in figure 8 by the divergence of the broken curves above 67 percent of the total air required. Set A, again, differs from the other two, showing a progressive increase in area and a corresponding decrease in the computed flame velocity as the size of the burner is increased.

Both methods of computation result in numerical values for the flame velocity which vary with the size of the burner port. In rich mixtures, the smaller the burner the higher is the apparent flame velocity.[10] In lean mixtures, the smaller the burner the lower is the apparent flame velocity.

When computed from angle measurements the numerical values for flame velocity were substantially the same in the vicinity of the maximum with burner ports from 9.60 mm down to 4.45 mm in diameter. The 2.75-mm burner showed a result about 11 percent lower at the maximum. In the rich mixtures the agreement was very poor, the 2.75-mm burner showing a numerical result twice that shown by the 9.60-mm burner.

When computed from area measurements, the numerical values for flame velocity are substantially the same for all the burners at about 67 percent of the total air required and diverge markedly in both directions. The 2.75-mm burner shows a result over 30 percent less than that shown by the 9.60-mm burner at the maximum. In the rich mixtures the spread of the results from all the burners is only about one-third as great as the spread shown when the results are computed from angle measurements. The curves for the 9.60-mm burner computed by both methods are in good agreement from about 60 to 75 percent of the total air required.

As has been stated previously in this paper, excellent agreement was found between the maxima of the flame-velocity curves for CO–O_2 mixtures (containing the same amount of water vapor in both cases), one curve being obtained from computations based on the angle of the flame surface on a 3.85-mm burner, and the other curve from results obtained by Stevens using the bubble method. In view of the above, and of the findings of Ubbelohde and Koelliker [4] and Ubbelohde and Hofsäss [11], it is concluded that when the burner method is used, computations on the basis of the angle of the flame

[10] Ubbelohde and Hofsäss [11] discuss some of the sources of error inherent in several of the methods of measuring the cone and computing the flame velocity. They mention that the result obtained depends upon the secondary combustion and is too high. This error disappears as the composition of the mixture approaches the theoretical, and it is larger with smaller burners.

surface at the mean velocity diameter yield results which are substantially correct for mixtures in which the flow is laminar, in which the flame velocity is near its maximum, and for burners not much smaller than 4 mm in diameter.

It is also concluded that only if the shape of the flame surface did not depart markedly from that of a geometrical cone could computations based on the actual area of the flame surface be expected to yield substantially the same results as those based on the angle, and only then could either be considered to be approximately correct. This requires that the tip of the flame surface have a reasonably sharp point, and that the area of its base exceed the area of the burner port by only a negligible amount. These conditions exist only in the vicinity of the maximum flame velocity and on relatively large ports. Few of the flames from which figure 8 is derived sufficiently approximate this condition.

That the same numerical result was obtained for the maximum flame velocity on all but the smallest of the four burners when the computation was made on the basis of the angle, shows that the angle is affected much less than the area by changes of burner size.

3. EFFECT OF THE OVERHANGING FLAME

It has been mentioned that if the base of the flame had the same diameter as the burner port, and if changing the size of the port had no effect upon the shape of the flame surface, the areas of the surfaces of two or more flames, when treated as shown in figure 7, should be equal. Reference to figure 7 makes it apparent that the flame base is larger than the port. This is true not only in mixtures low in primary air, as mentioned by Corsiglia, and in which it is very pronounced, but all of the negatives made during this study show that overhang always occurs to some extent.[11] In many cases the radius of the flame base was over 30 percent larger than the radius of the port.

There is no question that such differences must exert considerable influence upon the results obtained when the flame velocity is computed by different methods, such as those discussed above, but it is improbable that the effects upon the flame velocity set forth in table 2 can be accounted for wholly on this basis. In order to determine the magnitude of the overhang, measurements were made on the negatives used in the determination of flame velocity. These measurements embrace seven gases, mixtures ranging from low to high primary air, the same gas mixture on ports of different size, and the same mixture on the same port at different mixture velocities. The relation of overhang to the composition of the mixture, to the size of the port, and to the mixture velocity may be brought out most simply by a study of the measurements of the flames shown in figure 7, and of those from which the curves of figure 6 and the data of table 1(B) are derived. Table 3 presents the data from the sources just mentioned. The averages of overhang measurements for each port and each mixture are shown in table 4.

[11] Ubbelohde and Koelliker [4] mention that the bases of most inner cones project laterally out over the burner wall and are suspended an appreciable distance above it. The explanation given does not seem entirely satisfactory, and this question will be discussed in another part of this paper.

TABLE 3.—*Overhang as related to composition, port size, and mixture velocity*

Port diameter	Composition of mixture—% of the total air required					
	62.5%		89.5%		103.5%	
	Overhang	S_M	Overhang	S_M	Overhang	S_M
mm	mm	cm/sec	mm	cm/sec	mm	cm/sec
2.75	0.4	143	0.4	190	0.5	140
	.5	85	(•) .5	129–222		
	.5	144	.5	121		
			.4	193		
4.45	1.0	85	.6	129	.5	145
	.9	95	.6	120	.6	140
6.50	.8	85	.5	106	.5	120
	.8	81	.6	120	.6	141
9.60	.7	85	.5	121	.5	140
	.6	89	.3	118	.3	133

• Six flames of table 1(B) all had overhangs of 0.5 mm, but S_M varied from 129 to 222 cm/sec.

TABLE 4.—*Averages of the data of table 3*

Port diameter	Composition of the mixture—% of total air required			Average overhang for the port	
	62.5% Avg overhang	89.5% Avg overhang	103.5% Avg overhang	Distance	Percentage of port radius
mm	mm	mm	mm	mm	percent
2.75	0.5	0.5	0.5	0.5	36
4.45	.9	.6	.6	.7	31
6.50	.8	.6	.6	.6	18
9.60	.6	.4	.4	.5	10
Avg. overhang for the mixture	.7	.5	.5		

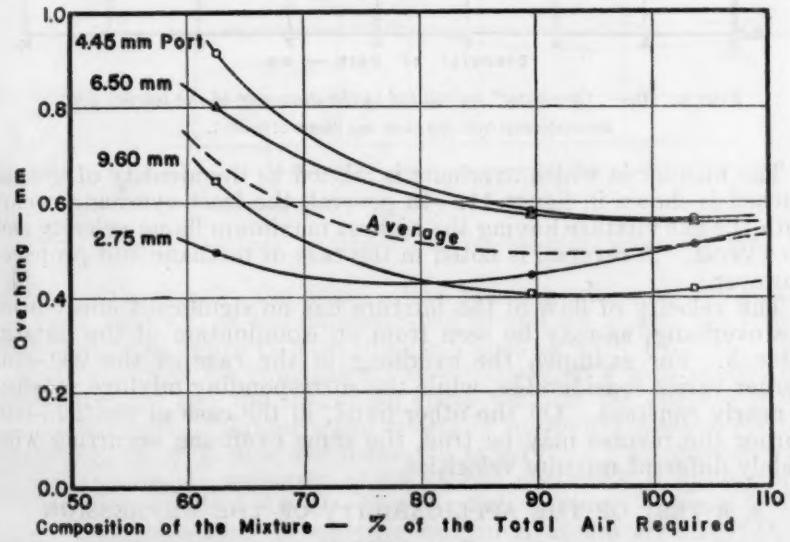

FIGURE 9.—*The relation of "overhang" to the composition of the combustible mixture.*

Measurements from the flames and ports of figure 7.

The average overhang on a given port has been plotted as ordinate and the composition of the mixture as abscissa in figure 9. These

curves, with additional data in figure 11 show that the overhang is large in mixtures containing little primary air, decreases as the proportion of air is increased, and passes through a minimum in mixtures containing somewhat more air than the theoretical proportion. Although the data at hand do not all show it, the overhang again becomes larger with mixtures containing a large excess of air.

The average overhang for a given mixture has been plotted as ordinate and the size of the port as abscissa in figure 10, which shows the overhang to be slightly greater on the 4.45 and 6.50-mm burners than on the 9.60- or the 2.75-mm burners. The difference between the largest and smallest overhang shown by the average curve is about 0.2 mm on ports which vary from 2.75 to 9.60 mm, which is surprisingly small. In terms of the percentage of port radius, therefore, the overhang is much larger in the case of the smaller ports, as is shown in the right hand column of table 4.

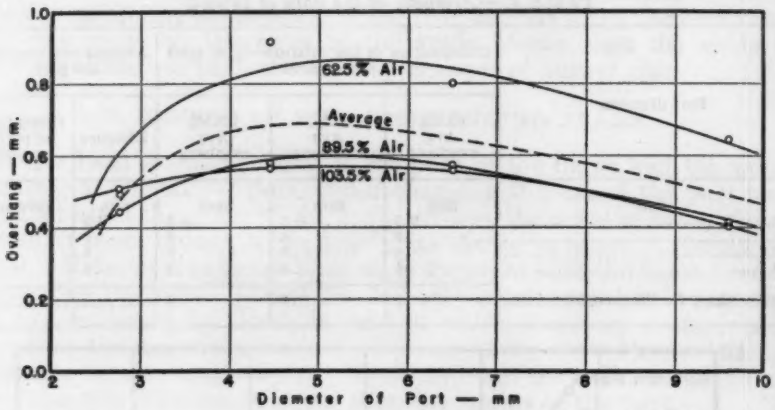

FIGURE 10.—*"Overhang" as related to the diameter of the burner port.*

Measurements from the ports and flames of figure 7.

The manner in which overhang is related to the identity of the gas burned is shown in figure 11. In general, the least overhang occurs with the gas mixture having the highest maximum flame velocity and vice versa. A reversal is noted in the case of methane and propane, however.

The velocity of flow of the mixture has no significant effect upon the overhang, as may be seen from an examination of the data in table 3. For example, the overhang in the case of the 9.60-mm burner varies considerably, while the corresponding mixture velocity is nearly constant. On the other hand, in the case of the 2.75-mm burner the reverse may be true, the same overhang occurring with widely different mixture velocities.

4. A TEST OF THE APPLICABILITY OF THE EXPRESSION

$$D_{\overline{v}}=0.707\ D$$

It is obvious that the correctness of the foregoing numerical results for the velocity of flame relative to the combustible mixture, and many of the conclusions based upon them, must rest upon the applicability

of the assumption that $D_{\overline{r}}=0.707\ D$, since this factor was used in all the computations of flame velocity based on measurements of the angle α which have been presented in this paper.

The theoretical derivation of this factor has been given on page 12. Experimental data have been collected by workers in hydraulics who used much larger pipes. These data, while not conclusive, tend to indicate that the above factor is probably as close or closer to the truth than measurements of velocities by present means are capable of giving experimentally, so long as the flow remains laminar.

The relatively large departures from the shape of a geometrical cone exhibited by the flames of the 2.75-mm burner (shown in fig. 7) and by those of set A with low primary air, and the fact that different numerical values for the flame velocity were obtained from measurements of these flames, suggested the possibility that some factor other than 0.707 might lead to more concordant results for the entire

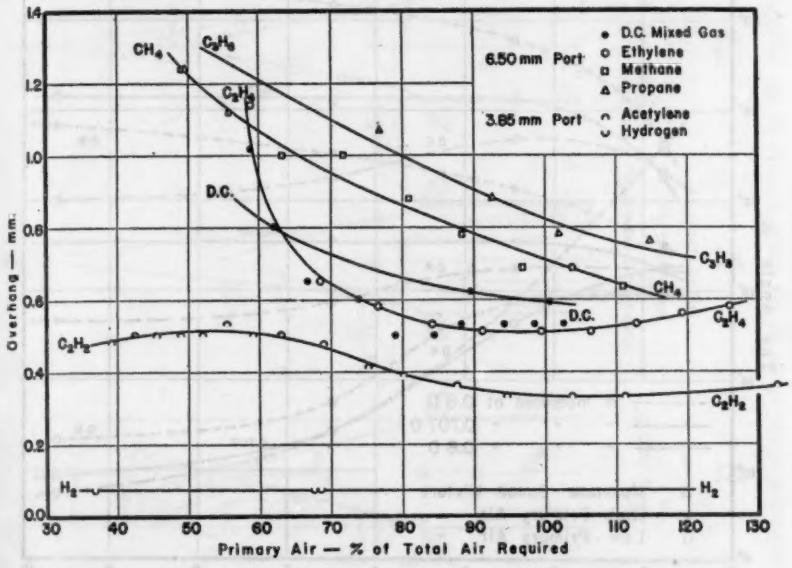

FIGURE 11.—*"Overhang" as related to the identity of the combustible gas.*

group. Accordingly, the angle α was remeasured for all the flames shown in figure 7, at the diameters 0.6 D and 0.8 D and the results were plotted in figure 12 with those obtained at 0.707 D.

It is seen that for both the mixture containing a high proportion of primary air and the maximum speed mixture the angle α is the same for the three larger burners and is somewhat smaller for the 2.75-mm burner when α was measured at 0.707 D. α increases with increasing D when measured at 0.8 D, and decreases with increasing D when measured at 0.6 D. For the rich mixtures α tends to decrease with increasing D whether measured at 0.6 D, 0.707 D, or 0.8 D.

The constancy of the value of α when measured at 0.707 D (in the cases of the lean and maximum speed mixtures when using the three larger burners) and its variation in opposite directions when α was

measured at 0.6 D and 0.8 D, indicates that the range of variation of this factor within which the value of α is independent of the size of the burner port is very limited; and also that the factor which yields a constant value of α lies much closer to 0.7 than to 0.6 or 0.8.

The above findings point to the conclusion that within a limited range of port sizes and a limited range of composition of the combustible mixture, there is a very limited portion of the flame surface the slope of which has not been affected by the distortion at the base or at the tip.

This conclusion is partially corroborative of the conclusion of Ubbelohde [4] mentioned on page 11 that the rounded tip and curved base represented deviations from the normal, but indicates that the

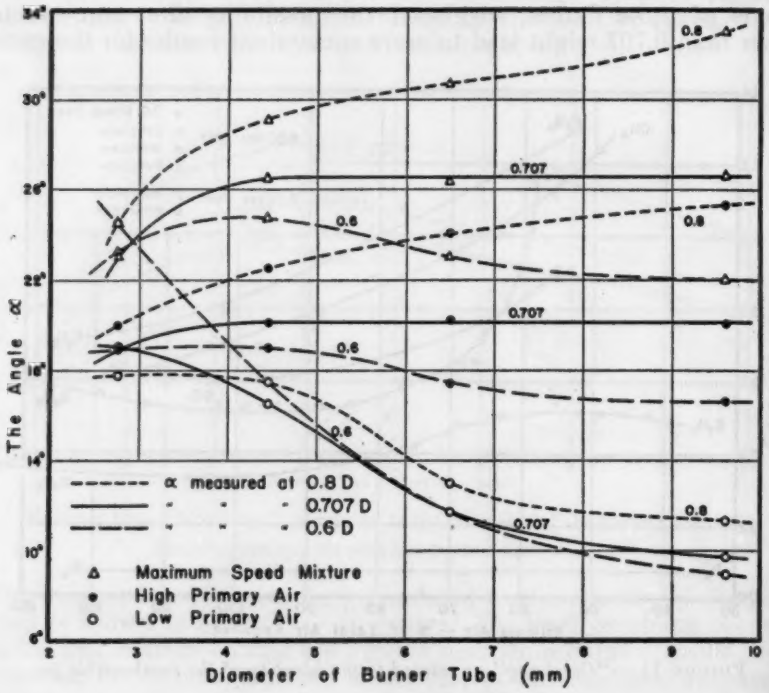

FIGURE 12.—*Location of the part of the flame surface at which α is independent of the diameter of the burner tube.*

Measurements from the flames of figure 7.

deviations extend much further from tip and base than he supposed. Ubbelohde considered that the straight portion of the flame surface was unaffected by these disturbing influences and measured the angle between this and the axis. As will be seen from the discussion of figure 13 (III), the entire flame surface, unaffected by secondary influences, should be concave upward rather than straight. In this connection it is significant that when α was measured at 0.707 D, on flames with which the angle was found to be independent of the diameter of the port, the points marked on the images all fell on concave portions of the flame surfaces.

The part of the flame surface involved when α is measured at 0.707 D, using suitable burners and mixtures, is probably affected little or not at all by those things which affect the tip and base, and which may even overlap in such cases as those of the rich mixture on the 2.75-mm burner.

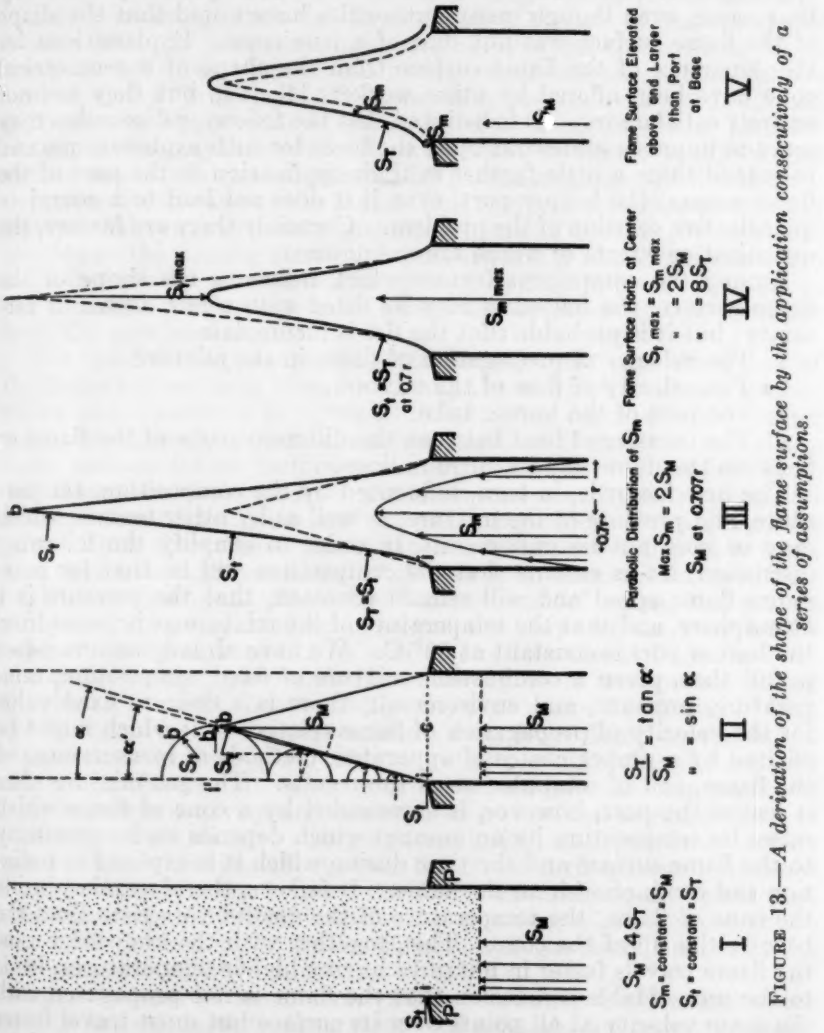

FIGURE 13.—*A derivation of the shape of the flame surface by the application consecutively of a series of assumptions.*

In view of the above, it seems probable that the expression $S_T = S_M \sin \alpha$ is capable of yielding numerical results which are independent of the diameter of the port. But it is also probable that this is true only in case the composition of the mixture is near the theoretical and the burner port is over 4 mm in diameter.

VI. SHAPE OF THE FLAME SURFACE AS A RESULTANT OF SEVERAL VARIABLE COMPONENTS

The shape of the figure assumed by the flame front resulting when a burning stream of combustible mixture issues from a burner tube approximates sufficiently to a cone to have been generally called by that name, even though many authorities have noted that the shape of the flame surface was not that of a true cone. Explanations for the departure of the flame surface from the shape of a geometrical cone have been offered by other workers [4], [12], but they are not entirely satisfactory. It is believed that the following discussion may serve to improve somewhat upon the basis for such explanations, and to extend them a little further in their application to the part of the flame nearest the burner port, even if it does not lead to a complete quantitative solution of the problem. Certainly there are factors, the quantitative effects of which are unknown.

Among the component factors which influence the shape of the flame surface, the following may be listed with a fair degree of certainty; but it is probable that the list is incomplete.

1. The velocity of propagation of flame in the mixture.
2. The velocity of flow of the mixture.
3. The port of the burner tube.
4. The transfer of heat between the different parts of the flame or between the flame and its surroundings.

The first factor is, in turn, influenced by the composition, temperature, and pressure of the mixture, as well as by other factors, which may or may not be important. In order to simplify the following discussion, let us assume that the composition will be that for maximum flame speed and will remain constant, that the pressure is 1 atmosphere, and that the temperature of the mixture as it issues from the burner port is constant at 50° C. We have already assumed (see p. 20) that, given a combustible mixture of fixed composition, temperature, pressure, and environment, there is a definite fixed value for the velocity of propagation of flame relative to it which might be elicited by a proper choice of apparatus, methods of measurement of the flame, and of computation of the results. The gas mixture after it leaves the port, however, is surrounded by a cone of flame which raises its temperature by an amount which depends on its proximity to the flame surface and the time during which it is exposed to radiation and conduction from the flame. It follows, therefore, that inside the cone of flame, the temperature of the gas mixture rises from the base to the tip of the cone. This, together with the knowledge that the flame travels faster in mixtures having higher temperatures, leads to the unavoidable conclusion that the flame is not propagated with the same velocity at all points over its surface but must travel faster at some points than at others.

The second factor is determined only indirectly in the present study. The volume of gas passing per unit of time is divided by the area of the burner port, which yields the average or mean velocity of flow of the gas mixture through the port. Assuming laminar flow,

which has already been justified,[12] there are several facts to be noted. On both theoretical and experimental grounds it can be stated: (1) that the distribution of velocities will be parabolic; (2) that the gas mixture will flow with its average velocity at a distance from its axis of 0.7 the radius of the circular port; and (3) that the maximum velocity at the axis will be twice the average velocity. In addition, it has been found that the diameter of a stream of unburned gas issuing from the port remains substantially equal to the diameter of the port for some 10 to 15 diameters—until the sharp boundary is broken up by turbulence. This indicates that there is no significant expansion of the stream to be expected as a result of any pressure change on leaving the port. There is, however, reason to expect that the stream of mixture surrounded by a cone of flame will rise in temperature after it leaves the port. This increase of temperature may be expected to cause a corresponding expansion equal in all directions relative to the moving stream, and consequently to deflect it outward from the axis by an amount which is proportional to the increase in the absolute temperature and which also increases as the distance from the axis increases.

The third factor, the port, exerts its influence upon the shape of the flame surface in at least two ways, one of which has been treated above and illustrated in figure 7. Restricting discussion to circular ports, the diameter affects the shape less than it does the size of the flame surface (other factors remaining constant). The effect illustrated may be accounted for if the dimensions of the temperature-gradient zones [13] remain about the same, regardless of the size of the port. Thus the same dimension becomes larger relative to a small port than to a large one and the effect is to broaden the flame surface relative to the port. Secondly, the material of which the port is made might be expected to influence the shape of the flare at the base of the flame surface. A material of low thermal conductivity would, by becoming hotter itself, allow the flame to approach nearer the rim of the port than would be the case where a material of high conductivity forces the temperature drop from flame to the initial temperature to take place almost entirely within the gas mixture alone. In the case at hand, where the port is made of material of high heat conductivity and maintained at the same temperature as the combustible mixture emerging from it, it is not clear how the port can exert any cooling effect upon the flame surface that would not also be exerted by the mixture itself at some distance above the port rim. Consequently, it is doubtful if the cooling effect of the port can play as important a part in the distortion of the flame surface at the base as has so often been attributed to it.

Other sources of heat, such as the secondary combustion which usually surrounds the primary cone of a flame, influence the shape of the primary flame surface. First, the flare at the base of the cone is slightly decreased and, in effect, drawn closer to the rim of the port; and, secondly, the heat transmitted to the unburned mixture is in-

[12] With the assumption of laminar flow, which has been justified, there has also been made a second assumption which has not been justified; i. e., that the parabolic distribution of velocity which exists within the tube persists during and after emergence from the port, at least until the tip of the cone is reached. Direct experimental evidence on this point is lacking. From purely theoretical considerations one must conclude that some modification will occur which would take the form of a decrease in the velocity of flow at the center of the stream and in an increase at the surface. Whether the change is great enough to be significant in the short space involved is not known.

[13] See discussion of gradient layer on p. 38.

creased, causing an increase in the flame velocity, which, in turn, results in a decrease in the size of this cone of mixture. The effect depends, of course, upon the composition of the primary mixture, being large when the proportion of primary air is low, and negligibly small when the proportion of air approaches or exceeds the theoretical ratio.

An attempt has been made in figure 13 to illustrate some of the possible effects of several factors considered separately on the ultimate shape of the surface of a flame. I represents a port P, through which a combustible mixture is flowing vertically upward.

Let S_t be the velocity of propagation of the flame surface relative to the mixture, or its speed of transformation by the flame, at any point. Let S_m be the velocity of the combustible mixture at any point. Let S_M be the mean velocity of the combustible mixture, and α the angle between flame surface and axis. It will be shown shortly that S_T may now be defined by the equation $S_T=S_M \sin \alpha$ (when α is measured at the point on the radius where S_M is found, namely, 0.7 the distance from center to rim of the port). The velocity of flow, S_m, is for the moment considered to be uniform across the section of the port and equally numerically to the mean velocity of flow in a tube passing gas at the same rate. This is represented symbolically by S_M. The composition and mean velocity of the mixture are so chosen that $S_M=4S_T$, where S_T is the rate at which flame is propagated relative to the mixture.

If the combustible mixture be ignited at any point, i, the flame will travel with equal velocity in all directions in the mixture, its surface, therefore, being spherical.

In II, the direction of travel of the flame is indicated as radial by the vectors S_t and S_T, which are equal, and whose length indicates the velocity of travel of the flame. During the time required for the flame to travel from i to the center of the stream, the mixture has moved upward from i to i′, so that the flame front arrives at b′ just as if it had started from i′ in a stationary mixture. However, in traveling, the spherical flame front, simultaneously rising vertically and expanding radially, describes the bounding line ib. The direction of advance of the elements of flame front which together constitute the line ib is, of course, radial in any sphere. The radius of a circle which passes through the point at which a line is tangent to the circle must be perpendicular to the tangent line. Therefore, the flame front must advance in a direction normal to itself. (See Huyghens' principle of the propagation of light). With the flame advancing in a direction normal to itself, it is now evident that S_T, the vector forming a part of the radius i′b, divided by the vector S_M is equal to sin α, the angle between surface and axis of the conical flame front. The relationship $S_T=S_M \sin \alpha$ is thus derived directly from the direction of propagation of the flame front, and serves to define S_T in terms of S_M and α, which have been defined above.

Thus far, we have made three arbitrary assumptions, i. e., $S_M=4S_T$, S_m is constant and equal to S_M, and S_t is constant and equal to S_T. The second of these, if true, would greatly simplify the determination of flame velocity since one need only adjust S_M to make sin α equal 1, in which case the advancing spherical element would describe the bounding line ic, forming a plane surface at the mouth of the port; $\alpha=90°$, and $S_T=S_M$.

Actually, within the burner tube, S_m is distributed parabolically over the section of the port as indicated in III. This having been determined by experiment, the following facts may be derived theoretically as well as experimentally. (1) S_m max$=2S_M$; and (2) S_M occurs at 0.7 r from the axis. Assuming that the parabolic distribution of velocity remains unchanged for at least 4 diameters beyond the port, III has been constructed to conform to these conditions; and the conical surface derived in II, and shown dotted in III, has been modified accordingly. In moving from the port rim to the axis, the flame simultaneously rises less near the rim, the same distance as before at 0.7 r, and twice as far at the center. The resulting flame surface is indicated by the solid line, ib, S_t still being assumed constant and equal to S_T.

Obviously the shape delineated in III does not correspond to that of an actual flame. For one thing, no flame has a perfectly sharp point, but is rounded off somewhat as indicated by the solid line in IV. Regardless of the factors which may be operating to produce the effect, it is apparent that at the center the surface must be horizontal. Here α equals 90° and consequently $S_t=S_m$; or, the direction of advance of the flame front being normal to its surface must be vertically downward in the same line as the velocity of the mixture, and, since the surface moves neither upward nor downward, S_t must equal S_m. In either case one arrives at the same result. S_t at the center must equal S_m max, which is equal to $2S_M$. But S_M, in turn, has been assumed from the beginning to equal $4S_T$. Therefore, S_t at the tip is 8 times S_T; and the third of our original arbitary assumptions (that S_t is constant and equal to S_T) has been shown to be invalid as far as the tip of the flame is concerned. The first still holds, for IV was so drawn that the direction of advance of S_T in IV is the same as that in II. Therefore, S_M still equals $4S_T$.

While the solid line delineating the flame surface in IV corresponds approximately to the outline of an actual flame over most of its length, it fails to do so at the base where the flame approaches nearest the rim of the port. The base of an actual flame has a larger diameter than the port and locates itself at a measurable distance above it, as is indicated in a somewhat exaggerated manner in V. For purposes of discussion we may assume that in the exceedingly thin flame front there is some definite temperature which is the same over the entire surface of the flame. The port is maintained at a temperature of 50° C by continuously replacing the water in the jacket surrounding the burner by fresh water at 50°. It seems reasonable to suppose that the flame would actually touch the port if the port were at the flame temperature, and conversely, that the flame does not approach nearer the port than it does because the distance separating them is required in which to raise the gas mixture from the temperature of the port to the temperature of the flame front.

That portion of the combustible mixture in contact with the rim of the port has an upward velocity which is substantially zero. That near the wall has only a slightly greater velocity. When this mixture rises above the level of the port rim into the vicinity of the flame front it receives heat by conduction and radiation as does the port. It expands by an amount corresponding to its rise in temperature, and having only a slight vertical motion its expansion may be so great in comparison that the resulting direction of its motion may be as much

outward as upward, as indicated by the small arrows at the left rim in V. In addition to this lateral expansion, it has been supposed that by the time the primary mixture at the rim of the port has reached the short distance from the rim at which the flame can persist, some interdiffusion of the primary mixture with the outside air will have taken place.[14]

Since the shape of the flame surface is a resultant of the velocity and direction of the mixture and the flame propagation, among other factors, this view of the situation at the port rim can readily account for the outward flare of the flame surface at this point, and consequently for the overhang of the flame relative to the port.

The magnitude of S_m is here largely determined by thermal expansion, and the space between flame and port may be considered to represent the distance ahead of the flame surface at which the source of heat at the temperature of the flame is able to maintain a temperature of 50° C by whatever means against the motion of the oncoming mixture. The flame does not dip down inside the rim of the port. The velocity of the mixture becomes greater as the center is approached. The temperature of the mixture is maintained at 50° C by being continuously replaced by fresh mixture at 50° C at a rate which is greater than that at which the flame is able to advance, even near the rim of the port, and at a still faster rate as the center is approached. For these reasons, regardless of which mechanism of propagation may be assumed to operate, it seems probable that there may be a thin gradient layer, less than 1 mm thick, underlying the entire flame surface, in which the temperature rises rapidly from that of the mixture near the center to that of the flame front, and the thickness of which may be inferred from the distance of approach of the flame to the port.

This conclusion is supported by such evidence as the sharpness of the outline of the surface of an advancing spherical flame front of $CO—O_2$ exploding in a bubble photographed by transmitted light [13]. Both the bubble and the flame are evidenced by the change in the optical properties of the material through which the light passes. In the case of the flame, this is caused by the difference between the temperature of the unburned gases ahead of the reaction zone and the much higher temperature of the gases constituting the reaction zone.

If this change had been gradual, a proportionately slow change in the optical properties and a correspondingly diffuse image would have resulted. Actually, the image of the flame front is surprisingly sharp, which indicated a correspondingly steep temperature gradient. Furthermore a thermocouple, introduced from below into the center of the volume outlined by the mixture, and moved laterally toward the flame surface, shows only a gradual rise in temperature until it is practically in contact with the flame, when it rises very rapidly.

[14] Ubbelohde and Koelliker [4], in explaining why the flame lifts off the port under certain conditions, assume that outside or secondary air diffuses or flows inward under the lower rim of the flame and by increasing the proportion of air in the combustible mixture at this point may, in lean mixtures, cause the flame velocity to be lowered even to zero, thus allowing the flame to leave the port.

Some experiments in which fine carbon particles (soot) were introduced into the air around the burner throw light on the validity of this explanation. When the particles of soot entered the primary air openings of an ordinary bunsen burner they became incandescent on passing through the inner cone of the flame and indicated clearly the direction of flow of the gases in which they were suspended. When the jacketed burner shown in figure 2 was supplied with primary air from the laboratory air line no incandescent particles were observed, showing that air surrounding the burner does not flow in under the base of the flame at the port. Any explanation of phenomena associated with the base of the flame must, therefore, be explained on some basis other than by the accession of secondary air into the combustible mixture by any process other than diffusion.

Such a gradient layer, greatly exaggerated in thickness, is indicated in V by the dotted line underlying the flame surface. There is at hand insufficient evidence to decide whether or not the gradient layer changes in thickness toward the tip, but it is evident that when the opposite sides of its inner surface come together, so that the two layers mutually affect each other, the rapid acceleration of the flame movement and the rounding off of the tip of the flame surface are inevitable.

As has been mentioned above on page 35, a rise in temperature may be expected to result in a corresponding expansion of the unburned mixture. It follows from what has just passed that most of the lateral motion imparted to the mixture will be imposed in this thin gradient layer, and consequently will affect the position of the mean velocity diameter only slightly, even though the mixture may be traveling in a direction normal to the flame surface as it passes through it. That the mixture probably does pass through the flame in approximately this direction is indicated by the direction of the emergence of fine carbon particles introduced as soot into the air around a bunsen burner. The arrow marked S_n, passing through the gradient layer in V, indicates the probable direction of flow of the mixture as it approaches the flame surface.

On account of the sharp changes in the optical properties of the gases, as shown by spark photographs of flame fronts, as well as the other evidence for the presence of a thin gradient layer, it does not seem possible, on the basis of an increase in the temperature of the combustible mixture, to account for as great an increase in the flame velocity at the tip of the flame as the derivation given in figure 13 indicates. Neither does it seem possible on this basis to account for appreciable increases in the flame velocity extending downward much below the tip of the flame.

The unreasonably large increase in flame velocity at the tip and the relatively large disparity in shape between the solid and dotted outlines of the flame surface in IV of figure 13 may be accounted for if the parabolic distribution of velocity does not persist unchanged beyond the port, as was assumed.

It is certainly true that after emerging from the port the moving stream is surrounded by a stationary mass of air which exerts a frictional retarding effect just as the metal walls of the tube do. The surrounding air, however, is not rigid and cannot maintain itself stationary against the tendency of the moving stream to set it in motion. Laminas of surrounding air can only be set in motion by the forward drag of laminas of the moving gas stream next inside them. These laminas, in turn, have a higher velocity than they had when in contact with the rigid walls of the burner tube.

The energy required to set in motion laminas of surrounding air must come from the kinetic energy of the moving stream, with a consequent decrease in its velocity as a whole, since no further pressure gradient exists after the stream emerges from the port. Superposed upon this effect, the laminas near the center of the moving stream have their velocities reduced to correspond to the increased velocity of those at the surface, as a result of the lack of a rigid stationary retarding effect. This redistribution of velocities is such as to maintain the momentum of the stream as a whole at the rate of decrease occasioned by the loss of energy just mentioned.

The magnitude of these combined effects may be expected to vary with different gases. The solid outline in IV of figure 13 would result

if S_m max had a value more nearly 1.1 S_M than 2.0 S_M. This would lead to a value of S_t at the tip of 4.5 S_T instead of 8 S_T. It would also permit the supposition that S_t remained substantially equal to S_T until the overlapping of the gradient zones at the tip occurred. A fourfold increase at this point still seems high but not entirely unreasonable.

Some experimental work has been done by various people and several postulates have been offered concerning mechanisms of propagation of flame and the transfer of energy by radiation, by activated particles, etc. [14], which have a bearing for the most part on the character of the flame front and gradient layer, but which would affect in no significant way the derivation of the shape of the flame surface just presented. Their discussion is beyond the scope of this paper.

A local value of S_t at the tip, which is actually several times as great as S_T, must be the result of changes in the physical or chemical condition of the gas mixture. Without attempting in this paper to estimate the relative importance of such real or imaginary effects as those mentioned above, it is certain that if they occur at all their effects must be more pronounced near the tip and result in an inward bending of the flame surface.

The experimental fact that the shape of one part of the flame surface is modified by proximity to the burner, and that of another part by proximity to other parts of the flame, would lead us to expect what we find—that the most consistent results for flame velocity should be obtainable when using large burners rather than small ones, and when measurements are made on the flame surface at some distance from either base or tip rather than when the entire surface is used.

VII. SUMMARY AND CONCLUSIONS.

A description has been given of the equipment and procedure used by the authors to determine the velocity of propagation of flame in mixtures with air of carbon monoxide, hydrogen, acetylene, methane, ethylene, and propane. A modification of the general "burner method" was chosen after a review of the methods employed by other workers, and because the results obtained were to be applied to the study of burners. The angle α between the axis and the tangent to the flame surface was measured at a point 0.7 r from the axis, where the actual velocity of the stream of gas equals the mean velocity. The mean velocity of the mixture, S_M, was determined by dividing the measured volume rate of flow of the mixture by the area of the burner port. The flame velocity S_T was then computed from the relationship $S_T = S_M \sin \alpha$.

Attention is called to the fact that "flame velocity" like "flame temperature", etc., is not a characteristic of a gas itself, but a property of the system as a whole, including the apparatus; and the identity of the gas can be considered as only one of several factors which, taken together, determine the numerical values in a given case. Also, such data must be used with the knowledge that the numerical values may or may not be applicable to any particular case in question.

Data are presented in the form of curves, with the compositions of the mixtures plotted in terms of the air required to combine with the gas, to place the different fuels on as nearly the same basis as possible for comparison. It is concluded, however, that the only points on

the curves of two or more fuel gases which even approach suitability for a direct comparison are the maxima.

An attempt has been made to isolate and determine the effect, on the numerical result, of the velocity of flow of the combustible mixture, the diameter of the burner port, the method of measuring the photographs (angle between surface and axis, versus total area of flame surface), the overhanging base of the flame, and the assumed location of the mean velocity in the stream of combustible gas mixture. The assumption has been made that in any combustible mixture of gases of given composition, temperature, pressure, and environment, there is a definite fixed value for the velocity of propagation of flame relative to the mixture, which may be elicited by a proper choice of apparatus, methods of measurement and of computation; and that different values are obtained by different means because of effects imposed upon the *numerical result* by the methods of measurement and computation, or by the apparatus; and not because of differences in the flame velocity itself.

It was determined that the numerical result obtained by the method described was independent of the velocity of flow of the gas mixture within the precision of the measurements, the average deviation of the individual determinations from the mean being about 2 percent.

The base of the flame surface was found to be somewhat larger in diameter than the port and suspended a short distance above it. This "overhang" was found to be nearly the same for large as for small ports, and consequently was a larger fraction of the radius of the latter, amounting to more than 30 percent of the port radius in the case of the two smaller burners. This was sufficient to lower the numerical results considerably as compared with those obtained with larger burners, when the results were computed from measurements of the surface area of the flames. The larger ports produce flame surfaces with relatively sharp tips and sides which are concave outward near the base. With smaller ports the flame tends to become thimble-shaped, with the tip broadened into a dome. Similar changes in the shape of the flame surface occur with the same port as the proportion of air in the mixture is reduced. The relationship of overhang to the proportion of air in the gas mixture and to the identity of the combustible gas is also shown.

It is concluded that when the burner method is used, the shape of the flame surface must not depart markedly from that of a geometrical cone, if computations based on the actual area of the flame surface are expected to yield substantially the same results as those based on measurements of the angle between the flame surface and its axis, and only then can either result be considered to be approximately correct. To approximate sufficiently to a geometrical cone the flame must result from a mixture in laminar flow, in which the flame velocity is near its maximum, and when the burner ports are not much smaller than 4 mm in diameter. Under other conditions both methods of measurement yield results which depend on the size of the burner, especially when using mixtures containing much less than the theoretical proportion of air or burners smaller than 4 mm in diameter. However, the angle is affected much less than the area by the relative changes in overhang and shape of the flame which accompany changes in the size of the port.

The fact that the angle between the surface and axis of the flame is independent of the diameter of the burner tube when the angle is measured at a point 0.707 r from the axis, and varies in opposite directions when measured at 0.6 r and 0.8 r, (in the cases of the lean and maximum-speed mixtures when using the three larger burners) indicates that the angle is independent of the size of the burner only within a limited range of variation of this factor, and that the value of the factor which yields a constant value of the angle lies much closer to 0.7 than to either 0.6 or 0.8.

These and other facts lead to the conclusion that, even with ports larger than 4 mm and with mixtures in nearly theoretical proportions, there is a very limited portion of the flame surface which has been affected little or not at all (in slope) by the factors which cause the distortion at the base and at the tip.

Within these limitations it seems probable that the expression $S_T = S_M \sin \alpha$ is capable of yielding numerical results which are independent of the diameter of the port.

An attempt has been made to derive the shape of the flame surface by the application consecutively of a series of facts and of assumptions based on facts. The derivation leads to the conclusion that a local value of the flame velocity at the tip, which is several times the average as determined, may exist as the result of changes in the physical or chemical condition of the mixture. Hence, the tip of the cone is rounded off. It is demonstrated, by an application of Huyghens' principle, that the flame front advances in a direction normal to its surface.

Since the temperature of the mixture is maintained inside the cone of flame by the mixture being continuously replaced at a rate greater than that at which the flame can advance, it seems probable that most of the temperature rise and most of the lateral motion produced by expansion may take place within a thin gradient layer underlying the entire flame surface, and that the thickness of the layer may be inferred from the distance of approach of the flame to the port. It is not clear how the port can exert any cooling effect upon the flame surface that would not also be exerted by the mixture itself at some distance above the port rim. Consequently, it is doubtful if the cooling effect of the port can play as important a part in the distortion of the flame surface at the base as has been attributed to it. This distortion may be more reasonably accounted for by the effect of heat from the flame upon the direction and magnitude of the motion of the gas mixture at the rim of the port.

The rounding off of the flame surface well below the tip is probably not the result of a progressive increase in flame velocity caused by an increase in the temperature of the mixture, but is more likely caused by a redistribution of velocities in the stream of mixture after leaving the burner tube.

Finally, it is concluded that while the range of operations within which the burner method is capable of giving reliable results is restricted considerably by the effect of several experimental variables on the shape of the flame surface, yet it appears to be as simple and useful as any of the methods available at present. However, a knowledge of its limitations is essential if erroneous conclusions from results obtained with it are to be avoided.

The authors desire to make acknowledgment to Messrs. John H. Eiseman, Nelson L. Miller, and Cecil J. Merritt for able assistance in conducting the experimental work involved in collecting the data presented in this paper.

VIII. REFERENCES

[1] R. Bunsen, Pogg. Ann. **131,** 161 (1866).
[2] M. Gouy, Ann. chim. Phys. [5] **18,** 27 (1879).
[3] W. Michelson, *Flame velocity of gas mixtures.* Ann. Physik [3] **37,** 1–24 (1889).
[4] L. Ubbelohde and E. Koelliker, *Information about the inner cone of the bunsen flame.* J. Gasbeleucht. **59,** 49–57 (1916).
[5] F. W. Stevens, Nat. Advisory Comm. Aeronaut. Rep. 305, (1929).
[6] F. W. Stevens, *A Constant Pressure Bomb.* Nat. Advisory Comm. Aeronaut. Rep. 186 ,(1923); J. Am. Chem. Soc. **48,** 1896 (1926).
[7] L. Ubbelohde and M. Hofsäss, *The flame velocity in the inner cone of the bunsen flame.* J. Gasbeleucht. **56,** 1253–62 (1913).
[8] H. Mache, Die Physik der Verbrennungserscheinungen (Leipzig, 1918).
[9] W. R. Chapman and R. V. Wheeler, *The Movement of the medium in which the flame travels.* J. Chem. Soc. 38–46 (**1927**).
[10] J. Corsiglia, *New method for determining ignition velocity of air and gas mixtures.* Am. Gas Assn. Mo. **13,** 437–42 (1931).
[11] L. Ubbelohde and M. Hofsäss, *The flame velocity in the inner cone of the bunsen flame.* J. Gasbeleucht, **56,** 1225–32 (1913).
[12] K. Bunte and W. Litterscheidt, *Ignition velocity of gas mixtures.* Gas. u. Wasserfach **73,** 837–42 (1930).
[13] E. F. Fiock and C. H. Roeder, Nat. Advisory Comm. Aeronaut. Tech. Rep. 532, (1935).
[14] B. Lewis and G. von Elbe. *On the theory of flame propagation.* J. Chem. Phys. **2,** 537–46 (1934).

WASHINGTON, April 21, 1936.

U. S. DEPARTMENT OF COMMERCE NATIONAL BUREAU OF STANDARDS

RESEARCH PAPER RP901

Part of Journal of Research of the National Bureau of Standards, Volume 17, July 1936

INTENSITY DISTRIBUTION IN THE LINE EMISSION SPECTRUM OF CESIUM

By Fred L. Mohler

ABSTRACT

The intensity in a series of lines is $J_n = h\nu N_n A_n$, where N_n is the number of atoms per cubic centimeter in the nth state, and A_n is the rate of radiation per atom. A_n is proportional to n^{-3} for large values of n, while for a limited range of conditions N_n is known to have a temperature distribution.

Line intensities were measured by direct comparison with spectra of a strip lamp. Plots of log J/ν^4 versus log n give parallel curves for the S, D, and F series, and the form of the curve is nearly independent of current and pressure for pressures above 70 μ. Measurements of the D series corrected for self-absorption give plots of log Jn^3 versus term energy, which are straight lines with slopes consistent with measured values of reversal temperature for the P series. Measurements of intensity of two D series lines over a wide range of conditions show that the intensities are proportional to the continuous spectrum intensity at the higher pressures.

For pressures above 70 μ the excited states have a temperature distribution from $n=4$ to 14. For the D series $A_n = \frac{6.4\times 10^8}{n^3}\frac{\lambda_n}{5635}$. The values of A/ν^3 are about twice the theoretical hydrogen values. The values for the F series are also about twice the hydrogen values, while for the S series they are 16 times the hydrogen values.

There is evidently an equilibrium between the number of ions and the number of excited atoms at high pressure, and in the same range of discharge conditions the temperature distribution of excited states is found.

CONTENTS

	Page
I. Introduction	45
II. Experimental results	47
1. Relative intensities in the S, D, and F series	47
2. Intensity of the D series for a columnar discharge	47
3. Intensity variation with current and pressure	50
III. Discussion	51
1. Population of excited states	51
2. Transition probabilities	53
3. Line spectra and continuous spectra	54

I. INTRODUCTION

This is one of a series of papers[1] on the electrical discharge in cesium vapor. Published papers include data on the intensity variation of the first doublet of the principal series, on the intensity of the continuous recombination spectrum, and on the number of excited atoms in the states 6^2 P to 11^2 P.

[1] F. L. Mohler, *Power input and dissipation in the positive column of a caesium discharge*, BS J. Research **9**, 35 (1932) RP455; *Collisions of the first and second kind in the positive column of a caesium discharge*, BS J. Research **9**, 93 (1932) RP485; *Recombination radiation in the cesium positive column*, BS J. Research **10**, 771 (1933) RP565; *Reversal temperature and population of excited states in the cesium discharge*, J. Research NBS **16**, 227 (1936) RP869.

This is a study of the intensity distribution in the subordinate and fundamental series. There are numerous papers on intensity distribution in line emission spectra but, in general, there are unknown factors involved which preclude a direct comparison of experiment and theory. Spectrophotometric studies[2] of flames and carbon arcs containing alkali salts have, however, given some information on transition probabilities in the alkali spectra.

The number of quanta emitted per cubic centimeter per second in a transition nlj to $n'l'j'$ is

$$J/h\nu = N_{nlj} A^{n'l'j'}_{nlj} \tag{1}$$

where J is the radiation in ergs, N is the number of atoms per cubic centimeter in the initial state, and A_n is the transition probability or rate of radiation per atom. Two extreme cases are of interest. If the pressure and current are so low that every atom radiates before it interacts with other atoms or electrons N is proportional to $1/A_n$ and J is a measure of the rate of production of excited states. In the other extreme, where interactions are frequent in comparison to $1/A_n$, there will be a random distribution of population between the different states N_{nlj}, and the population will cease to depend on A_n. This random distribution is probably established at pressures above a few microns.

For the case of thermal equilibrium at a temperature T,

$$N_{nlj} = N_a \frac{2j+1}{2j_a+1} e^{-E_n/kT}, \tag{2}$$

where N_a is the number of atoms in the normal state, E_n the energy of the excited state, and $2j+1$ and $2j_a+1$ the weights of the two states. In another paper,[3] it is shown that for a limited range of conditions the principal series lines have a nearly constant reversal temperature beyond the third line. If the reversal temperature is constant N_{nlj} of equation 1 can be expressed by equation 2 with T equal to the reversal temperature.

Equation 1 is only applicable where self-absorption is negligible. For this reason it is not feasible to measure J for the principal series and it is necessary to use the subordinate and fundamental series. For these series there are no theoretical values for the transition probabilities. A_n is, in general, a complicated function of the quantum numbers, but for large values of n it becomes proportional to $1/n^3$. In this work the effective quantum number (the square root of the Rydberg denominator) will be used for n. This has the advantage that terms of equal n values have equal energies. Furthermore, it is probable that in a comparison of transition probabilities with hydrogen the effective quantum number and not the total quantum number should be used. For the first terms of the cesium series the numbers are approximately 1.87 for 6S; 2.36 and 2.33 for 6P; 2.54 for 5D and 3.97 for 4F.

[2] Ornstein and Key, Physica 1, 945 (1934); Van der Held and Heierman, Physica 3, 31 (1936).
[3] See footnote 1.

II. EXPERIMENTAL RESULTS

1. RELATIVE INTENSITIES IN THE S, D, AND F SERIES

Before the systematic study of the columnar discharge was started, the author made a series of measurements of intensity of nearly all of the emission lines in the visible region, using a discharge between a hot-wire cathode and a surrounding cylindrical anode. The discharge was viewed parallel to the axis of the cylinder along a line about a centimeter from the cathode. The spectrum was photographed with a 3-prism Steinheil spectrograph. The spectrum of a calibrated strip lamp was superposed on that of the discharge and intensities measured by photographic densitometry between nearly equal densities. The line intensity for equal densities is equal to $J(\lambda)\ \delta\lambda$, where $J(\lambda)$ is given by Wien's law and $\delta\ \lambda$ is the slit width expressed in wavelength units.

At relatively high pressures there was no perceptible change in intensity distribution with change of current and pressure. Three sets of measurements with a current of about 0.5 ampere and pressures of 130, 290, and 500 microns of mercury gave intensities for 32 lines, which remained quite accurately proportional, and two arbitrary constants reduced the three sets of values to equality within experimental uncertainty. The mean values are plotted in figure 1. The logarithmic scale is used for convenience. J/ν^4 is proportional to the matrix element, squared, times the population of the upper state. The abscissa is the log of the effective quantum number. The curves plotted are the red components of the F series, both components of the D series, and the red components of the S series. There is some self-absorption of the stronger lines, and the form of the curves is slightly distorted from this effect.

2. INTENSITY OF THE D SERIES FOR A COLUMNAR DISCHARGE

For a comparison with other experiments on the cesium discharge, intensity measurements have been repeated, using a columnar discharge in a tube 1.8 cm in diameter. The discharge was viewed diametrically across the tube. The intensity measurements were based on a series of exposures to a strip lamp on each plate. Self-absorption was measured by means of a discharge tube with two anodes in parallel arms. The line of sight passed diametrically through the two arms. An exposure with both discharges running was compared with a double exposure to the two discharges separately. Except for a small difference due to reciprocity failure of the photographic plate, the higher series lines are equally dense in the two cases, while the strongest lines are weaker on the exposure with both discharges running. The correction to be applied to a single discharge tube is taken to be half the measured difference between two tubes running simultaneously and separately. Table 1 gives corrections for a few cases. The values for 5635 A are based on another experiment sighting across a tube and along the axis of a tube 19 cm long.

73059—36——4

TABLE 1.—*Correction to be added to log J for self-absorption*

	150 μ, 2 amp	150 μ, 0.5 amp	33 μ, 2 amp
$6P_{1/2}$-7D 6724 A	0.105	0.071	0.08
$6P_{1/2}$-9D 5664 A	.040	.018	.018
$6P_{1/2}$-10D 5635 A	.013	.006	.006

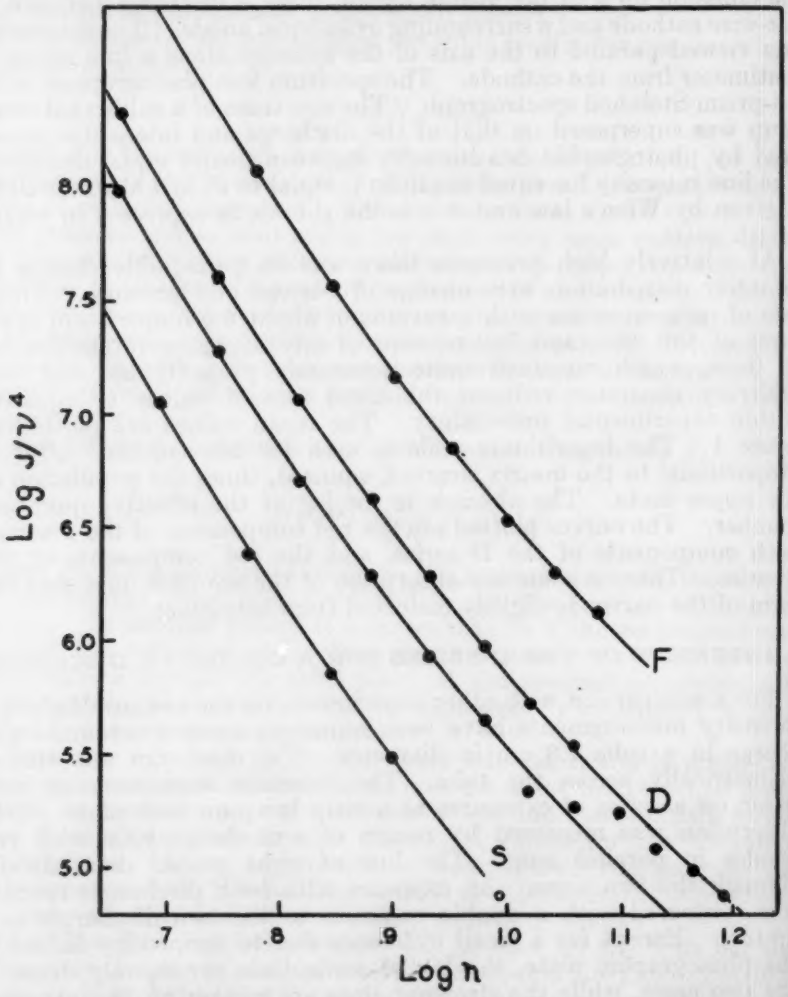

FIGURE 1.—*Intensity distribution in the* S, D, *and* F *series for a high-pressure discharge.*

The red components of the F and S series, and both components of the D series, are plotted. J/ν^4 is in arbitrary units, and n is effective quantum number.

There is an appreciable background of continuous spectrum near the limit, and correction has been applied to the last three lines for this.

Most of the measurements have been limited to seven lines of the diffuse series. Table 2 lists the lines and the values of log J and corrections for a typical series of measurements. The first two lines

are violet components of the series, and 0.30 has been added to log J to give the value of the red component.

TABLE 2.—*Measurements and computations for a 1-ampere discharge at a pressure of 150 μ*

Transition	Wave length	n	Measured log J	Corrections	Log J $6P_{3/2}-nD$	Log n^3J	[1] E_n Electron volt
	A						
$6P_{1/2}$-7D	6724	4.52	4.62	0.30 +.09	5.01	6.98	0.668
$6P_{1/2}$-9D	5664	6.52	3.44	.30 +.03	3.77	6.22	.318
$6P_{1/2}$-10D	5635	7.52	3.40	+.01	3.41	6.04	.239
$6P_{3/2}$-11D	5503	8.52	3.15		3.15	5.95	.186
$6P_{3/2}$-13D	5351	10.52	2.76	−.01	2.75	5.81	.122
$6P_{3/2}$-15D	5267	12.52	2.47	−.02	2.45	5.74	.087
$6P_{3/2}$-16D	5240	13.52	2.39	−.06	2.33	5.73	.075

[1] E_n is the negative energy of the initial state measured from the ionization potential.

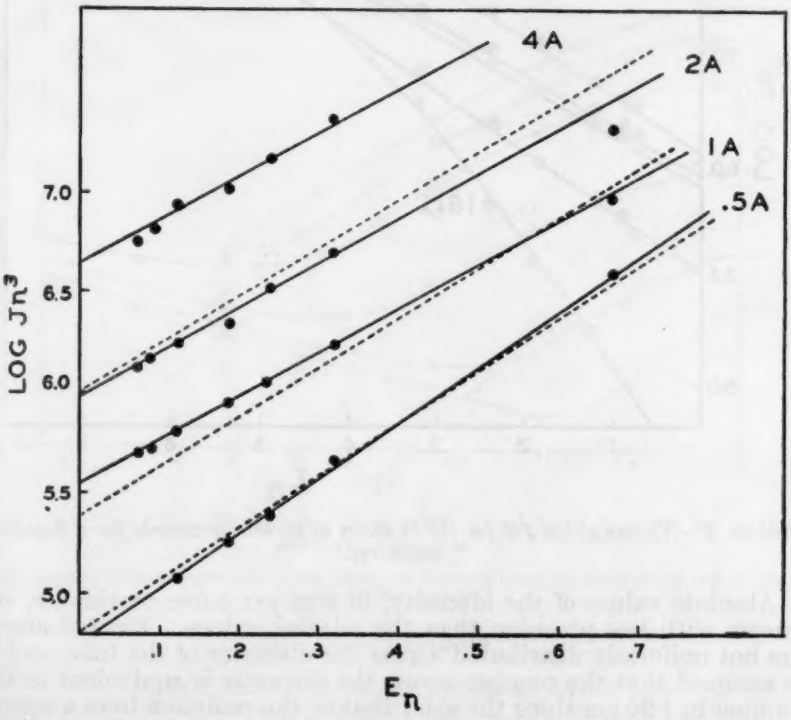

FIGURE 2.—*Values of log Jn^3 for the* D *series for various currents at a pressure of 150 μ.*

E_n is the negative energy of the upper state in electron volts. Broken lines are computed from the reversal temperatures of the P series.

It follows from considerations given in the introduction that in each series Jn^3 is proportional to the population of the states, and, if the distribution of excited states approximates a thermal distribution, a natural choice of coordinates is log Jn^3 versus the energy of the state. Figure 2 shows the results for four different currents at a pressure of

150 microns of mercury. Figure 3 shows results at a number of pressures for a 2-ampere discharge. In Figure 2 there are included, as broken lines, the values log N_n computed from the observed reversal temperatures of the higher principal series lines.[4] A single arbitrary constant is added to fit the three broken lines to the scale of log Jn^3.

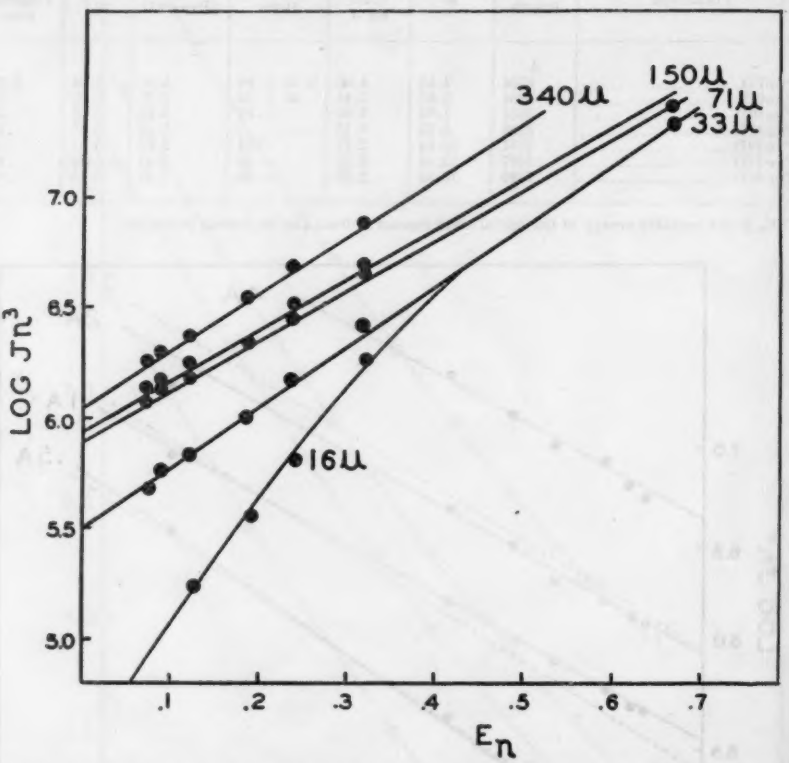

FIGURE 3.—*Values of log Jn^3 for the* D *series at various pressures for a 2-ampere discharge.*

Absolute values of the intensity, in ergs per cubic centimeter, are known with less precision than the relative values. Excited atoms are not uniformly distributed across the diameter of the tube, and it is assumed that the number across the diameter is equivalent to the number in 1.26 cm along the axis; that is, the radiation from a square centimeter comes from 1.26 cm.[3] The plotted and tabulated values are on an arbitrary scale and 4.26 must be subtracted to obtain values of log J in terms of ergs per cubic centimeter per second.

3. INTENSITY VARIATION WITH CURRENT AND PRESSURE

Measurements of the intensity of two superposed diffuse series lines were made over a very wide range of current and pressure. A columnar discharge through a tube about 20 cm long was viewed end on by a low-dispersion spectroscope and intensity measured by

[4] See footnote 1.

visual matching of the image of a strip lamp superposed on the image of the discharge. The settings were made on the unresolved lines $6P_{1/2}$-10D at 5466 A and $6P_{3/2}$-11D at 5503 A. The very low dispersion permitted measurements at low intensity. Figure 4 gives results [5] plotted in terms of log J, in arbitrary units, versus the log of the pressure, in microns, for currents ranging from 4 to 0.3 ampere. At higher pressures the intensity of the continuous spectrum beyond the 6P limit is proportional to the line intensity. Broken lines show values of log J for the continuous spectrum at lower pressures. A constant has been added to log J for the continuous spectrum to make it coincide with the line-intensity values. Other lines of the diffuse series change in the same general way with pressure. For lines of higher quantum number the intensity begins to rise with pressure at a lower pressure. The fundamental series is very faint at low pressure.

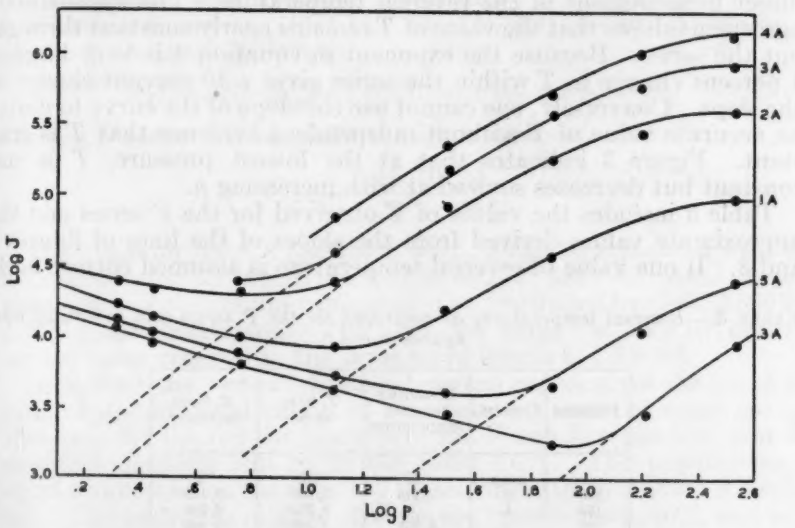

FIGURE 4.—*Log J for diffuse series lines 5466* A *and 5503* A *versus log of the pressure in microns.*

Broken lines give the relative intensity of the continuous spectrum below the range where it is proportional to the line spectrum.

III. DISCUSSION

1. POPULATION OF EXCITED STATES

The purpose of this study was to obtain information concerning both transition probabilities and the population of excited states, but the reasoning is complicated by the limitations of experimental and theoretical data. An inspection of theoretical hydrogen values [6] of transition probabilities, matrix elements squared, etc., indicates that $A_n h\nu n^3$ remains constant even for small values of n, and it is assumed that it is constant for the diffuse series of cesium from 6P-7D

[5] F. L. Mohler, BS J. Research 10, 776 (1931) RP565, gives the same data plotted as a function of the electron concentration.
[6] Bethe, Handbuchder Physik 24, 442.

to the limit. From equations 1 and 2 and this relation, it follows that

$$Jn^3=k'N_a\frac{g_n}{g_a}e^{-E_n/kT}, \tag{3}$$

where k' is the constant value of $Ahvn^3$, and g's are the weights of the states. For the intensity of both components of the diffuse doublets,

$$\log Jn^3=\log 5k'+\log N_a-5.04\times10^3\ E_n/T, \tag{4}$$

where E_n is the energy of the nth state in electron volts. T is the reversal temperature of the nth line, and, if it is constant, the plot of log Jn^3 versus E will give a straight line with a slope proportional to $1/T$. Figure 2 shows a satisfactory agreement between the straight lines derived from intensity measurements and the lines based on direct measurement of the reversal temperature. The approximate agreement shows that the value of T remains nearly constant throughout the series. Because the exponent in equation 3 is very large, a 1 percent change in T within the series gives a 10 percent change in the slope. Conversely, one cannot use the slope of the curve to derive an accurate value of T without independent evidence that T is constant. Figure 3 indicates that at the lowest pressure, T is not constant but decreases somewhat with increasing n.

Table 3 includes the values of T observed for the P series and the approximate values derived from the slopes of the lines of figures 2 and 3. If one value of reversal temperature is assumed correct fairly

TABLE 3.—*Reversal temperatures as measured for the* P *series and computed from figures 2 and 3*

Pressure	Current	Measured reversal temperature	T, from slope	T, from intensity
μ	amp	°K	°K	°K
340	2	2, 115	1, 980	2, 140
150	4	----------	2, 380	2, 380
150	2	2, 205	2, 300	2, 200
150	1	2, 030	2, 310	2, 080
150	0.5	1, 938	1, 840	1, 938
71	2	2, 270	2, 240	2, 260
33	2	----------	1, 860	2, 290
16	2	----------	----------	2, 210

accurate values of the relative temperatures can be computed from the difference in log Jn^3 at one wave length. From equation 4,

$$5.04\times10^3\ E_n\left(\frac{1}{T_2}-\frac{1}{T_1}\right)=\log\ J_1n^3-\log\ J_2n^3+\log\ N_{a,2}-\log\ N_{a,1},$$

where subscripts 1 and 2 refer to two conditions of current and pressure. Table 3 gives, in the last column, values of T based on the intensity of 5635 A and on T=1,938° K at 0.5 ampere and 150 μ. This is probably the best of the three values of T, while the value derived from the slope is the least accurate. The large discrepancy for the two values given for a 2-ampere discharge, at 33 μ, indicates that T decreases with n at this pressure, and it is obvious from figure 3 that it does this at 16 μ.

The fact that the curves for the S and F series in figure 1 are parallel to the D series, indicates that all the series S, P, D, and F have the same reversal temperature for values of n above 5. For equal values of n the populations are assumed to be in the ratio 1:3:5:7. Numerical values are given by equation 2 with values of T from table 3. N_n approaches a constant value as n becomes large. This limiting value for S terms ranges from 2.2×10^5 at 0.5 ampere to 1.6×10^7 at 4 amperes for 150 μ, and it does not change much with pressure.

2. TRANSITION PROBABILITIES

The absolute value of A_n can be computed from the values of J and N_n. The J value taken as standard for the last column of table 3, viz, the intensity of 5635 A at 0.5 ampere and 150 μ will be used. The numerical value of log J is 1.17, in ergs per cubic centimeter. For comparison with hydrogen the intensity of the complete doublet is convenient and log $J=1.35$. Log N_n for the two D states of weight 5, at 1,938° K, is 6.63.

$$A_n=J/(h\nu.N_n)=1.5\times10^6 \text{ per sec for } n=7.52$$

For the D series from $n=4.52$ to higher numbers,

$$A_n=\frac{6.4\times10^8}{n^3}\frac{\lambda_n}{5635}.$$

The value for 5635 A for which $n=7.52$ can be compared with the hydrogen value for the transition 8_2 to 2_1 at 3889 A. As A_n is proportional to ν^3 the cesium value should be multiplied by $(5635/3889)^3=3.02$ for the comparison. The hydrogen value [7] is 2.1×10^6 and the cesium value reduced to the same wave length is 4.5×10^6.

In figure 1 the vertical distance between curves gives the log of the ratio of J/ν^4 at equal values of n or between terms of equal energy. The ratio for the red components of the F and D series is 5, and the complete doublets will be in the ratio 5.6:1. The populations at equal n values are in the ratio of 7:5, and the ratio of A/ν^3 is $5\times5.6/7=4.0$. The hydrogen ratio of A/ν^3 for the transitions 8_3 to 3_2 and 8_2 to 2_1 is 5.3.

For the D and S series the ratio of J/ν^4 is 10.5, and as the populations are in the ratio 5:1, the values of A/ν^3 are in the ratio 2.1:1. The hydrogen ratio is 16.7:1. While the transition probabilities in the D and F series are of the same magnitude as the theoretical hydrogen values, the cesium value for the S series is much higher.

Van der Held and Heierman [8] obtained values for transition probabilities in potassium from measurements of the intensity of emission by a flame of known temperature containing potassium at a measured concentration. The value for A_n for the D doublet 4966 and 4952, $n=7.75$ is 0.38×10^6 as compared with 1.5×10^6 found in cesium for $n=7.52$. The value for the S doublet 4956 A and 4941 A is 1.01×10^6, while the corresponding value here is 0.71×10^6. The intensity variation in the potassium diffuse series is extremely abnormal for small values of n.

Ornstein and Key [9] have published relative A values for cesium based on measurements of the emission of a carbon arc containing

[7] Handbuchder Physik **24**, p. 444.
[8] Van der Held and Heierman, Physica **3**, 31 (1936).
[9] Ornstein and Key, Physica **1**, 945 (1934).

cesium chloride, and on flame spectra measured by Miss Bleeker.[10] The ratio of the S and D series is about that found here, but the variation of A with n is much faster than $1/n^3$. Miss Bleeker has, however, concluded from her measurements that the population of D and S states did not have a temperature distribution. Certainly the intensity in a series drops more rapidly with increasing n in a flame at 2,700° K than it does in the discharge at an effective temperature of 2,300° K, and the results scarcely disprove the general rule that A varies as $1/n^3$ for large values of n.

3. LINE SPECTRA AND CONTINUOUS SPECTRA

In figure 4 it is seen that the intensity of diffuse series lines remains proportional to the continuous spectrum for higher currents and pressures, and from other data it is known that this is also true for the S and F series. With decreasing pressure the line intensity rises above the continuous spectrum. This indicates that at high pressures there is an equilibrium between the number of ionized states and the excited states which is maintained by recombination and ionization of excited states. At low pressures direct excitation by electron impact becomes predominant in maintaining the excitation. One important factor in this pressure change is known from studies of photoionization by line absorption.[11] Radiation from excited states is quenched by atomic collision and for states of n greater than 4.3 the quenching results in ionization in 15 to 100 percent of the collisions. At 40 μ about 0.9 of the radiation is quenched. This increase of the ionization at the expense of the excited states will, with increasing pressure, bring the number of excited states into equilibrium with the number of ions. It is seen from the experimental results that a temperature distribution of the population of excited states is found in the range where ionized and excited states are in equilibrium and it is evidently not generally true at lower pressures.

It is shown in this work that the transition probabilities in the D and F series have approximately hydrogen values as measured at pressures from 70 to 350 μ and in this range the continuous and line intensities are proportional. Published measurements of continuous intensity combined with measurements of the number of electrons per cubic centimeter [12] have given values for the collision area q for recombination into the 6P state. The results are not consistent with the line-transition probabilities. At pressures below 5 μ, q has a value comparable to the theoretical hydrogen value and consistent with the A values found for the cesium lines at high pressure, but the recombination measurements gave values of q that increased rapidly with pressure to values far in excess of the hydrogen value in the pressure range where line-transition probabilities could be measured. The author now suspects that electron-concentration measurements made by the usual probe methods are systematically too low at high pressure and that q is actually a constant. q is a transition probability and the theoretical difficulties in understanding how it could change with pressure led to this attempt to evaluate line-transition probabilities by a method independent of probe measurements.

WASHINGTON, April 24, 1936.

[10] Bleeker, Z. phys. Chem. **120**, 63 (1926).
[11] Mohler and Boeckner, BS J. Research **5**, 51 (1930) RP 186.
[12] Mohler, *Recombination radiation in the cesium positive column*, BS J. Research **10**, 771 (1933) RP565.

U. S. Department of Commerce National Bureau of Standards

RESEARCH PAPER RP902

Part of Journal of Research of the National Bureau of Standards, Volume 17, July 1936

SOLUBILITY OF CALCIUM 2-METHYLBUTYRATE IN WATER

By David F. Houston

ABSTRACT

This paper presents new data for the solubility of calcium 2-methylbutyrate in water from 0 to 100° C. Earlier information concerning the solubility and hydration of this salt is compared with the present results. A transition from the pentahydrate to the hemihydrate is found to occur at 36.5° C, at which temperature the solubility reaches a maximum value of 29.90 g of anhydrous salt per 100 g of water. The solubility rises to this maximum from 23.05 g of anhydrous salt per 100 g of water at 0° C, and then decreases to a value of 19.80 g of anhydrous salt per 100 g of water at 100° C.

CONTENTS

		Page
I.	Introduction	55
II.	Materials	56
III.	Solubility	56
IV.	Hydration	57
V.	References	58

I. INTRODUCTION

Definite information concerning the solubility and the hydration of calcium 2-methylbutyrate was desired in the course of an investigation at this Bureau of some salts of the fatty acids. A survey of the literature disclosed the fact that the existing information was confusing and apparently in error, and indicated the desirability of a redetermination of these properties.

In 1887 Sedlitzky [1][1] determined the solubilities of the calcium salts of 2-methylbutyric, isovaleric, and isobutyric acids. In the same year, Krasnicki [2] determined the solubilities of the calcium and barium salts of formic, acetic, and propionic acids. The results of both investigators give curves which are, in some cases, concave to the temperature axis of the temperature-concentration diagram. The results of later investigators [3] show solubility curves of fatty-acid salts which are all convex to the temperature axis, and these authors point out that the data of the earlier investigators are often in error. The values obtained by Sedlitzky for the solubility of calcium 2-methylbutyrate[2] in water over the range from 0 to 80° C are the only ones available for this salt. The curve expressing these data is strongly concave to the temperature axis, and thus appears

[1] Figures in brackets here and elsewhere in the text relate to the reference numbers given at the end of this paper.

[2] Unless otherwise indicated, all references to the acid and its salt in this paper are to the *dl*- or inactive form.

to be incorrect. A new determination of the solubility over the range from 0 to 100° C is presented in this paper.

According to Milojković [4], the salt exists in three different forms at different temperatures: a pentahydrate at 0° C, a trihydrate at 23 to 26° C, and a monohydrate at 85 to 90° C. Other authors [5] who have dealt with this salt refer only to the pentahydrate. The results of the present investigation serve to remove the existing confusion concerning the hydration of the salt.

II. MATERIALS

Secondary butyl bromide was prepared [6] from secondary butyl alcohol,[3] and fractionated to give a product boiling at 91.3 ± 0.1° C at 760 mm. From this bromide, 2-methylbutyric acid was formed through the Grignard reaction according to the procedure given in Organic Syntheses [7]. A fraction boiling at 174 to 177° C at 757 mm was collected and treated in aqueous solution with a slight excess of calcium carbonate containing $\angle 0.005$ percent of barium and $\angle 0.001$ percent of heavy metals as lead. The solution was refluxed to complete the reaction and was filtered from residual solids. It was extracted with ether to remove any unreacted acid, and the salt was fractionally crystallized. Samples of each fraction were dried at 105° C, and calcium was determined in the anhydrous material by treating it in aqueous solution with dilute sulfuric acid, evaporating, driving off the excess acid, and igniting the $CaSO_4$ formed.

Ca (theory for anhydrous salt) 16.54 percent.

Ca (found in fractions dried at 105° C) 16.52, 16.24, 16.46, 16.51, 16.48, 16.43, 16.43, 16.43, and 16.48 percent.

III. SOLUBILITY

The apparatus and procedure for determining the solubility of the salt have been described in detail in a previous article [3e]. In brief, the apparatus was such that filtering was done in the body of the solution, and samples were filtered by pressure rather than by suction, to avoid loss of solvent. The solubility at 0° C was determined in a bath of melting ice. At all other temperatures the constant-temperature bath previously described was used. The weight of anhydrous salt in a known weight of saturated solution was determined by evaporation of the solution to a residue of constant weight at 105° C. The results were calculated to the weight of anhydrous salt per 100 g of water. The values obtained by this method are in complete agreement on duplicate samples with those gotten by determining the amount of calcium as calcium sulfate, and calculating from it the quantity of anhydrous salt.

The results of the solubility determinations are shown in figure 1 by the solid curve drawn through the experimental points. Each point is the average of duplicate determinations. For ready comparison, the data of Sedlitzky are represented by a dotted line in the same figure. The solubilities at 10-degree intervals and at the transition point, taken from the curve expressing the present results, are shown below.

[3] Stanco Distributors, New York, N. Y., kindly supplied a quantity of this alcohol. Their assistance is gratefully acknowledged.

Temperature, in °C	0	10	20	30	36.5	40	50	60	70	80	90	100
Grams of anhydrous salt per 100 g of water	23.05	23.60	24.55	27.15	29.90	29.10	26.60	24.45	22.80	21.40	20.35	19.80

Duplicate samples usually checked within 0.05 g of anhydrous salt per 100 g of water, and determinations approaching equilibrium at any one temperature from saturation conditions at higher and lower temperatures located the desired points within 0.1 g of anhydrous salt per 100 g of water. This is considered to be the accuracy herein obtained.

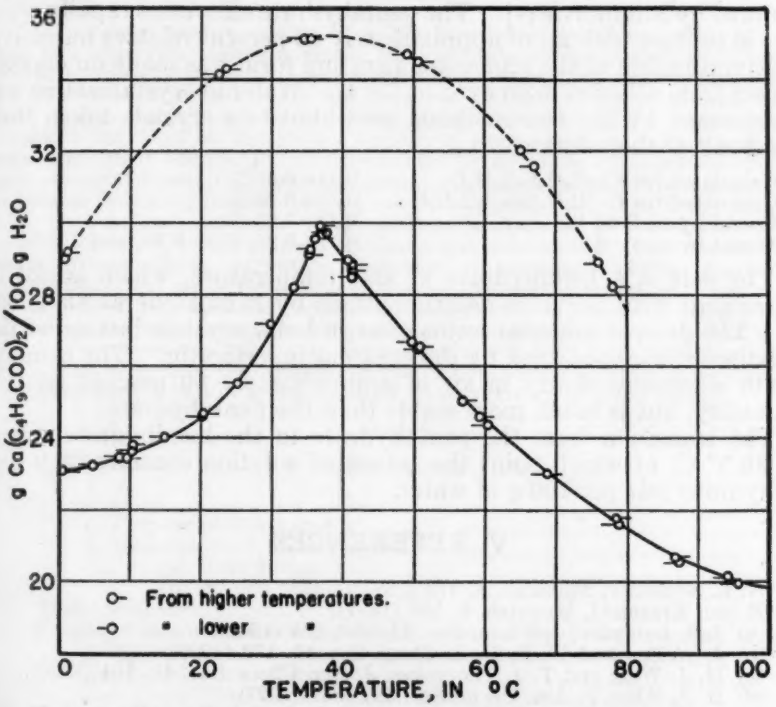

FIGURE 1.—*Solubility of calcium 2-methylbutyrate in water.*

IV. HYDRATION

It is evident from the solubility curve that only two forms of the salt exist in equilibrium with saturated solutions in the temperature range from 0 to 100° C. Moreover, microscopical examination [4] indicates that the same crystal form is obtained from solution at 0, 8, and 25° C. These data show that there can not be two different hydrates in stable equilibrium with saturated solutions at temperatures between 36.5° C and 0° C.

Crystals were grown from solution in a desiccator over sulfuric acid at room temperature (approx. 25° C), and water of crystalliza-

[4] Microscopical examination was made by C. P. Saylor.

tion was determined on crystals taken from the body of the solution. They were dried in one of two ways: (a) by pressing them between filter paper, and (b) by centrifugal filtration, using an apparatus [8] devised during this investigation. The water of crystallization was then determined by heating to constant weight at 105° C. The results are in agreement for both methods of drying.

Calculated for $Ca(C_5H_9O_2)_2.5H_2O$	$H_2O=27.11$ percent
Calculated for $Ca(C_5H_9O_2)_2.4\frac{1}{2}H_2O$	$H_2O=25.08$ percent
Calculated for $Ca(C_5H_9O_2)_2.3H_2O$	$H_2O=18.23$ percent
Found by method (a)	$H_2O=26.77$ percent
Found by method (b)	$H_2O=26.40$ percent

These values agree with those of previous investigators [5] who found the pentahydrate, but offer no confirmation of the trihydrate claimed by Milojković [4]. The pentahydrate effloresces rapidly when left in contact with air of approximately 60 percent relative humidity.

Investigation of the higher-temperature form was made on crystals grown from solution in an oven at 60° C. Water of crystallization was determined by the two methods used above on crystals taken from the body of the solution.

Calculated for $Ca(C_5H_9O_2)_2.H_2O$	$H_2O=6.92\%$.
Calculated for $Ca(C_5H_9O_2)_2.1/2\ H_2O$	$H_2O=3.86\%$.
Found by method (a)	$H_2O=3.63\%$.
Found by method (b)	$H_2O=3.28$, 3.28, 3.80, and 3.59%.

The salt is a hemihydrate at this temperature, which is not in agreement with previous determinations by Milojković at 85 to 90° C. The present material forms clear, tabular crystals instead of the gelatinous mass obtained by the previous investigator. The hemihydrate effloresces slowly in air of approximately 60 percent relative humidity, but is much more stable than the pentahydrate.

The transition from the pentahydrate to the hemihydrate occurs at 36.5° C, at which point the saturated solution contains 29.9 g of anhydrous salt per 100 g of water.

V. REFERENCES

[1] N. L. Sedlitzky, Monatsh. **8,** 573 (1887).
[2] E. von Krasnicki, Monatsh. **8,** 595 (1887).
[3] (a) J. S. Lumsden, J. Chem. Soc. **81,** 350, 363 (1902).
(b) J. Walker and W. Fyffe, J. Chem. Soc. **83,** 173 (1903).
(c) H. J. Wing and T. J. Thompson, J. Am. Chem. Soc. **48,** 104 (1926).
(d) H. J. Wing, J. Am. Chem. Soc. **49,** 2859 (1927).
(e) F. W. Ashton, D. F. Houston and C. P. Saylor, BS J. Research **11,** 233 (1933) RP587.
[4] D. Milojković, Monatsh. **14,** 702 (1893).
[5] (a) A. Pagenstecher, Liebig's Ann. **195,** 119 (1879).
(b) M. Conrad and C. A. Bischoff, Liebig's Ann. **204,** 152 (1880).
(c) E. Schmidt, Liebig's Ann. **208,** 258 (1881).
(d) N. L. Sedlitzky, reference [1] of this paper.
(e) H. Taverne, Rec. trav. chim. **13,** 197 (1894). (Salt of *d*-acid.)
(f) O. Schutz and W. Marckwald, Ber. deut. chem. Ges. **29,** 52 (1896). (Salt of *l*-acid.)
[6] D. F. Houston, J. Am. Chem. Soc. **55,** 4131 (1933).
[7] Organic Syntheses **5,** 75–77 (J. Wiley & Sons, New York, N. Y., 1925.)
[8] D. F. Houston and C. P. Saylor, Ind. Eng. Chem., Anal. Ed. **8,** (July 15, 1936).

WASHINGTON, April 27, 1936.

U. S. Department of Commerce National Bureau of Standards

RESEARCH PAPER RP903

Part of Journal of Research of the National Bureau of Standards, Volume 16, July 1936

DETERMINATION OF THE BRINELL NUMBER OF METALS

By Serge N. Petrenko*, Walter Ramberg, and Bruce Wilson

ABSTRACT

The procedure used in making Brinell tests must be closely controlled in order that two observers testing a given metal at different locations should obtain Brinell numbers that are in close accord. Small variations in testing procedure will be inevitable so that it becomes important to know the effect of these variations on the magnitude of the Brinell number obtained. The present paper considers the effect on the Brinell number of such variations with the help of data available in the literature supplemented by new tests wherever the existing data seemed deficient. Attention is given to the effect on the Brinell number of variations in testing procedure, i. e., rate of applying load, time under nominal load, error in load, and error in measuring the diameter of indentation. The effect of variables residing in the specimen is discussed next under the separate heads of nonuniform properties, curvature of surface, thickness, spacing of indentations, and angle between load line and normal to specimen. Variations in the type of ball used were considered last, particular attention being paid to differences in elastic deformation and in permanent compression of the ball under load. The paper concludes with recommendations for a test procedure which would lead to greater concordance in the Brinell numbers obtained by different observers using a ball of given diameter on a specimen of given metal.

CONTENTS

	Page
I. Introduction	60
1. Purpose of this paper	60
2. Description of Brinell test	60
(a) Test fixture	60
(b) Brinell formula	61
II. Test specimens	61
III. Causes of discrepancies in the determination of the Brinell number	63
1. Apparatus and procedure	63
(a) Rate of applying load	63
(b) Time under nominal load	65
(c) Error in load	67
(d) Error in measuring the diameter of indentation	68
2. Specimen	71
(a) Nonuniform properties	71
(b) Curvature of surface	72
(c) Thickness	73
(d) Spacing of indentations	75
(1) From edge	75
(2) From adjacent indentations	77
(e) Angle between load line and normal to specimen	77
3. Indenting ball	79
(a) Error in diameter	79
(b) Nonspherical shape	80
(c) Deformation of ball under load	81
(1) Elastic deformation	83
(2) Permanent deformation	87

*Deceased.

Page
IV. Recommendations for Brinell testing 90
1. Apparatus and procedure 91
2. Specimen 91
3. Indenting ball 91
V. Appendix 92
1. Error in the Brinell number due to curvature of specimen 92
2. Error in the Brinell number due to error in the computed contact area for a given diameter of indentation 94

I. INTRODUCTION

1. PURPOSE OF THIS PAPER

The Brinell test came into common use soon after its introduction by the Swedish engineer, J. A. Brinell,[1] in 1900. An extensive literature dealing with the test has grown up, but it has not yet been possible to arrive at an understanding of the test that will allow one to predict the Brinell number of a given material from its other physical properties. The chief value of the Brinell test, just as that of other indentation tests, lies in its simplicity, in the fact that it measures a combination of properties that has proved to be significant in the choice of metals, and that it can be used to check the uniformity of a given product by making a few indentations in that product and measuring their diameters.

It follows from the lack of a basic understanding of the Brinell test that it can be expected to give concordant results in the hands of different operators at different locations only if the test conditions are closely controlled and if the effect on the Brinell number of small changes in these conditions is understood. It is the purpose of this paper to bring together, and in places to supplement, present knowledge in regard to the effect on the Brinell number of small variations in the several variables entering into its determination. It is hoped that this will assist in further developing a standard procedure for Brinell testing. A short description of the Brinell test will aid in understanding the nature of these variables.

2. DESCRIPTION OF BRINELL TEST

(a) TEST FIXTURE

The apparatus necessary for a Brinell test consists of a machine for making an indentation with a sphere under a known load, and means for measuring the diameter of that indentation.

The machine that was used in making the tests at the National Bureau of Standards described in this paper is shown in figure 1. It consists of a heavy cast-iron frame A, an adjustable anvil B, and a hydraulic press C. The specimen is placed on the anvil B and is brought into contact with a 10-mm ball attached to plunger D, which, in turn, is connected to the ram of the hydraulic press. Hand pump E is used to force oil into the hydraulic press. The resulting compressive force set up between the ball and the specimen may be read off approximately on pressure gage F. With continued pumping the pressure will increase until it is just sufficient to lift the crossbar G and the dead weights H, which are connected to the pressure chamber by a ball piston without packing. The pressure in the cylinder and, therefore, the force exerted by the ball will remain practically con-

[1] Communications Congrès International des Méthodes d'Essai des Matériaux de Construction, Paris, 2, 83–94. (1900.)

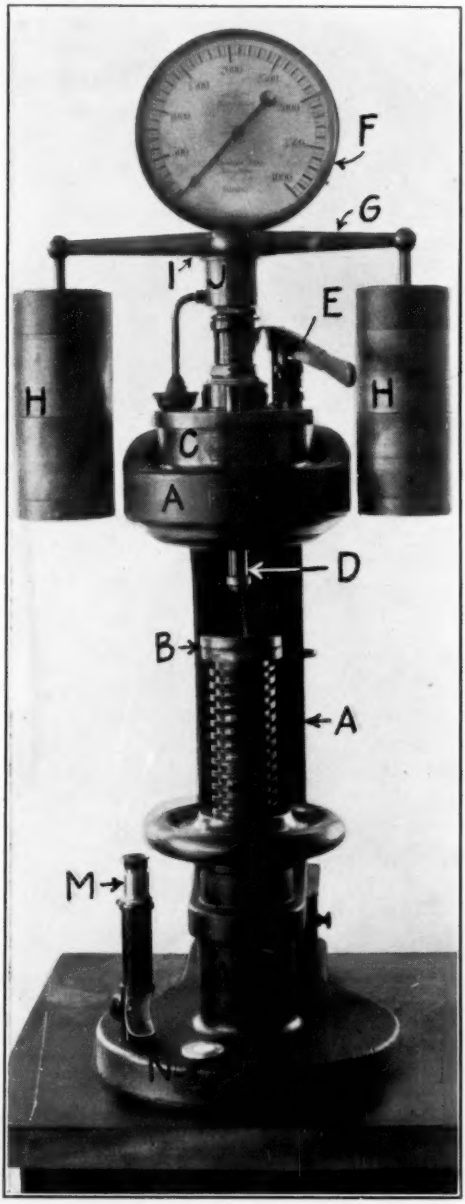

FIGURE 1.—*Machine for making Brinell test and microscope for measuring diameter of indentation.*

stant as long as the piston remains raised to a position of floating equilibrium.

This machine was chosen because investigation showed that the motion of the indenting tool had no appreciable lateral play and differences caused by frictional forces in the ball piston were too small to be observed in calibrating with a proving ring. Previous tests with an improvised dead-weight Brinell machine had shown that errors as great as 5 or 10 percent could be produced by very small rocking of the ball under load.

A load of 3,000 kg is commonly used for metals having a Brinell number greater than 100 and one of 500 kg for metals having a Brinell number less than 100.

Figure 1 also shows the Brinell microscope M, that was used in most of the tests at the National Bureau of Standards to measure the diameters of the Brinell indentations. This microscope has a fixed 7-mm scale, which may be read directly to 0.1 mm and to 0.01 mm, by estimation.

(b) BRINELL FORMULA

The Brinell number was defined by Brinell as the average axial stress over the surface A of the indentation produced by a steel ball, assuming that surface to be spherical, as it would be for an infinitely rigid spherical ball. This leads to the formula

$$H=\frac{P}{A}=\frac{2P}{\pi d^2}\left(1+\sqrt{1-\left(\frac{d}{D}\right)^2}\right), \tag{1}$$

where

P=load (kg),
D=ball diameter (mm), and
d=indentation diameter (mm).

Both P and D must be specified in giving the Brinell number, since it varies somewhat with each of these. Since the work of Brinell, suitable balls of other materials than steel have become available. As the indentation diameter, on the same metal, may differ for balls of different material (see p. 83) it is now necessary to specify also the material of the ball. Tables for H with P=3,000 kg, D=10 mm and with P=500 kg, D=10 mm have been computed from this formula, which give the Brinell number corresponding to the observed diameter d of the indentation.[2]

II. TEST SPECIMENS

The materials used in this investigation are listed and described in table 1. They are tabulated according to lot numbers, ranging from 10 to 90. Not all lots available in the laboratory were used for this investigation and only those used are listed.

[2] Misc. Pub. BS 62 (1924).

TABLE 1.—*Materials used in investigation*

Lot	Material	Approximate chemical composition (in percent)														Condition
		Al	Cu	Si	Fe	Mn	Mg	Sn	Pb	Zn	Ni	C	Cr	V	W	
10	Aluminum alloy SAE 30	90.80	7.95	0.58	0.59	0.08										Cast.
11	Aluminum alloy 2S	99.01	0.19	.35	.44	.01										Rolled.
12	Duralumin	94.36	3.71	.35	.49	.60	0.49									Heat treated.
13	Magnesium						(a)									Extruded at 300° C.
14	Magnesium alloy	4.00				.30	95.70									Cast at 680° C.
15	Do	4.00				.30	95.70									Heat treated at 450° C, quenched in water.
16	Do	4.00				.30	95.70									Rolled at 450° C.
17	Do	4.00				.30	95.70									Extruded at 290° C.
20	Phosphor bronze		89.35		.04	.05		10.23	0.01							Annealed.
21	Do		89.35		.04	.05		10.23	.01							Cold-rolled.
22	Nickel silver		63.70		.17	.21				18.00	17.92					Annealed.
23	Do		63.75		.16	.19			.015	17.77	18.13					Cold-rolled.
24	Brass		65.12		.01				.08	34.79						Annealed.
25	Do		65.12		.01				.08	34.79						Cold-rolled.
27	Nickel steel										3.50					As received from mill.
28	Carbon tool steel											0.90				Annealed.
33	Monel metal		30.00	.10	2.00	1.75					66.00	.20				Hot-rolled.
34	Nickel		.20	.10	.50	.25					99.00	.10				Do.
35	Aluminum bronze	7.92	91.90							.18						Annealed.
36	Do	7.55	92.16							.29						Cold-rolled.
37	Copper		99.97													Annealed.
38	Do		99.97													Cold-rolled.
53	Carbon steel											.09				As received from mill.
54	Do											.28				Do.
55	Do											.68				Do.
56	Nickel-chromium steel										2.14	.30	0.82			Do.
57	Chromium steel											1.01	1.33			Do.
58	Chromium-vanadium steel											.30	1.11	0.25		Do.
59	Tungsten steel											.60	3.50		14.00	Do.
81	Brass															Cold-rolled.
82	Do															Do.
83	Duralumin															Do.
84	Carbon tool steel															Do.
85	Carbon steel															Do.
86	Do															Do.
89	Do															Do.
90	Do															Do.

a Commercially pure.

III. CAUSES OF DISCREPANCIES IN THE DETERMINATION OF THE BRINELL NUMBER

The causes of discrepancies in the determination of the Brinell number may be grouped as variations in the apparatus and procedure, in the specimen, and in the shape and material of the ball.

1. APPARATUS AND PROCEDURE

(a) RATE OF APPLYING LOAD

A rapid rate of applying load will affect the diameter of the Brinell indentation in two ways. It will add an inertia load and a friction load to the nominal load and thus increase the size of the indentation, and it will allow less time for the plastic flow of the material, and, in that way, decrease the size of the indentation.

The magnitude of the first of these two effects will depend both on the method of applying the load and on the type of machine used. It is probably small as long as the load is applied slowly and without jerking and as long as the friction forces opposing the motion of parts in the machine are small compared to the forces effecting that motion.

This last condition is easily satisfied in a machine of the design shown in figure 1. The friction force between the lower piston and cylinder in the hydraulic press C is probably less than 0.5 percent of the impressed load of 3,000 kg, and the force between the ball piston lifting the balancing weights and its sleeve is certainly less than 0.5 percent of the 24–kg weight lifted at maximum load, since the piston is constantly covered with oil.

In the absence of appreciable friction the only forces that may lead to a pressure greater than that required to maintain the weights G and H in floating equilibrium are the inertia forces due to an upward acceleration of the weights G and H. The acceleration of the indenting plunger D is, in general, so small as to be entirely negligible and it is, in addition, in an upward direction, i. e., in a direction leading to a lessening of the load rather than an overload.

The relative error due to an upward acceleration a of G and H will be equal to the ratio of the resulting inertia force to the weight of the floating parts, i. e., equal to the ratio of its upward acceleration a to the downward acceleration g of gravity

$$\frac{\Delta P}{P}=\frac{a}{g}. \tag{2}$$

The acceleration a will be large under two conditions, first, when the weights G and H are accelerated from zero velocity to a finite upward velocity at the instant at which the 3,000-kg load is reached for the first time, and second, when during the maintenance of maximum load the downward drift of the weights is reversed into an upward motion by a stroke of the pump E, in order to maintain the weights in floating equilibrium.

The acceleration mentioned first was greatly reduced in the machine of figure 1 by attaching to the fixed cylinder J a leaf spring I, which starts to raise the balancing weights at half load, i. e., 1,500 kg on the indenting ball or 12 kg on the ball piston, and so imparts an upward motion to G and H, allowing them to come to floating equi-

73059—36——5

librium with a small upward velocity. The travel of this spring is 0.3 cm. The average acceleration for an interval as small as 1 second from half load to full load would, therefore, be

$$a=\frac{2\times 0.3}{1^2}=0.6 \text{ cm/sec}^2.$$

If this acceleration were maintained at the instant of coming to floating equilibrium the overload would be

$$\frac{\Delta P}{P}=\frac{0.6}{981}=0.0006,$$

which is an entirely negligible overload.

In estimating the magnitude of the acceleration due to pumping, the weights were assumed to drift down at a rate of 0.1 cm/sec. This approximates the observed rate of drift for the machine shown in figure 1. If the floating parts were then accelerated by a stroke of the pump E rapidly enough to gain an upward velocity of 2.9 cm/sec within 1 second, the average acceleration would be 3 cm/sec^2, and the corresponding relative error due to dynamic overload would be

$$\frac{\Delta P}{P}=\frac{3}{981}=0.003.$$

This also is a negligibly small overload. It is believed that average accelerations greater than 3 cm/sec^2 do not occur in careful testing with machines of the type shown in figure 1.

The overload due to inertia is therefore negligibly small with a machine of the type shown in figure 1, in all practical cases, as long as the loads are applied smoothly.

The second effect, that is, the decrease in indentation diameter with increasing rate of loading may, according to Guillery,[3] [4] become appreciable for average rates of loading of the order of 1,000 kg/sec, provided the maximum load is maintained a sufficiently short time (less than a minute). In the case of soft cast iron he obtained diameters that were 3 percent smaller for a loading interval of about 15 seconds than those for an interval of 4 minutes. C. Grard [5] states that there is no appreciable effect of the loading interval on the Brinell number provided the maximum load is maintained for more than 2 minutes.

In the absence of data covering different materials it was decided to make a short series of tests to provide further information on the subject. Two sets of five or more indentations each were made in 23 specimens of widely different materials which were selected from the group listed in table 1. The load was applied relatively slowly in making one set of indentations and rapidly in making the other; the relatively slow rate of loading was taken as 30 seconds from no load to full load for the 3,000-kg maximum load and 10 seconds for the 500-kg maximum load; for loads applied rapidly the loading interval was 6 seconds for the 3,000-kg load and 2 seconds for the 500-kg load. The rate of applying load was approximately uniform, i. e., the handle of pump E, figure 1, was operated at approximately a constant number of strokes per minute. The load was held at the maximum for 15

[3] Compt. Rend. 165, 468–471 (1917).
[4] Rev. Met. 18, 101–110 (1921).
[5] Trans. Sixth Int. Cong. Assn. Testing Materials, 1912, report III^3.

seconds in every test; actually it would have been desirable to make this interval zero, but since inaccuracies in timing are unavoidable it was felt that the value should not be too small, and 15 seconds was chosen in the belief that it would lead to comparable results.

The average diameters for each set of indentations are given in table 2. The specimens are identified in this table by lot numbers; their compositions may be found from table 1. It is seen that the average diameters of the indentations for all the steel specimens do not differ by as much as 0.01 mm; they agree within 0.02 mm for all remaining specimens, except those of nickel, copper, and brass. An examination of the individual readings for these metals showed that the individual readings differed more than the difference between the averages in all cases. The observed differences are in 9 cases positive, in 12 cases negative, and in 2 cases too small to detect. For all the specimens the effect of rate of loading up to 500 kg/sec appears to be smaller than the accidental variations in indentation diameter due to lack of homogeneity and due to other causes.

TABLE 2.—*Tests to determine the possible effect of the rate of application of load upon diameter of indentation*

Lot	Material	Load	Diameter of indentation [1]		Difference
			Load applied slowly	Load applied rapidly	
		kg	mm	mm	mm
38	Hard copper	3,000	6.794	6.744	−0.050
35	Soft aluminum bronze	3,000	6.426	6.410	−.016
20	Soft phosphor bronze	3,000	6.034	6.032	−.002
53	Low-carbon steel	3,000	5.932	5.935	+.003
22	Soft nickel silver	3,000	5.861	5.884	+.023
12	Duralumin	3,000	5.434	5.450	+.016
25	Hard brass	3,000	5.330	5.310	−.020
54	Medium carbon steel	3,000	5.331	5.332	+.001
86	Cold-rolled carbon steel	3,000	4.999	4.997	−.002
33	Monel metal	3,000	4.900	4.904	+.004
23	Hard nickel silver	3,000	4.618	4.608	−.010
11	Aluminum alloy 28	500	4.594	4.604	+.010
28	Carbon tool steel	3,000	4.546	4.543	−.003
21	Hard phosphor bronze	3,000	4.156	4.154	−.002
55	High-carbon steel	3,000	4.002	4.009	+.007
59	Tungsten steel	3,000	3.973	3.968	−.005
37	Soft copper	500	3.802	3.776	−.026
56	Nickel-chromium steel	3,000	3.754	3.756	+.002
58	Chromium-vanadium steel	3,000	3.725	3.722	−.003
24	Soft brass	500	3.942	3.520	+.028
57	Chromium steel	3,000	3.298	3.296	−.002
27	Nickel steel	3,000	3.104	3.104	.000
84	Carbon tool steel	3,000	3.103	3.103	.000

[1] Each value is the average of at least 5 determinations.

(b) TIME UNDER NOMINAL LOAD

The effect on the diameter of the Brinell indentation of the time under maximum load has been investigated by W. N. Thomas [6], W. Deutsch [7], M. Guillery [8], and P. Lieber.[9] Each one of these

[6] J. Iron and Steel Inst. **93**, 255–269 (1916).
[7] Forsch. Gebiete Ingenieurw. **M1**, 7–23 (1919).
[8] See footnotes 3 and 4.
[9] Z. Metallkunde **16**, 128–131 (1934).

investigators found that a certain time interval was required to allow the ball to penetrate to its position of static equilibrium.

In the case of mild steel Thomas found that some 5 to 10 minutes were required to come within 1 percent of the Brinell number for loading intervals as long as 1 hour.

Deutsch recommended a duration under maximum load of not less than 3 minutes in testing soft bearing metals. Guillery concluded that 3 minutes are required to bring the diameters of indentation on mild-steel specimens within 1 percent of the final equilibrium value. Lieber found that an interval of 15 minutes under maximum load is required for some very soft bearing metals to bring the Brinell number within 1 percent of the final value; he found that the Brinell numbers after 3 minutes at maximum load may be as much as 12 percent above the final value.

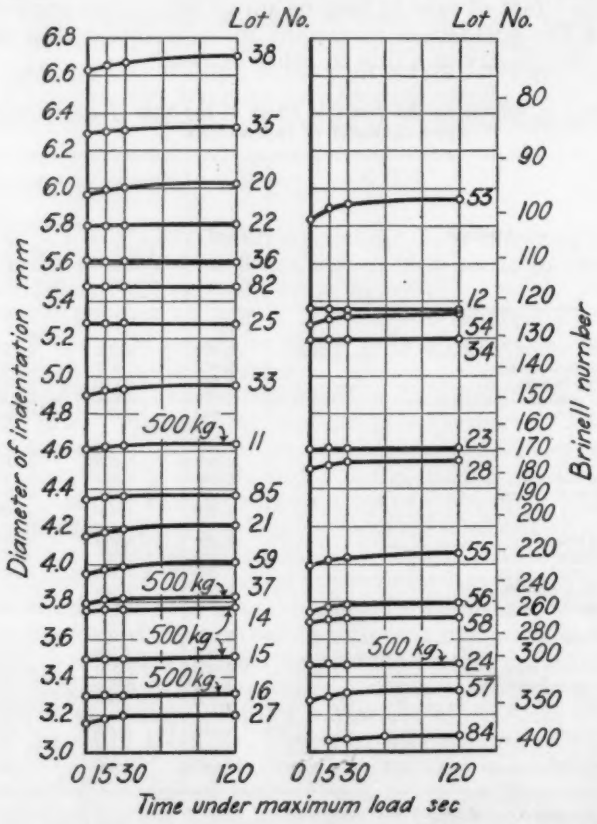

FIGURE 2.—*Variation in indentation diameter with time under maximum load.*

Brinell scale on right margin of figure applies to all curves except those marked 500 kg.

The investigators mentioned above confined their study of the time effect to mild steel, copper, and the soft bearing metals. It seemed worth-while to extend this research to a wider variety of materials selected from those listed in table 1.

The tests were made as follows: Four sets of five indentations each were made in each specimen, the time from no load to full load

being 10 seconds and the time under maximum load being 0, 15, 30, and 120 seconds, respectively, for the successive sets of five indentations each. A maximum load of 3,000 kg was used on all specimens, except those from lots no. 11, 14, 15, 16, 24, and 37, which were tested using a maximum load of 500 kg. The average diameter of indentation for each set is plotted against time under maximum load in figure 2. The Brinell numbers of all specimens, except those tested under 500-kg load, may be read from the vertical scale at the right of the figure. It is seen that the creep for most materials is quite rapid during the first 30 seconds under maximum load; it is much less rapid in the interval from 30 to 120 seconds. The Brinell number in this interval decreased more than 1 percent for only two of the materials tested, i. e., soft copper (specimen 38, 1.34 percent) and carbon steel (specimen 55, 1.30 percent). The decrease in Brinell number was between 0.5 percent and 1 percent for 10 of the 29 specimens tested, and it was below 0.5 percent for the remaining 17.

For most materials, then, the Brinell number varies less than 1 percent for loading intervals between 30 and 120 seconds.

(c) ERROR IN LOAD

The effect on the Brinell number of a relative error $\Delta P/P$ in the applied load is given by the Brinell formula, page 61, if it is assumed that this formula gives a Brinell number P/A independent of P in the region considered. Differentiation gives

$$\frac{\Delta H}{H}=\frac{1}{H}\frac{\partial H}{\partial P}\Delta P=\frac{\Delta P}{P}, \tag{3}$$

that is, the relative error in the Brinell number is equal to the relative error in the applied load. The assumption, on which the correctness of this equation is based, that the Brinell number is independent of the load, is true in first approximation only. The closeness of this approximation may be computed by using the empirical relation between load P and indentation diameter d established by E. Meyer [10] for a large number of metals indented by steel balls:

$$P=ad^n, \tag{4}$$

where a is a constant depending on the material and the ball diameter and n is a constant depending on the material alone. Meyer found values of n ranging from $n=1.91$ to $n=2.4$. The Brinell number may be written in terms of Meyer's law as [11]

$$H=\frac{2}{\pi D}a^{2/n}P^{1-2/n}\left(D+\sqrt{D^2-\left(\frac{P}{a}\right)^{2/n}}\right). \tag{5}$$

The change of the Brinell number with load was computed from this by differentiating with respect to P and substituting in equation 3. The resulting expression involves n and P/a. P/a was replaced by d^n and $\Delta H/H$ was calculated for the most unfavorable pairs of values of n and d. For $n=1.91$ and $d=7$ mm, $\Delta H/H=-0.26\,\Delta P/P$, and

[10] Forsch. Gebiete Ingenieurw. 65 (1909).
[11] H. O'Neill, J. Iron and Steel Inst. 107, I, 343-376 (1923).

for $n=2.4$ and $d=2$ mm, $\Delta H/H=+.16\ \Delta P/P$. It appears from this that $\Delta P/P$ on the right side of equation 3 must be multiplied by 0.74 in the first case and by 1.16 in the second to give a value of $\Delta H/H$ corrected for the variation of the Brinell number with load. This variation adds less than 20 percent to the correction as given by equation 3 in the most unfavorable cases that could be found. Assuming a 20-percent correction to equation 3, the applied load should be correct within 0.33 percent in order to keep the error in the Brinell number from that source within 0.4 percent.

(d) ERROR IN MEASURING THE DIAMETER OF INDENTATION

The area A entering in the expression P/A for the Brinell number is defined as the area of the surface of contact between the ball and the specimen under load. It is assumed in the derivation of the Brinell formula that A can be measured by the diameter of the indentation d left after removing the ball.

Actually there may be considerable uncertainty in the magnitude of this diameter, and hence in the value of the Brinell number P/A obtained. For some materials the edge of the indentation is very poorly defined, even when the surface finish is good. Sometimes there is a ridge around the indentation extending above the original surface of the specimen, and at other times the edge of the area of contact is below the original surface [12] as is illustrated in fig 3. In some cases there is no sharp line of demarcation between the indentation and the surrounding surface; one surface merely rounds off into the other. In all cases there is uncertainty as to the portion of the visible indentation which was actually in contact under load. At present no methods are known which will in all cases eliminate all uncertainty as to the actual contact area. The best that can be done is to insure that different observers will not secure too widely different results on the same indentation.

For some specimens, the indentations may be made more distinct by using balls etched with nitric acid, as suggested by Axel Hultgren.[13]

The borders of the indentation will be still more distinct if a ball of more rigid material than steel is used. Styri [14] found that indentations made with 5-mm Carboloy (tungsten-carbide) balls at 750-kg load have a remarkably clear outline, even on specimens having Brinell numbers as high as 780. This observation was confirmed by tests made at the National Bureau of Standards (p. 88). In these tests 10-mm Carboloy balls were used to indent specimens up to 750 Brinell at 3,000 kg. It must be borne in mind, however, that Carboloy balls will indicate considerably higher Brinell numbers than steel balls on a given specimen because of the difference in elastic properties; this is discussed on page 85.

In general, there will be an error Δd in reading the diameter d of the indentation. The relative error $\Delta H/H$ in the Brinell number due to a relative error $\Delta d/d$ may be computed from the Brinell formula 1 by differentiation

$$\frac{\Delta H}{H}=\frac{1}{H}\frac{\partial H}{\partial d}\Delta d=-\left[1+\frac{1}{\sqrt{1-\left(\frac{d}{D}\right)^2}}\right]\frac{\Delta d}{d} \tag{6}$$

[12] F. E. Ross and R. C. Brumfield, Proc. Am. Soc. Testing Materials **22**, part II, 312-334 (1922).
[13] Axel Hultgren, Mech. Eng. **43**, 445 (1921).
[14] Metals and Alloys **3**, 273-274 (1932).

FIGURE 3.—*Sections of Brinell indentations on two different materials.*

[A, Copper; B, aluminum.]

UNIV. OF MICH.

The minus sign indicates that an increase in indentation diameter corresponds to a decrease in Brinell number.

Figure 4 shows curves for the percentage error 100 $\Delta H/H$ in the Brinell number H plotted against H for values of d ranging from 0.005 to 0.050 mm. The error in the Brinell number is less than 1 percent, as long as the error in diameter does not exceed 0.01 mm.

Errors in reading the diameter of the indentation may be ascribed to two causes, first, to an error in the reading of the instruments used for measuring the diameter, and second, to indefiniteness of the boundary of the indentation itself.

The error in reading a Brinell microscope of common design, such as the one shown in figure 1, should not exceed 0.01 mm over the entire 7-mm scale, if the microscope is in proper adjustment. The adjustment of the microscope may be checked easily by placing it on a calibrated 7-mm scale, such as the scale marked on disk N shown next to the microscope in figure 1, and verifying that the image of this scale and the scale on the reticule coincide within 0.01 mm; this corresponds to 0.1 of a scale division.

No discussion was found in the literature of the magnitude of the error due to indefiniteness of the boundary of the indentation, although this error is probably the greatest single factor contributing to the lack of concordance in Brinell numbers obtained by different observers testing a given material. The following series of tests was made to provide some information on this point.

TABLE 3.—*Average errors in reading Brinell indentation diameters*

Observer→		1	2	3	4	5	Mean value
Diameter ↓	H	Average error [1]					
mm		mm	mm	mm	mm	mm	mm
2.418	644	0.0095	0.0054	0.0134	0.0113	0.0201	0.0120
2.676	524	.0050	.0064	.0156	.0217	.0194	.0136
3.082	392	.0037	.0025	.0135	.0124	.0068	.0078
3.716	267	.0052	.0035	.0045	.0110	.0143	.0077
4.177	209	.0034	.0050	.0088	.0122	.0151	.0089
4.660	166	.0049	.0054	.0069	.0081	.0206	.0092
Mean value		0.0053	0.0047	0.0104	0.0128	0.0160	0.0099

[1] Each value given is the average for 6 indentations.

Six groups of six Brinell indentations each were made on steel specimens whose surfaces had been ground plane and the diameter of each indentation, taken as the average of two mutually perpendicular diameters, measured at an angle of about 45 degrees to the direction of grinding, was obtained by two methods. First the diameter of each indentation was obtained with a traveling microscope which was read by estimation to 0.001 mm. Then the diameter of each indentation was obtained by each of five observers with the regular Brinell microscope (M, fig. 1), which was read by estimation to 0.01 mm. The observers were chosen from the staff of the Bureau's Engineering Mechanics Section. Observers 1 and 2 had had con-

siderable experience in measuring the diameters of Brinell indentations, observer 3 had had only a small amount of experience, while observers 4 and 5 were inexperienced.

The relatively more concordant results obtained with the traveling microscope were considered as correct, and the error for each observer for each indentation was computed by subtracting the diameter obtained with the traveling microscope from the diameter obtained with the regular microscope. These results are plotted in figure 5.

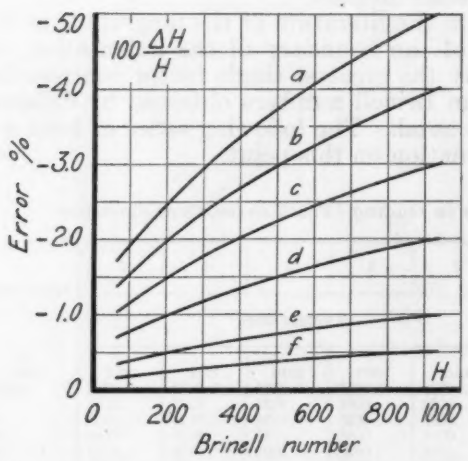

FIGURE 4.—*Error in Brinell number due to error in indentation diameter.*

	Error in indentation diameter (mm)
Curve a	0.05
Curve b	.04
Curve c	.03
Curve d	.02
Curve e	.01
Curve f	.005

The diameters of the six indentations of each group were nearly equal. The averages of the absolute values of the errors for each group were computed for each observer. They are given in table 3. The last line of table 3 lists mean values of the average errors for each observer, and the last column lists mean values for each group of indentations.

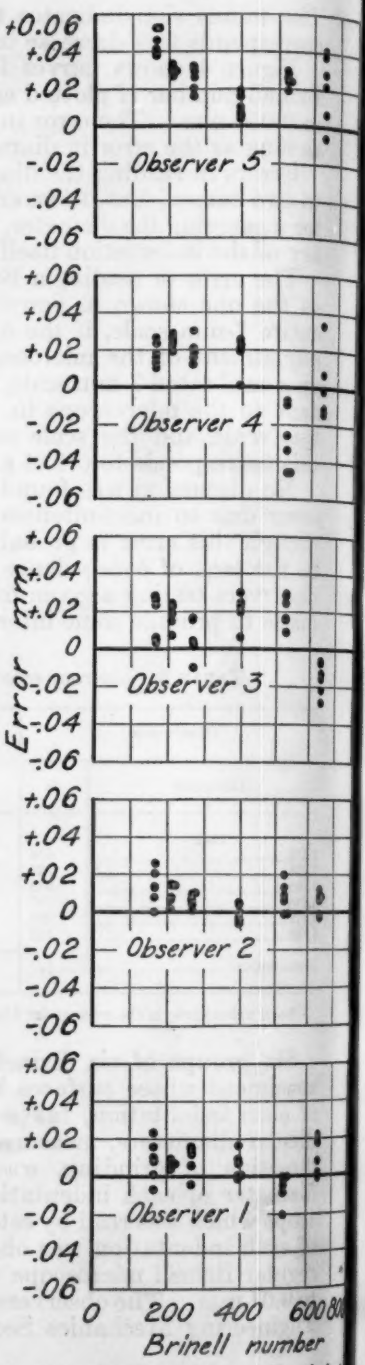

FIGURE 5.—*Errors in reading indentation diameters for five different observers*

[Observers 1 and 2 with considerable experience; observer 3 with a little experience; observers 4 and 5 with no experience.]

From these results the average percentage error in the Brinell number was computed for each observer for each group. These values are plotted in figure 6 as a function of the Brinell number.

The results for each observer shown in figure 5 indicate the presence of systematic as well as accidental errors. The systematic error changes with the Brinell number of the specimen in a different way for each observer. Both the systematic and the accidental errors were smaller for the experienced observers than for the remaining observers. Apparently a certain amount of experience improves an observer's ability to distinguish the boundary of the contact surface.

Figure 6 shows that the average percentage error in the Brinell number for the experienced observers was always less than 1 percent, while that for the inexperienced observers exceeded 2 percent in some cases.

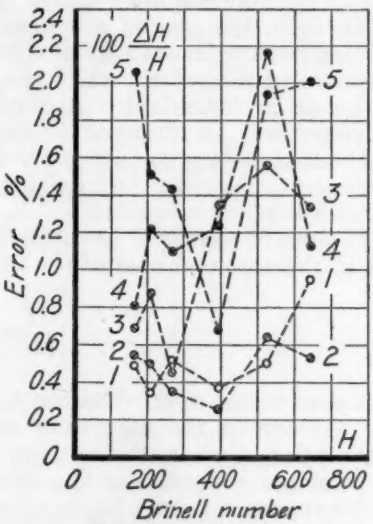

FIGURE 6.—*Average error in Brinell number due to uncertainty in reading indentation diameter.*

[Curves 1–1 and 2–2 represent results obtained by experienced observers; 3–3 by an observer with a little experience; 4–4 and 5–5 by observers with no previous experience.]

2. SPECIMEN

(a) NONUNIFORM PROPERTIES

If the compressive properties of a flat specimen are not uniform, e. g., if they change with the direction of rolling, this will be reflected in a noncircular shape of the indentation left after the Brinell test. Thus, if the material yields more easily under compressive stresses in the direction of rolling than at right angles to that direction, the indentation will be roughly elliptical with a maximum diameter in the direction of rolling and a minimum diameter at right angles to that direction. An average value of the Brinell number for an indentation with a noncircular boundary will be obtained if the diameter of the indentation is taken as the average of diameters in four directions, roughly 45 degrees apart.

It is assumed here that the surface of the specimen is finished by filing, machining, or grinding to such smoothness that the tool marks do not interfere with the measurement of the indentation diameter. For most materials there is no difficulty in finishing the specimen so that the error in the measured diameter caused by tool marks does not exceed 0.01 mm.

If the test used affects only a very small amount of the test material, there may be some question as to the proper interpretation of results because variations in indentation numbers may be due to local differences in the surface layer of the specimen and not to systematic variations in the body of the material. The standard Brinell test is probably comparatively free from uncertainties of this sort because in it a fairly large amount of the test material is affected. Variations in

the Brinell number greater than can be accounted for by the variations in the test procedure and in the indenting ball will actually indicate corresponding variations in those properties of the material in which the user is interested.

(b) CURVATURE OF SURFACE

It is frequently necessary in practice to measure the Brinell number on a curved surface rather than a plane surface. An indentation on a curved surface of a specimen having uniform properties will not have a circular boundary unless the curvature is constant in all directions, as in the case of a sphere. The question arises as to which diameters to measure and how to average them so as to obtain the "equivalent diameter", which may then be substituted in the Brinell tables or in formula 1. A good approximation to the equivalent diameter will be obtained when the diameters measured and the method of averaging are such that the area computed from the equivalent diameter approximates closely the area of the actual indentation.

The relative error in the Brinell number corresponding to an error ΔA in the assumed area of the indentation is then from 1:

$$\frac{\Delta H}{H}=-\frac{\Delta A}{A}. \tag{7}$$

A convenient approximation to the equivalent diameter would be the average of the maximum and the minimum diameters of the indentation, that is, the average of the diameters in the two planes of principal curvature. The corresponding value of ΔA is derived in the appendix 1, page 92, as a function of the principal curvatures of the specimen (equation 17, page 94), and the distance from the center of the indenting ball to the point of intersection of the load line with the original surface of the specimen. The area A of the surface of the sphere embedded in the specimen is given by equation 14 of appendix, page 93. Knowing both A and ΔA, the relative error in the Brinell number can be computed for various values of the Brinell number P/A.

Figure 7 shows the result for the indentation produced by a 10-mm ball under 3,000-kg load on cylindrical specimens of 20 mm and of 50 mm diameter, as well as on specimens having a concave cylindrical curvature of 10 mm radius and 25 mm radius, respectively. For two of the surfaces considered, the maximum radius of curvature of the specimen is twice that of the indenting ball, while for the remaining two it is 5 times the radius of curvature of the ball. For the extremely high ratio of 1:2 the error in Brinell number is less than 3 percent for the concave cylindrical surface and less than 1 percent for the convex cylindrical surface; for the ratio 1:5 the error is less than 0.3 percent for both concave and convex cylindrical surfaces. The cylindrical specimen is a rather severe test of the approximation; the errors involved would be larger only in the case of specimens with anticlastic curvature, i. e., specimens whose principal radii of curvature have opposite signs. Two cases of anticlastic curvature

were computed, one in which the specimen had radii of curvature of +10 mm and −10 mm and the other in which the radii were +25 mm and −25 mm (fig. 8). The error becomes as large as 6.5 percent in the first case, but it is less than 1 percent in the second case.

The error in the Brinell number due to curvature of the specimen may be reduced, in general, to less than 1 percent by using the average of the two principal diameters of the indentation as the equivalent diameter, provided the minimum radius of curvature of the specimen is equal to or greater than 5 times the radius of the indenting ball.

(c) THICKNESS

The material of the specimen is permanently deformed for an appreciable distance below the surface of the indentation. If this deformation extends to the lower surface of the specimen opposite the indentation, one of the following effects may result.

The support given by the hardened-steel anvil may effectively increase the resistance of the material directly under the ball, thereby causing the indentation to be smaller than one which would be produced in a thicker specimen of the same material.

The cohesion of the material directly under the ball may be insufficient to support the load and this portion may yield rapidly with increasing pressure. The diameter of the indentation may, therefore, be larger than one obtained on a thicker specimen.

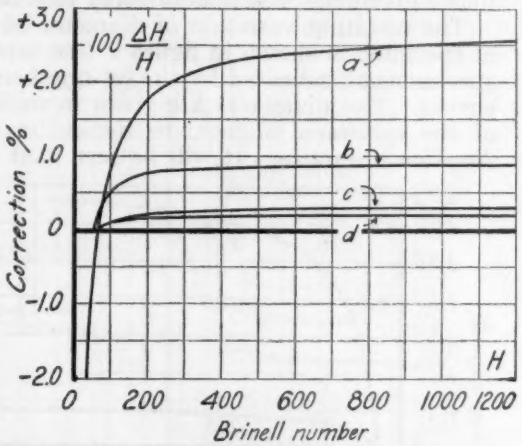

FIGURE 7.—*Correction due to cylindrical curvature to be added to Brinell number.*

[10-mm ball, under 3,000-kg load]

Curve	Cylindrical surface	Radius (mm)
a	Concave	10
b	Convex	10
c	Concave	25
d	Convex	25

The effect of thickness on the Brinell number of steel specimens has been investigated by H. Moore [1]*l* and by W. N. Thomas.[1]*t* Moore found an increase of about 3 percent if the depth of the indentation was one-third the thickness of the specimen. A ratio of 1:7 was considered safe by Moore to eliminate the effect of thickness. Thomas concluded from his tests that the effect of thickness was negligible for a 10-mm ball at 3,000-kg load, provided the specimen was at least 0.38 in. thick.

[1] Trans. Fifth Int. Cong. Assn. Testing Materials 1909, report II$_4$.
[1] J. Iron and Steel Inst. 93, 255-269 (1916).

It seemed desirable to add to these results by carrying out a series of tests on specimens of various materials. The following procedure was adopted in carrying out these tests. One surface of each specimen was machined so that the thickness of the specimen decreased uniformly approximately 0.05 in. for each inch of length. The other surface was polished with emery paper, without previous machining, and indentations were made about 1 inch apart. This spacing gave the desired variation in thickness and eliminated at the same time the effect of any given indentation on an adjacent one. The time under maximum load was in every case 30 seconds.

The resulting variation of diameter of indentation with thickness of specimen is shown in figure 9 (see table 1 for composition of test specimens as indicated by the lot numbers near the right end of each curve). The diameters are given in millimeters while the thickness of the specimen is given in inches, in accordance with the usual American practice. It will be seen that in most cases the diameter decreased with increasing thickness indicating that the weakening in the cohesion of the material usually predominates over the strengthening due to the backing of the steel plate below the specimen. For specimens 14, 35, and 37 the second effect appears to be more important than the first, since the diameters of the indentations were found to increase with increasing thickness.

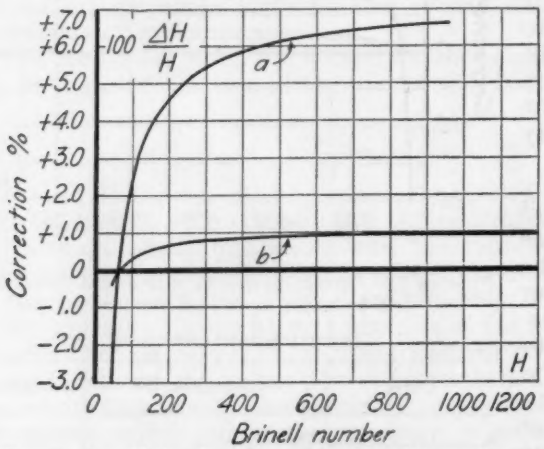

FIGURE 8.—*Corrections due to anticlastic curvature to be added to Brinell number*

[10-mm ball, under 3,000 kg load]

Curve a, anticlastic surface, principal radii 10 mm. Curve b, anticlastic surface, principal radii 25 mm.

The curves faired through the individual points have been used to determine a "critical" thickness, arbitrarily defined as the thickness at which the apparent Brinell number for the indentation differed by 1 percent from that for the thickest portion of the specimen. The corresponding thickness is indicated by a short vertical line on each curve; it varied between the limits of 0.08 in. and 0.32 in. For other metals, as well as for steel, a thickness of specimen of 0.4 in. may, therefore, be considered sufficient, in nearly all cases, to make negligible the effect of thickness on Brinell number. This thickness agrees closely with the thickness of 0.38 in. recommended by Thomas for steel specimens.[17]

It was noted that under each indentation made, where the thickness was less than the "critical" value, a spot of altered surface was visible on the under side of the specimen. As a large variety of engineering materials was used in this investigation, it seems safe to

[17] J. Iron and Steel Inst. **93**, 255–269 (1916).

assume that the absence of a visible spot on the under surface of the specimen indicates that the thickness of the specimen exceeds the critical thickness as defined above.

(d) SPACING OF INDENTATIONS

(1) *From Edge.*—If an indentation is made too near the edge of the specimen it may be both too large and too unsymmetrical.

H. Moore [18] concluded on the basis of tests on specimens of steel and of rolled brass that the center of the indentation should be at least 2½ times the diameter of the indentation distant from the edge to avoid errors from this source.

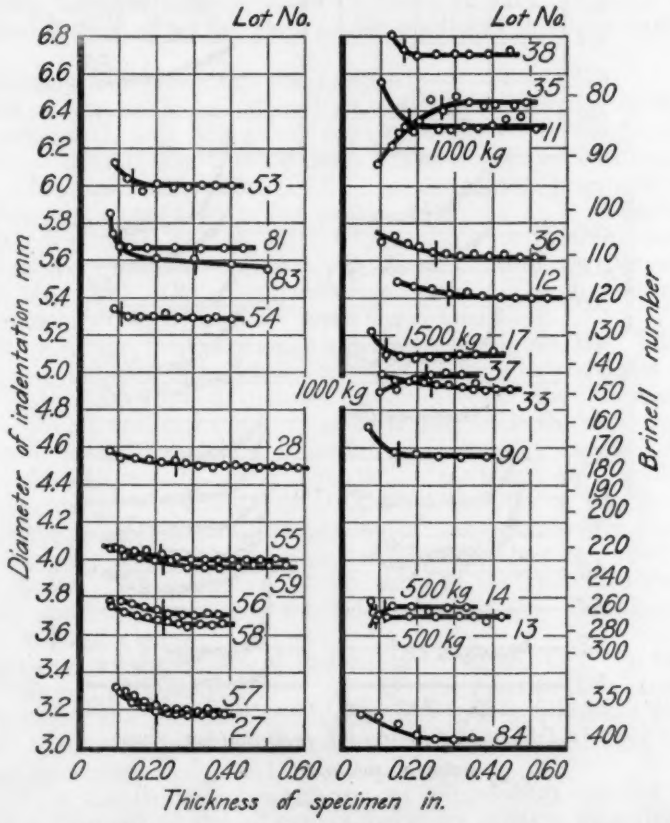

FIGURE 9.—*Variation in indentation diameter with thickness of specimen.*

[Brinell scale on right margin applies to all curves except those marked 500, 1,000, or 1,500 kg.]

It seemed desirable to extend these results to a wider variety of materials. Indentations were made on 23 different specimens selected from the materials listed in table 1. The thickness of each specimen was greater than 0.40 in. so as to make the effect of thickness negligible (see previous section). The time under load was in every case 30 seconds.

[18] See footnote 15.

Figure 10 shows the relation between the diameter of the indentation and the distance from the edge for each of the 23 specimens. As in figure 9 a value was found for the "critical" distance in each case, i. e., the distance at which the apparent Brinell number for the indentation differs by 1 percent from that obtained for the maximum distance. This value is indicated by a short vertical line. The ratio

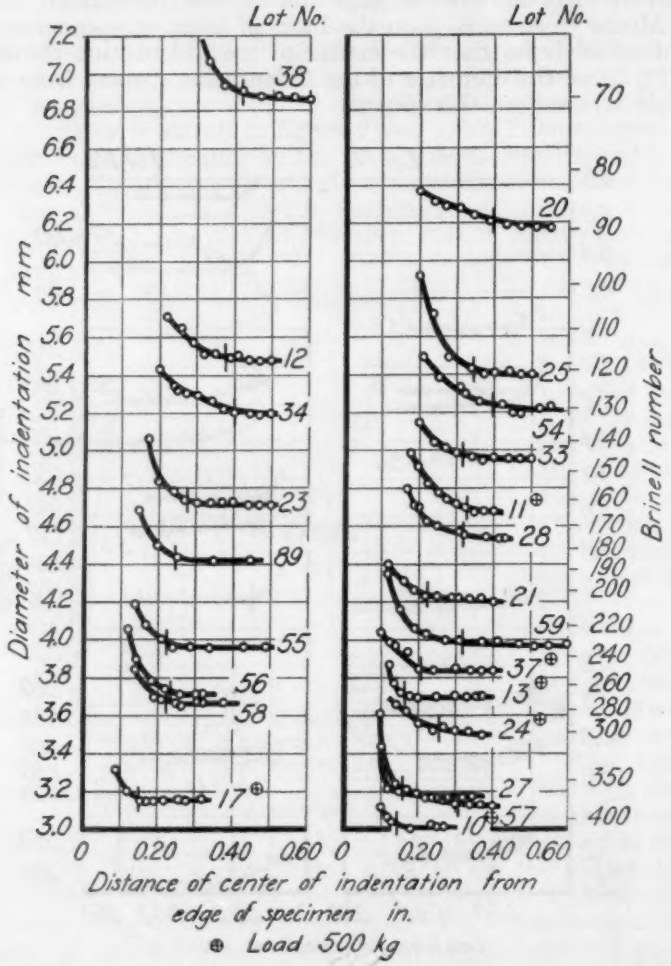

FIGURE 10.—*Variation in indentation diameter with distance of Brinell indentation from edge.*

[Brinell scale on right margin applies to all curves except those marked to indicate 500-kg load instead of 3,000 kg.]

of this critical distance to the diameter of the indentation was found to vary from 1.1 to 2.6.

The error in Brinell number due to edge spacing may be neglected if the distance of the center of the indentation from the edge of the specimen is equal to or greater than three times the diameter of the indentation.

(2) *From Adjacent Indentations.*—If an indentation is made too close to one made previously, at least three possibilities of error are introduced.

Deformation of the material resulting from a second indentation may extend into the one made first, decreasing its diameter along the line connecting their centers.

Lack of sufficient supporting material may make the second indentation too large.

Work-hardening of the material resulting from the first indentation may decrease the size of the second indentation.

The magnitude of the effect on the Brinell number of adjacent indentations was investigated for different specimens selected from the materials listed in table 1. The thickness of each specimen was greater than 0.40 in. and the time under load was in every case 30 seconds.

The following test procedure was adopted:

Six pairs of points A—A′, B—B′, C—C′, . . . were marked on the specimen, each pair being well separated from any neighboring pair and from the edges of the specimen. The points were so located that the distances AA′, BB′, CC′, . . . decreased progressively. Indentations were made with the points A, B, C, . . . as centers. The diameters parallel to AA′, BB′, CC′, . . . were then measured. Indentations were made at points A′, B′, C′, . . . and the diameters parallel to AA′, BB′, CC′, . . . were measured. The diameters of the indentations at A, B, C, . . . were again measured.

The results of the measurements are shown in figure 11. This is a plot of the distance between indentation centers as abscissas and $d_o - \Delta d$ as ordinates, where d_o denotes the diameter of the indentation before the second one was made close to it and Δd is the decrease in this diameter after the second indentation is made. In each case values for the distance between indentation centers were found for which there was no variation greater than 1 percent in the Brinell number for the indentation. The smallest of these values is indicated on the curve by a short vertical line and will hereafter be called the critical distance. For specimen 38 the ratio of the critical distance to the corresponding diameter of the indentation is 1.6. For all other specimens this ratio is less.

A comparison of diameters of indentations A, B, C, . . . made first, with those of indentations A′, B′, C′, . . . made last, showed the effect which the indentations made first had upon those made last. This effect was quite small and no critical distance larger than the largest one shown in figure 11 was found.

The error in the Brinell number due to indentation spacing will not exceed 1 percent if the distances between centers of adjacent indentations are equal to or greater than three times the diameter of the indentation.

(e) ANGLE BETWEEN LOAD LINE AND NORMAL TO SPECIMEN

It is not always practical to have the surface of the specimen at the point at which it is to be indented exactly normal to the load P producing the indentation. Usually there will be a small angle α between load line and normal to the surface; this will reduce the normal load from P to $P\cos\alpha$ and in addition will add a component of load $P\sin\alpha$ acting in a direction tangential to the surface of the

specimen. The reduction in the normal load may lead to an increase in the observed Brinell number, while the addition of the tangential component may elongate the indentation in the direction in which it acts and may lead to an increase in area and consequent decrease in the observed Brinell number. The question arises within what limits α must be kept to make the error in the Brinell number from this cause negligibly small.

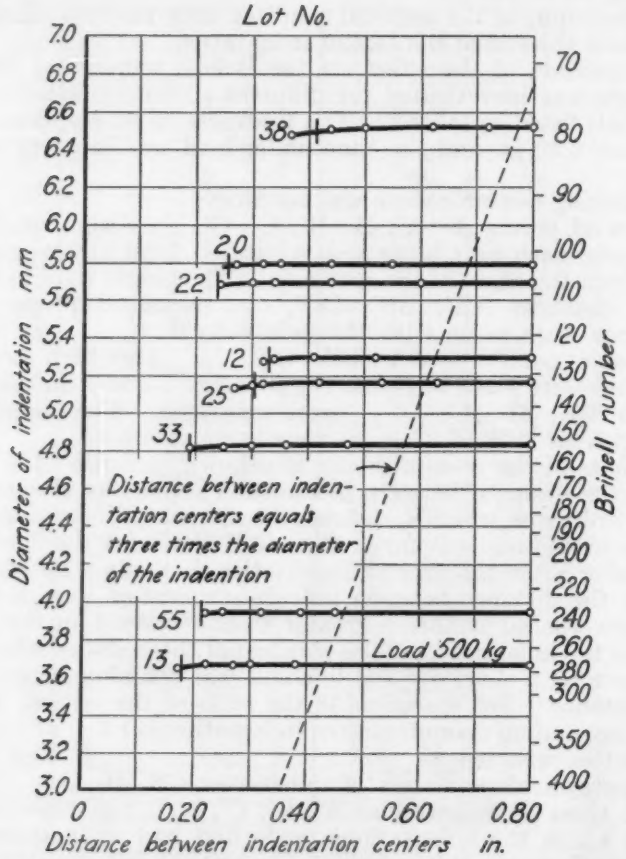

FIGURE 11.—*Variation in indentation diameter with distance of Brinell indentation from adjacent indentations.*

[Brinell scale on right margin applies to all curves except curve 13.]

An estimate of the error involved was obtained for a soft steel block (Brinell number 187) and a hard steel block (Brinell number 524) in the following manner.

The Brinell number of each steel block was determined from four or five indentations apiece under normal loading. A 2-degree wedge was then placed under the block and two further indentations were made; this was followed by the making of two indentations each with a 4-degree and a 6-degree wedge.

The resulting variation of the observed Brinell number with wedge angle is plotted in figure 12. Strictly speaking, the angle between the normal to the specimen and the load line will be larger than the wedge angle because of the play in the indenter D (fig. 1). Measurements showed that the maximum play possible was only about 0.5 degree. This is too small a variation to have any measurable effect on the Brinell number and it was accordingly neglected in plotting figure 12. Figure 12 also shows a plot of the percentage increase in the Brinell number due to the reduction in normal load computed from

$$\frac{\Delta H}{H}=\frac{\Delta P}{P}=1-\cos\alpha. \tag{17}$$

The percentage increase appears to be too small to be measured, and it is entirely overshadowed by the second effect which becomes appreciable for deviations from normal loading of 4 degrees or more. The error does not exceed 1 percent for angles of 2 degrees. The error exceeded 8 percent for the indentations on the hard-steel block with the 6-degree wedge.

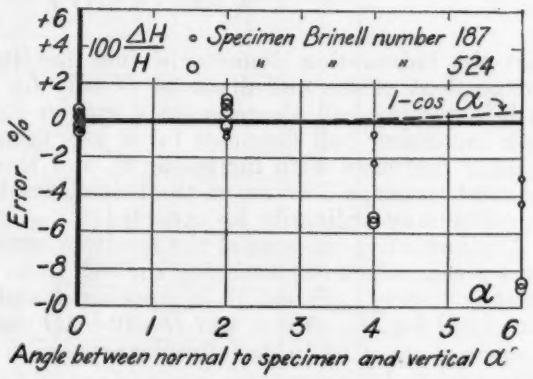

FIGURE 12.—*Error in Brinell number due to deviation from normal loading.*

The two specimens are sufficiently far apart in Brinell number to make it probable that the error will not exceed 1 percent for other steels also, as long as the deviation from normal loading does not exceed 2 degrees. The naked eye will suffice in most cases to check alignment within 2 degrees.

3. INDENTING BALL

The Brinell formula assumes that the indenting ball remains a sphere of nominal diameter (e. g. 10 mm) during the test. Actually this condition is never satisfied. The ball will, in general, deviate from the nominal diameter, its shape will not be truly spherical, and, furthermore, it will deform under load elastically and may deform permanently. Each of these conditions results in a curvature of the contact surface different from the nominal curvature which, in turn, leads to a difference in contact area and a corresponding change in the computed Brinell number.

(a) ERROR IN DIAMETER

If the indenting ball is spherical when not under load but has a diameter $D+\Delta D$ instead of the nominal diameter D, the resulting

[9] Forsch. Gebiete Ingenieurw. 65 (1909).

indentation diameter d will vary, in general, with ΔD. The magnitude of the variation has been studied by Meyer [19] for a number of metals indented with steel balls of various diameters. He found that this variation could be expressed by a formula of the type

$$P=ad^n=a_D\left(\frac{D}{D+\Delta D}\right)^{n-2}d^n, \tag{18}$$

where a is a constant depending on the material of the specimen, and on the nominal diameter D of the ball used, and where n is a constant of the material alone. Meyer found values of n ranging from 1.91 (for lead) to 2.38 (for a certain type of cast iron). For most metals n lies in the neighborhood of 2.2. It is seen by solving equation 18 for d

$$d=\left(\frac{P}{a}\right)^{1/n}\left(1+\frac{\Delta D}{D}\right)^{1-2/n}, \tag{19}$$

that the indentation diameter d (not the Brinell number) will be independent of the ball diameter D only for $n=2$; it will increase with increasing ball diameter for n greater than 2 and will decrease with increasing ball diameter for n less than 2. Since the Brinell number decreases with increasing d, and since n is greater than 2 for most metals, a decrease of the Brinell number with increasing ball diameter may ordinarily be expected.

A quantitative measure of the resulting error in the Brinell number for a given value of n, assuming the ball to be rigid, may be obtained by substituting equation 19 in equation 5 and calculating the difference in H for $D=10$ mm and $D=10+\Delta D$ mm. Eliminating a with the help of equation 19 the following expression results for $\Delta D/D$ small compared to 1.

$$\frac{\Delta H}{H}=\frac{\partial H}{\partial D}\frac{\Delta D}{D}=\frac{2}{n}\left(1-n+\frac{1}{\sqrt{1-\left(\frac{d}{D}\right)^2}}\right)\frac{\Delta D}{D}. \tag{20}$$

This coincides with the corresponding expression which would be obtained from equation 1 for the special case $n=2$ upon holding everything constant except D.

Figure 13 shows the percentage error 100 $\Delta H/H$ calculated for the extreme cases $n=1.91$ and $n=2.4$, as well as for the ideal case $n=2$ for deviations $\Delta D=0.10$ mm, and 1.00 mm from a nominal diameter of 10 mm. The percentage error for $\Delta D=0.10$ mm does not exceed 0.5 percent for Brinell numbers between 67 and 945.

The diameters of steel balls produced by modern manufacturing methods are within 0.015 mm of the nominal diameter. The error due to variation in diameter of such balls for any value of n observed by Meyer stays below 0.1 percent, which is entirely negligible.

(b) NONSPHERICAL SHAPE

If the indenting ball is nonspherical in shape when not under load, there will be a resulting error in the Brinell number. This may be

estimated from equation 20, provided the radii of curvature in the region of contact are known. ΔD may be taken as the difference between twice the average radius of curvature—i. e., the effective diameter of the ball in the region of contact—and the nominal diameter. Consider, for example, a ball ground to the shape of an ellipsoid of revolution with the minimum diameter of the ellipsoid coinciding with the line of action of the load on the ball. Such a ball will have an effective diameter at the point of loading larger than the average diameter by an amount $3\Delta D$, where $D+\Delta D$ is the diameter at the equator of the ellipsoid of revolution, and $D-\Delta D$ is its diameter along

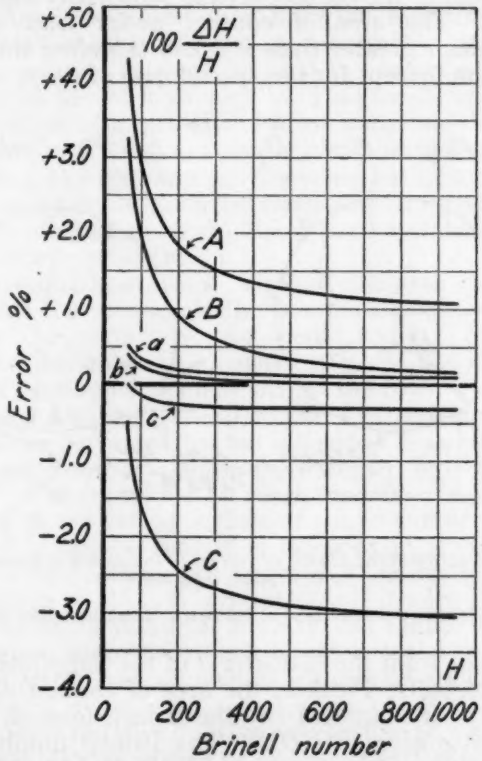

FIGURE 13.—*Error in Brinell number due to error in ball diameter.*

Curve	Error in ball diameter (mm)	n	Curve	Error in ball diameter (mm)	n
A	1.0	1.91	a	0.1	1.91
B	1.0	2.00	b	.1	2.00
C	1.0	2.40	c	.1	2.40

the load line (connecting the poles). The consequent error in the Brinell number will, according to equation 2, be less than $1.6\,\Delta D/D$ in practical cases (n between 1.91 and 2.4). The error would not exceed 0.24 percent if the tolerance in diameter is set at ± 0.015 mm.

(c) DEFORMATION OF BALL UNDER LOAD

The diagrammatic sketch of figure 14 will assist in a discussion of the effect of deformation of the ball on the Brinell number. Balls B_1 and B_2 are imagined to indent a given specimen under a given load, and both are taken to be spheres of the same diameter when not under load. Ball B_1 is an "ideal" Brinell ball; it is perfectly rigid and will not deform under load. If such a ball were possible, an "ideal" Brinell number could be determined by direct measurement of the indentation it produced. Ball B_2 is an actual Brinnell ball; it is made of deformable material and will yield under load elastically, and if the stress in the contact area is sufficiently high it will deform permanently. The area of contact under load approximates a sphere of radius r greater than $D/2$ and therefore the diameter d' of the indentation (except for the special case of $n=2$, see equation 19)

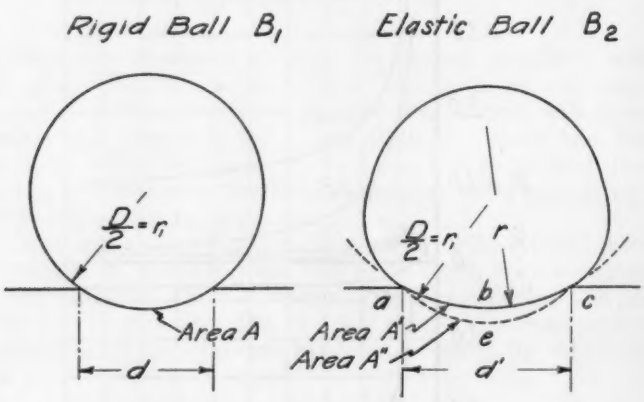

FIGURE 14.—*Diagrammatic sketch of two balls indenting a given specimen under a given load.*

[Ball B_1 is an ideal rigid Brinell ball and B_2 is an actual deformable Brinell ball.]

will be different from the diameter d of the indentation produced by the ideal rigid ball. Further, the area of contact corresponding to the diameter d' is computed (by the Brinell formula) as if it were a spherical calotte of radius $D/2$. The Brinell number so measured and computed, in contrast to the hypothetical ideal Brinell number, instead of being a characteristic mechanical constant of the specimen alone is also a function of the elastic and inelastic properties of the indenting ball which determine its shape under load.

The importance of this effect, especially for materials of high Brinell number, is shown clearly by tests made by Mailaender,[20] who found differences up to 10 percent between the Brinell number of a given specimen computed from indentations with a 5-mm diamond ball under 187.5-kg load and with a 5-mm steel ball under the same load. Styri[21] found differences of the same order between

[20] R. Mailaender, Stahl u. Eisen **45**, 1769–1773 (1925).
[21] H. Styri, Metals and Alloys **3**, 273–274 (1932).

the Brinell numbers computed from indentations with 5-mm Carboloy balls under 750-kg load and those with 5-mm steel balls under the same load.

Brinell defined his "hardness number" (nombre de dureté) in terms of the indentation produced by a ball of hardened steel (acier trempé).[22] According to this definition Brinell numbers computed from balls of other materials have "errors" depending upon the difference between their elastic moduli and the moduli of steel. In view of the increased use of Carboloy and diamond balls, it seems preferable to consider these effects not as errors but as differences between Brinell numbers measured under different conditions analogous to the difference between the 3,000-kg Brinell number and the 500-kg Brinell number of the same material.

Meyer's formula 18 could be used to evaluate this effect if Meyer had extended his work to very hard materials and had, in addition, obtained values of n for balls of other materials than steel, and if the value of the radius of curvature r of the loaded ball in the contact surface (fig. 14) were known. Knowing both r and n, the constant a of equation 18 could then be calculated from the diameter of the indentation d' and, in turn, the Brinell number for an ideal rigid ball from this constant a.

Even without knowing n, a rough estimate for r and d' may be obtained for the case of elastic deformation of the ball from Hertz's theory for the contact of two elastic bodies. Such an estimate is made below, followed by a consideration of the effect on the Brinell number of permanent deformation of the ball.

(1) *Elastic Deformation.*—The effect of elastic deformation of the ball would be measured by the difference between the Brinell number P/A' obtained for an elastic ball (B_2, fig. 14), and the Brinell number P/A obtained for an ideal rigid ball (B_1, fig. 14), where A' is the area of the actual surface of contact under load of the elastic ball (a b c in fig. 14) and A is the contact area of the ideal rigid ball. It is not possible to measure A' under load. To obtain an approximation to A', it is computed as if it were the area of a spherical indentation of diameter d' with the radius of curvature of the ball when not under load; that is, A' is replaced by A'', where A'' is the area of the contact surface intersecting the plane of the paper in figure 14 in a e c. The assumption of $A'=A''$ is convenient in that the Brinell number P/A'' corresponding to d' may be read directly from a Brinell table and may be compared with that corresponding to d. The error due to this assumption is less than 1 percent, as is shown in figure 19 in the appendix 2, p. 95.

In applying Hertz's theory it must be remembered that it is not strictly applicable to the case of the deformation of the indenting ball in the Brinell test for two reasons:

1. The specimen does not remain elastic during the test.

[22] Communications Congrés International des Méthodes d'Essai des Matériaux de Construction, Paris, 2, 85 (1900).

2. The diameter of the contact surface is not, in general, small compared to the diameter D of the indenting ball.

In spite of these limitations, however, the theory forms a useful basis for discussion of the effects of changes in ball diameter, load, and material of the ball on the Brinell number obtained on a given specimen. These effects become most pronounced for the case of indentations on very hard materials. This is just the case which is more closely approximated by the theory, since the indentation is small on hard materials and since the specimen is not as severely deformed as for softer materials.

According to Hertz's theory the radius a of the circle of contact is, for the special case of elastic contact between a ball and plane, given by [23]

$$a^3=\frac{3Pr_1}{16}(\theta_1+\theta_2), \tag{21}$$

where

P=normal load transmitted by the ball to the plane
r_1=radius of curvature ($D/2$) of the ball in its unloaded condition.
$\theta_1=\frac{4}{E_1}(1-\mu_1^2)$=elastic constant for the ball
$\theta_2=\frac{4}{E_2}(1-\mu_2^2)$=elastic constant for the plane
E_1=Young's modulus for the ball.
E_2=Young's modulus for the plane.
μ_1=Poisson's ratio for the ball.
μ_2=Poisson's ratio for the plane.

Assuming that a is the radius $\frac{d'}{2}$ of the actual indentation gives

$$d'^3=\frac{3}{2}Pr_1(\theta_1+\theta_2), \tag{22}$$

while the diameter of the indentation made by the ideal rigid ball ($\Theta_1=0$) would be given by

$$d^3=\frac{3}{2}Pr_1\theta_2. \tag{23}$$

Substituting this value in equation 22 gives

$$d^3=d'^3-\frac{3}{2}Pr_1\theta_1. \tag{24}$$

The Brinell number is obtained by substituting d' in the Brinell formula. The corrected Brinell number, which would be obtained with an ideal rigid ball, may be obtained by substituting d, computed from

[23] Gesammelte Werke, Barth, Leipzig, 1, 155-196 (1894/95).

equation 24 in the Brinell formula. This requires a knowledge of the elastic constant Θ_1 of the material of the Brinell ball. The elastic constants for some materials that have been used for Brinell balls are:

Steel. $\theta_1 = 1.770 \times 10^{-4}$ $kg^{-1}mm^2$

Carboloy. θ_1 lies between 0.770×10^{-4} and 0.834×10^{-4} $kg^{-1}mm^2$

Diamond. θ_1 lies between 0.2955×10^{-4} and 0.515×10^{-4} $kg^{-1}mm^2$.

The values for Carboloy were calculated from Young's modulus, as determined by tests at the National Bureau of Standards; Poisson's ratio was assumed to be between 0.16 and 0.32. The values for diamond were calculated from the bulk modulus given in International Critical Tables; Poisson's ratio was assumed to lie between 0.16 and 0.32.

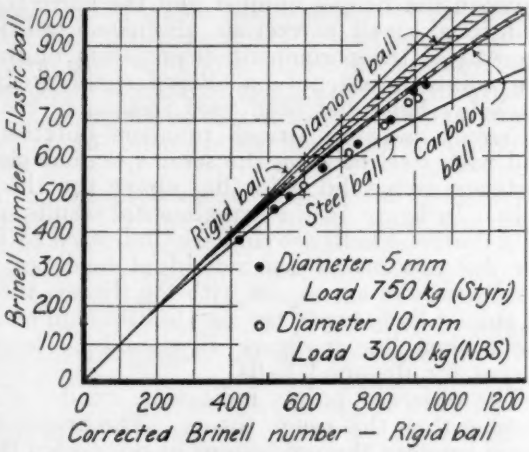

FIGURE 15.—*Theoretical and observed relations between Brinell numbers obtained with 10-mm balls of various materials under 3,000-kg load or 5-mm balls under 750-kg load.*

Figure 15 shows curves of Brinell number *vs* corrected Brinell number calculated from equations 23 and 24 for steel balls, Carboloy balls, and diamond balls of 10 mm diameter, under 3,000-kg load, or of 5 mm diameter, under 750-kg load. Figure 16 shows similar curves for steel balls and diamond balls of 5 mm diameter, under 187.5-kg load. The curves indicate roughly how the Brinell number should be expected to vary with the elastic properties of the ball. The variation increases from zero at low Brinell numbers to a large value at high Brinell numbers.

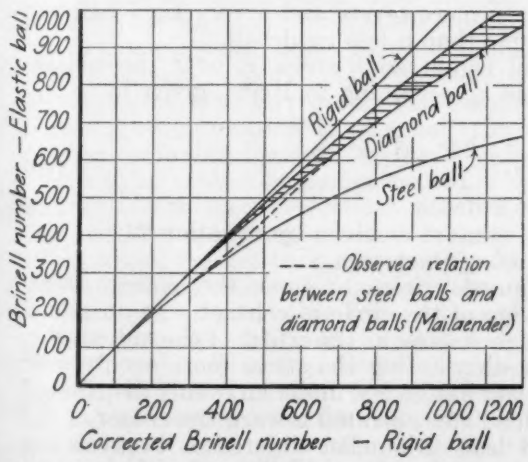

FIGURE 16.—*Theoretical and observed relations between Brinell numbers obtained with 5-mm balls of various materials under 187.5-kg load.*

Results taken from actual tests by Styri [24] using Carboloy balls and steel balls (fig. 15) and by Mailaender [25] using diamond balls and steel balls (fig. 16) have been replotted for comparison with this rough theory. Each point in figure 15 represents two determinations of the Brinell number on a given specimen, one made with a steel

[24] H. Styri, Metals and Alloys 3, 273–274 (1932).
[25] R. Mailaender, Stahl u. Eisen 45, 1769–1773 (1925).

ball and the other with a Carboloy ball. In plotting the points a corrected Brinell number was assigned to each specimen, on the assumption that the curve for the steel ball represented the relation between the Brinell number and the corrected Brinell number. An additional small correction (discussed later) was applied to take account of the permanent deformation of the balls. The trend of the points would not be altered significantly if the curve for the Carboloy balls had been used instead of that for steel balls. The difference between Brinell numbers obtained with Carboloy balls and with steel balls on the same specimen shown in figure 15 is the distance each solid point lies above the theoretical curve for steel balls. In figure 16 the experimental results obtained by Mailaender with diamond balls are similarly indicated by a broken line (Mailaender did not report his individual readings). If the experimental results were in agreement with the theory, the points shown in figure 15 should lie between the two limiting curves for Carboloy balls and the broken line in figure 16 should lie between the two limiting curves for diamond balls.

The observed points indicate a smaller difference in the Brinell number than this rough theory. The probable reason for this divergence between the predictions of the elastic theory and actual observations is to be sought in the difference between the actual stress distribution in the contact area and that assumed in Hertz's theory.

This difference in stress distribution has little effect on the deformation of balls indenting very soft material since the average stresses acting on the ball are so small in that case that there is no noticeable difference between the deformed shape of, say, a steel ball and a diamond ball. As the indentation becomes smaller with harder materials the stresses become more severe and a very rigid ball will be flattened to a lesser degree than a less rigid ball.

The distribution of axial compressive stress σ_z over the contact area between ball and plane is, according to Hertz, given by

$$\sigma_z=\frac{3P}{2\pi}\frac{\sqrt{a^2-x^2}}{a^3}, \tag{25}$$

where

a=radius of the circle of contact as given by equation 21

x=distance from center of contact area.

The stress decreases continuously from 1½ times the average stress at the center to 0 at the edge of the circle of contact. In an actual Brinell test the relatively high stresses at the center of the indentation will produce yielding, thus distributing the stress more evenly over the contact area. The ball will flatten less under an evenly distributed load than under the same load concentrated toward the center of the contact area. This would lead to smaller differences between the diameters of indentations obtained with steel balls and with diamond balls than those predicted from Hertz's theory. As the hardness of the specimen increases further the indentation becomes smaller and flatter and the stress distribution assumed by Hertz is more nearly approached. The difference between theory and experiment should, therefore, decrease in going to the harder materials. This is verified by the plots of figures 15 and 16. The difference, as shown in figure 15, between the Brinell numbers reported by Styri [26] for a given

[26] H. Styri, Metals and Alloys **3**, 273-274 (1932).

specimen with a 5-mm Carboloy ball and with a steel ball at 750-kg load comes close to that predicted by the theory at a "Carboloy" Brinell number of about 800. Figure 16 shows that the same agreement holds for the comparison of a diamond and a steel ball under 187.5-kg load at a "diamond" Brinell number of about 600.

Styri's results for the comparison of steel balls and Carboloy balls were checked at the National Bureau of Standards by tests on 10-mm balls. These tests will be described in detail later. The five points taken from these tests (fig. 15, open circles) fall close to the solid points taken from Styri's tests.

The small correction for the permanent compression of the balls is less than 5 in Brinell number for all of Styri's tests and less than 20 for the tests made with high-grade balls at the National Bureau of Standards. The observed difference in Brinell number on a given specimen made with a steel ball and a Carboloy ball was found to be as high as 70 in some cases. The differences in elastic deformation may, therefore, be several times greater than those caused by permanent deformation of the ball.

In the case of extremely hard specimens both effects will have to be considered, since the elastic theory in itself is not sufficient. Nevertheless, theory and tests show that the elastic deformation of the ball may lead to large differences in the measured Brinell number if balls with sufficiently different elastic properties are used. It is, therefore, necessary to specify the material of the ball in quoting Brinell numbers above 500.

(2) *Permanent Deformation.*—If the ball deforms permanently during the test the contact area will be flattened even more than in the case of elastic deformation, thus increasing still more the effective diameter of the ball. This effect produces an appreciable error in practical testing with high-grade steel balls only if the Brinell number of the specimen exceeds 500. For steels the diameters of the indentations increase with increase in ball diameter so that the greater the permanent deformation of the ball the lower will be the Brinell number computed from the resulting indentation.

It is important, for practical work, to specify the limits of Brinell number of the specimen within which a given Brinell ball may be used without introducing an uncertainty, caused by its permanent deformation, greater than a certain figure, e. g., 1 percent.

This problem has been considered by several workers in the field. Mailaender [27] carried out a comprehensive series of indentation tests with 10-mm steel balls of different hardness, indenting specimens from 110 to 680 Brinell under 3,000-kg load. The Brinell number of the ball, as estimated from the diameter of indentation in bringing one ball in contact with the other under 3,000-kg load, varied from 230 to 720.

Mailaender concluded from these tests that the diameter of the indentation remained independent of the Brinell number of the ball as long as the latter was at least 1.77 times the Brinell number of the specimen.

Hultgren [28] made an even more extended series of tests with 10-mm steel balls of various hardness under 3,000-kg load. His specimens

[27] R. Mailaender, Stahl u. Eisen **45**, 1769–1773 (1925).
[28] J. Iron and Steel Inst. **110**, II, 183–218 (1924).

ranged in Brinell number from 506 to 735. Instead of using either the Brinell number or the effective radius of curvature of the contact area of the ball as independent variable, he used the more easily measured shortening or permanent compression of the loaded diameter after the first test. Hultgren obtained a series of correction curves which show, for instance, that a permanent compression of 0.025 mm in the ball will lower the Brinell number computed from the indentation by about 25 and a compression of 0.010 mm by about 5.

Hultgren used five different makes of steel balls on each of five different specimens, four of which were chromium steel, while the fifth (specimen V) was high-speed steel. He made five or more indentations on each specimen with each make of ball and measured the permanent compression and the Brinell number for each indentation. From these individual values averages of the permanent compression of the ball after the first test and of the observed Brinell number H were obtained for each specimen and each type of ball.

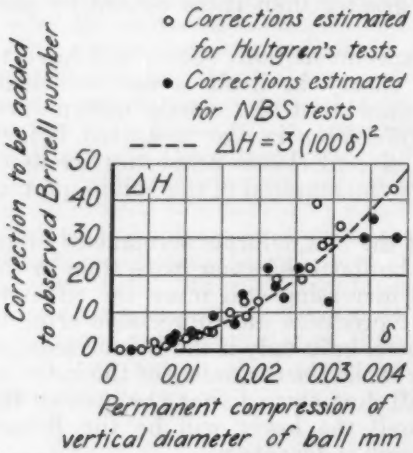

FIGURE 17.—*Estimated corrections in Brinell number due to permanent deformation of ball.*

[10-mm steel balls, 3,000-kg load]

A plot of Hultgren's corrections $\Delta H = H_e - H$ against δ, where H_e is a Brinell number corrected for the permanent compression δ of the ball, showed that all Hultgren's points, except those for specimen V, grouped themselves with considerable scatter about a parabola of the type $\Delta H = \alpha\delta^2$.

Obviously the scatter of the individual points depends on the value of this corrected Brinell number H_e. It was found that this scatter could be reduced and that at the same time the points for specimen V could be brought into closer agreement with the remaining points by extrapolating to new values of H_e in the following manner. Assume that the relation $\Delta H = \alpha\delta^2$ holds for each specimen, plot H against δ^2 for each individual test, and fair a straight line through the plotted points. H_e will then be the ordinate of the straight line for the abscissa $\delta = 0$. The values of H_e so determined were within 5 in Brinell number of those estimated by Hultgren, except for specimen V, for which 720 was obtained in place of Hultgren's value of 735. The differences ΔH between the average values of H for each type of ball for each specimen and the values H_e for each specimen, derived as described above, are plotted against δ as open circles in figure 17, for values of δ less than 0.04 mm. For larger deformations no relations even approximately consistent were found between ΔH and δ.

The solid points in figure 17 represent the results of a few check tests made at the National Bureau of Standards. Steel balls (10 mm in diameter) of three makes A, B, C, were used in these tests. A and B designated ordinary steel Brinell balls, while C designated steel balls cold-worked by the Hultgren process. In addition, a num-

ber of 10-mm Carboloy balls were used for comparison with steel balls. These also gave a further check on the effect of elastic deformation of the ball on the Brinell number, which was discussed in the previous section.

The test specimens consisted of five disks of chromium steel (SAE 52100) heat treated by the Division of Metallurgy of this Bureau to have Brinell numbers ranging from 500 to 700. Four indentations with each type of ball, A, B, and C, were made on each one of the five disks. A new steel ball was used for each indentation, and the diameter of each ball in the direction of loading was measured with a Zeiss optimeter before and after test. The permanent compressions corresponding to the difference of these two readings, together with the Brinell numbers corresponding to the observed indentation diameters, are listed in the first six columns of table 4. The last two columns give corresponding results obtained with Carboloy balls. Since only two Carboloy balls were available for each specimen each ball was used twice; the permanent compression listed is that measured after the first indentation. Some of the balls of group A showed compressions greater than 0.04 mm. The values for these balls (denoted by an "a") were not included in the averages given at the bottom of each group for the reason noted above.

TABLE 4.—*Results of tests to show effect of deformation of ball on Brinell number*

Type of ball→	A		B		C		Carboloy	
Specimen ↓	Brinell number	Compression of ball	Brinell number	Compression of ball	Brinell number	Compression of ball	Brinell number	Compression of ball
		mm		mm		mm		mm
1, H_c=511	508	0.0079	505	0.0094	512	0.0025	525	0.0000
	508	.0071	508	.0084	511	.0030	526	
	*491	*.0445	506	.0084	513	.0030	521	.0033
	510	.0086	507	.0089	509	.0025	522	
Average	509	.0079	506	.0088	511	.0028	524	.0016
Correction	2		2		0		0	
Corrected Brinell number	511		508		511		524	
2, H_c=592	582	.0191	575	.0183	584	.0102	610	.0066
	590	.0168	579	.0180	588	.0076	613	
	580	.0175	575	.0183	590	.0084	610	.0061
	588	.0137	580	.0168	593	.0066	612	
Average	585	.0168	577	.0178	589	.0082	611	.0064
Correction	9		10		2		1	
Corrected Brinell number	594		587		591		612	
3, H_c=652	640	.0231	630	.0272	646	.0122	685	.0091
	639	.0234	628	.0239	647	.0130	684	
	639	.0211	629	.0259	633	.0185	678	.0084
	636	.0259	632	.0246	647	.0119	679	
Average	638	.0234	630	.0254	643	.0139	682	.0088
Correction	17		19		6		2	
Corrected Brinell number	655		649		649		684	
4, H_c=690		*.2508	665	.0343	658	.0203	742	.0142
	678	.0290	656	.0338	670	.0203	737	
	*628	.0533	652	.0353	672	.0216	741	.0142
	676	.0300	666	.0335	674	.0224	736	
Average	677	.0295	660	.0342	668	.0212	739	.0142
Correction	26		35		13		6	
Corrected Brinell number	703		695		681		745	
5, H_c=697	*529	*.1334	665	.0366	684	.0221	754	.0152
	667	.0386	661	.0345	674	.0221	757	
		*.3856	661	.0350	673	.0239	741	.0132
	*554	*.1217	662	.0353	690	.0211	746	
Average	667	.0386	662	.0354	680	.0223	750	.0142
Correction	45		38		15		6	
Corrected Brinell number	712		700		695		756	

*Values not included in average because the deformation of the ball was greater than 0.04 mm.

Values for the corrected Brinell numbers H_c for the five specimens were obtained from the individual test results by fairing a straight line through a plot of H versus δ^2 using the procedure already described above in the discussion of Hultgren's results. The values of $\Delta H = H_c - H$ corresponding to these corrected Brinell numbers are plotted as solid points in figure 17. It is seen that the points fall roughly about a common curve with the points computed from Hultgren's data. The scatter of all points increases with increasing compression. A large part of this scatter is, no doubt, due to nonuniform response to heat treatment. The resulting lack of uniformity may be expected to increase with the Brinell number of the specimen and hence with the permanent compression produced in a given ball. All of the observed results are approximated roughly by the simple empirical formula

$$\Delta H = 3(100\delta)^2, \tag{26}$$

which is shown as a dotted line in figure 17. This formula was used to correct the average Brinell numbers listed in table 4. The corrections are less than 1 percent for Carboloy balls, less than 3 percent for steel balls C, but they exceed 5 percent for steel balls B, indenting the hardest specimen, and 6 percent for steel balls A.

The effect of permanent deformation of the Carboloy balls would be similar to that of the steel balls, though not necessarily of exactly the same magnitude. The Carboloy balls used in the tests were so uniform that any difference was masked by the experimental error. For that reason the Brinell numbers obtained with the Carboloy balls have been corrected by the same formula, 26, used with the steel balls.

The Brinell numbers obtained with Carboloy balls are in every case higher than those obtained with steel balls; this is due primarily to the greater rigidity of Carboloy as compared to steel (see previous section). The correction for permanent deformation of the ball reduced the maximum difference in the average Brinell numbers obtained with the three types of steel balls in every case except specimen 4, in which it increased it from 17 to 22. Much of this scatter is, as already mentioned, due to nonuniform response of the specimen to heat treatment.

Figure 17 shows that the error due to permanent deformation of the ball is below 5 Brinell numbers for balls showing a permanent compression of less than 0.01 mm after the first loading, and below 20 Brinell numbers for balls showing a permanent compression of less than 0.025 mm after the first loading. Table 4 shows that high-grade steel balls are available which show permanent sets less than 0.01 mm at 500 Brinell and less than 0.025 mm at 700 Brinell. The corresponding permanent compressions for Carboloy balls were found to be even less.

IV. RECOMMENDATIONS FOR BRINELL TESTING

It is possible, after having discussed in detail the effect of small variations in the several variables that enter into the determination of Brinell numbers, to draw up a list of recommendations designed to keep the combined error due to these variations down to a small figure. Such recommendations may assist in further standardization of the Brinell test and may in that way lead to greater concord-

ance between the Brinell numbers obtained by different observers using balls of given diameter on specimens of given material. These recommendations are based on tests of metal specimens having Brinell numbers greater than 70. They may not be sufficient for testing metals having Brinell numbers less than 70, such as soft bearing metals.

Grouping the individual factors in the order in which they are discussed above gives the following list of recommendations.

1. APPARATUS AND PROCEDURE

(a) The loading mechanism should be operated to give a uniform rate of loading not exceeding 500 kg/sec.

(b) The maximum load should be applied for 30 seconds.

(c) The error in the load applied by the machine should not exceed ½ percent. This should be checked by periodic calibration with a proving ring or other suitable device.

(d) The calibration of the apparatus used for measuring the diameter of the indentation should be checked frequently. The maximum error in the reading at any point on the scale should not exceed 0.01 mm. The indentation diameter should be read in two or more mutually perpendicular directions.

2. SPECIMEN

(a) The Brinell number should be computed from the average of diameter readings in at least four equally spaced directions if the indentation has a noncircular boundary. Care should be taken to polish the surface of the specimen to such a finish that the error in diameter reading due to tool marks does not exceed 0.01 mm.

(b) If the indentation is made on a curved specimen the minimum radius of curvature of the specimen should not be less than 25 mm for a 10-mm ball. The diameter of the indentation should be taken as the average of the two principal diameters.

(c) The specimen should be at least 0.4 in. thick.

(d) The distance of the center of the indentation from the edge of the specimen should be at least three times the diameter of the indentation.

(e) The distance between centers of adjacent indentations should be at least three times the diameter of the indentation.

(f) The angle between the load line and the normal to the specimen should not exceed 2 degrees.

3. INDENTING BALL

(a) The difference between the average diameter and the nominal (10 mm) diameter of the ball should not exceed 0.025 mm (0.001 in.). The average diameter should be the average of six or more different diameters of the ball.

(b) The difference between any individual diameter and the average diameter of new balls should not exceed 0.025 mm (0.001 in.).

(c) The material of the indenting ball (e. g. steel, Carboloy, diamond) must be specified in quoting Brinell numbers greater than 500.

The permanent compression of the loaded diameter of the ball after any indentation on a specimen having a Brinell number less

than 500 should not exceed 0.01 mm. If, however, steel balls are used on specimens having Brinell numbers greater than 500, the permanent compression after any indentation should not exceed 0.025 mm.

The use of Carboloy balls is recommended for indentations on any specimen having a Brinell number greater than 500.

V. APPENDIX

1. ERROR IN THE BRINELL NUMBER DUE TO CURVATURE OF SPECIMEN

The Brinell formula:

$$H=\frac{P}{A}=\frac{2P}{\pi d^2}\left(1+\sqrt{1-\left(\frac{d}{D}\right)^2}\right) \tag{1}$$

assumes the surface of indentation to be a section of a sphere of diameter D bounded by a circle of diameter d. The surface of intersection between sphere and specimen will no longer have a plane boundary if the specimen has two different principal radii of curvature R_1, R_2. Instead of being a circle it will be a closed curve roughly elliptical in shape and having two principal axes, one of length d_1 and the other of length d_2. The error in the Brinell number assuming the equivalent diameter to be equal to

$$d_3=\frac{d_1+d_2}{2} \tag{2}$$

will be computed below.

The relative error in the Brinell number due to an error ΔA in the measurement of area, is from formula 1

$$\frac{\Delta H}{H}=-\frac{\Delta A}{A}. \tag{3}$$

The error in area may, in this case, be written

$$\Delta A=A-A_3, \tag{4}$$

where

A = area of surface of the sphere embedded in the specimen.

A_3 = area of equivalent section of sphere given by equation 1, that is,

$$A_3=\frac{\pi d_3^2}{2}\,\frac{1}{1+\sqrt{1-\left(\frac{d_3}{D}\right)^2}}. \tag{5}$$

The computation of the relative error $\Delta H/H$ involves the derivation of the three quantities A, d_1, d_2.

The surface of intersection A of a sphere with a specimen having principal curvatures of $1/R_1$ and $1/R_2$ will be computed first.

Let the origin of coordinates be at the center of the indenting sphere (fig. 18) and let any point on the surface of the sphere be described in terms of the latitude θ and the longitude ϕ. The curve of intersection ABCF of the sphere with the specimen may then be expressed as $\theta_i(\phi)$. The surface of indentation A will be a portion of a sphere of radius $r=D/2$ bounded by this curve, i. e.,

$$A=\int_{\phi=0}^{2\pi}\int_{\theta=0}^{\theta_i}(r\sin\theta d\phi)rd\theta=4r^2\int_{\phi=0}^{\pi/2}(1-\cos\theta_i)d\phi. \tag{6}$$

The integration, equation 6, can be carried out if the shape of the curve of intersection $\theta_i(\phi)$ is known, or more specifically, if $\cos\theta_i$ can be expressed as a function of ϕ.

The curve of intersection $\theta_i(\phi)$ is the locus of points common to the indenting spherical surface and the surface of the specimen. It is convenient to describe all points on the surface of the specimen in terms of cylindrical coordinates z, s, ϕ having their origin at the point E at which the load line (fig. 18) intersects the surface of the specimen. The z-axis is taken as coinciding with the load line and directed into the interior of the specimen, s is the radial coordinate (normal to

z) and ϕ is the longitude already used in describing points on the indenting sphere. z, s, will be points on the surface of the sphere also (see fig. 18) if

$$z=\epsilon r-r\cos\theta_i=r(\epsilon-\cos\theta_i). \tag{7}$$

$$s=r\sin\theta_i. \tag{8}$$

It is assumed in describing the surface $z(s,\phi)$ of the specimen, that only a small portion of this surface will be indented. The surface may then be approximated by a surface of the second degree with origin at E having a curvature at that point equal to the actual curvature of the specimen. This surface may be described mathematically by

$$z=\frac{1}{2}\frac{s^2}{R}, \tag{9}$$

where $1/R$ is the curvature at the longitude considered. The curvature at any longitude is related to the principal curvatures ($1/R_1$ at $\phi=0$, $1/R_2$ at $\phi=\pi/2$) by Euler's equation [19]

$$\frac{1}{R}=\frac{\cos^2\phi}{R_1}+\frac{\sin^2\phi}{R_2}. \tag{10}$$

Solving equations 8, 9, and 10 for $\cos\theta_i$ gives

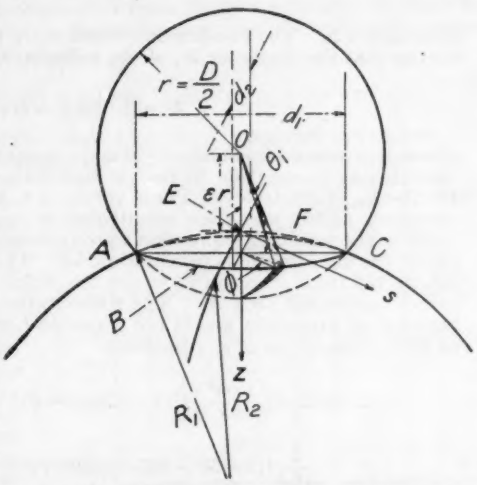

FIGURE 18.—*Diagrammatic sketch of intersection between a sphere and a curved surface.*

$$\cos\theta_i=\frac{R}{r}\left[1\pm\sqrt{1-2\frac{r}{R}\epsilon+\frac{r^2}{R^2}}\right]. \tag{11}$$

The negative sign in front of the radical applies here since $\cos\theta_i$ cannot be greater than 1 and since R/r is, in general, large compared to 1, while ϵ cannot be greater than 1.

Substituting equation 11 in equation 6 gives the following expression for the area of the surface of intersection of sphere and specimen

$$A=4r^2\int_{\varphi=0}^{\pi/2}\left[1-\frac{R}{r}\left(1-\sqrt{1-2\frac{r}{R}\epsilon+\frac{r^2}{R^2}}\right)\right]d\phi, \tag{12}$$

where the integrand is a known function of ϕ obtained by substituting in it equation 10 for 1/R. The resulting expression is not a simple integrable form but because $2\epsilon r/R+r^2/R^2$ are small it can be expanded in a series and integrated term by term.

It is convenient in carrying out this integration to substitute the ratios

$$\kappa=\frac{r}{\sqrt{R_1R_2}};\ \gamma=\frac{1}{2}\left(\frac{r}{R_1}+\frac{r}{R_2}\right), \tag{13}$$

which involve only the known radius r of the indenting sphere and the known principal curvatures $1/R_1$, $1/R_2$ of the specimen. The result of the integration in terms of these variables carried out to 5th order terms of κ, γ is equal to

$$A=2\pi r^2\Big\{(1-\epsilon)+(1-\epsilon^2)\Big[\frac{\gamma}{2}+\frac{1}{4}\epsilon(3\gamma^2-\kappa^2)-\frac{5}{16}(1-5\epsilon^2)(\gamma^3-\frac{3}{5}\gamma\kappa^2)$$

$$-\frac{35}{64}\epsilon(3-7\epsilon^2)(\gamma^4-\frac{6}{7}\gamma^2\kappa^2+\frac{6}{70}\kappa^4)+\frac{63}{128}(1-14\epsilon^2$$

$$+21\epsilon^4)(\gamma^5-\frac{10}{9}\gamma^3\kappa^2+\frac{5}{21}\gamma\kappa^4)+\ldots\Big]\Big\}, \tag{14}$$

[19] Blaschke, Differentialgeometrie (Springer, Berlin, I, 57, 1921).

where ϵr again represents the distance from the center of the indenting sphere to the point of intersection of the load line with the original surface of the specimen (fig. 18).

The area A_3 may be computed next by substituting the average diameter

$$d_3=2r_3=r_1+r_2 \tag{15}$$

in equation 5. The two principal radii r_1, r_2, may be derived from equation 11 by noting that the diameter $2r_i$ of the indentation in any direction is equal to

$$2r_i=2r\sin\theta_i=2r\sqrt{1-\cos^2\theta_i}. \tag{16}$$

Cos θ_i is given as a function of r/R and ϵ in equation 11. r_1 and r_2 were obtained by substituting in equation 16 the values obtained from equation 11, by letting $R=R_1$, $R=R_2$, respectively. These values of r_1, and r_2 were inserted in equation 15 to obtain d_3, and d_3 was then substituted in equation 5 to obtain A_3. The square roots in the resulting expression were removed by expansion into a series making use of the abbreviations in equation 13. This led to a formula which could be subtracted from equation 14 to get the difference between the area A and the assumed equivalent area A_3. The computation, while simple in principle, is cumbersome of execution and is not repeated here. The final expression carried out to fifth-order terms of κ, γ becomes

$$\begin{aligned}\Delta A=2\pi r^2\left(\frac{1-\epsilon^2}{8\epsilon}\right)\Big\{&[(1-2\epsilon^2)(\gamma^2-\kappa^2)]+\frac{1}{2\epsilon}[(1+8\epsilon^2-15\epsilon^4)(\gamma^3-\gamma\kappa^2)]\\&+\frac{1}{16\epsilon^2}[(3+5\epsilon^2+282\epsilon^4-406\epsilon^6)\gamma^4-(2+6\epsilon^2+332\epsilon^4-476\epsilon^6)\gamma^2\kappa^2\\&-(1-\epsilon^2-50\epsilon^4+70\epsilon^6)\kappa^4]+\frac{1}{32\epsilon^3}[(1-6\epsilon^2-233\epsilon^4+2448\epsilon^6\\&-2730\epsilon^8)\gamma^5+(2+16\epsilon^2+326\epsilon^4-3404\epsilon^6+3780\epsilon^8)\gamma^3\kappa^2\\&-(3+10\epsilon^2+93\epsilon^4-956\epsilon^6+1050\epsilon^8)\gamma\kappa^4]+\ldots\Big\}\end{aligned} \tag{17}$$

This expression is not applicable to the case in which half of the ball is embedded in the specimen ($\epsilon=0$). This, however, does not seriously detract from its usefulness. The diameter of a Brinell indentation does not exceed 70 percent of the diameter of the indenting ball in ordinary practice. It is apparent from this that $\epsilon>0.7$ in practical work.

ΔA must be zero if the indentation is circular, i. e., if $R_1=R_2$, as for a plane specimen or a spherical specimen; in that case $\kappa=\gamma$ in equation 13 and it is seen that the right side of equation 17 becomes equal to zero.

In the particu'ar case of a cylinder of radius R_1, $\kappa=0$ and equation 17 becomes

$$\begin{aligned}\Delta A=2\pi r^2\left(\frac{1-\epsilon^2}{8\epsilon}\right)\Big[&(1-2\epsilon^2)\gamma^3+\frac{1}{2\epsilon}(1+8\epsilon^2-15\epsilon^4)\gamma^3+\frac{1}{16\epsilon^2}(3+5\epsilon^2+282\epsilon^4\\&-406\epsilon^6)\gamma^4+\frac{1}{32\epsilon^3}(1-6\epsilon^2-233\epsilon^4+2448\epsilon^6-2730\epsilon^8)\gamma^5+\ldots\Big].\end{aligned} \tag{18}$$

2. ERROR IN THE BRINELL NUMBER DUE TO ERROR IN THE COMPUTED CONTACT AREA FOR A GIVEN DIAMETER OF INDENTATION

An error is introduced in the calculation of the Brinell number obtained with an elastic ball indenting a specimen to a diameter d' (fig. 14) by computing it from the Brinell formula as if it were a spherical calotte of radius $D/2$. (See p. 83.)

The error could be computed if the actual radius of curvature r (fig. 14) in the contact area of the loaded ball were known. An estimate of r may be obtained from Hertz's theory for the contact of an elastic ball and an elastic plane. The

radius of curvature r of the ball in the contact area is, according to Hertz, given by

$$r=\frac{\theta_1+\theta_2}{\theta_2}r_1. \tag{1}$$

The radius of curvature is doubled, if the contact takes place between a ball and a plane of the same material ($\theta_1=\theta_2$).

The elastic constant θ_2 may be eliminated from Hertz's equation 21, page 84, and from equation 1, and the following expression may be obtained for the curvature $1/r$ in the contact surface

$$\frac{1}{r}=\frac{1}{r_1}-\frac{3\theta_1}{16a^3}P. \tag{2}$$

In view of the limitations of Hertz's theory (p. 83), as applied to this case, it is not possible to calculate an exact value of r in figure 14. But it is possible to obtain an upper limit to r, and hence an upper limit to the difference between the Brinell number P/A' and P/A'' by substituting $d'/2$ for a in equation 23. The value obtained for r will be an upper limit because the substitution of $d'/2$ for a is equivalent to the replacement of the plastically deformed specimen by an elastically deformed specimen giving an indentation of the same diameter. It was shown on page 86 that the ball indenting a plastic specimen will be deformed less than the same ball indenting an elastic specimen to the same indentation diameter. Hence the radius of curvature will be less in the first case than in the second. For a 10-mm steel ball under 3,000-kg load ($r_1=5$ mm, $P=3{,}000$ kg, $E_1=2.1\ 10^4$ kg/mm^2, $\mu_1=0.25$) equation 2 above becomes

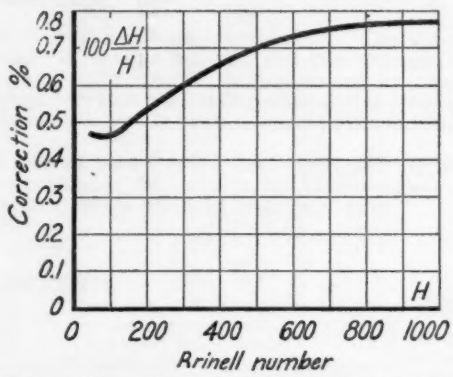

FIGURE 19.—*Upper limit to correction in Brinell number due to error in the computed contact area for a given indentation diameter.*

$$\frac{1}{r}=0.2-\frac{0.803}{d^3}\ \text{mm}^{-1}.$$

The average axial stress over the contact surface (equal to the corrected Brinell number) will then be obtained from the Brinell equation 1 by substituting in it $D=2r$ instead of $D=10$ mm. The error in the Brinell number can be computed by subtracting the Brinell number given by the tables from that just computed. Figure 19 shows the result of such a computation. The increase in the Brinell number computed on the assumption of a rigid 10-mm ball which would take account of this change in curvature, is found to be small; it ranges from 0.46 to 0.77 percent as the Brinell number is increased from 100 to 900. The actual percentage difference between P/A' and P/A'' is even less since the actual diminution in curvature of the ball must be less than that assumed in the derivation of figure 19.

WASHINGTON, March 26, 1936.

73059—36——7

U. S. DEPARTMENT OF COMMERCE NATIONAL BUREAU OF STANDARDS

RESEARCH PAPER RP904

Part of Journal of Research of the National Bureau of Standards, Vol. 17, July 1936

OXIDATION OF WOOL: PHOTOCHEMICAL OXIDATION[1]

By Arthur L. Smith and Milton Harris[2]

ABSTRACT

The photochemical decomposition of wool has been investigated. The deterioration, as evidenced by the decrease in cystine content and the increase in alkali-solubility, ammonia nitrogen, and sulfate sulfur, is accelerated by acids and decelerated by alkalies. The extent to which wool is degraded during irradiation is directly proportional to the decrease in cystine content and to the increase in alkali-solubility.

The sulfur content of untreated and of acid-treated wool decreased during irradiation. The data suggest that a portion of the sulfur in wool is converted to hydrogen sulfide, some of which is subsequently oxidized to sulfuric acid.

CONTENTS

		Page
I.	Introduction	97
II.	Materials and methods	98
III.	Results and discussion	98
IV.	References	100

I. INTRODUCTION

The photochemical decomposition of proteins, carbohydrates, fats and many nitrogenous substances is an oxidation process which is accelerated by acids and decelerated by alkalies [1, 2, 3, 4, 5, 6, 7].[3] In the case of proteins and other nitrogenous materials, this oxidation process is generally accompanied by the cleavage of ammonia [2, 3, 4]. In earlier studies on the photochemical decomposition of silk [1, 2], it was shown that the amount of this ammonia is a measure of the extent to which silk is damaged by exposure to light [1, 2].

Wool, which is relatively more stable to light than silk [8], is also oxidized during irradiation. The reaction, however, appears to be of a somewhat different nature, owing to the inherent differences in chemical constitution of the two proteins. The chief point of attack appears to be the disulfide group of the amino acid, cystine, which is present in wool but not in silk. This group is readily attacked by oxidizing agents and becomes more susceptible to the action of alkalies [9, 10]. The extent to which the wool is oxidized bears a functional relationship to the decrease in its cystine content and to the increase in the alkali-solubility of wool.

The present investigation was undertaken to extend our observations on reactions involving the disulfide group in wool and to determine the effect of irradiation on the sulfur and nitrogen in wool protein.

[1] This is the third paper of a series on studies relating to the oxidation of wool.

[2] Research associates at the National Bureau of Standards representing the American Association of Textile Chemists and Colorists.

[3] The numbers in brackets here and elsewhere in the text refer to the numbered references at the end of this paper.

II. MATERIALS AND METHODS

The wool used in these experiments was worsted top and worsted yarn, each of which had been purified by extraction with alcohol and ether and finally washed with distilled water. The wool was placed in thin layers on cardboard strips and held in place by clips at each end. The samples were exposed to the radiation of a glass-enclosed carbon arc [4] for definite periods of time. The distance from the axis of the arc to the wool was 10 inches.

The alkali-solubility was determined by a method previously described [9], the cystine content by the Sullivan method [11], the sulfate sulfur by the method of Mease [12] and the sulfuric acid by the pyridine method [13]. Ammonia nitrogen was determined by measuring that portion of the nitrogen which is liberated when the wool is boiled in a saturated solution of magnesium oxide. All data are calculated on the basis of the dry weight of the wool.

III. RESULTS AND DISCUSSION

The effect on worsted top wool of exposure to the radiation for different lengths of time up to 100 hours is shown in table 1. The alkali-solubility, ammonia nitrogen and sulfate sulfur increase and the cystine content decreases with increasing time of exposure. The values in the last two columns of table 1 are of special interest since they not only show that sulfuric acid is formed during exposure, but also that practically all the sulfate in the exposed wool is in the form of sulfuric acid. The formation of acid in irradiated wool has been previously noted or suggested by several investigators [14, 15, 16, 17] but only Von Bergen [18] actually demonstrated the presence of sulfuric acid.

TABLE 1.—*Effect on wool top of exposure to the radiation from a glass-enclosed carbon arc for different lengths of time*

Sample	Duration of exposure	Alkali-solubility	Cystine	Ammonia nitrogen	Sulfate sulfur	Sulfuric acid sulfur
	hr	%	%	mg/g	%	%
1	0	11.9	12.2	0.28	0.06	----------
2	5	14.5	11.9	.21	.07	----------
3	15	17.2	11.1	----------	----------	----------
4	30	21.9	10.4	.71	.22	----------
5	50	32.2	8.6	.68	.25	0.21
6	100	36.2	7.9	1.22	.37	.34

In figure 1, the increase in the alkali-solubility is shown to be directly proportional to the decrease in the cystine content. While previous work [10, 11] indicated a relationship, this is the first case in which it was found to be linear.

The effect of acid and alkali on the photochemical deterioration of wool was also investigated. Six-gram samples of wool yarn were soaked in 0.1 *N* solutions of hydrochloric acid and in sodium carbonate solutions of the same strength for 15 minutes at room temperature, centrifuged, and dried in an atmosphere of 65-percent relative humidity at a temperature of 70° F. Samples of untreated and of acid-

[4] Fade-Ometer, type F.D.A., Atlas Electric Devices Co., Chicago, Ill.

and alkali-treated yarns were exposed to the radiation for 100 hours. The effect of the exposures is shown in table 2. The deterioration of the wool, as shown by the decrease in the cystine content and the increase in the alkali-solubility and the ammonia nitrogen content, is greater in the acid-treated and less in the alkali-treated samples than in the untreated samples.

TABLE 2.—*Effect on untreated, acid-treated, and alkali-treated wool of exposure to the radiation from a glass-enclosed carbon arc for 100 hours* [1]

Treatment	Total sulfur	Total sulfur after pyridine extraction	Sulfate sulfur	Sulfuric acid sulfur	Cystine sulfur	Alkali-solubility	Ammonia nitrogen
	%	%	%	%	%	%	mg/g
Untreated and unexposed	3.61	----------	0.02	0.01	3.40	11.6	0.36
Untreated and exposed	3.43	3.25	.24	.27	1.92	53.0	1.65
0.1 *N* hydrochloric acid	3.35	3.30	.14	----------	1.66	67.8	2.24
0.1 *N* sodium carbonate	3.65	3.29	.24	----------	2.21	47.7	1.48

[1] These exposures were made on a different Fade-Ometer and the results of these experiments are not strictly comparable with those recorded in table 1.

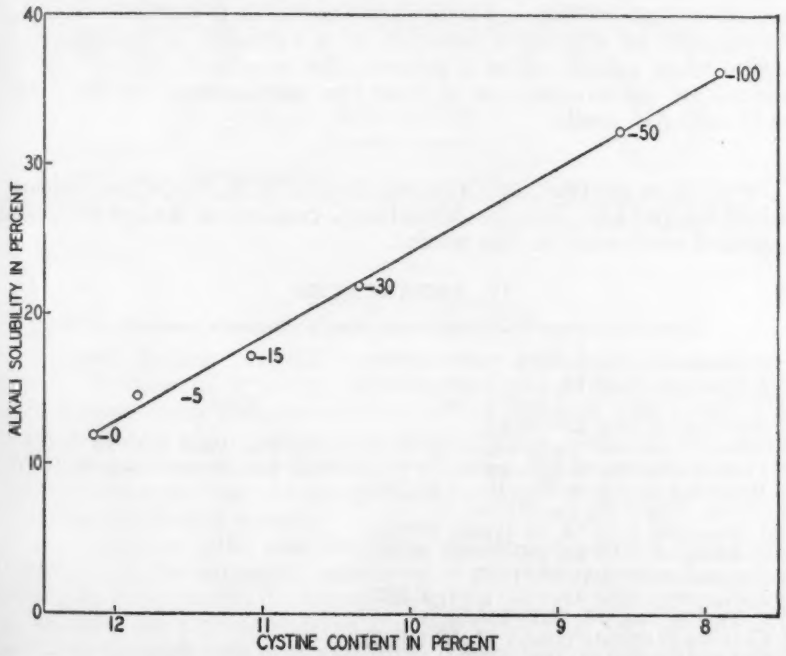

FIGURE 1.—*Relationship between the cystine content and the alkali-solubility of wool exposed to the radiation from a glass-enclosed carbon arc.*

The figures on the curve represent the duration of exposure, in hours.

The total sulfur content of the untreated and the acid-treated samples decreased during exposure. This suggests the possibility that irradiation converts a portion of the sulfur in wool to a volatile form, for example, hydrogen sulfide. Hydrogen sulfide is readily oxidized to sulfuric acid, which would account for the comparative ease with

which some of the disulfide sulfur in wool is converted to sulfate sulfur. In view of the great difficulty with which even small amounts of sulfur in wool are oxidized to sulfate by oxidizing reagents [19, 20], the ease of oxidation of sulfur to sulfate by irradiation cannot be emphasized too strongly. It should be noted that while the total sulfur and sulfate sulfur contents of the alkali-treated sample are higher than those of the acid-treated sample, the total sulfur after extraction of the wool with pyridine is the same for both samples. These results are also readily explained on the assumption that hydrogen sulfide is formed as an intermediate product. It is obvious that the hydrogen sulfide would be volatile in the presence of acids but would react with alkali to form a nonvolatile compound.

The experimental results reported in this paper indicate that although the photochemical decomposition of wool involves an oxidation reaction, the mechanism of the reaction is very different from that of such oxidizing reagents as hydrogen peroxide.[5] Further evidence supporting this is obtained by subjecting the exposed samples to the lead acetate test, described by the authors elsewhere [20]. The irradiated samples all gave strong positive reactions, indicating the presence of sulfide sulfur. Since it has previously been shown that the lead acetate test is negative when the sulfur is partially oxidized (for example by hydrogen peroxide to a sulfoxide or sulfone) and positive when sulfide sulfur is present, the results of the test clearly demonstrate the existence of at least two mechanisms for the oxidation of sulfur in wool.

The authors express their appreciation to G. E. Hopkins, Bigelow-Sanford Carpet Co., Inc., for furnishing a number of the light-exposed samples of wool used in this work.

IV. REFERENCES

[Bracketed numbers are citations corresponding to references in brackets in the text]

[1] J. Research NBS **7,** 1179 (1931) RP395.
[2] J. Research NBS **13,** 151 (1934) RP697.
[3] J. Phys. Chem. **32,** 1,263 (1928).
[4] Biochem. Z. **239,** 250 (1931).
[5] Fabrics Coordinating Research Dept. Sci. Ind. Res. First Rep. **10** (1926).
[6] Fabrics Coordinating Research Dept. Sci. Ind. Res. Second Rep. **95** (1930).
[7] Wyoming Agr. Exp. Sta. Bul. 131 (1922).
[8] Textile World **74,** 159 (1928).
[9] J. Research NBS **15,** 63 (1935) RP810.
[10] J. Research NBS **16,** 301 (1936) RP875.
[11] Public Health Rep. 86 (1930).
[12] J. Research NBS **13,** 617 (1934) RP731.
[13] J. Textile Inst. **26,** T87 (1935).
[14] Chimica Industria (Italy) **17,** 82 (1935).
[15] Compt. Rend. **183,** 596 (1926).
[16] Textile Argus **7,** 753 (1930).
[17] J. Textile Inst. **27,** T25 (1936).
[18] Melliand Textile Monthly **2,** 9 (1930).
[19] J. Biol. Chem. **110,** 343 (1935).
[20] J. Research NBS **16,** 309 (1936) RP876.

WASHINGTON, May 16, 1936.

[5] The available data do not warrant suggesting at this time a specific mechanism for the action of light on the cystine in wool. Experiments now in progress indicate that the first step is a splitting of the disulfide group, accompanied by the liberation of hydrogen sulfide, whereas in oxidation with hydrogen peroxide intermediate products of the sulfoxide, sulfone, etc., types are formed.

U. S. DEPARTMENT OF COMMERCE NATIONAL BUREAU OF STANDARDS

RESEARCH PAPER RP905

Part of Journal of Research of the National Bureau of Standards, Volume 17, July 1936

DROP OF POTENTIAL IN THE METALLIC ELECTRODES OF CERTAIN ELECTROLYTIC CELLS

By Chester Snow

ABSTRACT

In certain precise measurements of electrolytic resistance of solutions, the platinum electrodes are necessarily very thin so that one cannot neglect the drop of potential in them. Formulas are obtained for this drop in the case of two types of cylindrical cells, one in which the current is axial, the other partly axial and partly radial. The potential admits of accurate evaluation in the first case and the results obtained confirm the method outlined for the treatment of a general shape of cell.

CONTENTS

	Page
I. Introduction	101
II. Outline of method in general	103
III. Cylindrical cell with thin disk electrodes—current in axial direction	107
IV. A cell each of whose electrodes is a thin cylindrical shell closed by a thin disk	119
V. Summary	124

I. INTRODUCTION

In work during 1915–16 in connection with the examination of various sources of error in the equipment and technique then in use for measuring the conductivity of solutions and to develop precision methods and apparatus therefor, Taylor, Bennett, and Acree [1] studied a number of important electrical and chemical factors. One of these subjects was the proper design of the metal electrodes and the glass containing vessels.

In connection with this last item the above authors noted small deviations in the apparent resistance of solutions surrounding closely spaced disk electrodes 0.1 mm thick and 5 cm in diameter, depending on whether the current entered the disk through a post welded at the center or through this post and three others 120° apart at the edge of the disk. Because of possible corresponding variations in the distribution of the current through the electrodes and solution, and of the electrode phenomena and capacitance over the electrode surface, the above authors desired equations set up for the resistance of typical disk and cylindrical cup electrodes used in their work. With the magnitude of this small factor known accurately for stated conditions it is possible to determine separately the resistance of the solution

[1] J. Am. Chem. Soc. 38, 2396, 2403, 2415 (1916).

and the effects of the series capacitance at the electrode surfaces. With this object in view, the following treatment of the resistance of the metal electrodes themselves is presented.

The total current I (t) sent through an electrolytic cell when an emf E (t) is applied to it by means of electrodes is, in general, given to a first approximation by assuming that the current distribution throughout the electrodes and solution at every instant t is that which would be produced (ultimately) by a constant emf having this instantaneous value E (t), that is, the quasi-stationary state. Let V^0 be the potential of this first approximation in the electrodes or solution. The vector current density $i^0 = -\lambda \nabla V^0$ where the conductivity λ has the value λ_e in the electrodes and λ_s in the solution. At the contact surfaces S_1 and S_2 of electrodes with the solution this potential V^0 is continuous and the normal component i_n^0 of the current density is continuous. The constant contact potential difference between solution and metal is here ignored since it cancels out of the equations connecting current and applied emf when the electrodes are both of the same material and possess the same surface characteristics. Since the current density is solenoidal, the potential V^0 satisfies Laplace's equation, and for given shape of the solution volume T_s and electrode volumes T_1 and T_2 is determined by the above boundary conditions at the internal boundaries S_1 and S_2, together with the vanishing of the normal current at the external boundaries and the assignment of V^0 or the normal current densities at the entrance section S_{01} and exit section S_{02}, where the current is led into or out of the electrodes by the lead-wires. This first approximation is never sufficiently accurate to represent the results of experiments, but if the applied emf is sufficiently small these may be generally very accurately represented by assuming the existence of a polarization film of very small thickness Δ near the contact surfaces S_1 and S_2. This electrical double-layer, which is equivalent to a capacitance per unit area $k = \frac{\epsilon}{4\pi\Delta}$ (ϵ being the dielectric constant in the film), seems to be the predominant electrostatic effect, so that any simple distribution of charge on S_1 or S_2, or on the external boundaries, is negligible compared to it. This constitutes a condenser K_1 at S_1, K_2 at S_2, and the two being in series amount to a condenser K where

$$K_1 = kS_1,\ K_2 = kS_2,\ \text{and}\ \frac{1}{K} = \frac{1}{K_1} + \frac{1}{K_2} = \frac{1}{k}\left(\frac{1}{S_1} + \frac{1}{S_2}\right),\ \text{where}\ k = \frac{\epsilon}{4\pi\Delta} \quad (1)$$

If λ_0 is the conductivity of the film, the first condenser has an internal resistance R_{01} which amounts to a shunt on it and the second R_{02}, their resistance in series being R_0, where

$$R_{01} = \frac{\Delta}{\lambda_0 S_1},\ R_{02} = \frac{\Delta}{\lambda_0 S_2},\ \text{and}\ R_0 = R_{01} + R_{02} = \frac{\Delta}{\lambda_0}\left(\frac{1}{S_1} + \frac{1}{S_2}\right) \quad (2)$$

so that

$$\gamma \equiv \frac{4\pi\lambda_0}{\epsilon} = \frac{\lambda_0}{k\Delta} = \frac{1}{R_0 K} = \frac{1}{R_{01}K_1} = \frac{1}{R_{02}K_2} \quad (3)$$

The values of these electrolytic capacities, as evaluated by experiments,[2] are so large as to indicate that the film thickness Δ is exceedingly small compared to the thickness attainable in mica condensers or air condensers, so that the capacity k per unit area is enormous. Even when there is very little evidence of the film, we may adhere to this view that Δ is very small by assuming that the film conductivity λ_0 practically short-circuits the condenser. This viewpoint then leads to the second approximation, which is generally sufficient to fit the most accurate measurements. It consists merely in viewing the cell as a leaky [3] condenser (i.e., K shunted by R_0) in series with the resistance $R_s+R_{e1}+R_{e2}$ of solution and electrodes to the whole of which the emf $E(t)$ is applied. The current $I(t)$ is then determined by the equation (where Q is the total charge on K)

$$\left(D_t+\frac{1}{R_0K}\right)Q=I \tag{4a}$$

$$E=\frac{Q}{K}+(R_s+R_e)I, \text{ where } R_e=R_{e1}+R_{e2} \tag{4b}$$

with the initial conditions $E=I=0$ when $t<t_1$, so that $Q=0$ when $t=t_1+0$.

A justification, or rather formulation, of this assumption for the general case is made in the following section. Later a case is treated which is capable of a more accurate solution and this serves to confirm the assumption that the second approximation thus outlined is generally sufficient. The elimination of Q between (4a) and (4b) gives

$$\left[D_t+\left(\frac{1}{R_0}+\frac{1}{R_s+R_e}\right)\frac{1}{K}\right]I=\left(D_t+\frac{1}{R_0K}\right)\frac{E}{R_s+R_e} \tag{5a}$$

so that

$$I(t)=\frac{1}{R_s+R_e}\left[E(t)-\frac{1}{R(_s+R_e)K}\int_{t_1}^{t}E(\tau)e^{-\left(\frac{1}{R_0}+\frac{1}{R_s+R_0}\right)\frac{t-\tau}{K}}d\tau\right] \text{ for } t>t_1 \tag{5b}$$

In case the emf is simply periodic, $E(t)$=real part of $E_0e^{i\omega t}$ and when transients have died out, I is $R_e\, I_0e^{i\omega t}$, where the complex constant I_0 is given by

$$I_0=\frac{E_0}{R_s+R_e+\dfrac{R_0}{1+i\omega KR_0}}$$

II. OUTLINE OF METHOD IN GENERAL

The vector current density i is given at all points by $i=-\lambda\nabla V$, where $\lambda=\lambda_e$ in T_1 and T_2 and $\lambda=\lambda_s$ in T_s (6)

Since i is everywhere solenoidal, V must, at every instant, satisfy

$$\nabla^2V=0 \text{ in } T_1,\ T_2, \text{ and } T_s \tag{7}$$

[2] Taylor, Bennett, and Acree J. Am. Chem. Soc. 38 2408, 2427 (1916).
[3] Taylor, Bennett, and Acree J. Am. Chem Soc. 38 2408, 2415 (1916).

The boundary conditions at the small plane entrance-section S_{01} (fig. 1) and the small plane exit section S_{02} may be taken as

$$V=\frac{E(t)}{2}\text{(uniform) over } S_{01} \tag{8a}$$

$$V=\frac{-E(t)}{2}\text{(uniform) over } S_{02} \tag{8b}$$

In some cases, however, it is just as near the truth, and more convenient, to take instead of these, the boundary conditions

$i_{0n1}=\frac{I}{S_{01}}$ (uniform) over S_{01} and $V=\frac{E}{2}$ at some point on outer edge of S_{01} (8a′)

$i_{0n2}=\frac{I}{S_{02}}$ (uniform) over S_{02} and $V=\frac{-E}{2}$ at some point on outer edge of S'_{02} (8b′)

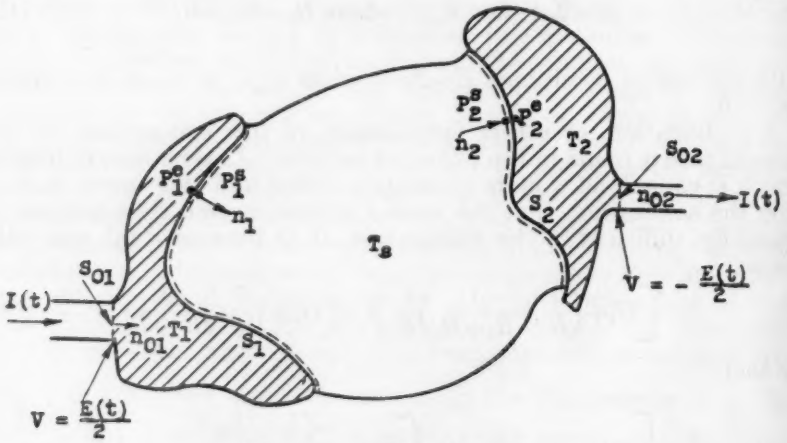

FIGURE 1.—*Electrolytic cell.*

Volumes T_1 and T_2 are electrodes and volume T_s, the solution.

The boundary conditions at the internal boundaries S_1 and S_2 are

$$i_{n_1} \text{ is continuous at } S_1 \tag{9a}$$

$$i_{n_2} \text{ is continuous at } S_2 \tag{9b}$$

and

$$(D_i+\gamma)(V_{e1}-V_{s1})=\frac{i_{n_1}}{k}=\frac{4\pi\Delta}{\epsilon}i_{n_1} \text{ at } S_1 \tag{10a}$$

$$(D_i+\gamma)(V_{s2}-V_{e2})=\frac{i_{n_2}}{k}=\frac{4\pi\Delta}{\epsilon}i_{n_2} \text{ at } S_2 \tag{10b}$$

and finally,

$$i_n=0 \text{ at all external boundaries of } T_1,\ T_2, \text{ and } T_s \tag{11}$$

The surface density of charge σ_1 on the element dS_1 of the condenser K_1 (at the point P_1^e of fig. 1) is

$$\sigma_1=k(V_{e_1}-V_{s1}) \tag{12a}$$

where V_{e1} is the potential at P_1^e in the electrode and V_{s1} at P_1^s in the solution. The conservation of electricity is represented by the equation

$$(D_t+\gamma)\sigma_1=i_{n_1} \tag{13a}$$

From the two latter equations, the boundary condition (10a) is derived. Equation 10b is similarly a consequence of

$$\sigma_2=k(V_{s2}-V_{e2}) \tag{12b}$$

and

$$(D+\gamma)\sigma_2=i_{n_2} \tag{13b}$$

The sense of the conditions (9) is that i_{n_1} at $P_1^e=i_{n_1}$ at $P_1^s=$ normal current density in the solution beyond the film which, of course, is considered to be of no thickness at all so far as we are concerned with the determination of the potential distribution outside it. If Q_1 and Q_2 are the total charges on condensers K_1 and K_2, then

$$Q_1\equiv\int\int_{S_1}\sigma_1 dS_1 \text{ and } Q_2\equiv\int\int_{S_2}\sigma_2 dS_2$$

and

$$\int\int_{S_1} i_{n_1}dS_1=\int\int i_{n_2}dS_2=I$$

Let $\overline{V}_{e1}=\frac{1}{S_1}\int\int_{S_1} V_{e1}dS_1=$average over S_1 of the electrode potential

and $\overline{V}_{s1}=$the average over S_1 of the solution potential and similarly let $\overline{V}_{s2}$ and $\overline{V}_{e2}$ denote averages over S_2. Then by integration of (12) and (13) over the respective surface S_1 and S_2 we obtain, by use of (1)

$$Q_1=K_1(\overline{V}_{e1}-\overline{V}_{s1}) \tag{14a}$$

$$(D_t+\gamma)Q_1=I \tag{15a}$$

and

$$Q_2=K_2(\overline{V}_{s_2}-\overline{V}_{e_2}) \tag{14b}$$

$$(D_t+\gamma)Q_2=I \tag{15b}$$

From (15a) and (15b) we obtain $(D_t+\gamma)\ (Q_1-Q_2)=0$. We assume that $E\ (t)$ (and hence $I\ (t)$, Q_1, and Q_2) is always finite, but that E and hence also I may be discontinuous at certain instants and that $E\equiv 0$ if $-\infty<t<t_1$, so that $Q_1\equiv Q_2\equiv I\equiv 0$ if $t<t_1$. But the last equation gives $Q_1-Q_2=Ce^{-\gamma t}$ when $t>t_1$, while (15a) and (15b) show that $Q_1(t_1+0)=Q_2(t_1+0)=0$ so that $C=0$, and we obtain

$Q_1=Q_2$ and $S_1(\overline{V}_{e1}-\overline{V}_{s1})=S_2(\overline{V}_{s2}-\overline{V}_{e2})$ at all times. (16)

Let $Q=Q_1=Q_2$. Then by (16) the two equations 15 are identical and may be written (by use of 3)

$$\left(D_t+\frac{1}{R_0K}\right)Q=I \text{ (which is the equation 4a)} \tag{17}$$

Also, by dividing (14a) by K_1 and (14b) by K_2 and adding, we find, by use of (1)

$$\frac{Q}{K}=\overline{V}_{s1}-\overline{V}_{e1}+\overline{V}_{s2}-\overline{V}_{e2} \text{ which may be written}$$

$$E=\frac{Q}{K}+(\overline{V}_{s1}-\overline{V}_{s2})+\left(\frac{E}{2}-\overline{V}_{e1}\right)+\left(\overline{V}_{e2}+\frac{E}{2}\right) \tag{18}$$

The first approximation V^0 for the potential distribution is determined by placing $\Delta=0$ in the second members of the two boundary conditions (10). The initial condition used in deriving (16) then shows in similar fashion that the conditions (10), reduce merely to the requirement of continuity of V^0 at S_1 and S_2 so that $\frac{V^0}{I}$ is a function of x, y, z only throughout the compound conductor $T_1+T_s+T_2$, which represents the potential distribution when it carries unit steady current. When V^0 is found one may compute the total resistance R of this compound conductor so that R will be a known function of λ_s, λ_e and the linear dimensions entering into the description of this compound conductor. In case R comes out as the sum of two functions in one of which only the conductivity, λ_s, appears, and only λ_e in the other, the first could be called the solution resistance R_s, the second the resistance R_e of the two electrodes. In general, λ_e and λ_s will be so involved in the expression for R that in order to resolve it into $R=R_s+R_{e1}+R_{e2}$ we must adopt some arbitrary definitions of these resistances.

Since $\frac{E}{2}$ is the potential at some chosen point on the edge of the entrance surface S_{01} and $\frac{-E}{2}$ its value at some part on the edge of S_{02}, we define arbitrarily

$$R_s\equiv\frac{\overline{V}^0_{s1}-\overline{V}^0_{s2}}{I},\ R_{e1}\equiv\frac{\frac{E}{2}-\overline{V}^0_{e1}}{I},\text{ and } R_{e2}\equiv\frac{\overline{V}^0_{e2}+\frac{E}{2}}{I} \tag{19a}$$

so that since $V^0_{e1}-V^0_{s1}=V^0_{s2}-V^0_{e2}=0$

$$\frac{E}{I}=R_s+R_{e1}+R_{e2}\equiv R \tag{19b}$$

When the first approximation V^0 for the potential has been found the use of V^0 for V in computing the mean potential drops in the second member of (18) gives

$$E=\frac{Q}{K}+(R_s+R_e)I, \text{ where } R_e=R_{e1}+R_{e2}, \tag{20}$$

which is equation 4b, so that (17) and (20) give the second approximation to the current, which is generally sufficient.

The conclusions so far are based merely upon the smallness of Δ. But the exact evaluation of the potential V^0 which is necessary to determine R is in general difficult. There is, however, another consideration equally important which results in a further simplification

in the evaluation of V^0. The metallic conductivity λ_e is so large in comparison with that λ_s of the solution that the principal part of th potential V_s^0 in the solution (say $V_s^{0\prime}$), may be obtained by assuming that the contact surfaces S_1 and S_2 are equipotential surfaces. This assumption determines the principal part of R_s by (19a) (say R_s') and also the principal parts say $i_{n1}^{0\prime}$, $i_{n2}^{0\prime}$ of the normal components of current i_{n1}^0 and i_{n2}^0 at S_1 and S_2. The principal part of the potential in the electrodes is then determined by making $i_{n1}=i_{n1}^{0\prime}$ at S_1, etc., together with the remaining boundary conditions. Then using (19), the principal part of the electrode resistance R_e, say R_e' is found. Since R_e' is proportional to $\frac{1}{\lambda_e}$ and R_s' to $\frac{1}{\lambda_s}$ it is evident that R_s' is so small relatively that no further modification of it will be necessary. Neither will it be necessary to go further with the evaluation of R_s, for any further terms would be of the order of $\frac{1}{\lambda_e^2}$ as will be seen in section III.

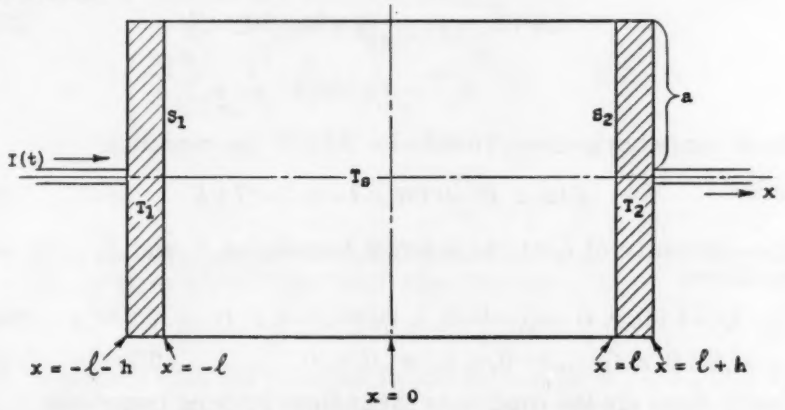

FIGURE 2.—*Section of a cylindrical shell by an axial plane.*

It should be noted that the electrode resistances thus defined are quite different from what would be obtained by evaluating the potential distribution *in the electrodes* on the assumption that S_1 and S_2 are equipotential surfaces. Such a boundary condition, while sufficient for the determination of the potential in the solution and its resistance R_s, is not applicable for determining electrode potentials. It is shown in section III that the electrode resistances obtained in this way are not even approximately correct.

III. CYLINDRICAL CELL WITH THIN DISK ELECTRODES—CURRENT IN AXIAL DIRECTION

Figure 2 represents a section by a plane through the x axis of a cylindrical cell which has as electrodes circular plates of radius a. The part $-l<x<l$ is filled with an electrolyte. The plates of thickness h, for $-l-h<x<-l$ and $l<x<l+h$ are circular disks of platinum very thin, say $h=0.02$ cm. The current $I(t)$ enters along a thin lead-in wire of radius b coaxial with the x axis, so that the potential V, either in the case of steady currents or variable with time, does

not depend upon the cylindrical coordinate θ, but only on the cylindrical coordinates x and r and the time t. As explained in equations 1 to 4

$$\left.\begin{aligned} K_1=K_2=\pi a^2k \text{ so that } K=\frac{\pi a^2k}{2}=\frac{\epsilon a^2}{8\Delta} \\ R_{01}=R_{02}=\frac{\Delta}{\pi a^2\lambda_0} \text{ so that } R_0=\frac{2\Delta}{\pi a^2\lambda_0} \end{aligned}\right\} \tag{21}$$

The boundary condition at the extreme left, where the current enters through the wire of small radius b (of the same order as h), will be taken

$$i_x(-l-h, r, t)=\frac{I(t)}{\pi b^2} \text{ when } 0\leqq r<b \tag{22a}$$

$$=0 \text{ when } b<r<a$$

At the extreme right

$$i_x(l+h, r, t)=\frac{I(t)}{\pi b^2} \text{ when } 0\leqq r<b \tag{22b}$$

$$=0 \text{ when } b<r<a$$

On all convex cylindrical boundaries there is the condition

$$i_r(x, a, t)=0 \text{ for } -l-h<x<l+h \tag{23}$$

The continuity of i_x at the internal boundaries S_1 and S_2 gives the conditions

$$i_x(-l+0, r, t)=i_x(-l-0, r, t)\,(\equiv i_x(-l, r, t)\text{----}0\leqq r<a \tag{24a}$$

$$i_x(l+0, r, t)=i_x(l-0, r, t)\,(\equiv i_x(l, r, t)\text{----------}0\leqq r<a \tag{24b}$$

Finally there are the conditions (5) at these internal boundaries

$$(D_t+\gamma)\sigma_1=i_x(-l, r, t), \text{ where } \sigma_1(r, t)=k[V(-l-0)-V(-l+0)] \tag{25a}$$

$$(D_t+\gamma)\sigma_2=i_x(l, r, t), \text{ where } \sigma_2(r, t)=k[V(l-0)-V(l+0)] \tag{25b}$$

Since V will be an odd function of x, this brings about a simplification in that σ_2 becomes equal to σ_1, and when one of the pair of equations 22, 24, or 25 is satisfied, the other will also be true.

For constructing the potential V we have the following type of particular solution of Laplace's equation

$$V=\left(A\sinh\frac{\alpha x}{a}+B\cosh\frac{\alpha x}{a}\right)J_0\left(\frac{\alpha r}{a}\right), \text{ where } J_0 \text{ is Bessel's function,}$$

the other solution of Bessel's equation being ruled out by the requirement of finiteness on the x-axis, where $r=0$.

Since $D_r J_0\left(\frac{\alpha r}{a}\right)=-\frac{\alpha}{a}J_1\left(\frac{\alpha r}{a}\right)$ the boundary condition (20) requires that α be a solution of the equation

$$J_1(\alpha)=0 \tag{26}$$

In what follows we use α_n to denote the nth positive root of this equation, of which there are an infinite number. We require the use of Dini's theorem for the development of a function of x, say $f(x)$, for the range $0 < x \leqq 1$, where $\int_0^1 f(x)dx$ converges absolutely

$$f(x)=c_0+\sum_{n=1}^{\infty}c_nJ_0(\alpha_n x), \tag{27}$$

where

$$c_0=2\int_0^1 xf(x)dx \text{ and } c_n=\frac{2}{J_0^2(a_n)}\int_0^1 xf(x)J_0(\alpha_n x)dx \text{ for } n>0$$

When the function has a finite discontinuity at $x=x_0$, the sum of this series is $\frac{1}{2}\left[f(x_0+0)+f(x_0-0)\right]$

As a special case of (27) we need the following development of the discontinuous function of r occurring in (22)

$$\left.\frac{I(t)}{\pi a^2}\left\{1+\frac{2a}{b}\sum_{n=1}^{\infty}\frac{J_1\left(\frac{\alpha_n b}{a}\right)}{\alpha_n J^2{}_0(\alpha_n)}\cdot J_0\left(\frac{\alpha_n r}{a}\right)\right\}\right.=\frac{I(t)}{\pi b^2} \text{ ------ if } 0\leqq r<b$$

$$=o \text{ -------- if } b<r\leqq a$$

$$=\frac{I(t)}{2\pi b^2} \text{ ---- if } r=b \tag{28}$$

If $E(t)$ is the difference of potential applied to the cell, i. e., between the wire surfaces where they touch the electrodes, then

$$E(t)=V(-l-h,\ b,\ t)-V(l+h,\ b,\ t) \tag{29}$$

It is evident that the potential in the three regions T_1, T_s, and T_2, must then have the following form

$$V(x,\ r,\ t)=\frac{1}{2}E(t)-I(t)\left\{\frac{x+l+h}{\pi a^2\lambda_s}+\right.$$

$$\left.\frac{2}{\pi b\lambda_s}\sum_{n=1}^{\infty}\frac{J_1\left(\frac{\alpha_n b}{a}\right)\left[\cosh\left(\frac{\alpha_n h}{a}\right)J_0\left(\frac{\alpha_n b}{a}\right)-\cosh\frac{\alpha_n}{a}(x+l)J_0\left(\frac{\alpha_n r}{a}\right)\right]}{\alpha_n{}^2\sinh\left(\frac{a_n h}{a}\right)J_0{}^2(\alpha_n)}\right\} \tag{30}$$

$$-\frac{1}{\pi a\lambda_s}\sum_{n=1}^{\infty}\frac{I_n(t)\left[\cosh\frac{\alpha_n}{a}(x+l+h)J_0\left(\frac{\alpha_n r}{a}\right)-J_0\left(\frac{\alpha_n b}{a}\right)\right]}{\alpha_n\sinh\left(\frac{\alpha_n h}{a}\right)}$$

when $-l-h<x<-l$

$$=-\frac{xI(t)}{\pi a^2\lambda_s}-\frac{1}{\pi a\lambda_s}\sum_{n=1}^{\infty}\frac{I_n(t)\sinh\left(\frac{\alpha_n x}{a}\right)}{\alpha_n\cosh\left(\frac{\alpha_n l}{a}\right)}J_0\left(\frac{\alpha_n r}{a}\right)$$

when $-l<x<l$

$$=-\frac{1}{2}E(t)+I(t)\left\{\frac{l+h-x}{\pi a^2\lambda_s}+\right.$$

$$\left.\frac{2}{\pi b\lambda_s}\sum_{n=1}^{\infty}\frac{J_1\left(\frac{\alpha_n b}{a}\right)\left[\cosh\left(\frac{\alpha_n h}{a}\right)J_0\left(\frac{\alpha_n b}{a}\right)-\cosh\frac{\alpha_n}{a}(x-l)J_0\left(\frac{\alpha_n r}{a}\right)\right]}{{\alpha_n}^2\sinh\left(\frac{\alpha_n h}{a}\right)J_0^2(\alpha_n)}\right\}$$

$$+\frac{1}{\pi a\lambda_s}\sum_{n=1}^{\infty}\frac{I_n(t)\left[\cosh\frac{\alpha_n}{a}(x-l-h)J_0\left(\frac{\alpha_n r}{a}\right)-J_0\left(\frac{\alpha_n b}{a}\right)\right]}{\alpha_n\sinh\left(\frac{\alpha_n h}{a}\right)}$$

when $l<x<l+h$

From this, the x component of current density is

$$i_x(x,r,t)=\frac{I(t)}{\pi a^2}\left\{1-\frac{2a}{b}\sum_{n=1}^{\infty}\frac{\sinh\frac{\alpha_n}{a}(x+l)J_1\left(\frac{\alpha_n b}{a}\right)J_0\left(\frac{\alpha_n r}{a}\right)}{\alpha_n\sinh\left(\frac{\alpha_n h}{a}\right)\cdot J^2{}_0(\alpha_n)}\right\} \tag{31}$$

$$+\frac{1}{\pi a^2}\sum_{n=1}^{\infty}\frac{I_n(t)\sinh\frac{\alpha_n}{a}(x+l+h)}{\sinh\left(\frac{\alpha_n h}{a}\right)}J_0\left(\frac{\alpha_n r}{a}\right)\text{when } -l-h<x<-l$$

$$=\frac{I(t)}{\pi a^2}+\frac{1}{\pi a^2}\sum_{n=1}^{\infty}\frac{I_n(t)\cosh\left(\frac{\alpha_n x}{a}\right)}{\cosh\left(\frac{\alpha_n l}{a}\right)}\cdot J_0\left(\frac{\alpha_n r}{a}\right)\text{when } -l<x<l$$

$$=\frac{I(t)}{\pi a^2}\left\{1+\frac{2a}{b}\sum_{n=1}^{\infty}\frac{\sinh\frac{\alpha_n}{a}(x-l)J_1\left(\frac{\alpha_n b}{a}\right)J_0\left(\frac{\alpha_n r}{a}\right)}{\alpha_n\sinh\left(\frac{\alpha_n h}{a}\right)J_0^2(\alpha_n)}\right\}$$

$$-\frac{1}{\pi a^2}\sum_{n=1}^{\infty}\frac{I_n(t)\sinh\frac{\alpha_n}{a}(x-l-h)J_0\left(\frac{\alpha_n r}{a}\right)}{\sinh\left(\frac{\alpha_n h}{a}\right)},\text{when } l<x<l+h.$$

Obviously (30) is a solution of (7) satisfying the condition (23) by reason of (26) and also the conditions (24). From (31) we find

$$i_z(l, r, t)=i_z(-l, r, t)=\frac{I(t)}{\pi a^2}+\frac{1}{\pi a^2}\sum_1^\infty I_n(t)J_0\left(\frac{\alpha_n r}{a}\right). \tag{32}$$

Also, the equation 31 shows by reference to (28) that the conditions (22) are also satisfied. Hence, all but the last conditions (25) are satisfied without placing any restrictions upon the coefficients $I_n(t)$. The first approximation V^0 will only differ from the more precise potential V by the manner in which we choose these coefficients I_n.

We introduce the abbreviations for $n=1, 2, 3, - - - \infty$

$$r_n\equiv\frac{2}{\pi a\lambda_e}\frac{J_0\left(\frac{\alpha_n b}{a}\right)}{\alpha_n \sinh\left(\frac{\alpha_n h}{a}\right)} \tag{33a}$$

$$\rho_n\equiv\frac{4}{\pi b\lambda_e}\frac{J_1\left(\frac{\alpha_n b}{a}\right)}{\alpha_n^2 J_0^2(\alpha_n) \sinh\left(\frac{\alpha_n h}{a}\right)} \tag{33b}$$

$$\frac{1}{\beta_n K}\equiv\frac{2}{\pi a\lambda_s\alpha_n}\left[\tanh\left(\frac{\alpha_n l}{a}\right)+\frac{\lambda_s}{\lambda_e}\coth\left(\frac{\alpha_n h}{a}\right)\right] \tag{33c}$$

$$R_e'\equiv\frac{2h}{\pi a^2\lambda_e}+\sum_{n=1}^\infty \rho_n \cosh\left(\frac{\alpha_n h}{a}\right)J_0\left(\frac{\alpha_n b}{a}\right) \tag{33d}$$

Then from (30) we find

$$V_{e1}\equiv V(-l-0, r, t)=\frac{E}{2}-\frac{R_e'}{2}I+\frac{1}{2}\sum_1^\infty r_n I_n+\frac{1}{2}\sum_1^\infty J_0\left(\frac{\alpha_n r}{a}\right)\left[\rho_n I-\frac{2I_n\coth\left(\frac{\alpha_n h}{a}\right)}{\pi a\lambda_e\alpha_n}\right] \tag{34a}$$

$$V_{s1}=V(-l+0, r, t)=\frac{l}{\pi a^2\lambda_s}I+\frac{1}{\pi a\lambda_s}\sum_1^\infty \frac{I_n J_0\left(\frac{\alpha_n r}{a}\right)\tanh\frac{\alpha_n l}{a}}{\alpha_n} \tag{34b}$$

so that

$$V_{e1}-V_{s1}=\frac{E}{2}-\left(\frac{l}{\pi a^2\lambda_s}+\frac{R_e'}{2}\right)I+\frac{1}{2}\sum_1^\infty r_n I_n+\frac{1}{2}\sum_1^\infty J_0\left(\frac{\alpha_n r}{a}\right)\left[\rho_n I-\frac{I_n}{\beta_n K}\right] \tag{34c}$$

and

$$V_{s2}=-V_{s1} \text{ and } V_{e2}=-V_{e1}$$

so that

$$\overline{V}_{e1}-\overline{V}_{e2}=\frac{2l}{\pi a^2\lambda_s}I \tag{35}$$

and

$$\frac{E}{2}-\overline{V}_{e1}=\overline{V}_{e2}+\frac{E}{2}=\frac{R_e'}{2}I-\frac{1}{2}\sum_1^\infty r_nI_n \tag{36}$$

Now the first approximation V^0 to the potential distribution is that determined by replacing the boundary conditions (25) by the mere requirement of continuity of V^0 at the internal boundaries S_1 and S_2. This, by (34c) would require that we choose the coefficient I_n as

$$I_n=I_n^0=k\beta_n\rho_nI^0 \tag{37}$$

which, being used in (36), give

$$\frac{\frac{E}{2}-V_{e1}^0}{I}=R_{e1}=R_{e2}=\frac{1}{2}R_e'-\frac{1}{2}K\sum_1^\infty r_n\rho_n\beta_n$$

so that the total electrode resistance is

$$R_e=R_e'-K\sum_1^\infty r_n\rho_n\beta_n=\frac{2h}{\pi a^2\lambda_e}+\sum_1^\infty \rho_n J_0\left(\frac{\alpha_n b}{a}\right)\cdot$$

$$\left\{\cosh\left(\frac{\alpha_n h}{a}\right)-\frac{\lambda_s}{\lambda_e\sinh\left(\frac{\alpha_n h}{a}\right)\left[\tanh\left(\frac{\alpha_n l}{a}\right)+\frac{\lambda_s}{\lambda_e}\coth\left(\frac{\alpha_n h}{a}\right)\right]}\right\} \tag{38}$$

$$=\frac{2h}{\pi a^2\lambda_e}+\frac{4}{\pi b\lambda_e}\sum_1^\infty\frac{J_0\left(\frac{\alpha_n b}{a}\right)J_1\left(\frac{\alpha_n b}{a}\right)}{\alpha_n^2J_0^2(\alpha_n)\sinh\left(\frac{\alpha_n h}{a}\right)}\cdot$$

$$\left\{\cosh\frac{\alpha_n h}{a}-\frac{\lambda_s}{\lambda_e\sinh\left(\frac{\alpha_n h}{a}\right)\left[\tanh\left(\frac{\alpha_n l}{a}\right)+\frac{\lambda_s}{\lambda_e}\coth\left(\frac{\alpha_n h}{a}\right)\right]}\right\}$$

On neglecting terms in $\frac{1}{\lambda^2_e}$ this becomes

$$R_e=\frac{2h}{\pi a^2\lambda_e}+\frac{4}{\pi b\lambda_e}\sum_1^\infty\frac{J_0\left(\frac{\alpha_n b}{a}\right)J_1\left(\frac{\alpha_n b}{a}\right)}{\alpha_n^2J_0^2(\alpha_n)\sinh\left(\frac{\alpha_n h}{a}\right)}$$

$$\left\{\cosh\left(\frac{\alpha_n h}{a}\right)-\frac{\lambda_s\coth\left(\frac{\alpha_n l}{a}\right)}{\lambda_e\sinh\left(\frac{\alpha_n h}{a}\right)}\right\} \tag{38'}$$

On neglecting terms in $\frac{1}{\lambda^2_e}$ this becomes

$$R_e=R_e'=\frac{2h}{\pi a^2\lambda_e}+\frac{4}{\pi b\lambda_e}\sum_1^\infty \frac{J_0\left(\frac{\alpha_n b}{a}\right)J_1\left(\frac{\alpha_n b}{a}\right)}{\alpha_n^2 J_0^2(\alpha_n)\tanh\left(\frac{\alpha_n h}{a}\right)} \qquad (38'')$$

which does not involve the conductivity λ_s of the solution, and is a function of the linear dimensions h, a, and b of the electrodes only.

Equation 35 gives $R_s=\frac{2l}{\pi a^2\lambda_s}$=resistance of the solution. (39)

If what we have called the second approximation to the current is sufficient, then (38″) and (39) give the total resistance $R=R_s+R'_e$ to be used in equation 4b. Equations 38 and 39 give the exact values of R_e and R_s defined by (19a) for they are derived from an exact evaluation of V^0. Since, however, (38″) differs from (39) by terms of the order $\frac{1}{\lambda_e}$, the results here obtained confirm the statements made after equation 20 as to the approximate method of evaluating R'_e.

To illustrate the general mode of the approximate evaluation of V^0, we note that the approximate potential distribution in the solution, based on the assumption that the contact surfaces S_1 and S_2 are equipotential surfaces, is given by taking $I_n=0$ as shown by (34b). Whatever value we take for I_n, the solution resistance is given by (39). The evaluation of the potential distribution throughout the electrodes, however, is made by assuming that the normal current there is continuous with that corresponding to this approximate potential in the solution, so that with $I_n=0$, the surfaces S_1 and S_2 are not equipotential, as shown by (34a). The value $I_n=0$ then leads to $R_e=R'_e$ by (36), as predicted in section II.

It is worth while to illustrate at this point the misconception that might arise from calling the resistance R_e, as defined in (19), the electrode resistance. That $\frac{R'_e}{2}$ is not the resistance of one electrode when the contact surface, say S_1, is equipotential is evident from the fact that to make S_1' equipotential (on the electrode side) we must, by equation 34a, take $I_n=I\frac{\pi a\lambda_e}{2}\rho_n\alpha_n\tanh\left(\frac{\alpha_n h}{a}\right)$ in which case we find

$$\frac{E}{2}-\overline{V}_{e1}=\frac{I}{2}\left[R'_e-\sum_1^\infty \frac{\rho_n J_0\left(\frac{\alpha_n h}{a}\right)}{\cosh\left(\frac{\alpha_n h}{a}\right)}\right]$$

which would give for the resistance of the electrodes, when S_1 and S_2 are equipotential surfaces

$$\frac{2h}{\pi a^2\lambda_e}+\sum_1^\infty \rho_n J_0\left(\frac{\alpha_n b}{a}\right)\left[\cosh\left(\frac{\alpha_n b}{a}\right)-\frac{1}{\cosh\left(\frac{\alpha_n h}{a}\right)}\right]$$

which is not even an approximation to the value R'_e when $\frac{b}{a}$ is small.

The present problem admits of an exact formulation of the current $I(t)$ produced by an arbitrary emf E from which it is easy to derive a third approximation. This enables one to estimate the degree of validity of the second approximation.

By (25) and (34c) we find

$$\frac{\pi a^2\sigma(r,\,t)}{K}=E-(R_s+R'_e)I+\sum_1^\infty r_nI_n+\sum_1^\infty J_0\left(\frac{\alpha_n r}{a}\right)\left[\rho_nI-\frac{I_n}{\beta_nK}\right] \quad (40)$$

Since the total charge $Q=2\int_0^a r\sigma dr$ this gives

$$E=\frac{Q}{K}+(R_s+R'_e)I-\sum_1^\infty r_nI_n \quad (41)$$

so that equation 40 may be written

$$\pi a^2\sigma(r,\,t)=Q+K\sum_1^\infty J_0\left(\frac{\alpha_n r}{a}\right)\left[\rho_nI-\frac{I_n}{\beta_nK}\right] \quad (42)$$

The boundary equation 25, which must be satisfied for all values of r in the exact solution, may be written by reference to (32)

$$(D_t+\gamma)\pi a^2\sigma(r,\,t)=I+\sum_1^\infty I_nJ_0\left(\frac{\alpha_n r}{a}\right) \quad (43)$$

Introducing into this the expression (42) for σ gives on equating corresponding coefficients of $J\left(\frac{\alpha_n r}{a}\right)$, the relations

$$(D_t+\gamma)Q=I \text{ (which is merely equation 4a)} \quad (44)$$

and

$$(D_t+\gamma+\beta_n)\,I_n=K\rho_n\beta_n(D_t+\gamma)\,I \text{ for } n=1,\,2,\,3,\,\ldots\ldots\ldots\infty \quad (45)$$

The integral of (44) is

$$Q(t)=\int_{t_1}^t I(\tau)e^{-\gamma(t-\tau)}d\tau \text{ for } t>t_1 \quad (46)$$

and the integral of (45) is

$$I_n(t)=K\beta_n\rho_nI(t)-K\beta_n^2\rho_n\int_{t_1}^t I(\tau)e^{-(\gamma+\beta_n)(t-\tau)}d\tau \text{ for } t>t_1 \quad (47)$$

With these values of Q and I_n the equation 41 becomes the following integral equation of Volterra's type to determine I (t) for $t>t_1$.

$$(R_s+R_e)e^{\gamma t}I(t)+\int_{t_1}^t e^{\gamma\tau}E(\tau).N(t-\tau)d\tau=e^{\gamma t}E(t) \quad (48)$$

where the nucleus N is defined by a convergent series for $\tau>0$

$$N(\tau)=\sum_{n=0}^{\infty}a_n e^{-\beta_n\tau} \tag{49}$$

where

$$a_0=\frac{1}{K},\ a_n=Kr_n\rho_n\beta_n^2,\ \beta_0=0, \text{ and for } n>0\ \beta_n \text{ is defined by (35c)} \tag{50}$$

If $F(\tau)$ denotes the resolving nucleus of the given nucleus N, then the unique solution of (48) is

$$\frac{e^{\gamma t}E(t)}{R_s+R_e}+\int_{t_1}^{t}e^{\gamma\tau}E(\tau)F(t-\tau)d\tau=e^{\gamma t}I(t) \tag{51}$$

Considering I given and E unknown, this is an integral equation of the same type as (48) with a nucleus F of the same type of function as N so that reciprocally (48) is the unique solution of (51) and N the resolving nucleus of F. The particular nature of the coefficients a_n is not essential in finding F. To show this we may construct, with the coefficients a_n, a function ψ of the complex variable β by

$$\psi(\beta)\equiv R_s+R_e-\sum_{n=0}^{\infty}\frac{a_n}{\beta-\beta_n} \text{ whose poles are at } \beta=\beta_n \tag{52}$$

Let β'_s for $s=0, 1, 2, \text{———} \infty$ denote the characteristic values which are solutions of the equation

$$\psi(\beta)=0 \tag{53}$$

Then

$$\frac{1}{2\pi i}\int\frac{d\beta'}{(\beta'-\beta)\psi(\beta')}=\frac{1}{R_s+R_e}=\frac{1}{\psi(\infty)} \tag{54}$$

where the integral is taken around a circle in the complex β' plane with center at the origin and infinite radius. Shrinking this path down to separate contours around the individual poles of the integrand which are at $\beta'=\beta$ and $\beta'=\beta'_s$ where $s=0, 1, 2, \text{———} \infty$, gives after evaluating each contour integral by Cauchy's theorem

$$\frac{1}{\psi(\beta)}=\frac{1}{R_s+R_e}-\sum_{n=0}^{\infty}\frac{A_n}{\beta-\beta'_n} \tag{55}$$

where

$$A_n=-\frac{1}{\psi'(\beta'_n)} \text{ for } n=0, 1, 2, \text{———} \left(\text{and } \psi'(\beta)\equiv\frac{d\psi(\beta)}{d\beta}\right) \tag{56}$$

Equation 55 is in a certain respect reciprocal to (52). If β takes on one of the values β_m ($m=0, 1, 2, \text{———}$), which is a pole of ψ (β) the first member of (55) vanishes, giving the relations

$$0=\frac{1}{R_s+R_e}-\sum_{n=0}^{\infty}\frac{A_n}{\beta_m-\beta'_n} \text{ for } m=0, 1, 2, 3\text{———}\infty \tag{57}$$

It is easy to see that the resolving nucleus F is given by

$$F(\tau)=\sum_{n=0}^{\infty}A_n e^{-\beta'_n\tau}$$

which is similar to (49) (58)

For if this series be substituted in the integral equation 48 with series (49) for N, the equation becomes

$$\int_{t_1}^{t}e^{\gamma\tau}E(\tau)d\tau\sum_{m=0}^{\infty}\left\{e^{-\beta'_m(t-\tau)}A_m\left[R_s+R_e=\sum_{n=0}^{\infty}\frac{a_n}{\beta'_m-\beta_n}\right]\right.$$
$$\left.+e^{-\beta_m(t-\tau)}a_m\left[\frac{1}{R_s+R_e}-\sum_{n=0}^{\infty}\frac{A_n}{\beta_m-\beta'_n}\right]\right\}=0$$

that is, by reference to (52) and (55)

$$\int_{t_1}^{t}e^{\gamma\tau}.E(\tau)d\tau\sum_{m=0}^{\infty}\left\{e^{-\beta'_m(t-\tau)}A_m\psi(\beta'_m)+e^{-\beta_m(t-\tau)}\frac{a_m}{\psi(\beta_n)}\right\}=0$$

Since β'_m is a zero of $\psi(\beta')$ and β_m a pole, this equation is satisfied for all values of t.

Hence the solution of the integral equation (48) is

$$I(t)=\frac{E(t)}{R_s+R_e}-\int_{t_1}^{t}d\tau E(\tau)e^{-\gamma(t-\tau)}\sum_{n=0}^{\infty}\frac{e^{-\beta'_n(t-\tau)}}{\psi'(\beta'_n)}\text{ for }t>t_1 \qquad (59)$$

where $E(t)=0$ if $t<t_1$

If $E(t)=R_eE_0e^{i\omega t}$ for $t>t_1$ this becomes, by reference to (55)

$$I(t)=R_e\left[\frac{E_0e^{i\omega t}}{\psi(-\gamma-i\omega)}\right]+R_eE_0\sum_{s=0}^{\infty}\frac{e^{-(\gamma+\beta'_n)(t-t_1)}e^{i\omega t_1}}{(\beta'_n+\gamma+i\omega)\psi'(\beta'_n)}\text{ for }t>t_1 \qquad (59')$$

so that the final periodic current is $I(t)=R_eI_0e^{i\omega t}$, where

$$I_0=\frac{E_0}{\psi(-\gamma-i\omega)} \qquad (59'')$$

To compute the roots β'_n of (53) we note that since λ_s is small ($\lambda_s\leqq.04$), while for platinum $\lambda_e=.8(10)^5$ the ratio $\frac{\lambda_s}{\lambda_e}\leqq5(10)^{-7}$ so that (33c) reduces practically to

$$\beta_nK=\frac{\pi a\lambda_s\alpha_n}{2}\coth\left(\frac{\alpha_nl}{a}\right) \qquad (60)$$

for $n>0$, so that the coefficients a_n defined by (50) are, when $\frac{h}{a}$ is small,

$$a_n=\frac{2a}{Kb}\left(\frac{a\lambda_s}{h\lambda_e}\right)^2\cdot\frac{J_0\left(\frac{\alpha_nb}{a}\right)J_1\left(\frac{\alpha_nb}{a}\right)\coth^2\left(\frac{\alpha_nl}{a}\right)}{\alpha_n^3J_0^2(\alpha_n)}\text{ for }n>0 \qquad (61)$$

The a_n's are exceedingly small $\left(\text{except } a_0=\frac{1}{K}\right)$ since if $\frac{a}{h}=100$, $\left(\frac{a\lambda_s}{h\lambda_e}\right)^2=2.5(10)^{-9}$. Hence writing (52) in the form

$$\psi(\beta)=(R_s+R_e)-\frac{1}{K\beta}-\sum_{n=1}^{\infty}\frac{a_n}{\beta-\beta_n} \tag{62}$$

it is evident that the series is negligibly small except when β is very near one of the values say β_s in which case the sth term is the only term of the series worth retaining. The nth zero β'_n of $\psi(\beta)$ is very close to the nth pole β_n so that β'_n is very approximately given by $(R_s+R_e)-\frac{1}{K\beta'_n}-\frac{a_n}{\beta'_n-\beta_n}=0$ so that

$$\beta'_n=\beta_n+\frac{a_n}{R_s+R_e} \text{ and } \frac{1}{\psi'(\beta'_n)}=\frac{a_n}{(R_s+R_e)^2}=-A_n \text{ for } n=0,1,2,3\ldots\infty \tag{63}$$

so that the resolving nucleus is

$$F(\tau)=\sum_0^{\infty}A_n e^{-\beta'_n\tau}=-\sum_0^{\infty}\frac{e^{-\beta'_n\tau}}{\psi'(\beta'_n)}=-\frac{1}{(R_s+R_e)^2}\sum_0^{\infty}a_n e^{-\beta'_n\tau} \tag{64}$$

or

$$F(\tau)=-\frac{1}{(R_s+R_e)^2K}\left\{e^{-\frac{\tau}{(R_s+R_e)K}}+K\sum_1^{\infty}a_n e^{-\beta_n\tau}\right\}, \text{ where } \beta_n \text{ is} \tag{64'}$$

given by (60) and a_n by (61) for $n>0$.

When $\frac{b}{a}$ is small, equation 61 may be written

$$a_n=\frac{\pi}{2K}\left(\frac{a\lambda_s}{h\lambda_e}\right)^2\frac{\coth\left(\frac{\alpha_n l}{a}\right)}{\alpha_n} \text{ since } \frac{\pi\alpha_n}{2}J_0^2(\alpha_n)=1 \text{ very approximately} \tag{61''}$$

Hence the equation 59 may be written

$$I(t)=\frac{1}{R_s+R_e}\left\{E(t)-\frac{1}{(R_s+R_e)K}\int_{t_1}^{t}d\tau E(\tau)e^{-\tau(t-\tau)}\right.$$
$$\left.\left[e^{-\frac{(t-\tau)}{(R_s+R_e)K}}+\left(\frac{a\lambda_s}{h\lambda_e}\right)^2\phi(t-\tau)\right]\right\} \tag{65}$$

where

$$\phi(\tau)=\frac{\pi}{2}\sum_{n=1}^{\infty}\frac{\coth^2\left(\frac{\alpha_n l}{a}\right)}{\alpha_n}e^{-\frac{\tau}{R_sK}\left(\frac{a_n l}{a}\right)}\coth\left(\frac{\alpha_n l}{a}\right) \tag{65a}$$

When l is of the same order of magnitude as a or larger, $\coth\frac{\alpha_n l}{a}=1$ very approximately so that

$$\phi(\tau)=\frac{\pi}{2}\sum_{n=1}^{\infty}\frac{e^{-\frac{\tau l a_n}{aR_sK}}}{\alpha_n} \text{ for } \tau>0 \tag{65b}$$

Since, however, $\alpha_n=(4n+1)\frac{\pi}{4}$ approximately, this may be written

$$\phi(\tau)=2\sum_{n=1}^{\infty}\frac{e^{-(4n+1)\left(\frac{\pi l\tau}{4aR_eK}\right)}}{4n+1}=\log\sqrt{\frac{1+z}{1-z}}+\tan^{-1}z-2z \tag{65c}$$

where $z=e^{-\frac{\pi l\tau}{4aR_eK}}$.

This approximation to $\phi(\tau)$ is sufficient for those cases where it is not entirely negligible. When, however, $\left(\frac{a\lambda s}{b\lambda_e}\right)^2\leqslant 3(10^{-9})$ as in the example quoted, the terms in $\phi(t-\tau)$ in (65) are negligible and it reduces to equation 5b obtained at first. This may be taken as confirmation of the statement that the second approximation to the current is in general sufficient. It remains to reduce the expression (38″) to a more convenient form for computation. If we assume that $\frac{h}{a}$ is small, without any assumption as to b except that $0<b<a$ we may neglect the first term $\frac{2h}{\pi a^2\lambda_e}$ in (38″) and in the series replace $\tanh\left(\frac{\alpha_n h}{a}\right)$ by $\frac{\alpha_n h}{a}$ which gives

$$R_e'=\frac{2}{\pi h\lambda_e}\cdot\left(\frac{2a}{b}\right)\sum_{1}^{\infty}\frac{J_0\left(\frac{\alpha_n b}{a}\right)J_1\left(\frac{\alpha_n b}{a}\right)}{\alpha_n{}^3J_0{}^2\alpha_n} \tag{65d}$$

Now by (28) when $\frac{r}{a}=\frac{b}{a}=x$ we find

$$\frac{2}{x}\sum_{1}^{\infty}\frac{J_0(\alpha_n x)J_1(\alpha_n x)}{\alpha_n J_0{}^2(\alpha_n)}=\frac{1}{2x^2}-1 \quad\text{——————}\quad \text{if } 0<x<1 \tag{66}$$

Multiplying this by $\frac{x}{2}\,dx$ and integrating from x to 1 gives

$$\sum_{1}^{\infty}\frac{J_0{}^2(\alpha_n x)}{\alpha_n{}^2J_0{}^2(n)}-\sum_{1}^{\infty}\frac{1}{\alpha_n{}^2}=-\tfrac{1}{2}(1-x^2+\log x) \quad\text{———}\quad \text{if } 0<x\leqslant l$$

Since $\sum_{1}^{\infty}\frac{1}{\alpha^2 n}=\frac{1}{8}$ this may be written

$$\sum_{1}^{\infty}\frac{J_0{}^2(\alpha_n x)}{\alpha_n{}^2J_0{}^2(\alpha_n)}=\frac{1}{2}\left[\log\frac{1}{x}-\frac{3}{4}+x^2\right] \quad\text{----}\quad \text{if } 0<x\leqslant 1 \tag{67}$$

Multiplying this by xdx and integrating from zero to x gives

$$\sum_1^\infty \left(\frac{J_0^2(\alpha_n x) + J_1^2(\alpha_n x)}{\alpha_n^2 J_0^2(\alpha_n)} \right) = \frac{1}{2}\left[\log \frac{1}{x} - \frac{1}{4} + \frac{x^2}{2} \right] \text{---- if } 0 < x \leqq 1 \quad (68)$$

whence, by (67)

$$\sum_1^\infty \frac{J_1^2(\alpha_n x)}{\alpha_n^2 J_0^2(\alpha_n)} = \frac{1}{4}(1 - x^2) \text{ -------- if } 0 < x \leqq 1 \quad (69)$$

Multiplying this by xdx and integrating from 0 to x gives

$$\sum_1^\infty \frac{J_0^2(\alpha_n x) + J_1^2(\alpha_n x)}{\alpha_n^2 J_0^2(\alpha_n)} - \frac{2}{x} \sum_1^\infty \frac{J_0(\alpha_n x) J_1(\alpha_n x)}{\alpha_n^3 J_0^2(\alpha_n)} = \frac{1}{4}\left(1 - \frac{x^2}{2}\right) \text{ if } 0 < x \leqq 1 \quad (70)$$

By use of (68) this becomes

$$\frac{2}{x} \sum_1^\infty \frac{J_0(\alpha_n x) J_1(\alpha_n x)}{\alpha_n^3 J_0^2(\alpha_n)} = \frac{1}{2}\left[\log \frac{1}{x} - \frac{3}{4}(1 - x^2) \right] \text{ if } 0 < x \leqq 1 \quad (71)$$

Placing $x = \frac{b}{a}$ in this gives

$$\frac{2a}{b} \sum_1^\infty \frac{J_0\left(\frac{\alpha_n b}{a}\right) J_1\left(\frac{\alpha_n b}{a}\right)}{\alpha_n^3 J_0^2(\alpha_n)} = \frac{1}{2}\left[\log \frac{a}{b} - \frac{3}{4}\left(1 - \frac{b^2}{a^2}\right) \right] \quad (72)$$

so that (65[d]) becomes finally

$$R_e' = \frac{1}{\pi h \lambda_e}\left\{ \log \frac{a}{b} - \frac{3}{4}\left(1 - \frac{b^2}{a^2}\right) \right\}, \quad (73)$$

which is the principal part of R_e' when $\frac{h}{a}$ is small, and $0 < b \leqq a$

IV. A CELL EACH OF WHOSE ELECTRODES IS A THIN CYLINDRICAL SHELL CLOSED BY A THIN DISK

In figure 3 is shown a section (by a plane through the axis) of a symmetrical cell. The cylindrical shell T^a, and the circular disk T^b, are filled with solution, these regions being fairly thin, of the order of 0.1 cm. The current enters the electrode T_1 through the face of the cylindrical shell T^a_1 at $x=0$ (trace $\overline{AA}_1$) where the potential has the uniform value $\frac{E(t)}{2}$. It leaves at the face of the shell T^a_2 at $x=0$

(trace A_2A_3), where the potential has the uniform value $-\frac{E(t)}{2}$. The total capacity K of both films is given by

$$\frac{1}{K}=\frac{1}{K^a{}_1+K^b{}_1}+\frac{1}{K^a{}_2+K^b{}_2}, \text{ where } \left\{\begin{array}{l} K^a{}_1=\frac{\epsilon a_1 l_1}{2\Delta},\ K^b{}_1=\frac{\epsilon a^2{}_1}{\Delta} \\ K^a{}_2=\frac{\epsilon a_2 l_2}{\Delta},\ K^b{}_2=\frac{\epsilon a^2{}_2}{\Delta} \end{array}\right\} \quad (74a)$$

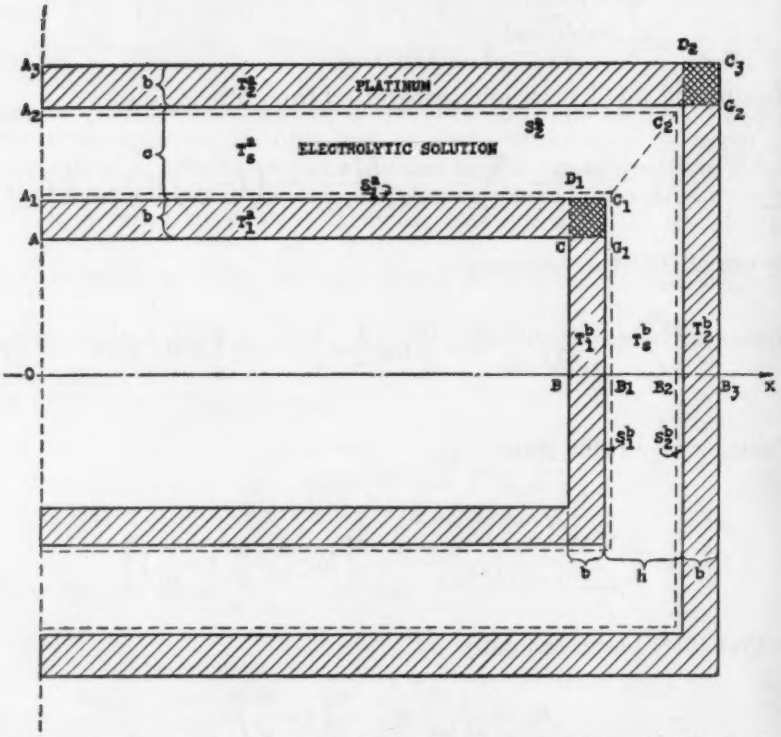

SECTION 3.—*Section of concentric cylinders by a plane through the axis.*

$\overline{0A}=a$	a_1 is of order of 1 cm	$\overline{OB}=l$
$0A_1=a_1=a+b$	l_1 is of order of 5 cm	$\overline{OB}_1=l_1=l+b$
$0A_2=a_2=a_1+c$	c and b of order 0.1 cm	$\overline{OB}_2=l_2=l_1+h$
$0A_3=a_3=a_2+b$	b of order 0.01 cm	$\overline{OB}_3=l_3=l_2+b$

The resistance R_0, which shunts the condenser K, is given by

$$\left\{\begin{array}{l} R_0=R_{01}+R_{02}, \text{ where } \frac{1}{R_{01}}=\frac{1}{R^a{}_{01}}+\frac{1}{R^b{}_{01}} \text{ and } \frac{1}{R_{02}}=\frac{1}{R^a{}_{02}}+\frac{1}{R^b{}_{02}} \\ R^a{}_{01}=\frac{\Delta}{2\pi a_1 b_1 \lambda_0},\ R^b{}_{01}=\frac{\Delta}{\pi a^2{}_1 \lambda_0} \\ R^a{}_{02}=\frac{\Delta}{2\pi a_2 b_2 \lambda_0},\ R^b{}_{02}=\frac{\Delta}{\pi a^2{}_2 \lambda_0} \end{array}\right\} \quad (74b)$$

Since the region T_s is everywhere thin, the first approximation to the resistance R_s of the solution, obtained by neglecting the variations of potential near the edges of C_1 and C_2, assuming a uniform radial component of current density in $T_s{}^a$, and a uniform axial component in $T_s{}^b$ is given by

$$\frac{1}{R_s}=\frac{1}{R_s{}^a}+\frac{1}{R_s{}^b}, \text{ where } \left\{\begin{aligned} R_s{}^a&=\frac{\log\frac{a_2}{a_1}}{2\pi\left(l_1+\frac{h}{2}\right)\lambda_s}\approx\frac{c}{2\pi a_1 l_1\lambda_s}\left[1-\frac{1}{2}\left(\frac{c}{a_1}+\frac{h}{l}\right)\right]\\ R_s{}^b&=\frac{h}{\pi\left(a_1+\frac{c}{2}\right)^2\lambda_s}\approx\frac{h}{\pi a^2\lambda_s}\left(1-\frac{c}{2a_1}\right)\end{aligned}\right\} \tag{75}$$

In these expressions the mean length of the shell $T_s{}^a$ is taken $\left(l_1+\frac{h}{2}\right)$ and the mean radius of the disk is $\left(a_1+\frac{c}{2}\right)$. In this way we attempt to make some allowance for the troublesome region near the edge C_1 and C_2. If the construction and measurement of dimensions of the solution-volume T_s were possible with any great precision, this expression for R_s would require a slight modification. All that is proposed here is an approximate evaluation of the electrode resistances R_{c1} and R_{c2}.

The total current is $I=I^a+I$ where I^a is that passing through the cylindrical shell $T_s{}^a$ and I^b that passing through the disk $T_s{}^b$.

For the two parts $T^a{}_1$ and $T^b{}_1$ of the electrode T_1 consider the potential

$$V(x,r)=\frac{E}{2}-\frac{I^b}{2\pi a_1 b\lambda_e}x+$$
$$\frac{I^a}{\pi a_1 l^2\lambda_e}\sum_{n=1}^{\infty}\frac{\sin\alpha_n x}{i\alpha^2{}_n}\left[\frac{Y_1(i\alpha_n a)J_0(i\alpha_n r)-J_1(i\alpha_n a)Y_0(i\alpha_n r)}{Y_1(i\alpha_n a)J_1(i\alpha_n a_1)-J_1(i\alpha_n a)Y_1(i\alpha_n a_1)}\right] \tag{76a}$$

$$\text{in } T_1{}^a \text{ where } \alpha_n=\frac{(2n-1)}{2l}\pi$$

and

$$V(x,r)=\frac{E}{2}-\frac{l}{2\pi a_1 b\lambda_e}\left(\frac{I^a}{2}+I^b\right)-\frac{2I^b}{\pi a\lambda_e}\sum_{n=1}^{\infty}\frac{\cosh\beta_n\left(\frac{x-l}{a}\right)J_0\left(\beta_n\frac{r}{a}\right)}{\beta_n{}^2\sinh\frac{\beta_n b}{a}J_1(\beta_n)} \tag{76b}$$

$$\text{in } T^b{}_1$$

where β_n is the nth positive unit of $J_0(\beta)=0$.

The equation 76a reduces at the face $x=0$ of $T^a{}_1$ to $V(0,r)=\frac{E}{2}$ as it should. Also $[D_r V(x,r)]_{r=a}=0$ ie., there is no current leaving the inner boundary of $T^a{}_1$. The current density at the surface $S^a{}_1$ i. e., $r=a$ is by (71a)

$$-\lambda_e[D_r V_{(x,\,r)}]_{r=a_1}=i_r(x,a_1)=\frac{I^a}{2\pi a_1 l}=\frac{I^a}{\pi a_1 l^2}\sum_{n=1}^{\infty}\frac{\sin\,(\alpha_n x)}{\alpha_n}$$

It is evident therefore that (76a) satisfies the reasonable boundary conditions at its external boundaries.

Over the section whose trace is $\overline{CD}_1$ i. e., $x=l$ we find from (76a)

$i_x(l,r)=-\lambda_e[D_xV(x,\ r)]_{x=l}=\dfrac{I^b}{2\pi a_1 b}$=uniform, which is a reasonable way of ignoring the fine structure of the field at this edge, since the total current through $\overline{CD}_1$ must be I^b the total which passes to the solution through the surface S^b_1. At S^a_1, $r=a_1$, (76a) becomes

$$V(x,a_1)=\frac{E}{2}-\frac{I^b}{2\pi a_1 b\lambda_e}x$$

$$+\frac{I^a}{\pi a_1 l^2\lambda_e}\sum_{n=1}^{\infty}\frac{\sin\ \alpha_n x}{i{\alpha_n}^2}\left[\frac{Y_1(i\alpha_n a)J_0(i\alpha_n a_1)-J_1(i\alpha_n a)Y_0(i\alpha_n a_1)}{Y_1(i\alpha_n a)J_1(i\alpha_n a_1)-J_1(i\alpha_n a)Y_1(i\alpha_n a_1)}\right] \quad (77).$$

Since $a_1=a+b$ where b is small, this series becomes

$$\sum_{n=1}^{\infty}\frac{\sin\ \alpha_n x}{i{\alpha_n}^2}\frac{1}{i\alpha_n b}\left[\frac{Y_1J_0-J_1Y_0}{Y_1J_1'-J_1Y_1'}\right]_{(i\alpha_n a)}=\sum_{1}^{\infty}\frac{\sin\ \alpha_n x}{i{\alpha_n}^2}\frac{1}{i\alpha_n b}\left[\frac{-\dfrac{2}{\pi i\alpha_n a}}{-\dfrac{2}{\pi i\alpha_n a}}\right]$$

$$=-\frac{1}{b}\sum_{n=1}^{\infty}\frac{\sin\ \alpha_n x}{{\alpha_n}^3}=-\frac{(2l)^3}{b}\frac{1}{\pi 3}\sum_{n=1}^{\infty}\frac{\sin\ (2n-1)\dfrac{\pi x}{2l}}{(2n-1)^3}$$

so that (77) becomes

$$V(x,\ a_1)=\frac{E}{2}-\frac{1}{2\pi a_1 b\lambda_e}\left[I_x{}^b+2lI^a\left(\frac{2}{\pi}\right)^3\sum_{n=1}^{\infty}\frac{\sin\ (2n-1)\dfrac{\pi x}{2l}}{(2n-1)^3}\right] \quad (77')$$

From this we find

$$2\pi a_1\int_0^l V(x,\ a_1)dx=2\pi a_1 l\left\{\frac{E}{2}-\frac{l}{2\pi a_1 b\lambda_e}\left[\frac{I^b}{2}+2I^a\left(\frac{2}{\pi}\right)^4\sum_{n=1}^{\infty}\frac{1}{(2n-1)^4}\right]\right\}$$

By means of the formulas

$$\left(\frac{2}{\pi}\right)^3\sum_{1}^{\infty}\frac{-1^{n+1}}{(2n-1)^3}=\frac{1}{4}\text{ and }\left(\frac{2}{\pi}\right)^4\sum_{1}^{\infty}\frac{1}{(2n-1)^4}=\frac{1}{6}$$

we thus find

$$2\pi a_1\int_0^l V(x,\ a_1)dx=2\pi a_1 l\left\{\frac{E}{2}-\frac{l}{2\pi a_1 b\lambda_e}\left(\frac{I^a}{3}+\frac{I^b}{2}\right)\right\} \quad (78)$$

and

$$V(l,\ a)=\frac{E}{2}-\frac{l}{2\pi a_1 b\lambda_e}\left(\frac{I^a}{2}+I^b\right) \quad (79)$$

Returning to the equation 76b this is evidently a solution in the region T^b_1 satisfying the boundary conditions

$V(x, a)=\frac{E}{2}-\frac{l}{2\pi a_1 b\lambda_e}\left(\frac{I^a}{2}+I^b\right)$ for $l<x<l+b$ (i. e., by 79 continuous at C,

$D_xV=0$ at $x=l$

$$D_xV=-\frac{I^b}{\pi a^2\lambda_e} \text{ at } x=l+b\left(=-\frac{I^b}{\pi a^2\lambda_e}2\sum_1^\infty\frac{J_0\left(\frac{\beta_r}{a}\right)}{\beta_n J_1(\beta_n)}\right) \tag{80}$$

From it we find

$$2\pi\int_0^a rV(l+b, r)dr=\pi a^2\left[\frac{E}{2}-\frac{l}{2\pi a_1 b\lambda_e}\left(\frac{I_a}{2}+I^b\right)\right]-\frac{a^2}{8b\lambda_e}I^b \tag{81}$$

where we have placed tanh $\frac{\beta_n b}{a}=\frac{\beta_n b}{a}$ and made use of the known sum

$$\sum_1^\infty\frac{1}{\beta_n{}^2}=\frac{1}{32}.$$

Hence, if $\overline{V}^0_{e1}$ denotes the average of V over $S_1=S^a{}_1+S^b{}_1$ we find, by use of (78) and (81)

$$\overline{V}^0_{e1}=\frac{E}{2}-\frac{1}{(b\lambda_e)(2\pi a_1 l+\pi a^2)}\left[\frac{l}{3}\left(l+\frac{3a}{4}\right)I^a+\frac{1}{2}\left(l+\frac{a}{2}\right)^2 I^b\right] \tag{82}$$

Since the current is determined principally by the solution resistance R_s and $R^a{}_s$ and $R^b{}_s$ are in parallel, we may replace I^a and I^b in (82) by

$$I^a=\frac{R^b{}_s}{R^a{}_s+R^b{}_s}I=\frac{hI}{h+\frac{a_1 c}{2l_1}} \text{ and } I^b=\frac{R^a{}_s}{R^a{}_s+R_s{}^b}I=\frac{\frac{a_1 c}{2l_1}}{h+\frac{a_1 c}{2l_1}}I \tag{83}$$

Hence the "resistance of the inner" electrode defined by (19a) is

$$R_{e1}=\frac{\frac{E}{2}-\overline{V}^0_{e1}}{I}=\frac{\frac{l}{3}\left(2l+\frac{3a}{2}\right)2l+\frac{1}{4}(2l+a)^2 a\frac{c}{h}}{2\pi ab\lambda_e(2l+a)\left(2l+a\frac{c}{h}\right)} \tag{84}$$

When the electrolytic solution has the same thickness everywhere, $c=h$ and this becomes

$$R_{e1}=\frac{l}{2\pi ab\lambda_e}\left[\frac{2l}{3(2l+a)}+\frac{al}{3(2l+a)^2}+\frac{a}{4l}\right] \tag{85}$$

Since $h=c$ is small it is similarly found as is evident from symmetry that the resistance R_{e2} of the outer electrode is practically the same as R_{e1}. To estimate the importance of this term, consider the case where $a=1$ cm, $l=5$ cm, $h=c=0.1$ cm, $b=0.01$ cm, $\lambda_s=0.04$ and $\lambda_e=0.8$ $(10)^5$. By (85) we find for the total electrode resistance $R_{e1}+R_{e2}=R_e=0.00073$ ohm, while (75) gives $R^a{}_s=0.79$ ohm, $R^b{}_s=7.95$ ohms, so that the total resistance of the electrolytic solution is

$$R_s=0.72 \text{ ohm.}$$

Hence, the electrode resistance is about one-thousandth of the solution resistance.

V. SUMMARY

In section II a plausible method of obtaining a first approximation to the effect of electrode-resistance was sketched without attempting a proof or inquiry into its limitations. The line of argument in a more detailed justification could be inferred from an examination of the equations obtained in section III for a particular shape of cells and electrodes. This exact mathematical solution confirms the method of section II as a first approximation. On the strength of this, the approximation is applied in section IV to a cylindrical cell of more complicated shape. The result of practical importance in the first case is the electrode resistance given by equation 73 and in the second case by (84). These electrode resistances were arbitrarily defined in equation 19 so that they would enter the first approximate equations of motion of electricity (4) in the familiar form. A possible source of misunderstanding due to the use of the name "electrode resistance" was pointed out in section II and illustrated in section III. The resolution of the total resistance into the sum of two parts, one being that of the solution, the other of the electrodes, is possible in the first approximation only. In a closer approximation in general, this concept goes to pieces, because the total current I is not confined to a single linear branch but is the sum of an infinite number of parallel current components having different paths and series capacities.

WASHINGTON, April 23, 1936.

U. S. Department of Commerce National Bureau of Standards

RESEARCH PAPER RP906

Part of Journal of Research of the National Bureau of Standards, Volume 17, July 1936

TERM ANALYSIS OF THE FIRST SPECTRUM OF VANADIUM (V_I)

By William F. Meggers and Henry Norris Russell[1]

ABSTRACT

All available data on 2525 V I lines (wave lengths, intensities, temperature classes, Zeeman effects, and absorption observations) subjected to analysis have aided in the identification of 60 doublet, 60 quartet, and 28 sextet terms. Combinations between these give 634 multiplets and account for 2,186 observed lines. Complete tables of lines and terms are presented.

The lowest term is $(d^3s^2)a^4F_{1\frac{1}{2}}$, but the strongest line (*raie ultime* of V I) is $(d^4s)a^5D_{4\frac{1}{2}}-(d^4p)y^5F^\circ_{5\frac{1}{2}}$ with wave length 4379.24 A, involving the simple *s-p* transition.

Line intensities, level intervals, and Zeeman effects indicate that this five-electron spectrum is governed, in the main, by LS coupling. The terms are all regular except for a few inversions, some of which appear to be explained by perturbations also accompanied by abnormal magnetic splitting.

Absorption data and temperature classification confirm the orientation of the terms and agree qualitatively with their energies of excitation.

Zeeman-effect observations for more than 900 lines greatly facilitated the analysis, and constitute convincing evidence for its correctness.

With the aid of the quantum theory, and comparisons with other spectra, the electronic configurations responsible for the observed terms have been identified in nearly all cases, but a few terms are left unassigned for various reasons.

A number of two-member series have been recognized; from them a corrected ionization potential of 6.71 volts has been computed for neutral vanadium atoms.

CONTENTS

	Page
I. Introduction	126
II. Observational data	126
1. Wave lengths	126
2. Intensities	128
3. Temperature classes	128
4. Zeeman effects	128
5. Absorption	129
III. Term analysis of V I (Z=23)	129
1. Lines of the V I spectrum	130
2. Terms of the V I spectrum	175
3. Electron configurations, theoretical and observed terms	185
(a) Low terms	185
(b) Middle odd terms	186
(c) High terms	188
4. Series and ionization potentials	189
IV. References	191

[1] Princeton University Observatory.

I. INTRODUCTION

A contribution of far-reaching importance to the term analysis of complex spectra was made by Catalán [1] [1] in 1922, when he announced new types of regularities (multiplets) in the spectra of manganese. Similar regularities were eagerly sought in other spectra, especially those of elements in the same period as manganese, primarily for the purpose of testing the alternation and displacement laws of spectral structure. Thus, after multiplets had been identified for scandium, titanium, chromium, manganese, and iron, to vanadium fell the distinction of disclosing the first spectral regularities in the 5th group of elements, thereby proving the general validity of the alternation law.

The first regularities in the arc spectrum of vanadium were announced in 1923, simultaneously by Meggers [2] and by Laporte [3]. Both recognized quartet and sextet multiplets accounting for several hundred lines. A paper on Zeeman effect and multiplet structure by Landé [4] gave further impetus to such analysis, and further results based on interpretations of observed Zeeman effects for vanadium lines were published by Meggers [5] and by Bechert and Sommer [6]. The analysis was continued by Meggers during the development of the theory of complex spectra [7] until the identified terms [8] accounted for about 1,000 lines. Except for a series-forming term identified in 1927 by Russell [9], the analysis rested until 1932, when it was resumed and carried to its present state of completion by cooperation of the present authors. A summary of the identified terms was published in 1934 by Miss Moore [10].

In order to bring this analysis to its present state, it was necessary to reobserve certain regions of the spectrum and to reexamine spectrograms for faint lines. By postponing this presentation, it was possible to exploit new photographic plates and spectrographs, which added much to the completeness and quality of the data. Most of the new observing was done at the National Bureau of Standards, while the extensions to the analysis all emanate from Princeton University. Since practically all conveniently observable data for V I lines have now been satisfactorily interpreted and correlated, the time has come for publication of final results.

II. OBSERVATIONAL DATA

The observed facts upon which this analysis of the V I spectrum is based consist of wave-length measurements, intensity estimates, temperature classification, Zeeman effects and absorption data, all of which are collected in table 1.

1. WAVE LENGTHS

Although a considerable number of spectroscopists have measured wave lengths of vanadium lines [11], no one has given satisfactory results for the entire spectrum, so, in lieu of remeasuring all lines, it has been necessary to use a composite list. The most complete table of vanadium arc spectrum measurements (1,642 lines, 2311.53 to 6812.63 A) was published in 1911 by Exner and Haschek [12], but the values are on Rowland's scale and the relative errors are rathe

[1] Numbers in brackets refer to references at the end of this paper.

large. More precise values on the International Scale were obtained by Kilby [13] (3126.224 to 3943.666 A), and especially by Ludwig [14] (2207.1 to 4646.402 A), whose results as tested by subsequently found spectral regularities appear to be correct within a few thousandths angstrom. These observers, however, measured only short intervals of the spectrum and omitted many faint lines. The region of longer waves (5500 to 9500 A) was explored in 1920 by Kiess and Meggers [15].

Efforts to advance the structural analysis of vanadium spectra soon indicated the necessity of remeasuring portions of them and extending observations in both directions. At the National Bureau of Standards the interval 4456 to 6700 A was remeasured in 1923, new observations in the ultraviolet (2081 to 2440 A) were made in 1925, new measurements in the infrared (6700 to 10500 A) in 1933 were extended to 12000 A in 1935, and finally, the ultraviolet (2081 to 2700 A) was once more observed with larger dispersion in 1936. These last observations were suggested by the term analysis which indicated that the earlier ultraviolet measurements were affected by systematic error. This systematic error was probably due to the fact that the iron lines used as standards below 2400 A were quite unreliable until new values by Burns and Walters [16] become available in 1929.

Since these new values of vanadium wave lengths are here being published for the first time, it may be justifiable to give some details of their measurement. Large concave grating spectrographs were employed, except in the ultraviolet, for which an exceptionally powerful quartz spectrograph became available in 1931. Dispersion constants of the spectrograms are as follows: 0.4 to 1.1 A/mm in the interval 2100 to 2700 A; 3.5 A/mm from 4456 to 9100 A; 10.2 A/mm from 8600 to 12000 A. All measurements were made relative to the international iron-arc secondary standards [17], supplemented in the ultraviolet by the above-mentioned values of Burns and Walters [16]. The earlier observations were made with vanadium chloride on graphite, but those since 1932 were secured with solid metal electrodes of highly purified vanadium kindly presented for these spectroscopic investigations by Jerome K. Strauss of the Vanadium Corporation of America.

A major difficulty encountered when describing the atomic spectra emitted by conventional sources is due to the confusing presence of molecular spectra arising from metallic oxides. In the arc spectrum of vanadium at atmospheric pressure partially resolved rotation structure of such bands [18] extending from the blue to the limit of observation in the infrared, inevitably masks many faint atomic lines and may in some cases falsify the wave-length measurements. The vanadium furnace spectrograms obtained by King [19] being free from oxide bands, were reexamined at Princeton for faint lines. Thus, in the range 2632 to 6607 A on King's plates, about 130 new lines were measured, the wave lengths of 155 others were checked, and 11 close doubles were resolved, including vanadium lines near strong iron lines or other impurities. Unfortunately, the infrared has not been observed without molecular spectra.

The hyperfine structure of some V I lines has been investigated by White [20], and by Kopfermann and Rasmussen [21], the latter definitely deducing from their measurements a nuclear-spin moment

of $I=9/2$ for vanadium atoms. In table 1 the symbol "*cm*" meaning "complex hyperfine structure measured", is attached to the 17 lines investigated with interferometers. No hyperfine structure in vanadium spectra has been resolved with ordinary spectrographs, but some infrared lines showing considerable width may merit further study with greater resolving power. For example, the line with mean wave length 8116.80 A appears to have a width of the order of 0.5 A. The present term analysis of the V I spectrum is quite independent of hyperfine structure, but further work in the latter field may be suggested and aided by it.

2. INTENSITIES

Except for four multiplets in each of which the relative intensities of lines have been measured by Frerichs [22] to test intensity rules, no quantitative measurements of intensities have been made in vanadium spectra and the usual practice of estimating such relative intensities has been followed. In the present case, we have quoted King's [19] arc-intensity estimates for the most part and attempted to supply the remainder on the same scale. Whereas other observers usually employ a scale of 1 to 10, King's scale has much greater range (1 to 200 for vanadium), and although empirical, it has been shown to be remarkably homogeneous and in possession of considerable quantitative value [23].

3. TEMPERATURE CLASSES

Comparison of the spectra of vanadium excited in a vacuum furnace at various temperatures enabled King [19] to separate some 1,600 vanadium lines (2340 to 6842 A) into a half dozen different classes corresponding closely to successive energy stages required for their excitation. This classification was of primary importance in the first search for regularities among vanadium lines and has been of great value in simplifying and generally confirming the complete analysis. King's temperature classes in roman numerals are quoted together with estimated arc intensities in the following list of lines. In the interval 2400 to 3200 A, King measured about 130 V I lines not mentioned before 1924.

4. ZEEMAN EFFECT

In 1911 the Zeeman effect for several hundred vanadium lines from 3665 to 6625 A was published by Babcock [24]. These observations were improved and extended and in 1923 were lent in manuscript form to those actively engaged in multiplet analysis. Except for a few patterns published by Bechert and Sommer [6] these data have remained in obscurity, but with the kind consent of Mr. Babcock, they are now fully presented, together with their interpretation in the following list of V I lines. A report on magnetic splitting factors (g and g sums) resulting from the present analysis was published last year by Russell and Babcock [25] so further details of this phase will be omitted here. The Zeeman effect observations quoted in table 1 are given in the usual form (normal triplet units) p components in parentheses followed by n components, the strongest in complex patterns being distinguished by boldface type. The same applies to calculated patterns, except that in some cases these are simplified to make their relation to the observations more obvious.

The calculated patterns are derived from the *observed* g-values obtained from Babcock's material and listed in table 1. When the observed components are wholly or partially resolved the full computed pattern is given. When only blends of the components of a given polarization are measurable, the calculated position of the blend is given. For the stronger lines this is assumed to coincide with the center of gravity of the theoretical group, as determined by the formulas of Shenstone and Blair [26]. Such cases are marked *b* in the list. For weaker lines, it is probable that the measurement applies more nearly to the strongest component of the group, which is, therefore, tabulated with the notation *s*.

The observed Zeeman effects have been most helpful in the identification of spectral terms and they afford the most convincing confirmation of the correctness of this analysis of the V I spectrum. "From the magnetic standpoint, this complex spectrum is conspicuously regular and orderly. Landé's formulas for the g-factors are closely followed, showing (as does the regular multiplet structure) that the departures from LS coupling are small. Most of the discordances are explicable as a result of simple perturbations between adjacent levels [25]."

5. ABSORPTION

Before the theory of complex spectra had been fully developed the apparent prominence of large azimuthal quantum numbers was regarded skeptically by many, and it was necessary to devise experimental proofs. The absorption spectrum of vanadium was promptly investigated by Gieseler and Grotrian [27] to determine the normal state of the atoms. They observed 52 absorption lines (2914.92 to 6251.81 A) when vanadium was vaporized in a furnace at 2,000° C. Since all of these lines originated either from a low quartet F or a slightly higher sextet D term, it was concluded that the normal state of vanadium atoms is described by a $^4F_{1\frac{1}{2}}$ level. Evidence of a similar nature, but less refined, is found in the self-reversal of lines in the vanadium arc.

King [28] extended his temperature classification of vanadium lines in the ultraviolet from 2340 to 2700 A by comparing arc intensities with those appearing in absorption by vapor at about 2,600° C.

The only other absorption data for vanadium are those of the solar spectrum. More than 600 vanadium lines have been identified in the spectrum of the solar disk, and most of these are enhanced two or more intensity units in the spot spectrum, so that many faint lines of vanadium appear only in sun spots [29].

III. TERM ANALYSIS OF V I (Z=23)

Since the terms of the V I spectrum are deduced directly from observed properties of the lines, we present in the following numbered subsections (1) a complete list of observational data in table 1, to which are added the term combinations for all classified lines, and calculated Zeeman effects to compare with observed; (2) the intrinsic facts concerning the established spectral terms in table 2; (3) discussions of electron configurations and terms; and (4) spectral series and ionization potentials.

1. LINES OF THE V I SPECTRUM

Table 1 exhibits in successive columns (1) the observer; (2) measured wave length; (3) intensity; (4) temperature class; (5) vacuum wave number; (6) term combination; (7) observed Zeeman effect; and (8) calculated pattern.

The key to the numerals in column (1) is as follows: 1=W. F. Meggers; 2=H. N. Russell; 3=Solar or sun-spot spectrum; 4=Exner and Haschek [12, 19]; 5=C. E. Moore; 6=W. Ludwig [14]; 7=C. M. Kilby [13]; and 8=A. S. King [28].

All wave lengths listed here are on the International Scale.

The letters *a*, *b*, *c*, etc., attached to wave lengths in column (2) have the following meaning:

a=*g* for higher level calculated from this line.
b=Observed and calculated Zeeman effects discordant.
c=Fe masks V line.
d=Blend with V II line.
e=Masked by V II line.
f=Ni masks V line.
g=Zeeman effect pattern changed by self-reversal.

The third and fourth columns contain the intensity and temperature class, respectively. For lines of known temperature class King's [19] intensities are given unless the intensity is in parenthesis, in which case it belongs to the observer in column (1). This is generally true of waves longer than 6400, and shorter than 2755 A. For all lines of unknown temperature class, the intensity is that of the author referred to in column (1). A few cases of temperature classes not published by King are given in parentheses. Intensities less than 0, i. e., 00, 000, and 0000, are entered as −1, −2, and −3, respectively. The intensities quoted from furnace spectra are inclosed in brackets.

Symbols accompanying some of the intensity numbers in column (3) have the following significance:

a=Absorption [27].
c=Complex, hyperfine structure (*hfs*).
cm=Complex *hfs* measured [20, 21].
d=Double.
E=Enhanced in spark.
h=Hazy, nebulous, or diffuse.
H=Very hazy.
l=Shaded to longer waves.
p=Part of band.
r=Self-reversed.
R=Strongly self-reversed.
w=Wide hyperfine structure.
W=Very wide hyperfine structure.

The vacuum wave numbers in column (5) were derived from the measured wave lengths with the aid of Kayser's Schwingungszahlen [30], except beyond 10000 A, where either Babcock's [31] method of using Kayser's table was employed or reciprocals were calculated from wave lengths corrected to vacuum by extrapolation of Meggers and Peters [32] dispersion formula for air.

The term combinations entered in column (6) show the quantum theoretical interpretation of the observed lines, the notation being that which is in general use [33]. In the case of blends, an attempt has been made to list the more important term combination first.

Lines which are completely masked have their multiplet designations in parentheses.

Symbols attached to Babcock's unresolved complex magnetic patterns in column (7) have the following meanings:
w_1=slightly widened; w_2=moderately widened;
w_3=greatly widened, while the apparent intensity distribution in such cases is qualitatively represented by letters as follows:
For unresolved *p* components B=⊢⊣; D=⊓; E=∧.
For unresolved *n* components A=⊣⊢; B=⊢⊣; C=⊓⊓.

As already explained, the letters *b* and *s*, with calculated patterns in column (8), indicate blended and strongest component values, respectively. Discordances are pointed out and often explained in footnotes. In such a complex spectrum, it would not be surprising if a few discordances arose from errors of observation or of judgment in separating overlapping Zeeman patterns of V I or of V I and V II lines. The recorded Zeeman data may be compared with values computed from Landé *g*-values by referring to a publication by Kiess and Meggers [34]. Considerable departures from such calculated values are usually accounted for by perturbation of adjacent levels [25].

The total number of classified lines is 2,186, divided among multiplicities as follows: 365 doublets, 1,173 quartets, 323 sextets, 277 doublet-quartet, 145 quartet-sextet, 12 doublet-sextet, and 13 from combinations with the three miscellaneous levels. The total number of assigned multiplet designations is 2,308, 120 lines being blended. Of the blends 118 have two designations each and 2 have three each. In addition, 73 lines which would otherwise appear in multiplets are masked; 61 by V I, 4 by V II, 2 by Ni, and 6 by Fe.

The combinations between sextets and doublets are of special interest, as this is the smallest atomic number for which they have been found. The combination $a^6D-z^2G°$ exhibits all five possible members of the multiplet, three of which (λλ 4200.19, 4179.42, 4159.70) have completely resolved Zeeman patterns, of very unusual type, which put their nature beyond any question. The remaining lines recorded as doublet-sextet combinations are sporadic and faint.

TABLE 1.—*Arc spectrum of vanadium* (V I)

(1)	(2)	(3)	(4)	(5)	(6)	(7)	(8)
Ref.	λ_{air} A	Int. arc	Temp. class	ν_{vac}cm^{-1}	Term combinations	Zeeman effect	
						Observed	Computed
1	11911.8	2		8392.7	$a^2F_{3½}-z^2F°_{4½}$		
1	11263.8	3		8875.6	$a^4G_{3½}-y^4F°_{4½}$		
1	11249.0	5		8887.2	$a^4G_{3½}-y^4F°_{3½}$		
1	11195.4	5		8929.8	$a^4G_{2½}-y^4F°_{3½}$		
1	11182.6	5		8940.0	$a^4G_{1½}-y^4F°_{2½}$		
1	11107.7	10		9000.3	$a^4S_{2½}-y^6P°_{3½}$		
1	10993.4	15		9093.9	$a^6S_{2½}-y^6P°_{2½}$		
1	10982.5	5hp?		9102.9	$a^4G_{2½}-z^2G°_{3½}$		
1	10848.0	20		9215.8	$a^6S_{2½}-y^6P°_{3½}$		
1	10824.8	6		9235.5			
1	10523.3	2p?		9500.1	$b^4P_{1½}-z^4P°_{½}$		
1	10479.4	4h		9539.9			
1	10458.4	2		9559.1	$b^4P_{2½}-z^4P°_{1½}$		
1	10392.4	2		9619.8	$a^4D_{2½}-z^6D°_{3½}$		
1	10383.72	3h		9627.83			
1	10283.4	1?		9721.7	$a^4D_{1½}-z^6D°_{2½}$		
1	10251.5	1?		9752.0	$b^4G_{3½}-z^4G°_{4½}$		

TABLE 1.—*Arc spectrum of vanadium* (V I)—Continued

(1)	(2)	(3)	(4)	(5)	(6)	(7)	(8)
						Zeeman effect	
Ref.	λ_{air} A	Int. arc	Temp. class	ν_{vac} cm^{-1}	Term combinations	Observed	Computed
1	10203.45	10		9797.93	$a^3P_{0\frac{1}{2}}-z^3D^0_{1\frac{1}{2}}$		
1	10193.66	5		9807.33	$a^3P_{1\frac{1}{2}}-z^3D^0_{1\frac{1}{2}}$		
1	10163.00	2		9836.92	$b^4P_{0\frac{1}{2}}-z^4P^0_{1\frac{1}{2}}$		
1	10138.82	5h		9860.38	$b^4P^0_{1\frac{1}{2}}-z^4P^0_{1\frac{1}{2}}$		
1	9865.44	10		10133.62	$a^3P^0_{1\frac{1}{2}}-z^3D^0_{2\frac{1}{2}}$		
1	9772.98	5+p		10229.49			
1	9738.50	15		10265.71	$b^4F^0_{1\frac{1}{2}}-y^4F^0_{1\frac{1}{2}}$		
1	9708.36	10		10297.58	$b^4F_{2\frac{1}{2}}-z^2G^0_{2\frac{1}{2}}$		
1	9691.58	40		10315.41	$b^4F_{2\frac{1}{2}}-y^4F^0_{2\frac{1}{2}}$		
1	9684.19	7		10323.28			
1	9670.9	5dp?		10337.5	$y^6D^0_{1\frac{1}{2}}-e^4F_{0\frac{1}{2}}$		
1	9668.9	3p?		10339.6	$b^4F_{1\frac{1}{2}}-y^4F^0_{2\frac{1}{2}}$		
1	9614.68	50		10397.92	$b^4F_{2\frac{1}{2}}-y^4F^0_{3\frac{1}{2}}$		
1	9611.60	80		10401.24	$b^4F_{4\frac{1}{2}}-y^4F^0_{4\frac{1}{2}}$		
1	9593.04	3p?		10421.37	$y^6D^0_{3\frac{1}{2}}-e^4F_{3\frac{1}{2}}$?		
1	9582.28	6h+p		10433.07	$b^4F_{2\frac{1}{2}}-y^4F^0_{2\frac{1}{2}}$		
1	9540.31	5		10478.97	$b^4D_{2\frac{1}{2}}-z^4F^0_{3\frac{1}{2}}$		
1	9536.53	3p?		10483.12	$y^6D^0_{4\frac{1}{2}}-e^4F_{3\frac{1}{2}}$		
1	9511.37	5h		10510.85			
1	9509.11	5h		10513.35	$1^\circ-f^0P_{2\frac{1}{2}}$		
1	9482.64	4		10542.70			
1	9480.25	5h		10545.36	$y^4D^0_{3\frac{1}{2}}-e^4F_{3\frac{1}{2}}$ $y^6D^0_{3\frac{1}{2}}-e^4F_{4\frac{1}{2}}$		
1	9476.14	10		10549.93	$b^4D_{2\frac{1}{2}}-z^4F^0_{3\frac{1}{2}}$ $b^4F_{2\frac{1}{2}}-y^4F^0_{2\frac{1}{2}}$		
1	9467.92	3h		10559.08			
1	9466.32	8h		10560.87	$b^4F_{2\frac{1}{2}}-y^4D_{1\frac{1}{2}}$		
1	9454.44	10		10574.14	$b^4F_{4\frac{1}{2}}-z^2G^0_{3\frac{1}{2}}$		
1	9445.74	10		10583.88	$y^6D^0_{4\frac{1}{2}}-e^6D_{3\frac{1}{2}}$		
1	9439.80	8h		10590.54			
1	9435.52	80		10595.35	$y^4D^0_{2\frac{1}{2}}-e^4F_{4\frac{1}{2}}$		
1	9411.32	30		10622.59	$y^6D^0_{3\frac{1}{2}}-e^6D_{2\frac{1}{2}}$		
1	9406.02	4h		10628.58	$b^4F_{3\frac{1}{2}}-y^4D^0_{2\frac{1}{2}}$		
1	9398.92	10		10636.60	$y^4D^0_{3\frac{1}{2}}-e^4F_{3\frac{1}{2}}$		
1	9384.83	30		10652.59	$y^6D^0_{2\frac{1}{2}}-e^6D_{1\frac{1}{2}}$		
1	9380.50	4		10657.49			
1	9369.80	5		10669.66			
1	9366.86	50		10673.01	$y^4D^0_{1\frac{1}{2}}-e^4F_{2\frac{1}{2}}$		
1	9362.76	2		10677.68	$b^4P_{2\frac{1}{2}}-y^4D^0_{1\frac{1}{2}}$		
1	9361.58	6		10679.03	$y^6D_{1\frac{1}{2}}-e^6D^0_{2\frac{1}{2}}$		
1	9341.10	100		10702.44	$y^6D^0_{3\frac{1}{2}}-e^6D_{4\frac{1}{2}}$		
1	9334.91	5h		10709.54	$b^4F_{4\frac{1}{2}}-y^4D^0_{3\frac{1}{2}}$		
1	9328.14	40		10717.31	$y^6D^0_{4\frac{1}{2}}-e^6D_{3\frac{1}{2}}$		
1	9324.46	5		10721.54	$y^6D^0_{2\frac{1}{2}}-e^6D_{2\frac{1}{2}}$		
1	9316.50	3		10730.70	$z^6G^0_{3\frac{1}{2}}-e^4F_{4\frac{1}{2}}$		
1	9313.54	4		10734.11	$y^4D^0_{1\frac{1}{2}}-e^4F_{1\frac{1}{2}}$ $b^4P_{1\frac{1}{2}}-y^4F^0_{1\frac{1}{2}}$		
1	9308.64	20		10739.76	$y^4D^0_{1\frac{1}{2}}-e^4F_{2\frac{1}{2}}$		
1	9290.34	10		10760.92	$y^6D^0_{3\frac{1}{2}}-e^6D_{1\frac{1}{2}}$		
1	9273.31	15		10780.68	$b^4P_{2\frac{1}{2}}-y^4D^0_{2\frac{1}{2}}$		
1	9255.59	20		10789.66	$y^6D^0_{1\frac{1}{2}}-e^6D_{2\frac{1}{2}}$		
1	9255.84	10		10801.03	$y^4D^0_{2\frac{1}{2}}-e^4F_{1\frac{1}{2}}$		
1	9242.89	30		10816.16	$y^6D^0_{2\frac{1}{2}}-e^6D_{3\frac{1}{2}}$		
1	9226.09	20		10835.87	$y^6D^0_{3\frac{1}{2}}-e^6D_{4\frac{1}{2}}$		
1	9217.22	4h		10846.28	$a^3P_{1\frac{1}{2}}-z^6P^0_{1\frac{1}{2}}$?		
1	9202.88	4		10863.18	$a^4P_{2\frac{1}{2}}-z^4D^0_{1\frac{1}{2}}$		
1	9168.76	20		10903.61	$y^4F^0_{1\frac{1}{2}}-e^4F_{0\frac{1}{2}}$ $y^4F^0_{1\frac{1}{2}}-e^4F_{2\frac{1}{2}}$		
1	9165.80	4		10907.13	$a^2H_{2\frac{1}{2}}-y^4F^0_{1\frac{1}{2}}$		
1	9164.84	40		10908.27	$b^4P_{1\frac{1}{2}}-y^4D^0_{2\frac{1}{2}}$		
1	9156.54	20		10918.16	$a^2H_{4\frac{1}{2}}-z^2G^0_{3\frac{1}{2}}$		
1	9113.74	6		10969.44	$a^4P_{1\frac{1}{2}}-z^4D^0_{0\frac{1}{2}}$		
1	9105.86	10		10978.93	$b^4P_{1\frac{1}{2}}-y^4D^0_{1\frac{1}{2}}$		
1	9100.78	8		10985.06	$y^4F^0_{1\frac{1}{2}}-e^4F_{2\frac{1}{2}}$		

TABLE 1.—*Arc spectrum of vanadium* (VI)—Continued

(1)	(2)	(3)	(4)	(5)	(6)	(7)	(8)
						Zeeman effect	
Ref.	λ_{air} A	Int. arc	Temp. class	ν_{vac} cm^{-1}	Term combinations	Observed	Computed
1	9085.26	40		11003.82	$a^4P_{3/2}-z^4D^0_{1/2}$		
1	9073.34	4		11018.28	$a^2H_{4/2}-y^4F^0_{3/2}$		
1	9046.68	50		11050.75	$a^4P_{1/2}-z^4D^0_{1/2}$		
1	9037.58	30		11061.87	$a^4P_{5/2}-z^4D^0_{3/2}$		
1	9022.70	20		11080.12	$a^2H_{3/2}-z^2G^0_{1/2}$		
1	9021.08	20		11082.11	$b^4P_{1/2}-y^4D^0_{1/2}$		
1	9003.08	5		11104.26	$b^4P_{3/2}-y^4D^0_{3/2}$		
1	8999.10	4		11109.17	$y^6D^0_{3/2}-e^6F_{3/2}$		
1	8971.62	40		11143.20	$a^4D_{3/2}-z^4D^0_{1/2}$		
1	8963.6	5		11153.2	$y^6D^0_{3/2}-e^6F_{4/2}$		
1	8949.2	4		11171.1	$b^4P_{5/2}-y^4D^0_{1/2}$		
1	8932.95	50*cw*		11191.44	$a^4P_{1/2}-z^4D^0_{3/2}$		
1	8931.62	7*hp*?		11193.11	$y^6D^0_{1/2}-e^6F_{3/2}$		
1	8919.85	100*cw*		11207.88	$a^4P_{3/2}-z^4D^0_{3/2}$		
1	8916.35	2*p*?		11212.27	$a^4H_{3/2}-y^4F^0_{3/2}$?		
1	8642.61	5+*p*?		11567.40			
1	8598.92	4+*p*		11626.18	$y^4D^0_{3/2}-e^4D_{2/2}$		
1	8580.37	8*h*		11651.31	$y^4D^0_{1/2}-e^4D_{1/2}$		
1	8551.48	3+*p*?		11690.67	$y^4D^0_{1/2}-e^4D_{3/2}$		
1	8541.98	20		11703.67	$b^2G_{4/2}-y^2G^0_{3/2}$		
1	8534.50	30		11713.93	$b^2G_{3/2}-y^2G^0_{3/2}$		
1	8505.63	10		11753.69	$y^4D^0_{3/2}-e^4D_{2/2}$		
1	8505.06	4		11754.48	$y^4D^0_{1/2}-e^4D_{1/2}$		
1	8502.94	5*d*?		11757.41	$y^4D^0_{3/2}-e^4D_{2/2}$ $b^2G_{4/2}-y^2G^0_{3/2}$		
1	8499.50	50		11762.17	$y^4D^0_{3/2}-e^4D_{3/2}$		
1	8493.61	5		11770.32	$z^2F^0_{3/2}-f^4F_{3/2}$?		
1	8431.63	10*h*+*p*?		11856.85	$y^4D^0_{3/2}-e^4D_{2/2}$		
1	8421.39	5		11871.27	$b^4D_{2/2}-z^4D^0_{3/2}$?		
1	8416.53	5		11878.12	$b^2G_{4/2}-y^2F^0_{3/2}$		
1	8414.39	5		11881.14	$b^2G_{3/2}-y^2F^0_{3/2}$		
1	8408.23	3		11889.85	$y^4D^0_{3/2}-e^4D_{3/2}$		
1	8402.79	15		11897.54			
1	8342.04	60		11984.19	$y^4F^0_{3/2}-e^4D_{2/2}$		
1	8331.21	40		11999.76	$y^4F^0_{3/2}-e^4D_{1/2}$		
1	8324.40	30		12009.58	$y^4F^0_{3/2}-e^4D_{2/2}$		
1	8282.35	100		12070.55	$y^4F^0_{3/2}-e^4D_{3/2}$		
1	8280.39	20		12073.41	$y^4F^0_{3/2}-e^4D_{1/2}$		
1	8267.61	2		12092.07	$b^2G_{4/2}-z^2H^0_{3/2}$		
1	8255.90	100c		12109.22	$a^4D_{3/2}-z^4D^0_{1/2}$		
1	8253.51	100*cw*		12112.73	$a^4D_{3/2}-z^4D^0_{3/2}$		
1	8241.61	60		12130.22	$a^4D_{1/2}-z^4D^0_{1/2}$		
1	8203.05	100		12187.24	$y^6F^0_{3/2}-e^6D_{4/2}$		
1	8198.87	80		12193.45	$a^4D_{3/2}-z^4D^0_{3/2}$		
1	8194.82	5		12199.48	$b^4D_{3/2}-w^4F^0_{3/2}$		
1	8187.33	70		12210.64	$y^6F^0_{3/2}-e^6D_{3/2}$		
1	8186.73	100		12211.54	$a^4D_{1/2}-z^4D^0_{1/2}$		
1	8180.19	15*h*		12221.30	$b^4D_{3/2}-w^4F^0_{3/2}$		
1	8171.34	40		12234.53	$y^6F^0_{3/2}-e^6D_{2/2}$		
1	8168.89	7*h*		12238.20	$y^4F^0_{3/2}-e^4D_{2/2}$		
1	8161.06	150*cw*		12249.95	$a^4D_{3/2}-z^4D^0_{3/2}$		
1	8154.55	20		12259.72	$y^6F^0_{3/2}-e^6D_{1/2}$		
1	8144.58	50		12274.73	$a^4D_{5/2}-z^4D^0_{3/2}$		
1	8136.80	20+*p*		12286.47	$y^6F^0_{1/2}-e^6D_{2/2}$		
1	8116.80	200c*W*		12316.74	$a^4D_{3/2}-z^4D^0_{1/2}$		
1	8109.88	15		12327.25	$y^6F^0_{3/2}-e^6D_{2/2}$		
1	8109.07	20*d*?		12328.49	$y^6F^0_{3/2}-e^6D_{3/2}$ $y^6F^0_{1/2}-e^6D_{1/2}$		
1	8108.60	30		12329.20	$y^6F^0_{3/2}-e^6D_{2/2}$ $y^6F^0_{1/2}-e^6D_{3/2}$		
1	8102.42	40		12338.60			
1	8093.48	100c		12352.23	$a^4D_{1/2}-z^4D^0_{1/2}$		
1	8028.13	20*cw*		12452.78			
1	8027.36	100*cw*		12453.97	$a^4D_{3/2}-z^4D^0_{3/2}$		
1	7947.36	6		12579.34	$z^6P^0_{3/2}-e^6D_{2/2}$		
1	7937.90	30		12594.33	$z^6P^0_{3/2}-e^6D_{3/2}$		

TABLE 1.—*Arc spectrum of vanadium* (V I)—Continued

(1)	(2)	(3)	(4)	(5)	(6)	(7)	(8)
						Zeeman effect	
Ref.	λ_{air} A	Int. arc	Temp. class	ν_{vac} cm^{-1}	Term combinations	Observed	Computed
1	7932.99	6		12602.13	$z^4P_{1/2}-c^4D_{3/2}$		
1	7826.88	3		12772.97	$b^2P_{1/2}-y^2S_{1/2}$		
1	7787.81	1		12837.05	$z^4F_{3/2}-e^2F_{3/2}$		
1	7736.63	1		12921.97	$a^2D_{3/2}-z^2F_{5/2}$		
1	7704.81	3		12975.34	$z^4P_{1/2}-e^4D_{3/2}$		
1	7701.36	2		12981.15	$b^2P_{3/2}-z^2S_{1/2}$		
1	7676.14	2		13023.80	$b^4P_{3/2}-z^6D_{3/2}$		
1	7662.97	2h		13046.17	$y^4D_{3/2}-f^4F_{3/2}$		
1	7661.02	2h		13049.51	$b^4P_{3/2}-z^4S_{1/2}$		
1	7638.03	3h		13088.78	$z^4P_{1/2}-e^4D_{1/2}$		
1	7624.80	15		13111.49	$z^4P_{3/2}-e^4D_{3/2}$		
1	7621.85	4dp?		13116.57	$y^4D_{3/2}-f^4F_{3/2}$		
1	7613.55	2h		13130.87	$y^6F_{3/2}-e^4D_{3/2}$		
1	7598.28	3h		13157.26	$b^2P_{3/2}-y^2S_{1/2}$		
1	7596.92	3p?		13159.61	$b^2P_{1/2}-z^4D_{1/2}$		
1	7591.24	3h		13169.46	$z^4P_{3/2}-e^4D_{1/2}$		
1	7578.75	5h		13191.16	$z^4P_{1/2}-e^4D_{1/2}$		
1	7573.93	2		13199.55	$b^4D_{3/2}-z^4F_{1/2}$?		
1	7570.26	2		13205.96	$b^4D_{1/2}-1^0$		
1	7554.63	2		13233.27	$z^4P_{3/2}-e^4D_{1/2}$		
1	7488.08	3h		13350.89	$b^4P_{1/2}-z^4S_{1/2}$		
1	7485.88	2h		13354.81	$b^4D_{1/2}-z^4F_{1/2}$		
1	7398.64	1		13512.29	$a^4G_{3/2}-y^4G_{1/2}$		
1	7395.20	3h		13518.58	$a^4G_{3/2}-y^4G_{3/2}$		
1	7389.14	2		13529.65	$a^4G_{5/2}-y^4G_{3/2}$		
1	7385.95	3		13535.50	$b^2P_{1/2}-z^2P_{3/2}$		
1	7381.95	1		13542.84	$b^4P_{1/2}-z^4S_{1/2}$		
1	7363.16	15		13577.39	$a^4G_{3/2}-y^4G_{1/2}$		
1	7362.49	4		13578.62	$b^2P_{1/2}-z^2P_{1/2}$ $b^2G_{7/2}-a^4D_{5/2}$		
1	7361.39	10		13580.65	$a^4G_{3/2}-y^4G_{1/2}$		
1	7358.64	4		13585.73	$b^4D_{3/2}-z^4F_{3/2}$		
1	7356.51	20		13589.66	$a^4G_{3/2}-y^4G_{3/2}$		
1	7338.92	30		13622.23	$a^4G_{5/2}-y^4G_{3/2}$		
1	7329.66	2		13639.44	$a^4G_{3/2}-y^4G_{3/2}$		
1	7327.76	1—		13643.00	$b^4H_{3/2}-z^4H_{1/2}$		
1	7321.44	4		13654.76	$a^4G_{7/2}-y^4G_{5/2}$		
1	7306.71	2		13682.28	$a^4G_{5/2}-y^4G_{3/2}$		
1	7291.90	1—		13710.07	$a^2F_{5/2}-z^4H_{7/2}$		
1	7264.28	8		13762.20	$b^4D_{3/2}-z^4F_{3/2}$		
1	7255.68	2		13778.51	$z^4F_{5/2}-e^4F_{3/2}$		
1	7239.26	1—		13809.77	$z^6D_{1/2}-f^6F_{3/2}$		
1	7228.36	1—		13830.58	$b^4D_{3/2}-z^6D_{3/2}$		
1	7186.79	1		13910.59	$z^6D_{3/2}-f^6F_{3/2}$ $a^2F_{7/2}-w^4F_{7/2}$		
1	7182.04	2		13919.78	$b^2P_{3/2}-z^2P_{3/2}$		
1	7159.90	1—		13962.84	$b^2P_{3/2}-z^2P_{1/2}$		
1	7151.36	2		13979.50	$b^4D_{5/2}-z^4D_{3/2}$		
1	7148.15	6		13985.78			
1	7102.53	2h		14075.62	$a^4G_{3/2}-z^4F_{3/2}$		
1	7092.08	4h		14096.36			
1	7063.69	1—		14153.02	$a^2G_{7/2}-y^2F_{5/2}$		
1	7026.05	10+p		14228.83	$a^2F_{5/2}-y^2G_{7/2}$		
1	6974.50	5		14334.00	$a^2F_{7/2}-y^2G_{9/2}$		
1	6940.92	2		14403.35	$a^2F_{5/2}-y^2F_{5/2}$		
1	6916.06	2		14455.12	$a^2F_{5/2}-y^2F_{7/2}$		
1	6893.99	3		14501.39	$a^2F_{7/2}-y^2F_{5/2}$		
1	6883.92	2		14522.60	$b^4P_{3/2}-y^4P_{1/2}$		
1	6871.53	4		14548.79	$b^4P_{3/2}-y^4P_{3/2}$		
1	6870.86	8		14550.21	$b^2H_{9/2}-z^2H_{9/2}$		
1	6841.89	(7)	III A	14611.82	$a^4D_{1/2}-z^4F_{1/2}$		
1	6839.58	6		14616.75	$b^2H_{9/2}-z^2H_{9/2}$		
1	6832.44	(10)	III A	14632.03	$a^4D_{3/2}-z^4F_{3/2}$		
1	6829.94	(10)	III A	14637.39	$a^4D_{5/2}-z^4F_{5/2}$		

TABLE 1.—*Arc spectrum of vanadium* (V I)—Continued

(1)	(2)	(3)	(4)	(5)	(6)	(7)	(8)
Ref.	λ_{air} A	Int. arc	Temp. class	ν_{vac} cm^{-1}	Term combinations	Zeeman effect	
						Observed	Computed
1	6819.13	2d?		14660.59	$a^3P_{1\frac{1}{2}}-z^4D_{2\frac{1}{2}}$		
1	6812.40	(20)	III A	14675.07	$a^4D_{0\frac{1}{2}}-z^4F_{1\frac{1}{2}}$		
1	6786.32	6		14731.47			
1	6784.98	(40)	III A	14734.38	$a^4D_{1\frac{1}{2}}-z^4F_{2\frac{1}{2}}$		
1	6777.29	2		14751.09	$b^4P_{1\frac{1}{2}}-y^4P_{0\frac{1}{2}}$		
1	6766.49	(60)	III A	14774.64	$a^4D_{2\frac{1}{2}}-z^4F_{3\frac{1}{2}}$		
1	6760.12	4		14788.56			
1	6753.00	(80c)	III A	14804.15	$a^4D_{3\frac{1}{2}}-z^4F_{4\frac{1}{2}}$		
1	6744.20	1		14823.47	$b^4P_{1\frac{1}{2}}-y^4P_{1\frac{1}{2}}$; $a^4P_{2\frac{1}{2}}-z^4P_{1\frac{1}{2}}$		
1	6732.02	2		14850.29	$b^4P_{1\frac{1}{2}}-y^4P_{2\frac{1}{2}}$		
1	6708.07	4		14903.31	$a^4P_{2\frac{1}{2}}-z^4P_{2\frac{1}{2}}$		
1	6693.66	1h		14935.40	$b^2G_{4\frac{1}{2}}-x^2G_{4\frac{1}{2}}$		
1	6677.82	1−		14970.82	$b^4F_{1\frac{1}{2}}-y^4G_{2\frac{1}{2}}$		
1	6662.38	(1)	IV A	15005.50	$b^4F_{2\frac{1}{2}}-y^4G_{3\frac{1}{2}}$		
1	6657.62	1−		15016.25	$b^4P_{0\frac{1}{2}}-y^4P_{1\frac{1}{2}}$		
1	6643.79	(2)	IV A	15047.50	$b^4F_{3\frac{1}{2}}-y^4G_{4\frac{1}{2}}$		
1	6633.26	(2)	III A	15071.38	$a^2G_{4\frac{1}{2}}-y^4F_{3\frac{1}{2}}$		
1	6624.86	(7)	III A	15090.49	$a^4P_{2\frac{1}{2}}-z^4P_{1\frac{1}{2}}$	(0? w_1) 1.50	(0) 1.43*b*
1	6623.51	(8)	IV A	15093.57	$b^4F_{4\frac{1}{2}}-y^4G_{5\frac{1}{2}}$		
1	6607.82	(3)	III A	15129.42	$a^2G_{3\frac{1}{2}}-z^2G_{3\frac{1}{2}}$		
2	6606.445	[0]		15132.56	$a^4D_{1\frac{1}{2}}-z^2D_{1\frac{1}{2}}$		
1	6605.98	(10)	III A	15133.63	$a^4P_{1\frac{1}{2}}-z^4P_{0\frac{1}{2}}$	(0.43) **1.32**, 2.12	(0.42) **1.28**, 2.12
1	6578.96	(2)	III A	15195.79	$a^4D_{0\frac{1}{2}}-z^2D_{1\frac{1}{2}}$		
1	6568.73	1h		15219.45	$a^4D_{3\frac{1}{2}}-z^2D_{2\frac{1}{2}}$; $b^2G_{4\frac{1}{2}}-w^4G_{3\frac{1}{2}}$		
1	6565.88	(3)	III A	15226.05	$a^4P_{0\frac{1}{2}}-z^4P_{0\frac{1}{2}}$	(0) 2.61	(0.02) 2.56*b*
2	6564.350	[2]		15229.60	$a^2G_{3\frac{1}{2}}-y^4F_{3\frac{1}{2}}$		
1	6558.02	(5)	III A	15244.30	$a^2G_{4\frac{1}{2}}-z^2G_{4\frac{1}{2}}$	(0.24) 1.11	(0.00) 1.13*b*
1	6550.02	(2)	IV	15262.91		(0) 1.08	
1	6543.51	(5)	III A	15278.12	$a^4P_{1\frac{1}{2}}-z^4P_{1\frac{1}{2}}$	(0) 1.74	(0.01) 1.70*b*
1	6531.44	(15)	II	15306.34	$a^4P_{2\frac{1}{2}}-z^4P_{1\frac{1}{2}}$	(0) 1.59	(0.09) 1.57*b*
2	6510.076	[−1]		15356.57	$a^4D_{2\frac{1}{2}}-z^2D_{2\frac{1}{2}}$		
1	6508.736	(2)	III	15359.73			
1	6504.164	(9)	II A	15370.54	$a^4P_{0\frac{1}{2}}-z^4P_{1\frac{1}{2}}$	(0.47) **1.30**, 2.20	(0.44) **1.27**, 2.15
1	6490.68	(2)	IV	15402.46	$a^2F_{3\frac{1}{2}}-y^2D_{2\frac{1}{2}}$		
1	6488.05	(4)	IV	15408.70	$a^2F_{3\frac{1}{2}}-y^2D_{3\frac{1}{2}}$	(0) 1.08	(0) 1.08*b*
1	6480.52	2h		15426.60	$y^6D_{3\frac{1}{2}}-e^6P_{3\frac{1}{2}}$		
1	6466.97	(2)	III A	15458.94	$a^4D_{1\frac{1}{2}}-z^2D_{2\frac{1}{2}}$		
1	6452.354	(10)	II A	15493.95	$a^4P_{1\frac{1}{2}}-z^4P_{2\frac{1}{2}}$	(0) 1.48	(0) 1.51*b*
1	6450.947	(2)	IV A	15497.33	$b^4F_{4\frac{1}{2}}-z^4F_{4\frac{1}{2}}$		
1	6447.82	(3)	IV A	15504.84	$b^4F_{3\frac{1}{2}}-z^4F_{3\frac{1}{2}}$		
1	6445.14	(1)	IV A	15511.38	$b^4F_{2\frac{1}{2}}-z^4F_{2\frac{1}{2}}$		
1	6438.08	(1)	IV A	15528.29	$b^2G_{3\frac{1}{2}}-y^2G_{3\frac{1}{2}}$		
1	6435.148	(2)	III A	15535.37	$b^4F_{1\frac{1}{2}}-z^4F_{1\frac{1}{2}}$	(?) 0.41	(0.01) 0.38*b*
1	6433.17	(3)	III A	15540.16	$b^4F_{2\frac{1}{2}}-z^4F_{2\frac{1}{2}}$	(0) 1.07	(0.09) 1.03*b*
1	6431.620	(4)	III A	15543.89	$b^4F_{3\frac{1}{2}}-z^4F_{3\frac{1}{2}}$	(0) 1.22	(0.03) 1.22*b*
1	6430.471	(5)	III	15546.67	$b^4F_{4\frac{1}{2}}-z^4F_{4\frac{1}{2}}$	(0) 1.32	(0.04) 1.32*b*
1	6424.96	(1h)	IV	15560.02	$y^6D_{2\frac{1}{2}}-e^6P_{2\frac{1}{2}}$		
1	6423.219	(1)	IV A	15564.22	$b^4F_{1\frac{1}{2}}-z^4F_{2\frac{1}{2}}$		
1	6420.23	1−		15571.47	$b^2G_{4\frac{1}{2}}-z^2G_{3\frac{1}{2}}$		
1	6418.71	(1)	IV A	15575.16	$a^4G_{3\frac{1}{2}}-z^4H_{3\frac{1}{2}}$		
1	6417.017	(2)	IV A	15579.27	$b^4F_{3\frac{1}{2}}-z^4F_{2\frac{1}{2}}$		
1	6411.26	1		15593.26	$b^4F_{2\frac{1}{2}}-z^4F_{1\frac{1}{2}}$; $a^2F_{3\frac{1}{2}}-w^4D_{2\frac{1}{2}}$?		
1	6407.07	2		15603.45	$b^4D_{1\frac{1}{2}}-z^2D_{1\frac{1}{2}}$		
1	6405.961	1		15606.16	$a^4G_{4\frac{1}{2}}-z^4H_{4\frac{1}{2}}$; $a^2D_{1\frac{1}{2}}-y^4P_{1\frac{1}{2}}$?		
1	6393.270	2	III	15637.14	$a^4G_{3\frac{1}{2}}-z^4H_{3\frac{1}{2}}$	(0? w_1) 0.78	(0) 0.79*b*
1	6385.62	1		15655.87	$a^4G_{2\frac{1}{2}}-z^4H_{3\frac{1}{2}}$		
1	6384.46	1h		15658.71	$y^6D_{1\frac{1}{2}}-e^6P_{2\frac{1}{2}}$		
1	6381.26	2h		15666.56	$y^6D_{0\frac{1}{2}}-f^4D_{1\frac{1}{2}}$		
1	6379.338	3	III	15671.28	$a^4G_{2\frac{1}{2}}-z^4H_{2\frac{1}{2}}$	(0) 0.97	(0) 1.02*b*
1	6374.484	1	III A	15683.21	$a^4G_{2\frac{1}{2}}-w^4F_{2\frac{1}{2}}$	(0) 0.64	(0) 0.64*b*

TABLE 1.—*Arc spectrum of vanadium* (V I)—Continued

(1)	(2)	(3)	(4)	(5)	(6)	(7)	(8)
Ref.	λ_{air} A	Int. arc	Temp. class	ν_{vac} cm^{-1}	Term combinations	Zeeman effect: Observed	Zeeman effect: Computed
2	6369.217	[−3]		15696.19	$b^3G_{3\frac{1}{2}}-w^2F^0_{3\frac{1}{2}}$		
1	6361.259	3	III	15715.82	$a^4G_{4\frac{1}{2}}-z^4H^0_{5\frac{1}{2}}$ $(b^3G_{3\frac{1}{2}}-y^2G^0_{4\frac{1}{2}})$	(0) 1.03	(0) 1.05*b*
1	6358.819	3	III	15721.85	$a^4G_{3\frac{1}{2}}-z^4H^0_{3\frac{1}{2}}$	(0) 1.09	(0) 1.04*b*
1	6357.297	4	III	15725.61	$a^4H_{3\frac{1}{2}}-y^4G^0_{3\frac{1}{2}}$	(0) 0.80	(0) 0.80*b*
1	6355.582	1	II A	15729.86	$a^4G_{3\frac{1}{2}}-w^4F^0_{3\frac{1}{2}}$	(0) 0.90	(0) 0.90*b*
2	6354.306	[−1]		15733.02	$b^4F_{1\frac{1}{2}}-z^4G^0_{1\frac{1}{2}}$?		
1	6349.477	5	III	15744.98	$a^4H_{4\frac{1}{2}}-y^4G^0_{4\frac{1}{2}}$	(0) 0.94	(0) 0.95*b*
1	6343.944	1	IV	15758.71	$b^3G_{4\frac{1}{2}}-z^2G^0_{4\frac{1}{2}}$ $y^6D^0_{3\frac{1}{2}}-f^5F_{3\frac{1}{2}}$		
1	6340.18	1h		15768.07	$y^6D^0_{3\frac{1}{2}}-f^5F_{4\frac{1}{2}}$		
1	6339.090	5	III	15770.78	$a^4H_{3\frac{1}{2}}-y^4G^0_{3\frac{1}{2}}$	(0) 1.03	(0) 1.03*b*
2	6333.634	[0]		15784.37	$a^4H_{3\frac{1}{2}}-y^4G^0_{2\frac{1}{2}}$		
1	6326.845	6	III	15801.31	$a^4H_{4\frac{1}{2}}-y^4G^0_{4\frac{1}{2}}$	(0) 1.09	(0) 1.10*b*
1	6324.675	2	III	15806.73	$a^4G_{4\frac{1}{2}}-w^4F^0_{3\frac{1}{2}}$	(0) 1.11	(0) 1.06*b*
1	6321.229	2	IV	15815.35	$y^6D^0_{3\frac{1}{2}}-f^5D_{4\frac{1}{2}}$	(0) 1.54	(0. 41) 1.55*b*
1	6318.367	*tr*	IV A	15822.50	$a^4H_{4\frac{1}{2}}-y^4G^0_{4\frac{1}{2}}$ $b^4D_{3\frac{1}{2}}-x^4P^0_{2\frac{1}{2}}$		
1	6311.53	3	III	15839.66	$y^6D^0_{3\frac{1}{2}}-f^5F_{2\frac{1}{2}}$	(0) $1.06w_1$	(0) 1.14*b*
1	6309.718	1	IV	15844.19	$b^4D_{2\frac{1}{2}}-x^4P^0_{1\frac{1}{2}}$	(0) $1.34w_1$	(0) 1.33*b*
2	6306.499	[0]		15852.28	$b^4F_{2\frac{1}{2}}-z^4G^0_{2\frac{1}{2}}$		
1	6304.334	2	IV	15857.72	$y^6D^0_{2\frac{1}{2}}-f^5F_{2\frac{1}{2}}$		
1	6298.69	*tr*	IV A	15871.93	$b^3G_{4\frac{1}{2}}-w^2F^0_{3\frac{1}{2}}$ $a^4G_{3\frac{1}{2}}-w^4F^0_{3\frac{1}{2}}$		
1	6296.518	15	I	15877.41	$a^6D_{4\frac{1}{2}}-z^6D^0_{3\frac{1}{2}}$ $(z^4F^0_{4\frac{1}{2}}-f^4F_{3\frac{1}{2}})$	(0) 1.50	(0) 1.46*b*
1	6292.858	20		15886.64	$a^6D_{3\frac{1}{2}}-z^6D^0_{3\frac{1}{2}}$	(0) 1.52	(0) 1.47*b*
1	6286.94	2		15901.59	$y^6D^0_{2\frac{1}{2}}-f^5F_{2\frac{1}{2}}$		
1	6285.185	20	I	15906.04	$a^6D_{2\frac{1}{2}}-z^6D^0_{1\frac{1}{2}}$	(0) 1.50	(0) 1.50*b*
1	6282.36	2	III	15913.21	$a^4G_{2\frac{1}{2}}-w^4F^0_{1\frac{1}{2}}$	(0) 1.16	(0) **1.13***s*
1	6280.93	2h		15916.82	$z^4F^0_{2\frac{1}{2}}-f^4F_{1\frac{1}{2}}$		
1	6274.670	15	I	15932.70	$a^6D_{1\frac{1}{2}}-z^6D^0_{0\frac{1}{2}}$	(0.60) **1.26**, 2.49	(0.69) **1.13**, 2.51
1	6268.841	8	II A	15947.51	$a^6D_{4\frac{1}{2}}-z^6F^0_{5\frac{1}{2}}$ $a^6D_{3\frac{1}{2}}-z^6F^0_{4\frac{1}{2}}$		
1	6266.32	7	II A	15953.92	$a^6D_{2\frac{1}{2}}-z^6F^0_{1\frac{1}{2}}$	(0.25, 0.67) 1.41, 1.92, **2.39.**	(**0.23**, 0.70) 0.91, 1.37, 1.84, **2.31**
1	6261.236	5	II A	15966.88	$a^6D_{1\frac{1}{2}}-z^6F^0_{2\frac{1}{2}}$	(1.12) 0.78, 3.06	(1.13) 0.69, **2.95**
1	6258.595	8	II A	15973.62	$a^6D_{2\frac{1}{2}}-z^6D^0_{2\frac{1}{2}}$ $(a^4G_{4\frac{1}{2}}-w^4F^0_{3\frac{1}{2}})$	(0) 3.20	(0.05) 3.25*b*
1	6256.906	8	II A	15977.92	$a^6D_{3\frac{1}{2}}-z^6D^0_{3\frac{1}{2}}$	(0) 1.61	(0.07) 1.60*b*
1	6251.83	30*a*	I	15990.89	$a^6D_{2\frac{1}{2}}-z^6D^0_{2\frac{1}{2}}$	(0) 1.55	(0.09) 1.54*b*
1	6249.30	*tr*	IV A	15997.39	$b^4F_{2\frac{1}{2}}-z^4G^0_{3\frac{1}{2}}$		
1	6247.544	2h		16001.87	$b^4D_{1\frac{1}{2}}-x^4P^0_{1\frac{1}{2}}$		
1	6245.214	2	II A	16007.84	$a^6D_{0\frac{1}{2}}-z^6F^0_{1\frac{1}{2}}$	(1.94) 1.47	(1.86) 1.42*b*
1	6243.49	3	III A	16012.27	$a^4D_{2\frac{1}{2}}-z^6P^0_{1\frac{1}{2}}$		
1	6243.11	30*a*	I	16013.24	$a^6D_{4\frac{1}{2}}-z^6D^0_{4\frac{1}{2}}$	(0) $1.54w_1$ C	(0.09) 1.54*b*
1	6242.80	15	I	16014.04	$a^4D_{2\frac{1}{2}}-z^6D^0_{3\frac{1}{2}}$	(0.80) 0.96	(0.77) **0.99**, 2.53
1	6240.137	6	II A	16020.86	$a^6D_{1\frac{1}{2}}-z^6F^0_{1\frac{1}{2}}$	(1.05) 0.85, **1.51**, 2.12	(0.34, 1.02) 0.80, **1.48**, 2.16
1	6238.22	*tr*	IV	16025.80	$b^4D_{2\frac{1}{2}}-x^4P^0_{2\frac{1}{2}}$		
1	6236.278	1	IV	16030.78	$z^4F^0_{2\frac{1}{2}}-f^4F_{2\frac{1}{2}}$	(0?w_3 D) $1.02w_3$ A	(0.12) 1.01*b*
1	6233.187	12	I A	16038.73	$a^6D_{2\frac{1}{2}}-z^6F^0_{2\frac{1}{2}}$ $(z^4F^0_{3\frac{1}{2}}-f^4F_{2\frac{1}{2}})$	(0.74) $1.44w_3$ C	(0.72) 1.44*b*
1	6230.736	30	I	16045.04	$a^6D_{1\frac{1}{2}}-z^6D^0_{2\frac{1}{2}}$ $(z^4F^0_{2\frac{1}{2}}-f^4F_{2\frac{1}{2}})$		
1	6224.507	15	I	16061.10	$a^6D_{2\frac{1}{2}}-z^6F^0_{2\frac{1}{2}}$ $(a^6D_{2\frac{1}{2}}-z^6F^0_{1\frac{1}{2}}?)$		
1	6221.216	1	III A	16069.59	$a^4D_{2\frac{1}{2}}-z^6P^0_{1\frac{1}{2}}$	(0.55)?	(**0.49**, 1.48) −**0.13**, 0.86 1.85, 2.83
1	°6218.328	3	IV	16077.06	$z^4F^0_{1\frac{1}{2}}-f^4F_{2\frac{1}{2}}$	(0) 1.32	(0.07) 1.32*b*
1	6216.368	30	I	16082.12	$a^6D_{3\frac{1}{2}}-z^6D^0_{2\frac{1}{2}}$	(0) 1.45	(0) **1.44***s*
1	6214.743	1	IV	16086.33			
1	6213.874	15	I	16088.58	$a^6D_{4\frac{1}{2}}-z^6F^0_{5\frac{1}{2}}$	(0.45) 1.48	(0.52) 1.45*b*
2	6207.251	[5]		16105.75	$a^6D_{3\frac{1}{2}}-z^6F^0_{3\frac{1}{2}}$		
2	6200.644	[0]		16122.91	$a^4D_{2\frac{1}{2}}-z^6P^0_{2\frac{1}{2}}$		

TABLE 1.—*Arc spectrum of vanadium* (V I)—Continued

(1)	(2)	(3)	(4)	(5)	(6)	(7)	(8)
Ref.	λ_{air} A	Int. arc	Temp. class	ν_{vac} cm^{-1}	Term combinations	Zeeman effect: Observed	Zeeman effect: Computed
1	6199.202	30	I	16126.65	$\begin{cases} a^6D_{3½}-z^6D^0_{1½} \\ (a^4F_{3½}-z^6G^0_{3½}) \end{cases}$	(0) 1.47	(0) 1.58*b*
1	6190.490	1	III A	16149.35	$a^4D_{2½}-z^6P^0_{2½}$	(1.17)?	(1.09) 1.60*b*
1	*b*6189.350	3	II A	16152.32	$a^6D_{2½}-z^6F^0_{3½}$	(?) 1.00w_2 A	(0) 0.87*b*
1	6184.93	1*h*		16163.87	$x^6D^0_{1½}-f^6P_{2½}$		
2	6184.026	[−17]		16166.23	$b^4F_{1½}-z^4G^0_{1½}$		
1	6181.841	1	III A	16171.95	$a^4D_{1½}-z^6P^0_{1½}$		
1	6170.340	8	I A	16202.09	$a^6D_{3½}-z^6F^0_{4½}$		
2	6161.913	[0]		16224.25	$a^4F_{2½}-z^6G^0_{3½}$		
2	6157.763	[1]		16235.18	$a^4D_{0½}-z^6P^0_{1½}$		
2	6152.416	[1]		16249.29	$a^4F_{3½}-z^6G^0_{4½}$		
2	6151.509	[1]		16251.68	$\begin{cases} a^4D_{1½}-z^6P^0_{2½} \\ a^6D_{2½}-y^6F^0_{1½} \end{cases}$		
1	6150.132	15	I	16255.33	$a^6D_{4½}-z^6F^0_{5½}$	(? w_3 D) 1.15w_3 A	(0) 1.18*b*
1	6135.36	15	II	16294.47	$a^4D_{1½}-z^4P^0_{0½}$	(0.68) **0.51**, 1.80	(0.67) **0.52**, 1.87
1	6135.07	2	III A	16295.25	$a^2G_{3½}-z^6F^0_{4½}$		
2	6128.543	[0]		16312.58	$a^4F_{3½}-z^6G^0_{3½}$		
1	6128.30	2	III A	16313.24	$a^4D_{1½}-y^6F^0_{0½}$	(0.88) **0**, 2.12	(0.89) 0.31, **2.08**
1	6119.505	40	I	16336.68	$a^4D_{2½}-z^4P^0_{1½}$	(0.19, 0.55) **0.81**, 1.20, 1.56, —	(**0.18**, 0.54) **0.81**, 1.17, 1.54, 1.89
1	6111.622	25	II	16357.75	$a^4D_{0½}-z^4P^0_{0½}$	(1.27) 1.27	(1.27) 1.27*b*
2	6110.214	[3]		16361.52	$a^4F_{1½}-z^6G^0_{1½}$		
2	6109.176	[1]		16364.30	$a^4F_{4½}-z^6G^0_{5½}$		
1	*b*6106.967	2	III A	16370.23	$a^2G_{4½}-z^2F^0_{3½}$	(0) 1.02	(0) 1.34*b*
1	6104.669	*tr*	III A	16376.38	$a^4D_{0½}-y^6F^0_{0½}$		
1	6097.42	1		16395.86	$a^4D_{3½}-y^6F^0_{4½}$		
2	6093.866	[3]		16405.42	$a^4F_{3½}-z^6G^0_{4½}$		
3	6090.515	−3		16414.44	$a^4D_{3½}-y^6F^0_{3½}$		
1	6090.184	50	I	16415.33	$a^4D_{3½}-z^4P^0_{2½}$		
2	6089.473	[3]		16417.24	$a^4D_{2½}-y^6F^0_{1½}$		
1	6087.485	1	III A	16422.61	$a^4D_{1½}-y^6F^0_{2½}$		
1	6086.55	2		16425.14	$a^4P_{2½}-y^4D^0_{1½}$		
2	6082.789	[2]		16435.29	$a^4F_{3½}-z^6G^0_{3½}$		
1	6081.421	25	I	16439.00	$a^4D_{1½}-z^4P^0_{1½}$	(−, **0.79**) 0.90, 1.45, 1.99	(0.25, **0.77**) 0.94, **1.45**, 1.96
2	6077.367	[2]		16449.95	$a^4F_{1½}-z^6G^0_{2½}$		
1	6067.245	1	III	16477.40	$b^4G_{2½}-z^2H^0_{3½}$	(0) 0.94	(0) 0.92*b*
1	6063.372	*tr*	III A	16487.92	$a^4H_{3½}-z^4G^0_{3½}$	(0) 0.76	(0) 0.80*b*
1	6058.113	5	II A	16502.23	$a^4D_{0½}-z^4P^0_{1½}$	(0.83) 0.86, **2.56**	(0.85) 0.85, **2.56**
1	*b*6054.445	2		16512.24	$b^2G_{4½}-f^4D^0_{3½}$	(?) 0.90	(0) 0.68*b*
1	6048.636	*tr*	III A	16528.10	$a^4P_{2½}-y^4D^0_{2½}$		
1	6039.690	25	I	16552.57	$a^4D_{2½}-z^4P^0_{2½}$	(0.51w_2B) 1.46w_2C	(0.52) 1.47*b*
1	6025.384	1	III A	16591.87	$a^4H_{4½}-z^4G^0_{4½}$	(0) 0.92	(0) 0.92*b*
1	6024.161	1		16595.24	$z^2F^0_{3½}-e^2F_{3½}$		
1	6021.725	*tr*	IV	16601.96		(0) 1.04	
1	*b*6017.90	*tr*	III A	16612.51	$a^4P_{1½}-y^4D^0_{1½}$	(0.74) 0	(0.74) 1.43*b*
1	6016.093	1	IV	16617.50	$b^2G_{4½}-z^2H^0_{3½}$	(0) 1.05	(0) 1.08*b*
1	6008.648	*tr*	III A	16638.08	$a^4P_{0½}-y^4D^0_{0½}$	(1.41) 1.24.	(1.32) 1.26*b*
1	6002.601	4	II A	16654.84	$a^4D_{1½}-e^4P^0_{1½}$	(?) 2.03w_1	(0) 1.89*b*
1	6002.273	2	II A	16655.76	$a^4P_{2½}-y^4D^0_{3½}$	(0) 1.16	(0) 1.19*b*
1	5984.602	1	III A	16704.93	$a^4P_{2½}-y^4D^0_{1½}$		
1	5980.748	2	III A	16715.70	$a^4P_{1½}-y^4D^0_{2½}$	(0) 1.02	(0) 1.07*b*
1	5978.881	2	III A	16720.92	$a^4H_{4½}-z^4G^0_{4½}$	(0) 1.02	(0) **1.01***s*
1	5975.323	2		16730.87	$z^2F^0_{2½}-e^2F_{2½}$		
1	5924.560	2	III A	16874.23	$a^4H_{5½}-z^4G^0_{5½}$	(0) 1.11	(0) 1.12*b*
1	5879.41	1−		17003.82	$y^6F^0_{3½}-e^6G_{3½}$		
1	5863.16	*tr*	IV A	17050.94	$a^4G_{3½}-z^4F^0_{3½}$		
1	5858.13	1*h*		17065.57	$y^6F^0_{4½}-e^6G_{4½}$		
4	5855.49	*tr*	IV A	17073.27	$b^4F_{1½}-w^4F^0_{1½}$		
4	5853.75	1	IV A	17078.34	$b^4P_{1½}-x^4D^0_{½}$		
1	5850.286	2	III A	17088.46	$b^4P_{2½}-x^4D^0_{1½}$	(0.56) 1.52	(0.55) 1.42*b*
1	5846.306	8	III	17100.09	$y^6F^0_{1½}-e^6G_{0½}$	(0) 1.18	(0) 1.18*b*
2	5839.357	0*h*		17120.44	$b^4F_{0½}-x^4D^0_{1½}$		
2	5839.043	[1]		17121.36	$y^6F^0_{1½}-e^6G_{1½}$		

TABLE 1.—*Arc spectrum of vanadium* (V I)—Continued

(1)	(2)	(3)	(4)	(5)	(6)	(7)	(8)
Ref.	λ_{air} A	Int. arc	Temp. class	ν_{vac}cm^{-1}	Term combinations	Zeeman effect: Observed	Zeeman effect: Computed
1	5830.719	7	III	17145.80	$y^4F_{1\frac{1}{2}}-e^4G_{2\frac{1}{2}}$	(0) 1.10	(0) 1.12*b*
1	5826.59	1	III	17157.96	$b^4F_{2\frac{1}{2}}-w^4F_{3\frac{1}{2}}$		
1	5817.532	5	III	17184.67	$y^4F_{3\frac{1}{2}}-e^4G_{3\frac{1}{2}}$	(?w_2) 1.00w_2	(0) 0.98*b*
1	b5817.063	3	III	17186.05	$b^4P_{1\frac{1}{2}}-z^4D_{1\frac{1}{2}}$	(0.79) 0.77	(0.26, **0.77**) 0.91, **1.42**, 1.94
1	5814.76	1	IV	17192.86	$a^4G_{3\frac{1}{2}}-z^4F_{3\frac{1}{2}}$		
1	5807.14	3	III	17215.44	$y^6F_{3\frac{1}{2}}-e^6G_{3\frac{1}{2}}$	(?) 0.87	(0) 0.89*b*
1	5798.905	2	IV	17239.87	$y^4F_{1\frac{1}{2}}-e^4G_{2\frac{1}{2}}$		
1	5797.352	1–		17244.48	$y^4F_{2\frac{1}{2}}-e^4G_{3\frac{1}{2}}$		
1	5790.533	1	III A	17264.80	$b^4F_{3\frac{1}{2}}-w^4F_{3\frac{1}{2}}$		
1	5788.549	3	III	17270.71	$b^4P_{2\frac{1}{2}}-z^4D_{2\frac{1}{2}}$	(0? w_3D) 1.13	(0.12) 1.20*b*
1	5786.153	7	III	17277.86	$z^4G_{3\frac{1}{2}}-f^4F_{3\frac{1}{2}}$ $z^4G_{2\frac{1}{2}}-f^4F_{3\frac{1}{2}}$	(0.31) 1.39 (0? w_1D) 0.98w_1A	(1.26) 1.34*b* (0) 0.86*b* (0) 1.05*b*
1	5784.360	5	III	17283.22	$z^4G_{3\frac{1}{2}}-f^4F_{4\frac{1}{2}}$	(0? w_1D) 1.12w_1A	(0) 1.04*b*
1	5783.509	2	III	17285.76	$z^4G_{3\frac{1}{2}}-f^4F_{3\frac{1}{2}}$		
1	5782.842	1	IV	17287.75	$a^4G_{3\frac{1}{2}}-z^4F_{3\frac{1}{2}}$		
1	5782.001	2	III A	17288.48	$a^4D_{3\frac{1}{2}}-y^4F_{3\frac{1}{2}}$ $b^4P_{1\frac{1}{2}}-y^4P_{2\frac{1}{2}}$		
1	b5776.670	4	II A	17306.23	$a^4D_{3\frac{1}{2}}-z^4G_{3\frac{1}{2}}$	(1.41) 0.91	(1.39) 1.15*b*
1	5772.402	6	III	17319.03	$b^4P_{2\frac{1}{2}}-z^4D_{1\frac{1}{2}}$	(0? w_2D) 1.12w_2A	(0) 1.11*b*
1	5770.55	3		17324.60	$y^6F_{3\frac{1}{2}}-f^6F_{3\frac{1}{2}}$	(0) 1.42	(0.00) 1.40*b*
1	5770.02	1*h*		17326.19	$z^6P_{3\frac{1}{2}}-e^6P_{2\frac{1}{2}}$		
1	5761.411	2	III A	17352.06	$a^4D_{2\frac{1}{2}}-y^4F_{1\frac{1}{2}}$	(**0.53**, 1.32) 2.91	(**0.47**, 1.40) −0.05, 0.89, 1.82, **2.75**
1	5755.085	3*H*		17371.13			
1	5752.711	3	III	17378.30	$b^4P_{0\frac{1}{2}}-z^4D_{1\frac{1}{2}}^{\dagger}$	(0.60) **0.47**, 1.97	(0.72) **0.45**, 1.88
1	5750.643	2	III	17384.55	$b^4F_{4\frac{1}{2}}-w^4F_{3\frac{1}{2}}$	(0) 1.34	(0.04) 1.30*b*
1	5748.860	4	III	17389.94	$b^4P_{1\frac{1}{2}}-z^4D_{2\frac{1}{2}}$ $a^2F_{2\frac{1}{2}}-z^4D_{1\frac{1}{2}}$?	(0) 0.82	(0) 1.00*b* (0) 0.84*b*
1	5748.412	1		17391.30	$b^2P_{1\frac{1}{2}}-y^4P_{1\frac{1}{2}}$		
1	5747.706	2	III	17393.43	$b^2H_{5\frac{1}{2}}-z^4G_{4\frac{1}{2}}$	(0) 1.06	(0) 1.15*b*
1	5743.438	18	II	17406.39	$a^4D_{3\frac{1}{2}}-y^4F_{4\frac{1}{2}}$	(0.78 w_3 D) 1.26 w_2 A	(0.71) 1.27*b*
1	5737.040	25	II	17425.77	$a^4D_{2\frac{1}{2}}-y^4F_{2\frac{1}{2}}$	(0.56, **0.85**) 0.49, 0.85, 1.18, 1.55	(0.19, 0.56, **0.93**) 0.42, **0.79**, **1.17**, 1.54, 1.91
1	5734.004	5	III	17435.00	$a^2F_{2\frac{1}{2}}-z^4G_{3\frac{1}{2}}$ $z^4G_{2\frac{1}{2}}-f^4F_{2\frac{1}{2}}$	(0) 0.94	
1	5733.403	1	IV	17436.82	$z^6P_{3\frac{1}{2}}-e^6P_{3\frac{1}{2}}$?		
1	5733.099	1	IV	17437.74	$b^2H_{4\frac{1}{2}}-z^4G_{3\frac{1}{2}}$	(0) 0.94	(0) 1.01*b*
1	5731.257	30	II	17443.35	$a^4D_{2\frac{1}{2}}-z^4G_{3\frac{1}{2}}$	(0.20, 0.64, 1.07) **0.72**, 1.14, 1.59	(**0.22**, 0.65, 1.08) **0.16**, 0.27, 0.70, 1.14, 1.57, 2.00
4	5729.89	*tr.*	IV A	17447.51	$a^2D_{1\frac{1}{2}}-y^2S_{\frac{1}{2}}$		
1	5727.662	20	II	17454.30	$a^4D_{1\frac{1}{2}}-y^4F_{1\frac{1}{2}}$	(0.37, **1.17**) 0, 0.82, 1.57	(0.39, **1.16**) 0.03, **0.81**, 1.58
1	5727.024	60	I	17456.25	$a^4D_{3\frac{1}{2}}-y^4F_{3\frac{1}{2}}$	(?w_1 D) 0.94 w_3 C	(0) 0.95*b*
1	b5725.633	6	III	17460.49	$a^2F_{3\frac{1}{2}}-z^2G_{4\frac{1}{2}}$	(0) 1.03	(0) 0.89*b*
1	5720.578	1		17475.92	$z^4G_{3\frac{1}{2}}-f^4F_{3\frac{1}{2}}$		
1	5716.219	3	IV	17489.24		(0) 1.16	
1	5713.582	1		17497.31	$b^4P_{1\frac{1}{2}}-z^2P_{1\frac{1}{2}}$		
1	5711.92	1–		17502.41	$a^4G_{3\frac{1}{2}}-z^4D_{2\frac{1}{2}}$		
1	5708.959	2	III	17511.48	$b^2P_{1\frac{1}{2}}-z^2D_{1\frac{1}{2}}$	(0) 0.93	(0) 0.95*b*
1	5707.765	1	IV	17515.15	$b^2H_{4\frac{1}{2}}-z^2G_{4\frac{1}{2}}$		
1	5706.973	30	I	17517.58	$a^4D_{2\frac{1}{2}}-y^4F_{1\frac{1}{2}}$	(0.25) 0.22, **0.59**	(0.21) 0.21, **0.63**
1	5706.135	2	IV	17520.15			
1	5704.374	2	IV	17525.56			
1	b5703.562	40	I	17528.06	$a^4D_{1\frac{1}{2}}-y^4F_{2\frac{1}{2}}$	(?w_3 D) 0.94	(0) 0.82*b*
1	5698.509	60	I	17543.59	$a^4D_{2\frac{1}{2}}-y^4F_{3\frac{1}{2}}$		
1	5691.125	1	IV	17566.36	$z^2F_{3\frac{1}{2}}-f^6D_{3\frac{1}{2}}$		
1	5687.764	1	IV	17576.73	$b^2P_{1\frac{1}{2}}-z^2F_{2\frac{1}{2}}$		
2	5683.658	1		17589.43	$b^4F_{4\frac{1}{2}}-y^4G_{5\frac{1}{2}}$		
1	5683.230	2	III	17590.76			
1	5676.529	1–		17611.52	$b^4P_{0\frac{1}{2}}-z^4D_{1\frac{1}{2}}$		
1	5670.827	30*cm*	I	17629.23	$a^4D_{3\frac{1}{2}}-z^4G_{4\frac{1}{2}}$		
1	5668.369	12	II	17636.88	$a^4D_{3\frac{1}{2}}-y^4D_{3\frac{1}{2}}$	(0) 1.48	(0) 1.45*b*
1	5665.246	1	IV	17646.53	$b^4P_{0\frac{1}{2}}-z^2P_{1\frac{1}{2}}$ $a^4F_{2\frac{1}{2}}-z^2F_{3\frac{1}{2}}$		
1	5658.432	1–		17667.84	$z^6P_{3\frac{1}{2}}-f^6F_{4\frac{1}{2}}$		

TABLE 1.—*Arc spectrum of vanadium* (V I)—Continued

(1) Ref.	(2) λ_{air} A	(3) Int. arc	(4) Temp. class	(5) ν_{vac} cm^{-1}	(6) Term combinations	(7) Zeeman effect Observed	(8) Zeeman effect Computed
1	5657.449	12	II	17670.92	$a^4D_{3½}-y^4D^0_{5½}$	(0w_1) 1.49w_1	(0) 1.48*b*
1	5656.895	1	IV	17672.65	$b^2P_{½}-y^2P^0_{½}$	(0) 0.75	(0.04) 0.70*b*
1	5656.29	2h		17674.55	$a^2F_{2½}-z^2D^0_{3½}$	(0.59) 0.93	(0.59) 1.00*b*
1	5652.030	1		17686.61		(0) 0.93w_1	
1	5651.50	1	IV	17689.53	$b^4P_{0½}-z^4P^0_{½}$		
1	5646.112	10	II	17706.40	$a^4D_{1½}-y^4D^0_{3½}$	(0.60) 0.60, **1.80**	(0.63) 0.57, **1.82**
1	5643.363	1h		17715.03	$z^6P^0_{3½}-f^{16}D_{4½}$		
1	5635.516	3		17739.69	$a^2F_{3½}-z^2F^0_{3½}$	(0) 0.87w_1	(0.07) 0.88*b*
1	5633.900	2		17744.77	$a^2F_{3½}-w^4G^0_{3½}$	(0.38) 1.09	(0.24) 1.10*b*
1	5632.469	1	II A	17749.30	$a^4F_{4½}-z^6D^0_{3½}$		
1	5627.628	30	I	17764.55	$a^4D_{3½}-y^4D^0_{3½}$	(0w_1) 1.42w_1	(0) 1.39*b*
1	5626.014	8	II	17769.65	$a^4D_{0½}-y^4D^0_{½}$	Unaffected	(0.03) 0.03
1	5624.895	10	II	17773.19	$a^4D_{1½}-y^4D^0_{1½}$	(0) 1.20	(0.03) 1.18*b*
1	5624.605	20	I	17774.11	$a^4D_{2½}-y^4D^0_{2½}$	(0) 1.36	(0) 1.34*b*
1	5624.223	2		17775.31	$b^2P_{½}-y^2P^0_{½}$	(0) 1.46	(0) **1.42***a*
1	5622.075	2		17782.09	$a^4H_{3½}-z^4H^0_{3½}$	(0) 0.67	(0.09) 0.66*b*
1	b5620.46	1h		17787.20	$a^4H_{3½}-z^4H^0_{3½}$ $b^2G_{4½}-w^4F^0_{4½}$?	(0.38)? w_1	(0) 1.37*b* (0.71) 1.20*b*
1	5619.56	1		17790.08	$a^4D_{3½}-y^6D^0_{3½}$		
1	b5616.66	1		17799.27	$b^2H_{4½}-w^4G^0_{3½}$	(0) 0.76	(0) 0.65*b*
1	5610.20	1		17819.75	$a^4F_{4½}-z^6F^0_{3½}$ $a^2F_{3½}-w^4G^0_{3½}$		
1	5604.943	8	II	17836.46	$a^4D_{0½}-y^4D^0_{1½}$	(0.58) 0.60, **1.81**	(0.58) 0.58, **1.75**
1	5604.205	1	IV	17838.81	$b^4F_{3½}-y^4F^0_{3½}$ $a^4H_{4½}-z^4H^0_{3½}$	(0) 0.97	(0.44) 0.95*b* (0.15) 0.96*b*
1	5601.380	2	III	17847.80	$a^2F_{3½}-z^2F^0_{3½}$	(0.27) 1.08w_1	(0.27) 1.10*b*
1	5597.822	1	III A	17859.15	$a^4D_{2½}-y^6D^0_{3½}$		
1	5592.962	1	II A	17874.67	$a^4F_{1½}-z^6D^0_{½}$ $b^2H_{4½}-w^4G^0_{3½}$?		
1	5592.409	12	I	17876.44	$a^4D_{1½}-y^4D^0_{2½}$	(0?w_1 D) 1.50w_1 A	(0) 1.45*b*
1	5588.487	1	III A	17888.98	$a^4D_{2½}-y^6D^0_{2½}$	(0.48) 1.55w_2 C	(0.56) 1.49*b*
1	5586.007	2	III	17896.92	$a^4H_{3½}-z^4H^0_{3½}$	(0) 1.11	(0.04) 1.10*b*
1	5584.738	3		17900.99	$a^4H_{4½}-z^4H^0_{3½}$	(0) 1.17	(0.16) 1.20*b*
1	5584.490	10	I	17901.78	$a^4D_{2½}-y^4D^0_{2½}$	(0) 1.50	(0) **1.49***a*
1	5582.638	1		17907.72	$a^2D_{2½}-z^4D^0_{1½}$	(0) 1.16	(0) 1.17*b*
1	5579.35	1–		17918.27		(0) 1.02	
1	5578.400	1h		17921.33	$a^4D_{1½}-y^6D^0_{2½}$	(1.06) 0	(1.02) **0.17**, 2.22
1	5576.510	2		17927.40	$a^4D_{2½}-y^6D^0_{3½}$		
1	5573.992	1	II A	17935.50	$a^4F_{3½}-z^6F^0_{3½}$	(0) 1.11w_1	(0) 1.10*b*
1	5565.93	1		17961.48	$a^4D_{1½}-y^6D^0_{1½}$	(?w_1) 1.60	(0.94) 1.52*b*
1	5561.670	2	III A	17975.24	$a^2P_{½}-z^2S^0_{½}$	(0.81) 1.47	(0.83) 1.47*b*
3	5560.56	–2		17978.82	$a^4F_{3½}-z^6D^0_{3½}$		
1	5558.752	3	III	17984.67	$a^2P_{1½}-z^2S^0_{½}$ $a^4D_{2½}-y^6D^0_{3½}$	(0.58) **0.63**, 1.74	(0.55) **0.65**, 1.75
1	5557.453	1	II A	17988.87	$a^4F_{3½}-z^6D^0_{3½}$	(0.38) **0**,—	(**0.38**, 1.13) —**0.12**, 0.63, 1.38, 2.14
1	5547.060	8	II	18022.51	$a^4D_{3½}-y^6D^0_{3½}$	(0?w_1) 1.78w_1	(0) 1.69*b*
1	5545.933	2	III A	18026.24	$a^4D_{2½}-y^6D^0_{2½}$	(0?w_1 D) 1.97w_1 B?	(0) 1.87*b*
4	5544.89	1		18029.64	$a^4D_{1½}-y^6D^0_{1½}$		
4	5542.69	1	II A	18036.77	$a^4F_{3½}-z^6F^0_{3½}$	(0) 0.96	(0) 0.91*b*
1	b5535.382	1		18060.60	$a^4F_{2½}-z^6D^0_{3½}$	(0) 1.14	(1.24) 1.30*b*
1	5533.833	1	IV	18065.65	$b^4H_{3½}-y^4H^0_{3½}$	(0) 1.09	(0) 1.08*b*
1	5527.72	1		18085.63	$a^4F_{1½}-z^4D^0_{½}$		
1	5517.198	1	II A	18120.13	$a^4F_{1½}-z^6F^0_{½}$	(0.42) 0, 0.79	(0.42) –0.02, **0.82**
2	5516.807	[2]		18121.40	$a^4F_{2½}-z^6F^0_{2½}$		
2	5515.371	[4]		18126.12	$a^4F_{1½}-z^6D^0_{½}$		
1	5515.083	1	II A	18127.08	$a^4F_{4½}-z^6F^0_{3½}$	(0) 1.75	(0) 1.73*b*
1	5511.181	1	IV	18139.91	$b^4H_{3½}-z^4I^0_{3½}$	(?w_1 D) 1.69w_1 B	(0) 1.55*b*
1	5508.610	1		18148.37	$a^2F_{2½}-z^2G^0_{3½}$	(0) 1.19	(0) 1.15*b*
1	5507.753	8	III	18151.22	$b^2H_{4½}-z^2G^0_{3½}$ $a^2P_{½}-y^2S^0_{½}$	(0w_1 D) 0.75	(0) 0.77*b*
1	b5505.881	1		18157.37	$b^4H_{4½}-y^6H^0_{3½}$	(0.45)	(0.67) 0.82*b*
1	5504.838	2	III	18160.81	$a^2F_{3½}-y^2S^0_{½}$	(0.52) **0.70**, 1.71	(0.50) **0.70**, 1.70
2	5500.816	[2]		18174.09	$a^4F_{4½}-z^6F^0_{4½}$		
2	5496.020	[3]		18189.94	$a^4F_{3½}-z^4F^0_{3½}$		
1	5489.940	2	III	18210.09	$a^2D_{1½}-z^2P^0_{½}$	(0?) 1.03	(0) 1.03*b*
1	5487.915	10	III	18216.81	$b^2H_{3½}-z^2G^0_{3½}$	(0) 1.14	(0) 1.15*b*

TABLE 1.—*Arc spectrum of vanadium* (V I)—Continued

(1)	(2)	(3)	(4)	(5)	(6)	(7)	(8)
Ref.	λ_{air} Å	Int. arc	Temp. class	ν_{vac} cm^{-1}	Term combinations	Zeeman effect: Observed	Zeeman effect: Computed
1	5487.220	2	III	18219.12	$a^3D_{2\frac{1}{2}}-z^3P^0_{1\frac{1}{2}}$	(0) 1.14	(0) 1.13*b*
2	5482.471	[1]		18234.90	$a^4F_{3\frac{1}{2}}-z^6F^0_{3\frac{1}{2}}$		
1	5467.792	2		18283.86	$a^3F_{2\frac{1}{2}}-z^4G^0_{2\frac{1}{2}}$	(0) 0.92	(0) 0.89*b*
1	5463.996	1		18296.56		($?w_1$ D) $1.54w_2$ B	
1	5458.133	1	IV	18316.20	$a^3F_{2\frac{1}{2}}-w^3F^0_{2\frac{1}{2}}$	(0) 0.85	(0.04) 0.85*b*
1	5454.822	2		18327.32		(0) 1.28	
1	5450.68	1–		18341.25	$\begin{cases} b^4F_{2\frac{1}{2}}-w^4D^0_{2\frac{1}{2}} \\ b^4F_{2\frac{1}{2}}-z^4F^0_{1\frac{1}{2}} \end{cases}$	(0) 1.16	$\begin{cases} (0)\ 1.12b \\ (0)\ 1.19b \end{cases}$
1	5445.86	1*h*		18357.48	$b^4F_{1\frac{1}{2}}-w^4D^0_{1\frac{1}{2}}$	($?w_3$ D) $1.22w_1$ A?	(0) 1.24*b*
1	5443.235	2		18366.33	$z^4D^0_{3\frac{1}{2}}-f^4F_{3\frac{1}{2}}$		
1	5437.659	1	IV	18385.18	$b^3H_{3\frac{1}{2}}-z^3I^0_{3\frac{1}{2}}$	(0.79?) 1.06	(0.63) 1.01*b*
1	5434.168	3	IV	18396.98	$a^3F_{3\frac{1}{2}}-w^3F^0_{3\frac{1}{2}}$	($?w_1$ D) $1.10w_1$ B?	(0.18) 1.11*b*
1	5429.484	2		18412.85	$z^4D^0_{3\frac{1}{2}}-f^4F_{2\frac{1}{2}}$		
1	5424.106	4	III	18431.11	$\begin{cases} a^3F_{2\frac{1}{2}}-w^3D^0_{1\frac{1}{2}} \\ a^3H_{3\frac{1}{2}}-z^3H^0_{3\frac{1}{2}} \end{cases}$	(0?w_1 D) 0.93	(0) **0.95***s*
1	5421.654	1		18439.45	$z^4D^0_{1\frac{1}{2}}-f^4F_{1\frac{1}{2}}$		
1	5420.040	1		18444.93		(0?w_1 D) 1.56	
1	5418.076	2	IV	18451.63	$b^3H_{4\frac{1}{2}}-w^3F^0_{3\frac{1}{2}}$	($?w_2$ D) $0.52w_3$ A	(0) 0.61*b*
1	5415.277	10	III	18461.16	$b^3H_{3\frac{1}{2}}-z^3I^0_{3\frac{1}{2}}$	(0?) 1.06 diffuse	(0) 1.00*b*
1	5401.945	8	III	18506.72	$\begin{cases} b^3H_{4\frac{1}{2}}-z^3I^0_{3\frac{1}{2}} \\ b^3G_{3\frac{1}{2}}-z^3F^0_{2\frac{1}{2}} \end{cases}$	(? w_2 D) 0.97	(0) 1.01*b*
1	[b]5397.873	1	IV	18520.68	$z^4D^0_{\frac{1}{2}}-f^4F_{1\frac{1}{2}}$	(0.21) 0.58	(0.25) 0.21, **0.71**
	[c]5393.185	10 Fe	IV	18536.78	$a^3H_{4\frac{1}{2}}-z^3H^0_{4\frac{1}{2}}$		
1	5388.296	1	III	18553.60	$z^4D^0_{1\frac{1}{2}}-f^4F_{2\frac{1}{2}}$	(0?) 0.87 diffuse	(0) 0.90*b*
1	5385.134	3	III	18564.50	$z^4D^0_{2\frac{1}{2}}-f^4F_{4\frac{1}{2}}$	(0 w_1 D) 1.14 w_1 B	(0) 1.12*b*
1	[c]5383.436	2	IV	18570.37	$z^4D^0_{3\frac{1}{2}}-f^4F_{3\frac{1}{2}}$	(0?) 1.07 diffuse	(0) 1.06*b*
1	5363.530	1		18639.27	$a_4H_{3\frac{1}{2}}-z^3H^0_{4\frac{1}{2}}$		
1	5353.420	5	III	18674.47	$a^3F_{3\frac{1}{2}}-w^3D^0_{3\frac{1}{2}}$	(0) 1.08	(0) 1.08*b*
1	5338.61	1		18726.28	$a^3F_{2\frac{1}{2}}-w^3D^0_{2\frac{1}{2}}$		
1	5335.588	2*h*		18736.89		($?w_2$ D) $1.10w_1$	
1	5334.309	1		18741.37	$b^3H_{4\frac{1}{2}}-v^3G^0_{3\frac{1}{2}}$		
1	5330.425	1	III A	18755.02	$a^4D_{3\frac{1}{2}}-z^4F^0_{3\frac{1}{2}}$		
1	[b]5329.281	1		18759.05	$b^4F_{4\frac{1}{2}}-v^4F^0_{4\frac{1}{2}}$	(0) 1.36	(0.37) 1.36*b*
1	5328.823	2		18760.66	$z^6F^0_{3\frac{1}{2}}-e^6D_{4\frac{1}{2}}$	(? w_2 D) 1.29 w_2 C?	(0) 1.28 *b*
1	5319.087	2*h*		18795.00	$b^4P_{1\frac{1}{2}}-w^4D^0_{2\frac{1}{2}}$?	(0) 0.82 w_1 A	(0) **0.73***s*
1	5316.885	2		18802.79	$b^4P_{2\frac{1}{2}}-z^4F^0_{3\frac{1}{2}}$	(0? w_1 D) 0.38 w_3 A	(0) **0.38***s*
1	[b]5315.219	4		18808.67	$z^6F^0_{1\frac{1}{2}}-e^6D_{2\frac{1}{2}}$	(? w_2) $1.10\,w_2$B	(0) 0.92*b*
1	5314.462	2		18811.36	$a^3D_{2\frac{1}{2}}-y^3G^0_{3\frac{1}{2}}$		
1	5302.157	5		18855.02	$z^6F^0_{\frac{1}{2}}-e^6D_{2\frac{1}{2}}$	(0) 1.48	
1	5294.04	3*h*		18883.92	$z^6D^0_{\frac{1}{2}}-e^6D_{2\frac{1}{2}}$	(0) 1.28	(0) **1.24***s*
1	5290.724	2		18895.77		(0) 1.20	
1	5290.289	2*h*		18897.32	$b^4P_{1\frac{1}{2}}-z^4F^0_{1\frac{1}{2}}$	(0) 0.75	(0) **0.78***s*
1	5287.640	5		18906.78		(0) 1.00	
1	5282.516	1	IV	18925.13	$z^6D^0_{1\frac{1}{2}}-e^6D_{2\frac{1}{2}}$	(? w_2 D) 1.47 w_1 C	(0) 1.50*b*
1	5261.910	2		18927.30	$z^4F^0_{1\frac{1}{2}}-e^6D_{1\frac{1}{2}}$		
1	5280.435	2*h*		18932.58	$a^3D_{2\frac{1}{2}}-y^3F^0_{2\frac{1}{2}}$	(0) $0.82w_1$	(0) **0.96***s*
1	[b]5275.69	2*h*		18949.62	$z^6F^0_{2\frac{1}{2}}-e^6D_{3\frac{1}{2}}$	(0.61) 1.27?	(1.06) 1.46*b*
1	5272.697	1	IV	18960.36	$z^6D^0_{2\frac{1}{2}}-e^6D_{1\frac{1}{2}}$	($?w_1$) $1.38w_1$	(0) 1.36*b*
1	5271.049	1	IV	18966.29	$a^3P_{1\frac{1}{2}}-z^3P^0_{1\frac{1}{2}}$	(0) 1.22	(0.03) 1.21*b*
1	5270.35	3*d*?		18968.81	$z^6F^0_{3\frac{1}{2}}-e^6D_{3\frac{1}{2}}$		
1	[b]5266.118	4		18984.05	$\begin{cases} b^2G_{4\frac{1}{2}}-v^2F^0_{3\frac{1}{2}} \\ z^6F^0_{\frac{1}{2}}-e^6D_{1\frac{1}{2}} \end{cases}$	(0?) w_2 D 1.08	(0) 1.28*b*
1	5264.34	2*h*		18990.47	$z^6D^0_{\frac{1}{2}}-e^6D_{2\frac{1}{2}}$	(0? w_2 D) 1.04	(0) **1.10***s*
1	5260.978	1	IV	19002.61	$z^4D^0_{\frac{1}{2}}-e^6D_{1\frac{1}{2}}$	(0) 1.56	(0.26) 1.52*b*
1	5260.350	3		19004.86		(0) 0.79	
1	5258.162	1		19012.77	$a^3D_{1\frac{1}{2}}-y^3F^0_{2\frac{1}{2}}$	(0) 0.68	(0) **0.67***s*
1	5256.24	1*h*		19019.72	$z^6D^0_{1\frac{1}{2}}-e^6D_{2\frac{1}{2}}$	(0) 1.58	(0.24) 1.60*b*
1	5248.593	1		19047.44	$b^4P_{2\frac{1}{2}}-v^4D^0_{3\frac{1}{2}}$?		
1	5240.878	9	III	19075.48	$b^3H_{3\frac{1}{2}}-z^3H^0_{3\frac{1}{2}}$	(0) 1.11	(0.09) 1.09*b*
1	[b]5240.198	1	III	19077.95	$z^6F^0_{1\frac{1}{2}}-e^6F_{1\frac{1}{2}}$	(0) 1.56	(0) 1.39*b*
1	5234.088	8	III	19100.22	$b^3H_{4\frac{1}{2}}-z^3H^0_{4\frac{1}{2}}$	(0? w_1 D) 0.89	(0.11) 0.90*b*
1	5233.752	2	IV	19101.45	$z^6F^0_{\frac{1}{2}}-e^6F_{2\frac{1}{2}}$	(0) 1.59	(0) **1.55***s*
1	5227.592	1*h*		19123.96	$z^6D^0_{2\frac{1}{2}}-e^6D_{3\frac{1}{2}}$		
1	[b]5225.767	3	III	19130.64	$z^6F^0_{2\frac{1}{2}}-e^6F_{3\frac{1}{2}}$	(0) 1.52	(0) 1.26*b*

TABLE 1.—*Arc spectrum of vanadium* (V I)—Continued

(1)	(2)	(3)	(4)	(5)	(6)	(7)	(8)
Ref.	λ_{air} A	Int. arc	Temp. class	ν_{vac} cm^{-1}	Term combinations	Zeeman effect: Observed	Zeeman effect: Computed
1	b5223.636	1		19138.45	$z^6D^0_{3/2}-e^6D_{3/2}$	(0) 1.51	(0) 1.34*b*
1	5216.595	3	IV	19164.27	$z^6F^0_{3/2}-e^6F_{1/2}$	(0) 1.64	(0) **1.62***s*
1	5213.651	1	III	19175.10	$b^4P_{3/2}-v^4D^0_{3/2}$	(w_1) 1.14w_1	(0) 1.11*b*
1	5212.237	3h		19180.30		(0) 1.01	
1	5207.683	3		19197.07	$b^2H_{11/2}-x^2H^0_{9/2}$	(0) 1.53	(0) 1.53*b*
1	5206.621	1	III	19200.99	$z^6F^0_{1/2}-e^6F_{3/2}$; $z^6D^0_{3/2}-e^6F_{3/2}$	(0.90) 2.08	(0.93) 0.21, **2.07**
1	5200.344	2		19224.16		(0) 0.41	
1	5195.394	5	III	19242.48	$z^6F^0_{3/2}-e^6F_{3/2}$	(0) 1.42	(0.15) 1.30*b*
1	5194.824	10	III	19244.59	$z^6F^0_{3/2}-e^6F_{2/2}$; $z^6F^0_{1/2}-e^6F_{1/2}$	(?) 1.55	{(0.04) 1.29*b*; (0.19) 1.40*b*
1	5193.626	1	III	19249.03	$z^6F^0_{1/2}-e^6F_{1/2}$	(0?) 1.12	(0.13) 1.09*b*
1	b5193.004	7	III	19251.33	$z^6F^0_{3/2}-e^6F_{3/2}$	(0) 1.45	(0.45) 1.47*b*
1	5192.022	1	IV	19254.98	$z^6F^0_{3/2}-e^6F_{3/2}$	(w_1) 0.57	(0.14) 0.58*b*
1	5190.684	1—		19259.94	$b^2H_{9/2}-x^4H^0_{7/2}$	(?) 1.10	(0.13) 1.10*b*
1	5188.882	1h		19266.63	$b^4P_{1/2}-v^4D^0_{1/2}$		
1	5182.828	1	IV	19289.13	$z^6D^0_{3/2}-e^6F_{3/2}$	(1.93) 1.22	(1.96) 1.24*b*
1	5180.752	1	IV	19296.86	$z^6D^0_{1/2}-e^6F_{1/2}$	(1.10) 0.68, **1.39**, 2.15	(0.36, **1.07**) 0.69, **1.40**, 2.12
1	5179.800	1—		19300.41		(0) 0.66	
1	5179.100	1	IV	19303.02	$z^6F^0_{1/2}-e^6F_{1/2}$	(0.75) 1.77	(0.74) 0.30, **1.79**
1	5178.554	1	IV	19305.05	$z^6D^0_{3/2}-e^6F_{3/2}$	(0.71) 1.55w_2	(0.61) 1.44*b*
1	5176.781	4	III	19311.67		(?w_2 D) 1.03	
1	5176.494	3		19312.74	$z^6D^0_{3/2}-e^6F_{3/2}$		
1	5174.533	2		19320.05	$z^6D^0_{3/2}-e^6F_{1/2}$	(0.43) 1.56w_1	(0.45) 1.49*b*
1	5172.110	3		19329.10	$z^6F^0_{1/2}-e^6F_{1/2}$	(0) 1.47	(0) 1.42*b*
1	5169.944	1	III	19337.19	$z^6D^0_{3/2}-e^6F_{1/2}$	(1.01) 0, 2.09	(1.08) **0.03**, 2.12
1	5166.789	1	IV	19349.01	$b^4P_{1/2}-v^4D^0_{1/2}$	(?w_1D) 0.90w_2A	(0) 0 98*b*
1	5164.892	4		19356.11	$z^6F^0_{3/2}-e^6F_{3/2}$	(0?w_2D) 1.48	(0) **1.46***s*
1	5159.350	3	III?	19376.91	$z^6D^0_{1/2}-e^6F_{3/2}$	(0.25, 0.73) 0.60w_2 A	(**0.23**, 0.69) **0.61**, 1.07, 1.53, 1.99
1	b5157.026	3		19385.64	$z^6F^0_{3/2}-e^6F_{1/2}$	(0) 1.50	(0) 1.69*b*
1	5148.724	4	III?	19416.89	$z^6D^0_{3/2}-e^6F_{1/2}$	(?w_2 D) 0.98w_2 A	(0) 1.02*b*
1	5148.428	2h		19418.00	$z^6F^0_{1/2}-e^6F_{3/2}$		
1	5139.536	6		19451.61	$a^2F_{3/2}-u^2G^0_{3/2}$	(?w_1 D) 0.86	(0) 0.73*b*
1	5138.431	5	III	19455.79	$z^6D^0_{3/2}-e^6F_{1/2}$	(?w_2) 1.18 w_1	(0) 1.20*b*
1	b5137.591	1		19458.97	$b^4P_{3/2}-v^4D^0_{1/2}$	(0.73)?	(0) 0.66*b*
1	5128.530	7	III	19493.35	$z^6D^0_{1/2}-e^6F_{3/2}$	(0?w_2) 1.53w_2	(0) 1.45*b*
1	5105.171	2	III?	19582.54		(0) 0.96	
1	b5086.847	1h		19653.09	$b^4P_{2/2}-u^4D^0_{3/2}$; $a^2D_{1/2}-v^4F^0_{3/2}$	(0) 1.39w_1	{(0.48) 1.43*b*; (0) 1.58*b*}
1	5075.672	2—		19696.35	$a^4G_{3/2}-w^4G^0_{3/2}$	(0) 1.27	(0.04) 1.26*b*
1	b5073.188	1—		19706.00	$a^4G_{3/2}-w^4G^0_{3/2}$	(0) 1.03	(0.30) 1.01*b*
1	5070.622	1		19715.97	$a^4G_{5/2}-w^4G^0_{5/2}$	(0) 1.17	(0.11) 1.16*b*
1	5064.131	3	V	19741.24		(0) 1.06	
1	5051.607	2	IV	19790.18	$b^2G_{3/2}-t^2G^0_{3/2}$	(0) 0.92	(0.12) 0.88*b*
1	5047.240	1	III A	19807.30	$b^4P_{3/2}-u^4D^0_{3/2}$	(0) 1.05	(0) 1.07*b*
1	5046.806	1—		19809.00	$a^4G_{3/2}-x^4F^0_{3/2}$		
1	5043.510	1—h		19821.95	$b^4P_{1/2}-u^4D^0_{1/2}$		
1	5032.956	1h		19863.52	$b^4D_{3/2}-w^2P^0_{3/2}$; $b^2H_{9/2}-y^2I^0_{9/2}$		
1	b5024.162	1h		19898.28	$b^2G_{4/2}-y^2H^0_{9/2}$	(?) 1.15w_1	(0.89) 0.99*b*
1	5014.620	5	III	19936.14	$b^2H_{9/2}-y^2I^0_{9/2}$; $b^2G_{4/2}-t^2G^0_{3/2}$	(0) 1.05	{(0) 1.00*b*; (0.26) 1.08*b*}
1	5010.018	1		19954.46	$b^4P_{1/2}-u^4D^0_{3/2}$	(0) 0.98	(0) 1.05*b*
1	5006.393	1—		19968.91	$a^4G_{5/2}-y^2H^0_{9/2}$		
1	5005.615	2		19972.01	$a^2D_{3/2}-y^2D^0_{3/2}$		
1	5002.320	4	IV	19985.17	$b^2H_{4/2}-y^2I^0_{3/2}$	(0?w_2D) 0.94	(0) 0.94*b*
2	4995.019	[3p?]		20014.37	$b^4P_{3/2}-u^4D^0_{3/2}$?		
1	4991.824	1—		20027.19		(0) 1.18	
1	4984.528	1—		20056.50	$b^2G_{4/2}-t^2H^0_{3/2}$		
1	4981.726	1—		20067.79		(0) 1.17	
1	4966.123	2	IV	20130.84	$z^2D^0_{3/2}-e^2F_{3/2}$	(0) 1.15	(0) 1.00*b*
1	4957.648	2		20165.25	$a^2P_{1/2}-w^4D^0_{3/2}$; $a^2P_{3/2}-w^4D^0_{3/2}$		

TABLE 1.—*Arc spectrum of vanadium* (V I)—Continued

(1)	(2)	(3)	(4)	(5)	(6)	(7)	(8)
Ref.	λ_{air} A	Int. arc	Temp. class	Vac cm^{-1}	Term combinations	Zeeman effect: Observed	Zeeman effect: Computed
1	4944.996	1h		20216.83	$a^2G_{4½}-z^4F_{3½}$		
1	4944.415	1—		20219.22	$a^2P_{2½}-z^4F_{1½}$	(0) 0.94	(0) 0.92*b*
1	4942.802	1	IV A	20225.82	$a^4G_{3½}-w^2F_{3½}$	(0.85) 1.01w_1C	(0) 1.11*b*
1	4935.101	1—		20257.37	$b^2G_{4½}-f^4G^0_{3½}$		
1	4933.616	1	IV	20263.47	$a^2F_{3½}-u^4F^0_{3½}$?	(0) 1.10	(0.21) 1.18*b*
1	4932.029	4	III A	20270.00	$a^4P_{2½}-y^4P^0_{1½}$	(0) 1.52	(0) 1.41*b*
1	4927.733	1—		20287.66	$a^4G_{2½}-w^2F^0_{2½}$		
1	4925.657	10	III	20296.22	$a^4P_{2½}-y^4P^0_{2½}$	(0) 1.62	(0.26) 1.61*b*
1	4923.785	1		20303.92	$b^2G_{3½}-u^2F^0_{3½}$	(? w_1D) 0.95	(0) **0.91***s*
1	4922.379	4		20309.72	$z^2D^0_{2½}-e^2F_{2½}$	(? w_2 D) 0.95	(0) 0.99*b*
1	4918.980	2		20323.76	$a^4G_{2½}-y^4H^0_{2½}$		
1	[b]4916.265	2	IV	20334.99	$a^4G_{4½}-y^4H^0_{4½}$?	(0) 0.91	(0.33) 1.09*b*
1	4913.093	2		20348.11		(? w_2 D) 1.19	
1	4909.18	1		20364.32	$a^4G_{2½}-y^4H^0_{3½}$, $a^4G_{3½}-z^2I^0_{3½}$		
1	4908.684	1	IV A	20366.40	$a^2P_{1½}-z^4F^0_{1½}$	(0) 1.01	
1	4906.90	1—		20373.82	$a^4G_{4½}-z^4G^0_{3½}$		
5	4906.718	1		20374.55	$b^2G_{3½}-u^2F^0_{3½}$		
1	4905.84	*tr*	IV A	20378.22			
1	4904.875	3	IV	20382.20		(0) 0.78	
2	4904.447	[7]	III *d*	20383.97	$a^4G_{4½}-y^4H^0_{5½}$		
2	4904.350	[9]		20384.39	$a^4G_{2½}-y^4H^0_{3½}$		
1	4904.285	8		20384.66	$a^4P_{1½}-y^4P^0_{0½}$	(0) 1.17	(0) **1.32***s*
1	4900.624	6	IV	20399.89	$a^4G_{3½}-y^4H^0_{4½}$	(0? w_1 D) 1.11	(0) 1.21*b*
1	4900.004	*tr*	IV A	20402.19	$a^4G_{2½}-z^4G^0_{2½}$	(0) 1.57	(0) 1.54*b*
1	4896.35	1	IV A	20417.71	$b^2G_{4½}-u^2F^0_{3½}$	(0) 1.07	(0) 1.10*b*
1	4894.218	4	III	20426.59	$a^4G_{3½}-y^4H^0_{3½}$	(0) 0.98	(0) 0.97*b*
1	4892.722	1h		20432.84	$b^2G_{3½}-u^2H^0_{4½}$	(0) 0.86	(0) 0.83*b*
1	4891.602	4	III	20437.52			
1	4891.222	1	IV	20439.10	$a^4G_{2½}-z^4G^0_{1½}$	(0) 1.00	(0.18) 0.99*b*
1	4890.090	1	IV	20443.84	$a^4G_{2½}-z^4G^0_{2½}$	(0) 0.60	(0.02) 0.60*b*
1	4886.821	2	III A	20457.51	$a^4P_{1½}-y^4P^0_{1½}$	(0) 1.74	(0.06) 1.72*b*
1	4885.649	2	IV	20462.41	$a^4G_{4½}-z^4G^0_{4½}$	(0) 1.17	(0.04) 1.14*b*
1	4882.183	2	III A	20476.94	$a^4P_{0½}-y^4P^0_{0½}$		
1	[b]4881.554	50*acm*	I	20479.58	$a^4F_{4½}-z^4D^0_{3½}$	(?w^2 D) 1.18w_1 C	(0) 0.98*b*
1	[b]4880.560	8	III	20483.75	$a^4P_{1½}-y^4P^0_{2½}$	(0) 0.90, 1.65	(**0.01**, 0.04) **1.63** 1.66, 1.69, 1.71
1	4877.219	*tr*	IV A	20497.77			
1	4875.462	40*acm*	I	20515.17	$a^4F_{3½}-z^4D^0_{3½}$	(?w_2D) 1.08w_2 C	(0) 1.01*b*
1	4873.00	1		20515.52		(?w_1D) 0.76	
1	4871.264	7		20522.84	$a^4G_{3½}-z^4G^0_{2½}$	(?w_1D) 1.25w_1 A	(0.22) 1.24*b*
1	4870.134	1		20527.60	$a^4G_{3½}-z^4G^0_{3½}$		
1	4867.986	2		20536.67		(?w_1D) 1.04w_1 C	
3	4864.85	−1		20549.90	$a^4P_{0½}-y^4P^0_{1½}$		
1	4864.741	40*acm*	1	20550.36	$a^4F_{3½}-z^4D^0_{2½}$	(?w_2D) 0.91w_2 A	(0) 0.86*b*
1	4862.625	5	IV	20559.30	($b^4D_{3½}-{}^4F^0_{3½}$?)	(0) 1.10	
1	4859.135	2	IV	20574.07		(0) 1.21	
1	4857.02	1—		20583.04	$a^4G_{4½}-z^4G^0_{3½}$	(0) 1.33	(0) 1.40*b*
1	4855.35	1—		20590.11		(0) 0.84	
1	4851.483	40*acm*	I	20606.52	$a^4F_{4½}-z^4D^0_{3½}$	(0.25w_2D) 0.19, **0.63**	(0.22) 0.18, **0.62**
1	4848.821	1	IV	20617.84	$b^2G_{3½}-u^2H^0_{3½}$, $a^2P_{0½}-y^2D^0_{1½}$	(0?w_2 D) 0.81	(0) **0.84***s*, (0) **0.78***s*
4	4848.60	3	III	20618.77			
1	[b]4846.620	1		20627.19	$a^2P_{1½}-y^2D^0_{1½}$	(?w_1D) 1.11w_2 A	(0.66) 0.96*b*
1	4843.018	2	IV	20642.53	($b^2G_{4½}-z^2D^0_{3½}$?	(?w_2D) 1.67 w_2B	
1	4833.804	1	IV	20681.88		(0) 1.11	
1	4833.027	3	IV A	20685.21	$a^2P_{1½}-y^2D^0_{2½}$	(0) 1.10	(0) 1.16*b*
1	4832.427	30	I	20687.78	$a^4F_{1½}-z^4D^0_{1½}$	(0.43, **1.20**) 0, **0.79**, 1.62	(0.40, **1.21**) 0, **0.80**, 1.61
1	4831.642	35	I	20691.13	$a^4F_{2½}-z^4D^0_{2½}$	(0.51, **0.83**) 1.28w_2	(0.18, 0.52, **0.86**) 0.49, 0.83, **1.18**, 1.53, 1.57
1	[b]4830.678	1	IV	20695.26	$b^2P_{1½}-z^2D^0_{1½}$	(0.82) 1.18	(0.63) 1.14*b*
1	4828.821	1	IV	20703.23	$b^4D_{2½}-{}^4F^0_{1½}$	(0) 0.90	(0) **0.90***s*

TABLE 1.—*Arc spectrum of vanadium* (V I)—Continued

(1)	(2)	(3)	(4)	(5)	(6)	(7)	(8)
Ref.	λ_{air} A	Int. arc	Temp. class	ν_{vac} cm^{-1}	Term combinations	Zeeman effect: Observed	Zeeman effect: Computed
1	b4827.458	30	I	20709.07	$a^4F_{3\frac{1}{2}}-z^4D^\circ_{3\frac{1}{2}}$	(0.56w_3 B) 1.33w_3 C	(0.74) 1.32*b*
1	4823.428	1		20726.37	$a^2P_{0\frac{1}{2}}-x^4D^\circ_{0\frac{1}{2}}$	(?w_1 D) 1.15	(0) 1.15*b*
1	4819.040	2	IV	20745.25		(0) 1.05	
1	4808.666	1		20790.00		(0) 1.34	
1	4807.537	25	III	20794.88	$z^6G^\circ_{3\frac{1}{2}}-e^6F_{3\frac{1}{2}}$	(0?w_2 D) 1.18w_2 A	(0) 1.18*b*
1	4803.042	1		20814.34	$b^4F_{3\frac{1}{2}}-x^2G^\circ_{3\frac{1}{2}}$		
1	4799.786	5	II A	20828.45	$a^4F_{1\frac{1}{2}}-z^4D^\circ_{1\frac{1}{2}}$	(**0.48**, 1.51) **0**, **0.92**, **1.85**, **2.81**.	(**0.48**, 1.43) −0.08, 0.88, 1.83, **2.78**.
1	4799.020	1	IV	20831.78	$b^4D_{2\frac{1}{2}}-t^4F^\circ_{1\frac{1}{2}}$	(?w_1) 0.52?	(0) 0.47*a*
1	4797.973	2	IV	20836.33	$b^4P_{2\frac{1}{2}}-y^4S^\circ_{1\frac{1}{2}}$	(0) 1.34	(0) 1.31*b*
1	b4796.930	20	III	20840.85	$z^6G^\circ_{3\frac{1}{2}}-e^6F_{4\frac{1}{2}}$	(0?w_3 D) 1.10w_3 A	(0) 0.88*b*
1	4795.104	3	IV	20848.80		(0) 0.94	
1	4792.954	3	IV	20858.14	$a^2F_{2\frac{1}{2}}-y^2D^\circ_{1\frac{1}{2}}$	(0) 0.86	(0) 0.82*b*
1	4786.515	20	III	20886.20	$z^6G^\circ_{3\frac{1}{2}}-e^6F_{3\frac{1}{2}}$	(0?w_3 D) 0.99w_3 A	(0) 1.03*b*
1	4784.480	5	II A	20895.10	$a^4F_{2\frac{1}{2}}-z^4D^\circ_{2\frac{1}{2}}$	(0) 2.18w_1 B	(0) 2.00*b*
1	b4781.342	*tr*	IV A	20908.80	$a^2F_{2\frac{1}{2}}-s^4D^\circ_{1\frac{1}{2}}$?	(0) 0.49	(0) 0.68*b*
1	4778.40	*tr*	IV	20921.69	$a^2F_{2\frac{1}{2}}-e^4D^\circ_{2\frac{1}{2}}$	(?w_1 D) 0.85	(0) 0.90*b*
1	4776.519	5	III	20929.92	$b^2P_{1\frac{1}{2}}-p^2D^\circ_{2\frac{1}{2}}$	(?w_1) 0.89w_1	(0.16) 0.97*b*
1	4776.364	10	III	20930.59	$z^6G^\circ_{3\frac{1}{2}}-e^6F_{2\frac{1}{2}}$	(0.34) 0.69, 1.44	(**0.10**, 0.30, 0.50) **0.60**, 0.80, 1.00, 1.20, 1.40, 1.60
1	4774.505	1−		20938.74	$b^4D_{1\frac{1}{2}}-x^4P^\circ_{0\frac{1}{2}}$		
1	4773.083	1	IV	20944.99		(0) 1.00	
1	b4772.588	2		20947.15	$b^4F_{1\frac{1}{2}}-x^4P^\circ_{1\frac{1}{2}}$	(0) 1.18	(0) 2.40*b*
1	4767.552	1−		20969.29	$b^4D_{2\frac{1}{2}}-t^4G^\circ_{2\frac{1}{2}}$		
1	4766.635	10	III	20973.31	$z^6G^\circ_{2\frac{1}{2}}-e^6F_{1\frac{1}{2}}$	(0?w_2) 0.67w_2 A	(0) 0.58*b*
4	4765.67	1	IV	20977.56	$b^2H_{4\frac{1}{2}}-u^4G^\circ_{3\frac{1}{2}}$	(0) 0.99	
2	4765.496	1		20978.33	$a^4G_{2\frac{1}{2}}-x^2H^\circ_{1\frac{1}{2}}$?		
1	4765.233	1h		20979.49		(0) 1.33	
1	4764.004	1		20984.90		(0) 1.07	
1	4761.880	1−		20994.26		(?w_1 D) 0.50	
1	4759.346	1		21005.43		(0) 1.41	
1	4759.018	1		21006.88	$a^4G_{2\frac{1}{2}}-x^2H^\circ_{1\frac{1}{2}}$		
1	4758.742	2	III A	21008.10	$a^4P_{2\frac{1}{2}}-z^6S^\circ_{1\frac{1}{2}}$?		
1	4757.50	8	III	21013.57	$z^6G^\circ_{1\frac{1}{2}}-e^6F_{1\frac{1}{2}}$	(0.34) 0.37	(0.36) 0.36*b*
1	4757.37	4	III	21014.14	$z^6G^\circ_{2\frac{1}{2}}-e^6F_{2\frac{1}{2}}$		
1	4753.957	7	IV	21029.25	$z^6G^\circ_{3\frac{1}{2}}-e^6F_{4\frac{1}{2}}$	(0.61w_2 B) 1.37w_2 C	(0.78) 1.32*b*
1	4751.849	1−		21038.58	$a^4G_{4\frac{1}{2}}-x^2H^\circ_{5\frac{1}{2}}$		
1	4751.574	6	III	21039.80	$b^4P_{2\frac{1}{2}}-x^4P^\circ_{1\frac{1}{2}}$	(0.11) 1.61	(0) 1.54*b*
1	4751.275	1		21041.11	$a^2F_{2\frac{1}{2}}-p^2D^\circ_{2\frac{1}{2}}$		
1	4750.990	8	III	21042.38	$z^6G^\circ_{3\frac{1}{2}}-e^6F_{3\frac{1}{2}}$	(0.85) —, 1.30	(0.11, 0.34, 0.57, **0.80**) 0.53, 0.76, 0.99, **1.21** 1.44, 1.67, 1.90
1	4748.525	7	III	21053.31	$z^6G^\circ_{2\frac{1}{2}}-e^6F_{2\frac{1}{2}}$	(1.09w_2 B) 1.15w_2 A	(1.14) 1.04*b*
2	4747.075	1	IV	21059.73			
1	4746.638	5	IV	21061.68	$z^6G^\circ_{1\frac{1}{2}}-e^6F_{1\frac{1}{2}}$	(1.63) **0.55**, 1.60	(0.52, **1.57**) −0.52 **0.52**, 1.57
1	4742.631	5	IV	21079.47	$b^2P_{0\frac{1}{2}}-y^2D^\circ_{1\frac{1}{2}}$	(0?w_2 D) 1.00w_1	(0) 0.98*b*
1	4739.607	1		21092.91	$\left\{\begin{matrix}b^4D_{3\frac{1}{2}}-t^4G^\circ_{3\frac{1}{2}}\\ a^2F_{2\frac{1}{2}}-p^2D^\circ_{2\frac{1}{2}}\end{matrix}\right.$		
4	4739.11	1	IV A	21095.13	$a^6D_{4\frac{1}{2}}-z^4F^\circ_{3\frac{1}{2}}$		
1	4738.318	1	IV	21098.66	$\left\{\begin{matrix}b^4F_{1\frac{1}{2}}-w^4G^\circ_{2\frac{1}{2}}\\ b^4F_{2\frac{1}{2}}-w^4G^\circ_{3\frac{1}{2}}\end{matrix}\right.$		
1	4737.746	1	IV	21101.21	$b^4F_{1\frac{1}{2}}-x^2F^\circ_{2\frac{1}{2}}$		
1	4731.95	1		21127.05	$\left\{\begin{matrix}a^2F_{2\frac{1}{2}}-p^2F^\circ_{3\frac{1}{2}}\\ b^4F_{4\frac{1}{2}}-w^4G^\circ_{5\frac{1}{2}}\end{matrix}\right.$ (0.59) 1.05w_2	$\left\{\begin{matrix}—, —\\ (0.52)\ 1.24b\end{matrix}\right.$
1	4731.556	1		21128.81	$\left\{\begin{matrix}a^4G_{2\frac{1}{2}}-x^4H^\circ_{3\frac{1}{2}}\\ b^4P_{2\frac{1}{2}}-x^2D^\circ_{2\frac{1}{2}}\end{matrix}\right.$		
1	4731.268	2		21130.10	$b^2P_{1\frac{1}{2}}-s^4D^\circ_{1\frac{1}{2}}$		
1	4730.394	3	III	21133.99	$b^4F_{2\frac{1}{2}}-w^4G^\circ_{2\frac{1}{2}}$	(0) 1.04	(0) 1.07*b*
1	4729.844	1−		21136.46	$b^2P_{1\frac{1}{2}}-u^2D^\circ_{2\frac{1}{2}}$		
1	4729.544	6	III	21137.80	$b^4P_{1\frac{1}{2}}-y^4S^\circ_{1\frac{1}{2}}$	(0.18) 1.77w_1	(0.24) 1.76*b*
1	4728.652	2		21141.79	$\left\{\begin{matrix}z^6G^\circ_{2\frac{1}{2}}-e^6F_{2\frac{1}{2}}\\ a^4G_{4\frac{1}{2}}-x^4H^\circ_{4\frac{1}{2}}\end{matrix}\right.$		
1	4723.430	1		21165.14	$z^6G^\circ_{3\frac{1}{2}}-e^6F_{3\frac{1}{2}}$		
1	4722.877	8	III	21167.65	$b^4F_{3\frac{1}{2}}-w^4G^\circ_{3\frac{1}{2}}$	(0) 1.12	(0) 1.15*b*

TABLE 1.—*Arc spectrum of vanadium* (V I)—Continued

(1)	(2)	(3)	(4)	(5)	(6)	(7)	(8)
Ref.	λ_{air} A	Int. arc	Temp. class	ν_{vac} cm^{-1}	Term combinations	Zeeman effect: Observed	Zeeman effect: Computed
1	4721.524	6	III	21173.70	$b^4F_{3/2}-w^4G^\circ_{3/2}$	(0) 1.05	(0) 1.08*b*
1	4721.246	2		21174.95		(0) 1.15	
1	4718.895	1—		21185.49	$z^6G^\circ_{3/2}-e^6F_{3/2}$		
1	4718.753	1—		21186.13	$b^4D_{1/2}-r^4D^\circ_{1/2}$		
1	4717.692	10	IV	21190.89	$a^4G_{3/2}-z^4H^\circ_{3/2}$	(0) 0.81	(0) 0.77*b*
1	4716.644	1—		21195.60	$a^4P_{1/2}-z^6S^\circ_{3/2}$		
1	4715.900	5	?	21198.95	$a\,^2F_{3/2}-u^2D^\circ_{3/2}$	(?) 0.98w_2	(0) 0.98*b*
1	4714.113	10	?	21206.90	$aG^\circ_{3/2}-z^4H^\circ_{3/2}$	(0) 0.96	(0) 0.88*b*
1	4713.448	2		21209.98	$b^4D_{3/2}-r^4D^\circ_{3/2}$		
1	4710.566	12	?	21222.95	$a^4G_{3/2}-z^4H^\circ_{3/2}$	(0) 1.04	(0) 1.05*b*
1	4709.728	4	?	21226.74		(0) 1.04	
1	4707.458	4	III A	21236.97	$b^4F_{3/2}-z^2F^\circ_{3/2}$	(0) 1.06	(0) 1.05*b*
1	4706.574	12	?	21240.96	$a^4G_{3/2}-z^4H^\circ_{3/2}$	(0?w_1) 1.09w_1	(0) 1.08*b*
1	4706.178	8	?	21242.75	$b^4P_{3/2}-z^4P^\circ_{3/2}$	(?w_2 D) 1.39w_2 A	(0) 1.37*b*
1	4705.099	4	?	21247.61	$a^2F_{3/2}-u^2D^\circ_{3/2}$	(0) 1.15	(0) 1.16*b*
1	4699.329	3	?	21273.70	$a^2H_{3/2}-z^2G^\circ_{3/2}$	(?) 1.11	(0) 1.12*b*
1	4686.926	6	?	21329.99	$b^4P_{3/2}-y^4S^\circ_{3/2}$	(0.39) **1.50**, —	(0.38) **1.47**, 2.22
1	4684.457	3		21341.23	$b^4P_{1/2}-z^4P^\circ_{3/2}$		
1	4682.763	2*h*		21348.96	$b^4D_{3/2}-r^4D^\circ_{3/2}$		
1	4680.904	2		21357.43	$a^2H_{1/2}-z^2G^\circ_{1/2}$		
1	4673.658	1		21390.54	$b^2H_{5/2}-w^4H^\circ_{5/2}$		
1	4670.483	25*cm*	III	21405.10	$a^4D_{3/2}-y^4P^\circ_{3/2}$	(?w_2) 1.14w_2	(0) 1.04*b*
2	4669.273	2		21410.64	$a^4F_{3/2}-z^4G^\circ_{3/2}$		
1	4666.149	4	III?	21424.97	$b^4P_{1/2}-z^4P^\circ_{1/2}$	(0.41)?	(0.41) **1.27**, 2.09
1	4656.546	1*h*		21469.16	$b^4D_{3/2}-2^5_{3/2}$		
1	4654.639	1*h*		21477.95	$b^4D_{3/2}-r^4D^\circ_{3/2}$		
1	4652.928	1		21485.85	$b^4F_{3/2}-z^2G^\circ_{3/2}$		
1	4648.880	2		21504.56	$b^2P_{1/2}-w^2P^\circ_{1/2}$		
1	4647.860	1		21509.28	$a^2F_{3/2}-z^2F^\circ_{3/2}$		
1	4646.396	15 *cm*	III	21516.06	$a^4D_{3/2}-y^4P^\circ_{3/2}$	(0.17, 0.55) **0.83**, 1.21, 1.62	(**0.19**, 0.58) **0.77**, 1.16, 1.55, 1.93
1	4645.971	1	III A	21518.03	$a^4F_{3/2}-z^4G^\circ_{3/2}$		
1	4644.452	3	III	21525.06	$a^2H_{1/2}-w^2G^\circ_{1/2}$	(?) 1.34	(0) 1.34?b
1	4640.735	7*cm*	III	21542.30	$a^4D_{3/2}-y^4P^\circ_{3/2}$	(0.47) 1.57w_2	(0.16, 0.48, **0.86**) 0.87, 1.19, **1.52**, 1.83, 2.15
2	4640.309	0		21544.28	$b^4P_{1/2}-z^4P^\circ_{1/2}$		
1	4640.062	8	III	21545.42	$a^4D_{1/2}-y^4P^\circ_{1/2}$	(0.73) 0.46	(0.74) **0.45**, 1.94
1	4636.166	2	IV	21563.53	$a^2H_{3/2}-w^2G^\circ_{3/2}$		
1	4635.176	15	I	21568.14	$a^4F_{3/2}-z^4G^\circ_{3/2}$	(0.63) 1.27w_2	(0.44) 1.22*b*
1	4630.038	1*h*		21592.07	$a^4P_{1/2}-z^4F^\circ_{3/2}$		
1	4626.480	7	III	21608.67	$a^4D_{3/2}-y^4P^\circ_{3/2}$	(1.34) **1.34**	(1.33) 1.33*b*
2	4624.657	1		21617.19	$b^4P_{3/2}-z^4P^\circ_{3/2}$		
1	4624.404	8	III	21618.38	$a^4D_{1/2}-y^4P^\circ_{1/2}$, $b^4F_{3/2}-w^2F^\circ_{3/2}$	(0.82w_1) 0.98, 1.52, 2.07	(0.27, **0.82**) 0.92, **1.47**, 2.01
1	4621.26	1—		21633.09	$a^2H_{3/2}-w^4G^\circ_{3/2}$		
1	b4619.771	25	I	21640.05	$a^4F_{3/2}-z^4G^\circ_{3/2}$	(0.67w_1 B) 1.49w_1 D	(0.71) 1.08*b*
1	4619.648	8	IV	21640.64		(0) 0.96	
1	4618.800	2		21644.60	$a^4D_{1/2}-y^4P^\circ_{3/2}$		
1	4616.850	1		21653.75	$b^4F_{3/2}-w^2F^\circ_{3/2}$		
1	4613.913	1—		21667.52	$a^2F_{3/2}-w^2P^\circ_{1/2}$, $b^4D_{1/2}-z^2P^\circ_{1/2}$		
1	4611.722	2	IV	21677.83	$b^4F_{1/2}-w^2F^\circ_{1/2}$	(**0.22**, 0.65) 0.62, 1.05, **1.48**	(**0.23**, 0.67) 0.17 0.62, 1.06, **1.51**
1	4610.925	2	III A	21681.57	$a^4D_{5/2}-z^4P^\circ_{3/2}$	(0.87) **2.58**, —	(0.86) 0.86, **2.57**
1	4609.646	4	III	21687.64	$a^2G_{1/2}-z^2H^\circ_{1/2}$	(0.56) 1.07w_2 D?	(0.56) 1.05*b*
1	4607.226	2		21698.97		(0) 0.54	
1	4606.146	15	I	21704.06	$a^4F_{3/2}-z^4G^\circ_{3/2}$, $b^4F_{1/2}-w^2F^\circ_{1/2}$	(0.68, **1.12**) —, 0.32, **0.78**, **1.25**, 1.71	(0.22, 0.68, **1.14**) —0.13, 0.33, **0.78**, 1.23, 1.69
1	4602.960	2	IV	21719.09	$a^2H_{1/2}-w^4G^\circ_{1/2}$	(0) 0.64	(0) 0.62*b*
1	4594.103	60*acm*	I	21760.97	$a^4F_{1/2}-z^4G^\circ_{1/2}$	(0) 1.13	(0) 1.15*b*
5	4591.991	[0]		21770.96	$b^4P_{3/2}-w^2F^\circ_{3/2}$		
1	4591.220	12	IV	21774.62	$b^2H_{3/2}-w^2H^\circ_{3/2}$	(0) 1.02	(0.54) 1.02*b*
1	4588.776	1	IV	21786.23	$b^4F_{3/2}-w^2F^\circ_{3/2}$	(0) 1.18	(0) **1.16***a*
1	4586.364	50*acm*	I	21797.68	$a^4F_{3/2}-z^4G^\circ_{1/2}$	(0?w_2 D) 1.05w_2 C	(0) **1.02***a*

TABLE 1.—*Arc spectrum of vanadium* (V I)—Continued

(1)	(2)	(3)	(4)	(5)	(6)	(7)	(8)
Ref.	λ_{air} A	Int. arc	Temp. class	ν_{vac} cm^{-1}	Term combinations	Zeeman effect: Observed	Zeeman effect: Computed
4	4585.93	2	IV	21799.74	$a^3G_{3½}-z^4H_{3½}$		
1	4583.783	5	III	21809.95	$b^4F_{2½}-y^4G^0_{3½}$	(0.63, **1.06**) 0.00, 0.37, 0.77, 1.18, 1.63	(0.22, 0.67, **1.12**) —0.07, 0.38, **0.82**, 1.27, 1.72
1	4581.227	2	IV	21822.12	$a^3H_{4½}-x_3F^0_{3½}$		
1	4580.394	40 *acm*	I	21826.14	$a^4F_{2½}-z^4G^0_{3½}$	(0) 0.90	(0) 0.90*b*
1	4579.198	7	IV	21831.80	$b^4F_{3½}-z^4G^0_{3½}$	(0.73w_2B) 1.22w_2 C	(0.59) 1.12*b*
1	4578.728	15	III	21834.03	$b^4F_{1½}-z^4G^0_{3½}$	(0?w_2D) 0.79w_2 B	(0) 0.76*b*
1	4577.642	1		21839.21	$a^4G_{3½}-y^2I^0_{4½}$		
1	4577.173	40*acm*	I	21841.44	$a^4F_{1½}-z^4G^0_{3½}$	(0?w_2D) 0.70w_2 B	(0) 0.66*b*
1	4571.783	15	III	21867.20	$b^4F_{2½}-z^4G^0_{3½}$	(0) 0.92	(0) **0.95***s*
1	4570.425	6	III	21873.70	$b^4F_{4½}-z^4G^0_{3½}$	(0.67w_2 B) 1.21w_2 D	(0.59) 1.23*b*
5	4565.513	[−1h]		21897.23	$a^4H_{3½}-w^4G^0_{3½}$?		
1	4564.581	2		21901.71	$a^2D_{1½}-z^2D^0_{1½}$	(0w_1 D) 0.97w_1 A	(0.11) 0.93*b*
1	4560.710	20	III	21920.29	$b^4F_{3½}-z^4G^0_{3½}$	(0) 1.02	(0) 1.03*b*
1	4553.056	7	IV	21957.14	$b^2H_{4½}-w^2H^0_{4½}$	(0.26) 0.95	(0.30) 0.95*b*
1	4551.860	3	IV	21962.91	$a^2D_{1½}-y^2P^0_{½}$	(0.15) 0.81, **1.07**	(0.11) 0.85, **1.08**
1	4549.644	10	IV	21973.60		(?w_2 D) 1.03	
1	4545.394	25	III	21994.13	$b^4F_{4½}-z^4G^0_{3½}$	(0) 1.08	(0) 1.02*b*
1	4540.014	6	IV	22020.22	$a^2H_{5½}-z^4I^0_{4½}$		
1	4537.663	6	IV	22031.62	$a^2D_{2½}-y^2P^0_{1½}$	(0) 1.19	(0) 1.17*b*
4	4535.57	1	IV	22041.79			
1	4533.940	4	IV	22049.71			
1	4530.808	4	IV	22064.97		(0) 1.10	
1	4529.589	8	III	22070.89	$a^2H_{4½}-z^2G^0_{3½}$	(0) 0.73	(0) 0.74b
1	4529.301	4	IV	22072.31	$b^4P_{1½}-w^2F^0_{2½}$	(?w_2 D) 1.02	
1	4528.302	1		22077.17	$a^2H_{4½}-y^2H^0_{4½}$		
1	4527.990	5	IV	22078.68		(0) 1.19	
1	4525.168	5	IV	22092.45	$b^4F_{1½}-t^4D^0_{½}$	(0.19) —, **0.58**	(0.20) 0.20, **0.59**
1	4524.218	15	III	22097.10	$a^2H_{5½}-z^2G^0_{4½}$	(0) 1.15	(0) **1.17***s*
4	4522.87	*tr*	IV	22103.68			
1	4520.168	3	III A	22116.88	$a^4D_{3½}-z^6S^0_{2½}$?		
1	4517.571	3	IV	22129.60		(0.37) **0.91**, —	
1	4515.558	2	IV	22139.47	$a^2H_{3½}-z^4I^0_{3½}$	(0) 1.13	(0) **1.14***s*
1	4514.191	6	III	22146.17	$b^4F_{2½}-t^4D^0_{1½}$	(?w_1) 0.85w_1	(0) **0.85***s*
1	4513.624	2	IV	22148.96	$a^4G_{3½}-u^4F^0_{4½}$	(0) 1.18	(0) 1.20*b*
1	4511.433	2	IV	22159.72	$a^4G_{4½}-u^4F^0_{4½}$	(0) 1.02	(0) 1.01*b*
1	4509.287	3	IV	22170.25	$b^4F_{1½}-t^4D^0_{½}$	(1.18) 0, 0.77, 1.56	(0.39, **1.18**) 0, **0.79**, 1.57
1	4506.577	2	IV	22183.59	$a^4G_{2½}-u^4F^0_{2½}$	(0) 0.88	(0) **0.86***s*
1	4506.210	1	IV	22185.39			
1	4506.094	2	IV	22185.98	$a^2D_{1½}-z^2D^0_{2½}$		
1	4501.972	8	III	22206.28	$a^2G_{4½}-y^2G^0_{4½}$	(0) 1.08	(0.37) 1.08*b*
1	4501.444	2		22208.87	$a^4G_{4½}-u^4F^0_{4½}$	(0.25) ?nw_2	(0.59) 1.22*b*
5	4501.256	1	IV	22209.82	$a^4H_{5½}-y^2H^0_{4½}$		
5	4500.853	1	IV	22211.80	$a^4G_{2½}-u^4F^0_{1½}$	(0) 0.59	(0) 0.63*b*
4	4499.76	1		22217.19	$a^2D_{2½}-z^2F^0_{2½}$		
1	4498.114	*tr*	IV A	22225.34	$a^4H_{4½}-t^2G^0_{4½}$	(?) 0.90, w_2 A	(0) 0.85 *b*
1	4497.710	1		22227.32	$b^2G_{3½}-t^2F^0_{3½}$		
1	4497.398	2	IV	22228.87	$b^2G_{3½}-t^2F^0_{2½}$	(0) 0.85	(0) 0.86*b*
1	4496.864	5	III	22231.51	$\{a^4H_{4½}-y^2H^0_{4½}$ $\{(a^2D_{1½}-z^2F^0_{2½})$		
1	4496.062	8	III	22235.47	$b^4F_{3½}-t^4D^0_{2½}$	(0? w_2 D) 1.01w_2 A	(0) 1.08*b*
1	4494.955	1	IV	22240.94		(0) 0.63	
4	4492.32	1	IV A	22253.97	$a^4D_{2½}-z^6S^0_{2½}$?		
4	4491.47	1	IV	22258.18	$\{a^2H_{4½}-z^2G^0_{4½}$ $\{z^2D^0_{2½}-h^6G_{3½}$?		
6	4491.162	2	III	22259.74	$a^2G_{4½}-y^2G^0_{3½}$	(?w_2 D) 1.55w_2 C	(0) 1.51 *b*
6	4490.815	5	III	22261.45	$a^4H_{4½}-y^2H^0_{3½}$	(?w_2 D) 1.33w_2 B	(0) 1.40*b*
6	4488.898	20	III	22270.96	$\{b^4F_{2½}-t^4D^0_{2½}$ $\{a^4H_{3½}-y^2H^0_{4½}$ $\{(b^2G_{4½}-t^2F^0_{3½})$	(? w_2 D) 0.99w_2 C	$\{$(0.61) 1.19*b* $\{$(0) **1.01***s*
4	4486.28	1		22283.97	$a^4H_{5½}-z^4I^0_{4½}$		
6	4480.041	6	III	22314.97	$a^4H_{5½}-z^4I^0_{5½}$	(0.69w_2 B) 1.06w_2 C	(0.63) 1.03*b*

TABLE 1.—*Arc spectrum of vanadium* (V I)—Continued

(1)	(2)	(3)	(4)	(5)	(6)	(7)	(8)
Ref.	λ_{air} A	Int. arc	Temp. class	ν_{vac} cm^{-1}	Term combinations	Zeeman effect: Observed	Zeeman effect: Computed
6	4475.882	2	IV	22335.73	$a^4H_{3½}-z^4H_{3½}$	(0.26) 0.89	(0.26) 0.90*b*
6	4474.721	12	III	22341.52	$a^2H_{3½}-z^2I_{3½}$ / $(a^4H_{3½}-z^4H_{3½})$	(0) 1.02	(0) 1.03*b*
6	4474.047	10	III	22344.88	$b^4F_{3½}-t^4D_{3½}$	(? w_1) 1.13w_2	(0) **1.17***s*
4	4473.26	1	IV	22348.82			
6	4471.781	1	IV	22356.20	$a^4D_{1½}-z^6S_{2½}$? / $b^2H_{3½}-p^2H_{3½}$		
4	4471.35	1		22358.36	$a^2F_{3½}-t^2G_{3½}$		
4	4470.86	1		22360.81	$a^4H_{3½}-p^2G_{3½}$?		
4	4470.39	1		22363.16	$a^2F_{2½}-t^4F_{1½}$		
6	4469.712	15	III	22366.55	$a^4H_{4½}-z^4H_{3½}$	(0) 0.98	(0) 1.01*b*
6	4468.764	4	III	22371.29	$a^2H_{4½}-w^2F_{3½}$	(0? w_1 D) 0.37w_1 A	(0) **0.37***s*
6	4468.008	8	III	22375.08	$a^4H_{3½}-z^4H_{3½}$	(0? w_1 D) 1.57w_1 B	(0) **1.64***s*
5	4467.624	1	IV	22377.00	$a^2D_{2½}-z^2F_{2½}$		
6	4466.857	2	IV A	22380.85	$a^2G_{4½}-y^2F_{3½}$	(0) 1.17	(0) 1.16*b*
6	4465.509	2	IV	22387.61	$b^4P_{2½}-t^4D_{2½}$	(0.53) 1.47w_2 C	(0.46) 1.44*b*
6	4464.769	2	IV	22391.32	$b^4F_{3½}-t^4D_{3½}$	(0.58) ?w_2 C	(0.38) 1.28*b*
4	4464.27	2	IV	22393.81	$b^2H_{3½}-t^2G_{3½}$	(0) 1.04	(0) 1.17*b*
6	4462.367	20	III	22403.36	$a^4H_{3½}-z^4H_{3½}$	(0) 1.01	(0) 1.02*b*
6	4460.989	4	IV	22410.20	$a^2F_{2½}-t^2G_{3½}$	(0) 0.92	(0) 0.95*b*
6	4460.302	50*a*	I	22413.74	$(a^6D_{4½}-z^6P_{3½}$ / $a^2G_{3½}-y^2G_{3½})$	(? w_2 D) 1.31w_2 A	(0) 1.27*b*
6	4459.766	30*a*	I	22416.43	$a^6D_{3½}-z^6P_{3½}$	(0.24, 0.46, 0.79) **0.75**, 1.05, 1.46, 1.76, 2.04, **2.36**	(**0.16**, 0.48, 0.80) **0.73**, 1.05 **1.37**, 1.69, 2.01, 2.33
4	4458.41	1	IV	22423.23	$a^2F_{3½}-z^2H_{3½}$		
6	4457.762	8	III	22426.51	$a^2H_{4½}-z^2I_{3½}$	(0) 0.97	(0) 1.03*b*
6	4457.484	15	I	22427.91	$a^6D_{2½}-z^6P_{1½}$	(0.36, **1.09**) **0.55**, 1.24, 2.01, 2.77	(**0.37**, 1.10) **0.51**, 1.24, 1.97, 2.71
6	4456.505	3	IV	22432.84		(0) 1.12	
6	4453.126	1	IV	22449.85	$b^4F_{4½}-z^2H_{3½}$		
6	4452.711	2	IV	22451.95	$a^4H_{3½}-z^6G_{3½}$	(0.20, 0.58, 0.97, 1.41) ?w_2 C	(**0.20**, 0.60, 1.00, 1.40) —0.35, 0.05, 0.45, 0.85, 1.25, 1.65, **2.05**, **2.45**
6	4452.022	20	III	22455.42	$a^4H_{4½}-z^4I_{3½}$	(0) 1.09	(0) 1.05*b*
6	*b*4450.909	4	IV	22461.04	$a^2F_{3½}-t^2G_{3½}$	(0) 1.02	(0) 0.87*b*
6	4449.578	5	III	22467.75	$a^2G_{3½}-y^2G_{3½}$	(0.16) 0.91	(0.09) 0.90*b*
4	4445.81	1	IV	22486.82	$b^4P_{1½}-t^4D_{2½}$		
6	4444.216	20*a*	I	22494.87	$a^6D_{1½}-z^6P_{1½}$	(0.24, **0.79**) 1.56, **2.11**, 2.67	(0.26, **0.73**) 1.56, **2.48**, 2.60
6	4443.342	5	IV	22499.29	$b^2G_{3½}-t^2H_{3½}$	(0) 1.01	(0) **1.04***s*
6	4441.688	25	I	22507.67	$a^6D_{2½}-z^6P_{2½}$	(0.50) 1.74w_2 C	(0.53) 1.76*b*
4	4438.98	1	IV	22521.41	$a^2F_{3½}-t^4F_{1½}$		
6	4437.842	20*a*	I	22527.18	$a^6D_{3½}-z^6P_{2½}$	(0.39) 1.61	(0.41) 1.60*b*
4	4437.39	1		22529.48	$a^4H_{4½}-z^2I_{3½}$		
4	4436.89	1		22532.01	$a^4H_{4½}-y^4H_{3½}$		
6	4436.140	15	I	22535.82	$a^6D_{3½}-z^6P_{3½}$	(0.47) **1.00**, 2.88	(0.47) **1.87**, 2.81
6	4434.602	5	III	22543.64	$b^4P_{3½}-t^4D_{3½}$	(? w_1D) 1.14w_2 A	(0) 1.11*b*
4	4432.88	1	IV A	22552.39	$a^4D_{3½}-x^4F_{3½}$		
6	4430.512	3	IV	22564.45	$b^4P_{1½}-t^4D_{1½}$	(0.26, 0.79) 0.89, **1.41**, 1.95	(0.25, **0.75**) 0.93, **1.43**, 1.93
6	4429.802	15	I	22568.06	$a^6D_{4½}-y^6F_{5½}$	(?w_2 D) 1.89w_2 B	(0) 1.80*b*
6	4428.519	15	I	22574.59	$a^6D_{1½}-z^6P_{2½}$	(0) 1.87w_1 B	(0) 1.87*b*
4	*b*4427.31	5	III	22580.76	$b^2G_{4½}-t^2H_{3½}$	(0) **0.94**, 1.54	(**0.02**, 0.07, 0.12, 0.17, 0.22) **0.84**, 0.89, 0.94, 0.99, 1.04, 1.08, 1.13, 1.18, 1.23, 1.28
6	4426.011	20	I	22587.39	$a^6D_{2½}-y^6F_{3½}$	(0.15, 0.43, 0.70) 2.31w_2 B	(**0.14**, 0.44, 0.74) 0.79, 1.09, 1.38, 1.67, 1.97, **2.27**
6	4425.724	4	III A	22588.85	$a^4H_{3½}-z^4G_{3½}$ / $a^2G_{3½}-y^2F_{3½}$		
6	4424.576	4	III A	22594.72	$a^2G_{4½}-z^2H_{3½}$	(0) 1.08	(0) 1.00*b*
6	4423.920	2	IV	22598.06	$b^4D_{1½}-q^4D_{2½}$?	(0) 1.07	
6	4423.210	8	III A	22601.68	$a^4D_{3½}-x^4F_{4½}$	(0) 1.18	(0) 1.20*b*
4	4422.48	2	IV	22605.41	$a^4H_{3½}-z^2I_{3½}$ / $a^2P_{2½}-z^2D_{3½}$	(?) 0.82	(0) **0.84***s* / (0) 0.95*b*

TABLE 1.—*Arc spectrum of vanadium* (V I)—Continued

(1)	(2)	(3)	(4)	(5)	(6)	(7)	(8)
Ref.	λ_{air} A	Int. arc	Temp. class	ν_{vac}cm^{-1}	Term combinations	Zeeman effect: Observed	Zeeman effect: Computed
6	4422.239	3	IV	22606.65	$a^4H_{4½}-v^4G^0_{5½}$ $(a^2P_{1½}-y^2S^0_{½})$	(0) 0.88	(0) 0.80*b*
6	4421.585	20	I	22610.00	$a^6D_{3½}-v^6F^0_{3½}$	(0.28, 0.87) 0.76, 1.34, 1.95, **2.55**	(**0.29**, 0.88) 0.73, 1.31, 1.90, **2.49**
6	4419.944	12	I	22618.38	$a^6D_{2½}-z^6P^0_{2½}$	(0) 1.76	(0) 1.75*b*
4	4418.45	1		22626.02	$a^2D_{2½}-y^2G^0_{3½}$		
6	4416.699	2	IV A	22635.01	$a^2G_{3½}-y^2F^0_{3½}$	(0) 0.89	(0) 0.92*b*
6	4416.480	20	I	22636.13	$a^6D_{1½}-y^6F^0_{2½}$	(1.21) 0.63, **3.10**	(1.20) 0.62, **3.02**
5	4415.062	2		22643.40	$a^4H_{3½}-v^4G^0_{4½}$ $b^4D_{3½}-q^4D^0_{3½}$		
6	4414.547	2	IV	22646.04	$a^4H_{3½}-z^4G^0_{3½}$		
4	4413.70	2	III A	22650.39	$a^4D_{3½}-x^4F^0_{4½}$	(0.79w_1B)?w_2 D	(0.74) 1.18*b*
6	4412.142	12	I	22658.39	$a^6D_{0½}-z^4P^0_{0½}$	(0.37) 2.94w_1B	(0.38) 2.92*b*
6	4408.515	90*a*	I	22677.01	$a^6D_{0½}-y^6F^0_{1½}$ $a^6D_{1½}-y^6F^0_{1½}$	(1.30) 0.85, 1.86	(1.94) 1.36*b* (0.40, **1.20**) 0.62, **1.42**, 2.22
6	4408.209	70*a*	I	22678.61	$a^6D_{2½}-y^6F^0_{3½}$ $(b^4P_{2½}-t^4D^0_{3½})$	(0.90)?	(0.83) 1.42*b*
6	4407.655	70*a*	I	22681.45	$a^6D_{3½}-y^6F^0_{4½}$	(0.56) 1.57w_2	(0.47) 1.45*b*
6	4406.649	80*a*	I	22686.63	$a^6D_{4½}-y^6F^0_{5½}$	(0.48) 1.49w_1C	(0.43) 1.47*b*
5	4406.141	6	III A	22689.24	$a^4D_{2½}-z^4F^0_{3½}$ $b^4P_{1½}-t^4D^0_{2½}$	(?w_2D) 1.09w_2 C	(0) 1.04*b* (0) 1.07*b*
6	4405.008	4	III A	22695.07	$a^6D_{2½}-z^4P^0_{1½}$ $a^4H_{4½}-v^4G^0_{5½}$		
6	4403.680	4	III	22701.93	$a^4H_{3½}-v^4G^0_{3½}$	(0) 1.13	(0) 1.07*b*
5	4401.140	[—]		22715.02	$b^4D_{2½}-u^4P^0_{1½}$		
6	4400.589	60*a*	II	22717.87	$a^6D_{0½}-y^6F^0_{1½}$	(1.12) 0, 2.18	(1.14) **0.12**, 2.16
6	4399.426	2	III	22723.88	$a^4D_{1½}-x^4F^0_{1½}$	(1.18) **0**, 0.80, 1.50	(0.41, **1.22**) −0.03, **0.79**, 1.60
4	4397.88	1		22731.87	$a^2F_{3½}-t^4G^0_{3½}$		
6	4397.414	1	IV	22734.27		(0) 1.01	
6	4395.243	80*a*	II	22745.51	$a^6D_{1½}-y^6F^0_{2½}$	(0.27, **0.86**) **0.43**, 1.01, 1.58, 2.14	(**0.29**, 0.88) **0.35**, 0.94, 1.53, 2.11
6	4394.814	3	III	22747.72	$a^3G_{3½}-z^3H^0_{3½}$	(0) 0.98	(0) 0.99*b*
6	4393.840	4	III A	22752.77	$a^4D_{1½}-x^4F^0_{2½}$	(0?w_1 D) 0.86w_1 A	(0) 0.88*b*
4	4393.09	4	III	22756.65	$b^4P_{0½}-t^4D^0_{1½}$	(0.72) 0.44	(0.71) **0.47**, 1.89
6	4392.078	5	II A	22761.90	$a^6D_{1½}-z^4P^0_{1½}$	(0.19) 1.82	(0.15) 1.76*b*
6	4391.681	2	IV	22763.96	$a^4H_{3½}-v^4G^0_{4½}$	(0.63)?	(0.54) 1.16*b*
6	4390.611	1	IV	22769.50	$a^3P_{0½}-y^3P^0_{1½}$		
6	4389.986	100*a*	II	22772.74	$a^6D_{2½}-y^6F^0_{3½}$		
4	4388.09	1		22782.58	$a^3F_{3½}-t^4G^0_{4½}$		
6	4387.215	3	III A	22787.13	$a^4D_{0½}-x^4F^0_{1½}$	(0.20) 0.60	(0.19) 0.19, **0.57**
4	4385.33	1	IV	22796.91	$a^4G_{3½}-u^4G^0_{3½}$		
6	4384.730	125*ra*	II	22800.04	$a^6D_{3½}-y^6F^0_{4½}$ $a^4F_{4½}-z^4F^0_{3½}$	(?w_2 D) 1.28w_2 C	(0) 1.20*b* (0) 1.37*b*
4	4384.19	1	III A	22802.84	$a^6D_{2½}-x^4P^0_{2½}$		
4	4381.76	1		22815.47	$a^4H_{4½}-v^4G^0_{3½}$?		
4	4381.23	1*h*		22818.24	$b^4D_{3½}-u^4P^0_{2½}$		
4	4381.03	1	IV A	22819.28	$a^4G_{4½}-u^4G^0_{3½}$ $a^4P_{1½}-x^4D^0_{1½}$ $a^6D_{3½}-z^4P^0_{2½}$		
6	4380.570	4	IV	22821.69	$a^4G_{3½}-u^4G^0_{4½}$	(0) 1.25	(0.18) 1.25*b*
6	4379.242	150*racm*	II	22828.61	$a^6D_{4½}-y^6F^0_{5½}$	(?w_2)1.29w_2	(0) 1.15*b*
4	4377.90	2	IV	22835.58	$a^4P_{2½}-x^4D^0_{2½}$	(0)1.35	(0.57) 1.42*b*
4	4376.80	1	IV	22841.38			
5	4376.057	0		22845.22	$a^4G_{2½}-u^4G^0_{2½}$?		
6	4375.315	4	IV	22849.10	$b^2G_{3½}-s^2G^0_{3½}$	(0)0.88	(0.15) 0.88*b*
6	4375.069	1	IV	22850.38			
6	4373.827	4	IV	22856.87	$a^4G_{4½}-u^4G^0_{4½}$	(0) 1.19	(0.19) 1.16*b*
6	4373.234	4	IV	22859.98	$b^2G_{4½}-s^2G^0_{4½}$	(0) 1.11	(0.07) 1.10*b*
6	4369.066	2	IV	22881.77	$a^4G_{4½}-u^4G^0_{3½}$	(0) 1.56	(0) **1.64***s*
6	4368.598	4	IV	22884.23	$a^4G_{3½}-u^4G^0_{3½}$	(0) 0.97	(0.09) 0.98*b*
6	4368.047	10	I	22887.12	$a^4F_{3½}-z^4F^0_{3½}$	(?w_2 D) 1.63w_2 B	(0) **1.75***s*
4	4367.07	1		22892.25	$b^2G_{4½}-s^2G^0_{3½}$		
4	4365.74	3	IV	22899.21	$a^2P_{1½}-x^2D^0_{1½}$		
6	4364.221	4	IV	22907.18	$a^4G_{2½}-u^4G^0_{3½}$	(0)0.56	(0.13) 0.56*b*
6	4363.531	5	II A	22910.81	$a^6D_{2½}-x^4P^0_{1½}$	(0?w_1) 1.59	(0.04) 1.60*b*
5	4363.357	1	IV	22911.71	$a^4P_{0½}-x^4D^0_{1½}$		

TABLE 1.—*Arc spectrum of vanadium* (V I)—Continued

(1)	(2)	(3)	(4)	(5)	(6)	(7)	(8)
Ref.	λ_{air} A	Int. arc	Temp. class	ν_{vac} cm^{-1}	Term combinations	Zeeman effect: Observed	Zeeman effect: Computed
6	4361.399	2	IV	22922.00	$a^4G_{3½}-u^4G^0_{3½}$	(?w_3 D) 1.66w_3 B	(0) 1.59*b*
4	4361.03	1		22923.95	$a^3F_{3½}-u^3F^0_{3½}$	(0) 0.83	(0.04) 0.85*b*
6	4360.592	3	IV	22926.24	$a^3D_{3½}-w^3F^0_{3½}$	(w_1) 0.86w_1	(0) **0.86***s*
6	4357.453	2	IV	22942.76	$a^2F_{3½}-u^2F^0_{3½}$ $a^2D_{1½}-w^2D^0_{1½}$	(0) 1.10 or (0) 1.38 diffuse.	(0.09 1.12*b* (0.24) 0.88*b*
6	4356.796	1	IV	22946.22	$a^4G_{2½}-u^4G^0_{3½}$	(**0.22**, 0.64, 1.03)?	(**0.20**, 0.60, 1.00)−0.01, 0.39, 0.80, 1.19, 1.59, **1.99**
6	4355.958	10	I	22950.64	$a^4F_{3½}-z^4F^0_{3½}$	(**0.29**, 0.88) 0.16, 0.70, 1.33, **1.92**	(**0.30**, 0.92) 0.09, 0.70, 1.31, **1.93**
6	4354.985	5	IV	22955.76	$a^2H_{5½}-x^2H^0_{5½}$	(0) 1.09	(0.13) 1.08*b*
6	4353.338	2	IV	22964.44	$a^2P_{1½}-z^2F^0_{2½}$	(0.15, 0.50)?	(**0.15**, 0.46) **0.63**, 0.74, 1.05, 1.35
6	4352.892	50*acm*	I	22966.81	$a^4F_{4½}-z^4F^0_{4½}$	(0) 1.30	(0.11) 1.30*b*
4	4352.47	2	IV	22969.03		(0.17)?	
6	4350.820	2	III A	22977.74	$a^6D_{1½}-z^4P^0_{2½}$		
6	4350.680	1	IV	22978.48			
4	4342.84	6	III	23019.94	$a^3H_{4½}-x^3H^0_{4½}$	(0) 0.90	(0.07) 0.89*b*
4	4342.21	4	III	23023.28	$a^4P_{1½}-z^4D^0_{½}$	(**0.18**, 0.57) 0.81, 1.15, —	(**0.20**, 0.61) **0.68**, 1.09, 1.50, 1.90
6	4341.016	40*acm*	I	23029.63	$a^4F_{2½}-z^4F^0_{3½}$	(0) 1.21	(0.09) 1.22*b*
6	4336.129	2	IV	23055.58	$b^3H_{4½}-u^3H^0_{4½}$	(0) 0.90	(**0.22**) 0.88*b*
6	4334.114	4	III A	23066.30	$a^4P_{2½}-z^4D^0_{3½}$	(?w_2 D) 1.06w_2 A	(0) 1.10*b*
6	4332.832	30*acm*	I	23073.13	$a^4F_{3½}-z^4F^0_{4½}$	(0) 1.00	(0.07) 1.00*b*
6	4332.380	1	IV	23075.54	$b^3H_{3½}-u^3H^0_{3½}$	(0) 1.08	(0.09) 1.07*b*
6	4330.033	30*acm*	I	23088.04	$a^4F_{1½}-z^4F^0_{1½}$	(0) 0.35	(0.01) 0.40*b*
5	4323.489	[−1]		23122.99	$a^4H_{3½}-x^3H^0_{3½}$		
4	4322.37	1		23128.98	$b^3P_{1½}-y^3P^0_{1½}$	(0) 0.38, **1.32**	(0.02, **0.05**) 1.32, **1.35**
4	4320.29	1		23140.11	$a^2H_{5½}-x^4H^0_{4½}$	(0.21) 1.11	
4	4319.96	1		23141.88	$a^2H_{4½}-x^4H^0_{3½}$		
4	4318.70	4		23148.63			
4	4315.83	1		23164.01	$a^4P_{2½}-w^4F^0_{3½}$?		
6	4313.896	3	IV	23174.40	$a^4H_{4½}-x^2H^0_{4½}$	(0.25) 0.94	(0.22) 0.91*b*
6	4309.801	20	I	23196.42	$a^4F_{3½}-z^4F^0_{4½}$ $(aG^4_{4½}-w^4H^0_{4½})$	(? w_2 D) 1.46 w_2 B	(0) 1.50*b*
6	4309.531	2	IV	23197.89	$a^4G_{3½}-w^4H^0_{3½}$		
4	4308.44	1		23203.74	$a^2D_{2½}-w^2D^0_{2½}$		
6	4307.188	12	I	23210.50	$a^4F_{1½}-z^4F^0_{2½}$ $(a^4G_{5½}w-H^6_{5½})$	(**0.31**, 0.92) 0?, 0.72, 1.37, **1.93**	(**0.29**, 0.87) 0.11, 0.69, 1.27, **1.85**
5	4306.594?	[−1]		23213.70	$a^4H_{3½}-x^3H^0_{4½}$		
6	4306.222	15	I	23215.70	$a^4F_{2½}-z^4F^0_{2½}$	(? w_3 D) 1.82w_3 B	(0) **1.78***s*
5	4305.482	3	IV	23219.70	$a^4H_{3½}-x^2H^0_{3½}$	(0, 0.38) 1.08	(0) 1.10*b*
6	4303.542	3	IV	23230.16		(? w_1 D) 0.85w_1 A	
5	4302.143	tr	IV A	23237.72	$a^2D_{1½}-w^2D^0_{2½}$	(?) 1.32w_1	(0) 1.34*b*
6	4298.048	12	III	23259.85	$a^4G_{2½}-w^4H^0_{3½}$	(0) 0.77	(0) **0.80***s*
6	4297.694	12	III	23261.77	$a^4G_{3½}-w^4H^0_{4½}$	(0) 0.94	(0) 0.85*b*
4	4297.10	1		23265.01	$a^2H_{3½}-u^2G^0_{3½}$	(0) 1.07	
6	4296.121	15	III	23270.29	$a^4G_{4½}-w^4H^0_{5½}$	(0) 1.04	(0) 0.95*b*
6	4291.828	15	III	23293.56	$a^4G_{5½}-w^4H^0_{6½}$	(0) 1.10	(0) 1.08*b*
6	4291.305	4	III	23296.40	$a^4H_{4½}-z^4H^0_{4½}$	(0.12, 0.44, 0.73, 1.05) 2.06w_3 B	(**0.13**, 0.40, 0.67, 0.94) 0.00, 0.27, 0.54, 0.81, 1.07, 1.34, 1.61, **1.88**
5	4288.819	1	IV A	23309.90	$a^4D_{1½}-z^2S^0_{½}$		
6	4287.823	4	IV	23315.31		(0) 1.03	
6	4286.428	5	III	23322.91	$a^4H_{3½}-x^4H^0_{3½}$	(?) w_3 D 1.61w_3 B	(0) 1.48*b*
6	4284.061	15	III	23335.80	$a^4H_{3½}-x^4H^0_{3½}$	(0) 0.68	(0.06) 0.66*b*
5	4282.924	(5)	(III)	23341.99	$a^4H_{6½}-x^4H^0_{5½}$	(?w_3 D) 1.46 w_3 B	
5	4278.992	2	III A	23363.44			
6	4276.966	12	III	23374.52	$a^4H_{4½}-x^4H^0_{4½}$	(0) 0.94	(0.04) 0.94*b*
6	4271.563	12	III	23404.08	$a^4H_{5½}-x^4H^0_{5½}$	(0) 1.08	(0.04) 1.10*b*
6	4270.332	4	IV	23410.82	$a^2D_{2½}-t^4D^0_{2½}$	(0) 1.18	(0.35) 1.25*b*
6	4269.768	5	III	23413.92	$a^4H_{3½}-x^4H^0_{4½}$	(0.15, 0.45, 0.75, 1.05) 1.96w_3 B	(**0.18**, 0.43, 0.71, 0.99) −0.06, 0.22, 0.50, 0.79 1.08, 1.36, 1.64, **1.93**
6	4268.652	20	III	23420.03	$a^4H_{6½}-x^4H^0_{5½}$	(0) 1.21	(0.21) 1.20*b*
4	4267.32	1	IV	23427.32			
4	4265.90	1	IV	23435.12	$b^4D_{3½}-z^6F^0_{3½}$?		

TABLE 1.—*Arc spectrum of vanadium* (V I)—Continued

(1) Ref.	(2) λ_{air} A	(3) Int. arc	(4) Temp. class	(5) ν_{vac} cm^{-1}	(6) Term combinations	(7) Zeeman effect Observed	(8) Zeeman effect Computed
6	4265.162	8n	III	23439.19		(0? w_2 D) 1.21w_2	
6	4262.169	6	III	23455.66	$a^4H_{4½}-x^4H^0_{3½}$	(?w_2 D) 1.67w_2 B	(0) 1.50*b*
6	4261.222	2	IV	23460.87	$b^2G_{3½}-q^4F^0_{4½}$		
6	4259.320	8	I	23471.33	$a^4F_{3½}-z^2D^0_{3½}$	(0.41) 1.31w_1 B	(**0.12**, 0.37) 0.6 (0.88 1.13, **1.38**
6	4257.375	6	III	23482.08	$a^4H_{3½}-x^4H^0_{3½}$	(? w_2 D) 1.55w_1 B	(0) 1.55*b*
4	a4252.80	1	IV	23507.35	$a^2H_{4½}-u^2G^0_{3½}$	(0) 0.93	(0) 0.93
4	4246.69	1	IV	23541.15	$a^2P_{1½}-w^2F^0_{2½}$		
6	4241.325	3	III	23570.93	$b^4F_{4½}-u^4F^0_{4½}$	(0) 1.52	(0) 1.48*b*
6	4240.368	4	III	23576.24	$b^4F_{3½}-u^4F^0_{3½}$	(? w_1 D) 1.54	(0) 1.50*b*
6	4240.089	3	IV	23577.80	$b^4F_{2½}-u^4F^0_{1½}$	(**0.24**, 0.72) 0.78, 1.23, **1.74**	(**0.25**, 0.76) 0.29, 0.79, 1.30, **1.81**
4	4238.97	2	IV	23584.01		(0) 1.22	
6	4236.618	1	III A	23597.11	$a^6D_{0½}-z^2G^0_{1½}$		
6	4235.765	10	III	23601.86	$b^4F_{1½}-u^4F^0_{1½}$	(0.20) 0.46	(0.21) 0.47*b*
6	4234.531	8	I	23608.75	$a^4F_{1½}-z^2D^0_{1½}$	(—, **0.54**) 0.18, 0.57, 0.96	(0.18, **0.54**) 0.22, **0.58**, 0.94
6	4234.010	12	I	23611.65	$b^4F_{2½}-u^4F^0_{2½}$ / $a^4F_{3½}-z^2D^0_{3½}$	(0) 1.05w_1 A	(0.11) 1.02*b*
6	4232.959	12	III	23617.51	$b^4F_{3½}-u^4F^0_{3½}$	(0) 1.23	(0.03) 1.22*b*
6	4232.466	15	III	23620.26	$b^4F_{4½}-u^4F^0_{4½}$	(0) 1.34	(0.04) 1.30*b*
6	4229.695	4	III	23635.73	$b^4F_{1½}-u^4F^0_{1½}$	(**0.28**, 0.93) 0, 0.67, 1.30, **1.91**	(**0.30**, 0.91) 0.09, 0.70, 1.30, **1.91**
6	4227.740	4	III	23646.66	$a^2P_{0½}-w^2D^0_{1½}$	(0) 0.87	(0) **0.88***s*
5	4226.622	(5)	(III)	23652.92	$b^4F_{2½}-u^4F^0_{2½}$	(?w_2 D) 1.61w_2 B	
5	4224.133	5	III	23666.85	$b^4F_{3½}-u^4F^0_{4½}$	(0?w_1 D)—, 1.50w_1 A	(0) 1.44*b*
4	4222.98	1	IV	23673.34	$z^6F^0_{½}-z^6G_{1½}$		
4	4222.33	2	IV	23676.99	$b^4P_{2½}-w^4P^0_{1½}$	(0) 1.54	(0) 1.50*b*
4	4221.04	1		23684.23	$b^4D_{0½}-p^4D^0_{0½}$		
4	4219.51	2	III A	23692.81	$a^6D_{3½}-y^4F^0_{2½}$		
6	4218.714	4	III A	23697.25	$a^6D_{4½}-y^4F^0_{3½}$	(**0.19**, 0.55, 0.96, 1.34) ?w_1 C	(**0.18**, 0.55, 0.92, 1.29, 0.23, 0.60, 0.97, .134, 1.70, 2.07, 2.44, **2.81**
4	4216.38	1	II A	23710.40	$a^6D_{2½}-y^4F^0_{1½}$ / $a^6D_{2½}-z^2G^0_{2½}$		
4	4213.94	1h		23724.12	$b^4D_{0½}-p^4D^0_{1½}$	(0.55) 0.75, 1.76	(0.56) 0.66, **1.78**
4	4210.85	1h		23741.52	$b^4D_{1½}-p^4D^0_{1½}$?		
6	h4209.857	20	I	23747.11	$a^6D_{4½}-y^4F^0_{3½}$	(?w_2 B) 1.43, 2.47w_2 C	0.14, 0.43, 0.72, 1.01, **1.30**) 0.22, 0.51, 0.80, 1.09, **1.38**, 1.66, 1.95, 2.24, 2.53
4	4206.68	1		23765.04	$b^4D_{2½}-p^4D^0_{1½}$	(0) 1.49	
4	4204.52	1		23777.25	$a^6D_{1½}-y^4F^0_{1½}$		
4	4200.89	1	III A	23797.79	$a^4F_{2½}-z^2D^0_{2½}$		
6	4200.190	4	III A	23801.77	$a^6D_{2½}-z^2G^0_{1½}$	(**0.34**, 1.04, 1.70) **0**, 0.72, 1.30	(**0.34**, 1.03, 1.72) —**0.80**, —0.11, 0.58, 1.26, 1.95, 2.64
6	4198.621	4	III A	23810.66	$a^6D_{3½}-y^4F^0_{2½}$	(—, 0.62, 1.01, **1.45**) **0.21**, 0.54, 0.95, 1.38, 1.76, 2.18, 2.60, —	(0.18, 0.56, 0.94, **1.32**) 0.21, 0.59, 0.97, **1.34**, 1.71, 2.09, 2.47
6	4197.606	2	IV	23816.24	$a^2H_{5½}-y^2H^0_{4½}$	(0) 1.05	(0) 1.03*b*
4	4197.29	1		23818.20	$a^6D_{0½}-y^4F^0_{1½}$		
5	a4195.601	1	IV	23827.80	$b^4D_{3½}-p^4D^0_{2½}$?	(0) 1.31	(0.26) 1.31*b*
4	4191.55	10	II	23850.81	$a^6D_{1½}-y^4F^0_{2½}$ / $b^4P_{2½}-w^4P^0_{2½}$	(**0.36**, 1.23) **0.20**, 0.60	(**0.42**, 1.26) —**0.28**, 0.56, 1.40, 2.24
6	4189.849	12	I	23860.51	$a^6D_{3½}-y^4F^0_{3½}$	(**0.16**, 0.49, 0.79, 1.08) **0.17**, 0.50, 0.80, 1.09, 1.41, 1.68	(**0.16**, 0.46, 0.76, 1.06) **0.17**, 0.47, 0.77, 1.07, 1.38, 1.69, 1.99, 2.29
5	4187.665	[1h]		23872.95	$a^4D_{1½}-x^4D^0_{½}$?	(0.56)?w_2	(0.56) 0.56, **1.75**
4	4186.80	1		23877.92	$a^4D_{2½}-x^4D^0_{1½}$	(0) 1.42	(0.13) 1.49*b*
6	4182.596	10	I	23901.89	$a^6D_{2½}-y^4F^0_{1½}$	(**0.24**, 0.72, 1.20) **0**, 0.43, 0.90, 1.43, —	(**0.22**, 0.68, 1.14) **0.01**, 0.47, 0.93, 1.38, **1.83**, 2.29
6	4182.082	2	IV	23904.82	$a^2H_{4½}-y^2H^0_{3½}$	(0) 0.92	(0) 0.97*b*
4	4180.89	1	IV	23911.66	$b^4D_{2½}-p^4D^0_{2½}$	(0) 1.48	(0) **1.50***s*

TABLE 1.—*Arc spectrum of vanadium* (V I)—Continued

(1)	(2)	(3)	(4)	(5)	(6)	(7)	(8)
Ref.	λ_{air} A	Int. arc	Temp. class	ν_{vac} cm^{-1}	Term combinations	Zeeman effect: Observed	Zeeman effect: Computed
6	4179.421	15	I	23920.05	$a^6D_{4½}-z^7G^0_{4½}$	(—, 0.54, 0.93, 1.28, **1.70**) **0.29**, 0.57, 0.98, 1.34, 1.71, 2.09, 2.48, 2.86, —	(0.19, 0.58, 0.97, 1.36, **1.75**) —0.23, 0.16, 0.55, 0.94, **1.33**, 1.71, 2.10, 2.49, 2.88
6	4177.071	2	IV	23933.50	$b^4D_{3½}-p^4D^0_{3½}$	(0) 1.37	(0.38) 1.38*b*
5	4176.793	[3]		23935.09	$a^4F_{1½}-z^7D^0_{1½}$		
5	4176.644	[00*p*?]		23935.94	$a^4D_{0½}-x^4D^0_{0½}$		
4	4175.16	1	IV A	23944.47	$a^4D_{3½}-x^4D^0_{3½}$	(0) 1.46	(0) 1.52*b*
6	4174.023	5	III	23950.98	$a^2P_{1½}-w^2D^0_{2½}$	(0) 1.19	(0) 1.15*b*
6	4171.308	3	IV	23966.57	$b^4P_{1½}-w^4P^0_{0½}$	(0.46) 1.26	(0.45) **1.23**, 2.13
6	4169.261	2	IV	23978.34	$b^4P_{1½}-w^4P^0_{1½}$	(0) 1.65	(0.11) 1.64*b*
4	4168.95	1		23980.13	$a^4D_{1½}-x^4D^0_{1½}$	(0) 1.17	(0.02) 1.19*b*
4	4167.04	1*h*		23991.11	$z^6F^0_{1½}-f^6F_{1½}$	(?) 1.37 diffuse	
4	4166.74	1*h*		23992.84	$z^6F^0_{1½}-f^6F_{4½}$	(0) 1.33	
4	4162.34	1		24018.19	$a^4H_{4½}-y^6H^0_{3½}$		
4	4160.40	1	III A	24029.39	$\{a^6D_{1½}-y^4D^0_{0½}$ $a^6D_{2½}-y^4D^0_{1½}\}$	(0.92)?w_2	{(0.94) 0.88, **2.76**, (**0.23**, 0.66) 0.94, 1.39, 1.83, **2.27**
3	4159.696	8	I	24033.47	$a^6D_{3½}-z^7G^0_{1½}$	(**0.20**, 0.61, 1.01, 1.45) **0.22**, 0.55, 0.93, 1.33, 1.76, —	(**0.21**, 0.61, 1.01, 1.41) —**0.28**, 0.12, 0.52, 0.92, 1.33, 1.74, 2.14, 2.54
3	4158.379	0		24041.08	$a^6D_{3½}-y^4D_{2½}$		
5	4157.960	1	III A	24053.50	$a^4D_{0½}-x^4D^0_{1½}$	(0.56) 0.56, **1.77**	(0.58) 0.58, **1.75**
5	4155.888	1	III A	24055.49	$a^6D_{4½}-y^4D^0_{3½}$		
4	4155.24	1		24059.22	$a^4H_{4½}-y^2I^0_{5½}$		
6	4153.332	2	III A	24070.30	$a^6D_{0½}-y^4D^0_{1½}$	(1.66) 1.58	(1.67) 1.62*b*
6	4152.602	2	IV	24074.18		(0.24) 1.00	
4	4151.37	1		24081.65	$a^4D_{3½}-x^4D^0_{3½}$		
4	4150.70	2	IV	24085.53		(0) 1.09	
6	4148.873	2	III A	24096.17	$a^6D_{1½}-y^4D^0_{1½}$	(0.32, **1.00**) 0.83, **1.49**, 2.15	(0.33, **0.98**)[0.84, **1.49**, 2.15
4	4147.77	2		24102.60	$z^6D^0_{3½}-f^6D_{3½}$		
4	4142.91	2	III	24130.86	$a^4D_{3½}-w^4F^0_{4½}$		
4	4142.66	2	III A	24132.32	$a^6D_{3½}-y^4D^0_{2½}$		
4	4141.85	2	III A	24137.04	$a^6D_{0½}-y^4D^0_{1½}$	(1.03) 0.13, 2.23	(1.07) **0.10**, 2.23
4	4141.37	2	IV	24139.84	$z^6D^0_{3½}-f^6F_{3½}$	(0?w_3 D) 0.59w_3*C*?	(0) **0.67***s*
6	4139.262	4	IV	24152.12	$b^4P_{1½}-w^4P^0_{2½}$	(0) 1.44	(0) 1.40*b*
4	4138.12	2*hd*?		24158.79	$b^4P_{0½}-w^4P^0_{1½}$		
5	4137.987	[1]		24159.55	$a^4D_{3½}-w^4F^0_{3½}$		
4	4137.02	1		24165.22	$z^6D^0_{3½}-f^6F_{3½}$?		
6	4136.395	3	III A	24168.85	$a^6D_{3½}-y^4D^0_{3½}$		
6	4136.116	4	III	24170.48	$b^4P_{0½}-w^4P^0_{1½}$	(0.51) 1.08	(0.50) **1.10**, 2.10
4	4135.29	1		24175.32	$a^4D_{3½}-x^4D^0_{2½}$		
4	4134.50	60*s*	I	24179.93	$a^6D_{4½}-y^6D^0_{3½}$	(0w_1D) 1.42w_1 C	(0) 1.43*b* (0) **1.44***s*
6	4133.781	3	III A	24184.13	$a^4D_{1½}-x^4D^0_{2½}$	(0) 1.48	
5	4132.877	[1]		24189.42	$a^4D_{3½}-z^5P^0_{2½}$		
6	4132.019	60*s*	I	24194.45	$a^6D_{3½}-y^6D^0_{2½}$	(0?w_2D) 1.44w_2 C	(0) 1.46*b*
4	4131.20	1	III A	24199.25	$a^6D_{1½}-y^4D^0_{2½}$	(0.23, 0.72)?w_3 A	(**0.24**, 0.72) **0.62**, 1.10, 1.58, 2.06
4	4130.40	1		24203.94	$z^6D^0_{2½}-f^6F_{4½}$		
6	4130.143	2		24205.44	$a^4P_{2½}-w^4F^0_{1½}$		
6	4128.868	5	III	24212.91	$b^4F_{1½}-s^4D^0_{0½}$	(0.22) 0.20, **0.60**	(0.20) 0.20, **0.59**
6	4128.077	60*s*	I	24217.55	$a^6D_{3½}-y^6D_{1½}$	(0w_1 D) 1.50w_1 C	(0) 1.42*b*
6	4124.080	5	III	24241.02	$a^4P_{2½}-w^4D^0_{3½}$	(0.56)w_2 C	(0.55) 1.42*b*
4	4123.56	60*s*	I	24244.07	$a^6D_{1½}-y^6D^0_{2½}$	(0.70) 1.12, 2.57	(0.71) **1.11**, 2.53
6	4123.196	6	III	24246.22	$b^4F_{2½}-s^4D^0_{1½}$		
4	4122.35	1*h*		24251.18	$z^6D^0_{1½}-f^6D_{4½}$		
6	4120.977	1	IV	24259.27	$a^4G_{5½}-z^6H^0_{4½}$		
6	4120.545	8	III	24261.81	$a^4D_{1½}-w^4F^0_{1½}$	(0.32, **0.97**) 0.22, **0.84**, 1.49	(0.34, **1.01**) 0.18, **0.86**, 1.53
6	4119.463	8	III	24268.18	$a^4D_{3½}-w^4F^0_{4½}$	(0.49, **0.83**) **0.52**, 0.85, 1.20, 1.55, 1.86	(0.18, 0.52, **0.86**) 0.49, 0.83, **1.18**, 1.53, 1.87
4	4119.10	1	IV	24270.32	$b^4F_{1½}-s^4D^0_{1½}$		
6	4118.648	8	III	24272.98	$a^4D_{3½}-w^4F^0_{3½}$	(0.54) 1.33	(0.62) 1.29*b*
6	4118.187	8	III	24275.70	$\{b^4F_{3½}-s^4D^0_{2½}$ $(b^4P_{2½}-z^4S^0_{1½})\}$	(0w_1) 1.14w_1	(0) 1.08*b*

TABLE 1.—*Arc spectrum of vanadium* (V I)—Continued

(1)	(2)	(3)	(4)	(5)	(6)	(7)	(8)
Ref.	λ_{air} A	Int. arc	Temp. class	ν_{vac} cm^{-1}	Term combinations	Zeeman effect: Observed	Zeeman effect: Computed
6	4116.700	4*a*	I A	24284.48	$a^6D_{1\frac{1}{2}}-y^6D^\circ_{1\frac{1}{2}}$		
3	4116.60	0		24285.06	$a^6D_{2\frac{1}{2}}-y^6D^\circ_{2\frac{1}{2}}$		
6	4116.479	50*a*	I	24285.77	$a^6D_{3\frac{1}{2}}-y^6D^\circ_{3\frac{1}{2}}$	(?) 1.60	(0.04) 1.60*b*
6	4115.484	2	III	24291.65	$a^4D_{1\frac{1}{2}}-z^4P^\circ_{1\frac{1}{2}}$		
6	4115.179	60*a*	I	24293.45	$a^6D_{3\frac{1}{2}}-y^6D^\circ_{3\frac{1}{2}}$	(?w_3D) 1.54	(0.15) 1.56*b*
6	4114.525	3	IV	24297.31	$b^4F_{1\frac{1}{2}}-u^4G^\circ_{2\frac{1}{2}}$		
6	4113.517	12	III	24303.27	$a^4P_{2\frac{1}{2}}-w^4D^\circ_{3\frac{1}{2}}$	(0?w_3D) 1.05w_3A	(0) 1.10*b*
6	4112.334	5	III	24310.27	$a^4G_{4\frac{1}{2}}-t^4F^\circ_{3\frac{1}{2}}$	(1.11) 1.74 or (0) 1.09	(0) **1.19***s*
6	4111.790	100R*a*	I	24313.47	$a^6D_{4\frac{1}{2}}-y^6D^\circ_{3\frac{1}{2}}$ $a^4G_{3\frac{1}{2}}-t^4F^\circ_{2\frac{1}{2}}$ $b^4F_{2\frac{1}{2}}-s^4D^\circ_{1\frac{1}{2}}$ $a^4D_{2\frac{1}{2}}-x^4D^\circ_{1\frac{1}{2}}$ $b^4F_{3\frac{1}{2}}-u^4G^\circ_{3\frac{1}{2}}$ $b^4F_{2\frac{1}{2}}-u^4G^\circ_{2\frac{1}{2}}$		
5	4110.761	1		24319.56	$a^4G_{4\frac{1}{2}}-y^4H^\circ_{4\frac{1}{2}}$ $a^4G_{3\frac{1}{2}}-t^4G^\circ_{3\frac{1}{2}}$		
6	4109.780	50*a*	I	24325.36	$a^6D_{0\frac{1}{2}}-y^6D^\circ_{1\frac{1}{2}}$ $a^4D_{0\frac{1}{2}}-w^4F^\circ_{1\frac{1}{2}}$	(0.71) **1.09**, 2.54	(0.72) **1.14**, 2.58
6	4109.043	2	IV	24329.73	$a^4P_{1\frac{1}{2}}-w^4D^\circ_{2\frac{1}{2}}$	(0?, 0.80) 0.88, 1.60?	(0.80) 0.90, **2.50**
6	4108.217	5	III	24334.62	$a^4G_{3\frac{1}{2}}-t^4F^\circ_{2\frac{1}{2}}$	(?w_1) 0.72	(0) 0.72*b*
6	4107.467	4	III	24339.06	$a^4P_{1\frac{1}{2}}-w^4D^\circ_{1\frac{1}{2}}$	(0.44, 1.35) 0.40, 1.27	(0.45, **1.35**) 0.35, **1.25**, 2.15
6	4105.166	60*a*	I	24352.70	$a^6D_{1\frac{1}{2}}-y^6D^\circ_{2\frac{1}{2}}$	(?) 1.48w_2C	(0) 1.42*b*
6	4104.779	15	III	24355.00	$b^4F_{4\frac{1}{2}}-s^4D^\circ_{3\frac{1}{2}}$	(?w_3) 1.38w_3	
6	4104.392	12	III	24357.30	$a^4G_{3\frac{1}{2}}-t^4F^\circ_{3\frac{1}{2}}$	(0) 1.36	(0) 1.36*b*
4	4103.41	1	IV	24363.15	$b^4P_{2\frac{1}{2}}-s^4D^\circ_{1\frac{1}{2}}$		
6	4102.163	20	II	24370.53	$a^4D_{1\frac{1}{2}}-w^4F^\circ_{2\frac{1}{2}}$	(0) 0.88	(0) 0.88*b*
5	4101.535	0		24374.24	$a^4G_{3\frac{1}{2}}-t^4F^\circ_{4\frac{1}{2}}$?		
5	4101.000	0		24377.44	$b^4D_{3\frac{1}{2}}-r^4F^\circ_{4\frac{1}{2}}$	(0) 0.94	
6	4099.796	60*a*	I	24384.60	$a^6D_{2\frac{1}{2}}-y^6D^\circ_{3\frac{1}{2}}$	(0) 1.44	(0) **1.50***s*
5	4098.850	0*h*		24390.22	$b^4D_{2\frac{1}{2}}-q^4F^\circ_{3\frac{1}{2}}$ $a^4H_{3\frac{1}{2}}-u^4F^\circ_{3\frac{1}{2}}$ $a^4H_{3\frac{1}{2}}-u^4F^\circ_{2\frac{1}{2}}$?		
6	4096.935	3	IV	24401.63	$b^4F_{2\frac{1}{2}}-s^4D^\circ_{1\frac{1}{2}}$	(0.61)?w_2C	(0.47) 1.30*b*
4	4096.50	1		24404.23	$a^4F_{3\frac{1}{2}}-z^6P^\circ_{3\frac{1}{2}}$		
6	4095.485	25	II	24410.27	$a^4D_{2\frac{1}{2}}-w^4F^\circ_{3\frac{1}{2}}$	(0) 1.06	(0) 0.97*b*
6	4094.285	3	IV	24417.42	$a^4G_{3\frac{1}{2}}-y^4H^\circ_{3\frac{1}{2}}$ $a^4G_{4\frac{1}{2}}-t^4F^\circ_{3\frac{1}{2}}$	(?2*p*) 1.19w_1 C	(0.98) 1.16*b* (0.33) 1.18*b*
4	4093.50	5	III	24422.11	$a^4P_{0\frac{1}{2}}-w^4D^\circ_{1\frac{1}{2}}$	(1.27) 1.35	(1.25) 1.34*b*
6	4092.694	50*a*	I	24426.91	$a^6D_{3\frac{1}{2}}-y^6D^\circ_{4\frac{1}{2}}$	(0) 1.40	(0) **1.40***s*
6	4092.417	8	III	24428.58	$a^4P_{1\frac{1}{2}}-w^4D^\circ_{2\frac{1}{2}}$ $b^4P_{2\frac{1}{2}}-s^4D^\circ_{2\frac{1}{2}}$	(**0.18**, 0.55) **0.76**, 1.15, 1.50	(**0.20**, 0.60) **0.70**, 1.10, 1.50, 1.90
6	4091.948	3	III	24431.37	$a^4P_{0\frac{1}{2}}-w^4D^\circ_{1\frac{1}{2}}$	(0.91) 0	(0.90) **−0.10**, 1.70
6	4090.587	25	I	24439.50	$a^4D_{3\frac{1}{2}}-w^4F^\circ_{3\frac{1}{2}}$ $(a^4F_{4\frac{1}{2}}-y^4F^\circ_{3\frac{1}{2}})$	(0) 1.13	(0) 1.14*b*
4	4084.75	1		24474.41	$a^4P_{2\frac{1}{2}}-1^\circ$		
4	4084.24	1		24477.47	$a^4G_{4\frac{1}{2}}-z^4H^\circ_{3\frac{1}{2}}$? $a^2F_{3\frac{1}{2}}-u^4P^\circ_{2\frac{1}{2}}$?		
6	4082.930	4	III	24485.34	$a^4P_{2\frac{1}{2}}-v^4F^\circ_{1\frac{1}{2}}$	(0.85) 0, 1.73	(0.87) **−0.01**, 1.73
5	4078.707	[−1]		24510.68	$a^4F_{3\frac{1}{2}}-z^6P^\circ_{3\frac{1}{2}}$		
5	4077.971	[−1]		24515.11	$a^4F_{3\frac{1}{2}}-z^6P^\circ_{2\frac{1}{2}}$		
5	4074.191	[0]		24537.85	$a^4G_{3\frac{1}{2}}-t^4G^\circ_{3\frac{1}{2}}$		
4	4072.16	3	III	24550.06	$a^4P_{2\frac{1}{2}}-v^4F^\circ_{3\frac{1}{2}}$	(**0.19**, 0.52, 0.86) **0.36**, —, —	(**0.18**, 0.52, 0.86) **0.35**, 0.69, 1.03, 1.38, 1.73, 2.07
6	4071.537	8	III	24553.85	$b^4P_{2\frac{1}{2}}-s^4D^\circ_{2\frac{1}{2}}$	(?w_1) 1.06w_2	(0) 1.17*b*
4	4070.78	4	II	24558.38	$a^4F_{4\frac{1}{2}}-y^6F^\circ_{4\frac{1}{2}}$	(0.38) 1.32w_1	(0.48) 1.35*b*
4	4068.00	4	II A	24575.22	$a^4F_{3\frac{1}{2}}-y^6F^\circ_{3\frac{1}{2}}$	(0) 1.06	(0) **1.12***s*
6	4067.742	3	IV	24576.75	$a^4G_{4\frac{1}{2}}-t^4G^\circ_{3\frac{1}{2}}$ $b^4P_{1\frac{1}{2}}-x^4S^\circ_{1\frac{1}{2}}$	(0.31) 1.18, 1.76	(0) 1.33*b* (0.16, **0.48**) 1.52, **1.84**, 2.16
5	4065.421	−1*d*?		24590.78	$a^4F_{3\frac{1}{2}}-z^6P^\circ_{2\frac{1}{2}}$		
6	4063.932	10	IV	24599.79	$a^4G_{3\frac{1}{2}}-t^4G^\circ_{3\frac{1}{2}}$	(0) 0.56	(0.02) 0.58*b*
4	4062.72	1		24607.14	$b^4P_{1\frac{1}{2}}-s^4D^\circ_{1\frac{1}{2}}$		

TABLE 1.—*Arc spectrum of vanadium* (V I)—Continued

(1)	(2)	(3)	(4)	(5)	(6)	(7)	(8)
Ref.	λ_{air} A	Int. arc	Temp. class	ν_{vac} cm^{-1}	Term combinations	Zeeman effect: Observed	Zeeman effect: Computed
4	4061.61	1		24613.87	$b^4P_{1\frac{1}{2}}-z^2D^1_{2\frac{1}{2}}$	(1.27) 0.45, 1.29	(0.38, **1.14**) 0.54, **1.20**
4	4060.85	1		24618.47	$a^4G_{3\frac{1}{2}}-f^4G^1_{4\frac{1}{2}}$	(0) 1.38	(0.13) 1.42*b*
6	4057.822	5		24636.83	$b^4F_{2\frac{1}{2}}-w^3D^1_{3\frac{1}{2}}$		
6	4057.069	10	III	24641.41	$a^4G_{3\frac{1}{2}}-f^4G^1_{3\frac{1}{2}}$	(0) 0.98	(0.21) 1.00*b*
5	4055.963	[0*hp*?]		24648.12	$a^4F_{1\frac{1}{2}}-z^4P^1_{1\frac{1}{2}}$		
4	4053.66	1		24662.13	$a^4P_{2\frac{1}{2}}-y^2D^1_{2\frac{1}{2}}$		
6	4053.267	3	IV	24664.51	$b^4P_{1\frac{1}{2}}-s^4D^1_{1\frac{1}{2}}$	(0.86) 0.83, 1.41	(0.29, **0.87**) 0.81, **1.30**, 1.97
4	4052.47	1	III A	24669.37	$a^4F_{2\frac{1}{2}}-y^6F^1_{3\frac{1}{2}}$	(0.53)?w_3 C	(0.50) 1.28*b*
6	[b]4051.356	12	III	24676.15	$a^4G_{3\frac{1}{2}}-f^4G^1_{3\frac{1}{2}}$	(0) 1.25	(0.31) 1.24*b*
6	4050.961	10	III	24678.55	$a^4G_{4\frac{1}{2}}-f^4G^1_{4\frac{1}{2}}$	(0) 1.15	(0.22) 1.17*b*
6	4048.619	4	II A	24692.83	$a^4F_{2\frac{1}{2}}-y^6F^1_{1\frac{1}{2}}$	(0) 0.97	(0) **0.99***s*
5	4047.380	1*h*		24700.39	$a^4F_{1\frac{1}{2}}-y^6F^1_{2\frac{1}{2}}$		
4	4046.87	1		24703.50	$a^4G_{2\frac{1}{2}}-f^4G^1_{3\frac{1}{2}}$		
6	4042.632	5	III	24729.40	$b^4P_{1\frac{1}{2}}-s^4D^1_{2\frac{1}{2}}$	(**0.19**, 0.56) **0.77**, 1.17, 1.56	(**0.17**, 0.52) **0.81**, 1.16, 1.51, 1.85
4	4041.60	3	V	24735.70			
4	4040.31	2	IV	24743.60	$a^4G_{3\frac{1}{2}}-f^4G^1_{2\frac{1}{2}}$		
5	4037.358	[−1*h*]		24761.70	$a^4F_{2\frac{1}{2}}-y^6F^1_{3\frac{1}{2}}$?		
5	4036.159	0		24769.06	$b^4P_{0\frac{1}{2}}-z^4S^1_{1\frac{1}{2}}$		
5	4035.896	[3]		24770.67	$a^4F_{1\frac{1}{2}}-z^4P^1_{2\frac{1}{2}}$		
4	4034.71	1	III A	24777.95	$a^4F_{2\frac{1}{2}}-z^4P^1_{1\frac{1}{2}}$		
5	4033.062	1		24788.08	$a^4F_{3\frac{1}{2}}-y^6F^1_{3\frac{1}{2}}$		
4	4032.85	2	III A	24789.35	$a^4F_{1\frac{1}{2}}-y^6F^1_{2\frac{1}{2}}$	(?) 0.90	(0) **0.89***s*
5	[b]4032.481	1	IV	24791.65	$a^4P_{1\frac{1}{2}}-y^2D^1_{1\frac{1}{2}}$	(0) 0.86	(1.36) 1.21*b*
6	[b]4031.831	5	IV	24795.64	$a^2F_{2\frac{1}{2}}-f^2F^1_{3\frac{1}{2}}$	(0) 1.09	(0.30) 1.00*b*
6	4031.220	2	IV	24799.41	$b^4P_{0\frac{1}{2}}-s^4D^1_{1\frac{1}{2}}$	(1.28) 1.31	(1.30) 1.30*b*
4	4030.12	1		24806.14	$b^4P_{0\frac{1}{2}}-s^2D^1_{1\frac{1}{2}}$		
4	4029.90	2	III A	24807.49	$a^4F_{3\frac{1}{2}}-z^4P^1_{2\frac{1}{2}}$		
4	4028.08	1		24818.76	$b^4D_{0\frac{1}{2}}-p^4F^1_{1\frac{1}{2}}$		
5	4026.200	[−1]		24830.32	$a^4F_{2\frac{1}{2}}-y^6F^1_{1\frac{1}{2}}$		
4	4025.30	1		24835.89	$b^4D_{1\frac{1}{2}}-p^4F^1_{1\frac{1}{2}}$	(0.73) 0.42, 0.93, **1.48**	(0.30, **0.90**) 0.30, **0.90**, 1.50
4	4024.40	1		24841.44	$b^4D_{1\frac{1}{2}}-f^2P^1_{1\frac{1}{2}}$		
6	4023.174	4	IV	24849.00	$b^4P_{1\frac{1}{2}}-s^2D^1_{2\frac{1}{2}}$ $a^2F_{2\frac{1}{2}}-f^2F^1_{3\frac{1}{2}}$		
5	4023.066	[−1?]		24849.67	$a^4P_{1\frac{1}{2}}-y^2D^1_{2\frac{1}{2}}$		
5	4022.111	[0]		24855.56	$a^4F_{2\frac{1}{2}}-y^6F^1_{2\frac{1}{2}}$		
4	4021.90	3	IV	24856.88	$b^4P_{0\frac{1}{2}}-s^4D^1_{1\frac{1}{2}}$	(0.73) **0.39**, 1.87	(0.75) **0.35**, 1.85
4	4021.44	1		24859.73	$b^4D_{2\frac{1}{2}}-p^4F^1_{2\frac{1}{2}}$		
4	4020.54	1		24865.30	$b^4D_{2\frac{1}{2}}-f^2P^1_{1\frac{1}{2}}$ $b^4P_{2\frac{1}{2}}-z^2P^1_{1\frac{1}{2}}$?		
4	4019.45	1		24872.03	$b^4D_{0\frac{1}{2}}-o^4D^1_{1\frac{1}{2}}$		
6	4016.699	1		24889.05	$b^4D_{1\frac{1}{2}}-o^4D^1_{2\frac{1}{2}}$		
4	4015.66	1		24895.50	$a^4G_{2\frac{1}{2}}-w^2F^1_{2\frac{1}{2}}$		
4	4015.35	1		24897.42	$a^2H_{4\frac{1}{2}}-w^4G^1_{3\frac{1}{2}}$		
4	4015.06	1	IV	24899.22	$b^4D_{2\frac{1}{2}}-p^4F^1_{2\frac{1}{2}}$		
5	4012.510	[1]		24915.04	$a^4F_{1\frac{1}{2}}-z^4P^1_{1\frac{1}{2}}$		
6	4011.315	3	III	24922.47	$a^4P_{2\frac{1}{2}}-s^4D^1_{2\frac{1}{2}}$	(0?w_2 D) 1.03w_2 A	(0) 1.10*b*
4	[c]4009.77	2	III	24932.06	$b^4D_{0\frac{1}{2}}-o^4D^1_{1\frac{1}{2}}$	(0.49) 0.59, 1.55	(0.43) 0.54, **1.39**
4	4007.01	1		24949.23	$b^4D_{1\frac{1}{2}}-o^4D^1_{2\frac{1}{2}}$ $a^4D_{2\frac{1}{2}}-y^2F^1_{3\frac{1}{2}}$?		
6	[b]4003.544	2	IV	24970.84	$b^4D_{2\frac{1}{2}}-p^4F^1_{3\frac{1}{2}}$	(0w_1) 1.06	(0) 0.73*b*
4	4003.18	*tr*	IV	24973.09	$b^4D_{2\frac{1}{2}}-o^4D^1_{2\frac{1}{2}}$		
4	4001.66	1	IV	24982.57	$a^4P_{1\frac{1}{2}}-s^4D^1_{2\frac{1}{2}}$		
6	[b]4000.081	1	III	24992.45	$b^4D_{2\frac{1}{2}}-p^4F^1_{2\frac{1}{2}}$ $a^4P_{0\frac{1}{2}}-s^4D^1_{1\frac{1}{2}}$	(0.50) 1.27?w_2	(1.27) 1.24*b* (0.78) **0.27**, 1.82
5	3999.939	0		24993.34	$a^4F_{2\frac{1}{2}}-z^4P^1_{2\frac{1}{2}}$		
6	3998.731	15	I	25000.89	$a^4H_{4\frac{1}{2}}-w^4G^1_{5\frac{1}{2}}$ $(b^2H_{4\frac{1}{2}}-f^2H^1_{5\frac{1}{2}})$	(0) 1.09	(0) 1.04*b*
6	3994.887	1	III	25024.95	$b^4D_{1\frac{1}{2}}-o^4D^1_{1\frac{1}{2}}$		
6	3992.801	12	I	25038.01	$a^4H_{4\frac{1}{2}}-w^4G^1_{4\frac{1}{2}}$ $(b^2H_{4\frac{1}{2}}-f^2H^1_{4\frac{1}{2}})$	(0) 1.02	(0) 0.90*b*
5	3991.083	1	III	25048.80	$b^4D_{2\frac{1}{2}}-o^4D^1_{3\frac{1}{2}}$		
6	3990.574	20	I	25051.99	$a^4H_{4\frac{1}{2}}-w^4G^1_{3\frac{1}{2}}$ $a^4H_{3\frac{1}{2}}-w^4G^1_{3\frac{1}{2}}$	(0) 0.88	(0) 0.85*b* (0) 0.80*b*

TABLE 1.—*Arc spectrum of vanadium* (V I)—Continued

(1)	(2)	(3)	(4)	(5)	(6)	(7)	(8)
Ref.	λ_{air} A	Int. arc	Temp. class	ν_{vac} cm^{-1}	Term combinations	Zeeman effect: Observed	Zeeman effect: Computed
6	3988.834	5	II	25062.92	$a^4H_{3\frac{1}{2}}$—$u^4G^0_{3\frac{1}{2}}$	(0.66) 1.13w_2 C	(0.58) 1.16*b*
4	3988.10	1		25067.55	$a^2F_{3\frac{1}{2}}$—$t^2H^0_{3\frac{1}{2}}$		
5	3987.634	1		25070.46	$b^4D_{3\frac{1}{2}}$—$o^4D^0_{3\frac{1}{2}}$		
6	3984.595	6	II	25089.58	$a^4H_{4\frac{1}{2}}$—$u^4G^0_{4\frac{1}{2}}$	(0.81w_2 B)? w_2 D	(0.93) 1.07*b*
6	3984.338	6	II	25091.19	$a^4H_{3\frac{1}{2}}$—$u^4G^0_{3\frac{1}{2}}$		
6	3980.526	3	III	25115.22		(0) 0.89	
6	3979.427	4	III	25122.16	$b^2H_{4\frac{1}{2}}$—$t^2H^0_{4\frac{1}{2}}$	(0w_1) 0.91	(0.04) 0.90*b*
6	3979.147	4	III	25123.93	$b^4D_{3\frac{1}{2}}$—$p^4G^0_{3\frac{1}{2}}$	(0) 1.13	(0) 1.10*b*
4	3978.34	1		25129.04	$a^4H_{3\frac{1}{2}}$—$u^4F^0_{3\frac{1}{2}}$		
6	3975.354	1	III	25147.90	$b^4D_{2\frac{1}{2}}$—$o^4D^0_{2\frac{1}{2}}$	(0) 1.42	(0) 1.70*b*
6	3973.363	2	III	25160.51	$b^2H_{4\frac{1}{2}}$—$t^2H^0_{4\frac{1}{2}}$		
5	3971.936	2	III	25169.55	$b^4D_{3\frac{1}{2}}$—$o^4D^0_{3\frac{1}{2}}$	(0) 1.36	(0) 1.45*b*
4	3964.50	2	III	25216.74	$z^6G^0_{5\frac{1}{2}}$—$e^6G_{5\frac{1}{2}}$		
6	3963.634	4	II	25222.26		(0) 1.01	
6	3950.230	4	III	25307.85		(0) 0.91	
4	3945.88	1	III	25335.76	$a^2D_{2\frac{1}{2}}$—$v^2D^0_{1\frac{1}{2}}$		
4	3945.17	2	III	25340.32	$z^6G^0_{3\frac{1}{2}}$—$e^6G_{3\frac{1}{2}}$		
4	3944.51	1	III	25344.56			
6	3943.666	12	I	25349.97	$a^4D_{3\frac{1}{2}}$—$w^4D^0_{2\frac{1}{2}}$	(0) 1.44	(0) 1.50*b*
4	3942.008	6	II	25360.63	$a^2G_{4\frac{1}{2}}$—$z^2G^0_{3\frac{1}{2}}$	(0?w_2) 1.70w_2 B	(0) 1.62*b*
6	3941.255	3	II	25365.48	$a^4H_{4\frac{1}{2}}$—$w^4H^0_{3\frac{1}{2}}$		
6	3940.596	2	II	25369.72	$a^2D_{1\frac{1}{2}}$—$v^2D^0_{1\frac{1}{2}}$	(0) 0.85	(0.07) 0.94*b*
6	3939.337	4	II	25377.82	$a^4H_{3\frac{1}{2}}$—$w^4H^0_{4\frac{1}{2}}$	(0?w_2 D) 1.59w_2 B	(0) 1.51*b*
4	3938.89	2h	I	25380.71	$z^6F^0_{4\frac{1}{2}}$—$e^6H_{3\frac{1}{2}}$		
6	3938.203	3	II	25385.12	$a^2F_{3\frac{1}{2}}$—$s^2G^0_{4\frac{1}{2}}$	(0) 1.00	(0) 1.01*b*
6	3937.528	3	II	25389.48	$a^4H_{6\frac{1}{2}}$—$w^4H^0_{5\frac{1}{2}}$	(0w_1 D) 1.50	(0) 1.46*b*
6	3936.286	5	I	25397.50	$a^4D_{2\frac{1}{2}}$—$w^4D^0_{1\frac{1}{2}}$	(**0.26**, 0.77) 0.48, 1.09, 1.60, **2.09**	(**0.28**, 0.83) 0.52, 1.08, 1.63, **2.18**
6	3935.140	6	II	25404.89	$a^4H_{3\frac{1}{2}}$—$w^4H^0_{3\frac{1}{2}}$	(0) 0.64	(0) 0.65*b*
6	3934.018	20	I	25412.13	$a^4D_{3\frac{1}{2}}$—$w^4D^0_{3\frac{1}{2}}$	(0) 1.37	(0.12) 1.37*b*
6	3931.345	5	II	25429.43	$a^4H_{4\frac{1}{2}}$—$w^4H^0_{3\frac{1}{2}}$	(0) 0.93	(0.07) 0.93*b*
6	3930.028	10	I	25437.93	$a^2G_{4\frac{1}{2}}$—$z^2G^0_{4\frac{1}{2}}$	(0) 1.04	(0.30) 1.09*b*
5	3929.491	−1*n*		25441.41	$z^6G^0_{3\frac{1}{2}}$—$f^6F_{3\frac{1}{2}}$		
7	3927.932	3		25451.51	$a^4H_{3\frac{1}{2}}$—$w^4H^0_{3\frac{1}{2}}$	(0w_1) 1.08w_1	(0.09) 1.09*b*
4	3926.67	1	III	25459.67	$z^6F^0_{3\frac{1}{2}}$—$f^6G_{3\frac{1}{2}}$	(0) 1.44	(0.36) 1.38*b*
6	3925.244	10	I	25468.94	$a^2F_{3\frac{1}{2}}$—$s^2G^0_{3\frac{1}{2}}$ $a^4F_{4\frac{1}{2}}$—$z^2G^0_{4\frac{1}{2}}$ $a^4H_{3\frac{1}{2}}$—$w^4H^0_{4\frac{1}{2}}$	(0) 0.03	(0) 0.97*b* (0) 1.91*b*
6	3924.661	10	II	25472.73	$a^4H_{4\frac{1}{2}}$—$w^4H^0_{4\frac{1}{2}}$	(0) 1.18	(0.21) 1.20*b*
6	3922.437	12	I	25487.23	$a^4D_{2\frac{1}{2}}$—$w^4D^0_{2\frac{1}{2}}$	(0) 1.33	(0.11) 1.32*b*
6	3921.914	6	I	25490.57	$a^4D_{1\frac{1}{2}}$—$w^4D^0_{0\frac{1}{2}}$	(0.53) 0.64, **1.69**	(0.56) 0.64, **1.75**
5	3921.749	0		25491.63	$z^6F^0_{1\frac{1}{2}}$—$f^6G_{0\frac{1}{2}}$		
6	3920.491	5	I	25499.82	$a^4D_{1\frac{1}{2}}$—$w^4D^0_{1\frac{1}{2}}$	(0.53) 0.60, **0.98**, 1.40	(0.20, **0.59**,) 0.60, **1.00**, 1.39
6	3919.990	2	III	25503.08	$a^4H_{4\frac{1}{2}}$—$w^4H^0_{5\frac{1}{2}}$		
4	3917.14	2	II	25521.66			
4	3915.36	2	II	25533.26			
6	3915.125	2	II	25534.77	$a^4H_{3\frac{1}{2}}$—$w^4H^0_{3\frac{1}{2}}$	(0) 1.60	(0) 1.55*b*
6	3914.329	5	I	25539.95			
4	3913.86	1	II A	25543.04	$a^4D_{1\frac{1}{2}}$—1°		
4	3913.56	2	III	25545.00			
6	3912.887	4	II A	25549.38	$a^4D_{2\frac{1}{2}}$—$w^4D^0_{2\frac{1}{2}}$	(0?w_2 D) 1.39 w_2 C	(0) 1.35*b*
6	3912.209	10	I	25553.80	$a^4D_{1\frac{1}{2}}$—$v^4F^0_{1\frac{1}{2}}$ $a^4D_{0\frac{1}{2}}$—$w^4D^0_{0\frac{1}{2}}$	(0, 0.46) 0.70, 1.04, 1.34	(0.17, **0.50**) 0.69, **1.03**, 1.36 (0.04) 0.04*b*
4	3911.71	1		25557.08			
6	3910.796	5	I	25563.04	$a^4D_{0\frac{1}{2}}$—w $D^0_{1\frac{1}{2}}$	(0.39) 0.41, **1.21**	(0.40) 0.40, **1.20**
6	3909.892	20	I	25568.95	$a^4F_{4\frac{1}{2}}$—$y^4F^0_{3\frac{1}{2}}$ $a^2G_{3\frac{1}{2}}$—$z^2G^0_{3\frac{1}{2}}$		
6	3909.677	4	III	25570.35	$a^2D_{2\frac{1}{2}}$—$s^2D^0_{2\frac{1}{2}}$	(0) 1.12	(0.07) 1.16*b*
4	3909.40	*tr*	IV	25572.18			
6	3908.311	4h	III	25579.27		(0) 1.20 unsymmetrical.	
4	3907.17	2h	II	25586.77		(0) 1.40	
7	3906.746	6	I	25589.53	$a^4D_{2\frac{1}{2}}$—$v^4F^0_{2\frac{1}{2}}$ $a^4D_{1\frac{1}{2}}$—$w^4D^0_{2\frac{1}{2}}$	(0) 1.45	(0.07 1.34*b* (0) 1.38*b*

TABLE 1.—*Arc spectrum of vanadium* (V I)—Continued

(1) Ref.	(2) λ_{air} A	(3) Int. arc	(4) Temp. class	(5) ν_{vac} cm^{-1}	(6) Term combinations	(7) Zeeman effect Observed	(8) Zeeman effect Computed
6	b3904.475	3	III	25604.41	$a^2D_{1½}-z^2D^0_{1½}$	(0.32) 1.49	(0) **1.49***s*
5	3904.402	2	III	25604.89	$z^4G^0_{3½}-e^4G_{4½}$; $a^2D_{2½}-v^2F^0_{2½}$		
6	3904.216	1	II A	25606.11	$a^4D_{0½}-1^\circ$	(0?w_2) 0.98	
6	3902.550	3	I	25617.04	$a^4D_{0½}-v^4F^0_{1½}$	(0.45) 1.28w_3	(0.43) 0.43, **1.29**
6	3902.260	50*r*	I	25618.94	$a^4F_{4½}-y^4F^0_{4½}$		
6	3901.681	2	II	25622.75	$a^4F_{3½}-p^4D^0_{3½}$		
6	3901.155	6	II	25626.20	$z^6F^0_{1½}-f^6G_{2½}$	(0w_1) 1.10w_2	(0) **1.15***s*
6	3900.168	6	II	25632.69	$z^6F^0_{3½}-f^6G_{4½}$	(0?w_1) 1.00w_2	(0) **1.19***s*
6	a3899.137	4	V E	25639.46	($a^2D_{1½}-v^2F^0_{2½}$)		
6	3898.271	5	II	25645.16			
5	3898.143	[4?]		25646.00	$a^3G_{3½}-x^2G^0_{4½}$		
6	3898.007	6	II	25646.88	$z^6F^0_{2½}-f^6G_{3½}$	(0?w_2) 1.17w_1	(0) 1.16*b*
6	3897.072	6	II	25653.06	$z^6F^0_{1½}-f^6G^0_{2½}$	(0) 1.02	(0) 0.92*b*
4	3896.81	2	III	25654.77	$a^3H_{3½}-w^2H^0_{3½}$		
6	3896.624	2	III	25656.00			
6	a3896.147	6	II	25659.15	$a^4D_{3½}-v^4F^0_{3½}$	(0) 0.27?	(0.53) 1.30*b*
4	3895.71	1		25662.01	$y^6F^0_{3½}-h^6G_{2½}$?		
6	b3894.028	4	II	25673.10	$z^6F^0_{1½}-f^6G_{2½}$	(0) 1.10	(0) 0.51*b*
4	3893.73	1	III	25675.00			
6	3892.864	25*a*	I	25680.77	$a^4F_{3½}-y^4F^0_{2½}$	(?w_3D) 1.59w_2 B	(0) 1.48*b*
6	3892.478	2	II	25683.33			
5	3891.227	2	II A	25691.58	$a^4D_{1½}-v^4F^0_{2½}$		
6	3891.115	4	II	25692.32			
6	3890.188	25*a*	I	25698.44	$a^4F_{3½}-z^2G^0_{3½}$; $z^6F^0_{3½}-f^6G_{3½}$	(0.86w_1 B) 1.04w_3 C	(0.82) 1.06*b*
6	3889.857	0		25700.62	$b^4F_{3½}-t^4F^0_{3½}$		
6	3889.236	1	III	25704.73	$b^4F_{3½}-t^4F^0_{4½}$		
6	b3888.331	3	III	25710.72	$a^2D_{1½}-u^2D^0_{1½}$	(0.33) 1.39w_2	(0.38) 0.78*b*
6	3888.081	2	III	25712.37	$b^4F_{3½}-t^2G^0_{3½}$		
4	3887.56	1		25715.79	$a^3H_{3½}-w^2H^0_{3½}$		
5	3886.687	−1		25721.59	$b^4F_{4½}-t^4F^0_{3½}$		
6	3886.584	6	I	25722.27	$a^3G_{4½}-w^4G^0_{3½}$	(0?w_1) 1.25w_1	(0) 1.25*b*
5	3886.200	[2]		25724.81	$b^4F_{1½}-t^4F^0_{1½}$		
6	3885.770	2	III	25727.66	$a^3G_{4½}-w^2G^0_{4½}$		
4	3885.55	1	IV	25729.10			
4	3885.33	1		25730.55	$b^4F_{4½}-v^2H^0_{4½}$		
6	3884.462	4	II	25736.32	$a^3G_{3½}-w^2G^0_{3½}$		
6	b3883.887	3	II	25740.14	$b^4F_{2½}-t^4F^0_{2½}$	(0) 0.97	(0.35) 0.97*b*
6	3880.265	1		25764.16	$b^4F_{1½}-t^4F^0_{2½}$		
6	3879.667	3?	III?	25768.13	$b^4F_{2½}-t^4F^0_{3½}$	(0) 1.17	(0.21) 1.18*b*
6	3879.225	2?	III?	25771.07	$a^4D_{3½}-y^2D^0_{3½}$		
4	3878.31	1		25777.18	$a^2D_{2½}-u^2D^0_{2½}$; $b^4F_{3½}-v^2H^0_{3½}$		
6	3876.740	1	III	25787.59			
6	3876.084	20	I	25791.95	$a^4F_{4½}-z^2G^0_{3½}$	(0.61) 1.12w_3 C	(0.56) 1.20*b*
6	3875.909	20	I	25793.12	$a^4F_{3½}-y^4F^0_{3½}$	(?) —, —, 1.56	(0) 1.45*b*
6	3875.425	3	I	25796.34	$a^4D_{2½}-v^4F^0_{1½}$		
6	3875.081	35	I	25798.63	$a^4F_{3½}-y^4F^0_{4½}$	(0.26) 1.17w_2 B	(0.15) 1.18*b*
6	3874.350	1	III	25803.49	$b^4F_{2½}-t^4F^0_{2½}$	(0?w_2 D) 1.29w_3 C	(0) 1.28*b*
6	3873.640	4	II	25808.22	$a^2G_{3½}-x^2D^0_{2½}$	(?w_3 D) 0.47w_3 A	(0) 0.57*b*
4	3873.21	1		25811.11	$a^2D_{1½}-u^2D^0_{2½}$		
7	3872.747	4h	II	25814.18	$a^4D_{3½}-v^4F^0_{4½}$; $a^2D_{1½}-x^2P^0_{2½}$		
6	3871.083	8	I	25825.27	$a^2G_{4½}-x^2F^0_{3½}$	(0) 1.17	(0) 1.27*b*
6	3870.581	2	II	25828.62	$b^4F_{4½}-t^4F^0_{4½}$	(0.30) 1.27	(0.30) 1.27*b*
6	3867.610	15	I	25848.47	$a^4F_{3½}-y^4F^0_{2½}$	(0) 1.28	(0) 1.28*b*
4	3867.33	2	II A	25850.35	$a^4D_{2½}-y^2D^0_{1½}$		
6	3864.862	35	I	25866.85	$a^4F_{3½}-y^4F^0_{3½}$	(0) 0.98	(0.07) 1.00*b*
4	3864.55	1	IV	25870.14			
5	3864.300	[3]		25870.60	$a^2G_{3½}-w^4G^0_{3½}$		
6	3864.110	3	I	25871.87			
6	a3863.864	6	II	25873.52	$a^2G_{2½}-x^2F^0_{2½}$	(0) 0.86	(0) 0.87*b*
5	3863.629	1		25875.09	$b^4F_{2½}-t^4F^0_{2½}$		

TABLE 1.—*Arc spectrum of vanadium* (V I)—Continued

(1)	(2)	(3)	(4)	(5)	(6)	(7)	(8)
Ref.	λ_{air} A	Int. arc	Temp. class	ν_{vac} cm^{-1}	Term combinations	Zeeman effect: Observed	Zeeman effect: Computed
4	3863.40	1		25876.64	$a^3H_{4½}-w^3H_{5½}$		
6	3862.218	12	I	25884.55	$a^4F_{3½}-z^4G_{4½}$	(0) 0.82	(0) 0.81*b*
6	3861.593	0*h*	II	25888.73	$\{a^2D_{2½}-z^2P_{1½}$, $b^4F_{4½}-y^2H_{5½}?$		
6	3859.336	6	II	25903.87	$a^4D_{3½}-x^4D_{3½}$	(0) 1.52	(0) 1.53*b*
6	3858.680	5	II A	25908.28	$a^4D_{2½}-y_2D_{3½}$	(0.38) 1.23	(0.37) 1.26*b*
4	3857.87	1*h*		25913.72	$z^6G_{3½}-f^6F_{3½}$		
4	3857.70	1		25914.86	$y^6F_{3½}-h^6G_{3½}$		
6	3855.855	60*ra*	I	25927.26	$a^4F_{4½}-y^4D_{3½}$		
6	3855.370	30*a*	I	25930.52	$\{a^4F_{1½}-y^4F_{1½}$, $a^2G_{3½}-w^4G_{3½}$	(0?w_1) 0.38	(0.03) 0.41*b*
5	3854.860	1*h*		25933.95	$z^6G_{3½}-f^6F_{4½}?$		
4	3854.58	1		25935.83	$a^3G_{3½}-w^3G_{4½}$		
4	3854.08	1	III	25939.19			
6	3852.099	2	II A	25952.55	$a^4D_{1½}-y^3D_{1½}$	(0.65) 0.51, **0.95** 1.40	(0.24, **0.70**) 0.49, **0.96** 1.43
6	3851.173	5	I	25958.78	$a^4D_{2½}-v^4D_{1½}$	(?w_1) 1.67w_1	(0) 1.58*b*
5	3850.158	[3*p*?]		25965.62	$\{b^2G_{3½}-s^2H_{4½}$, $b^4F_{3½}-t^4G_{3½}$		
6	3849.324	6	I	25971.25			
6	[d]3847.331	20	I	25984.69	$a^4F_{2½}-y^4F_{3½}$	(0?w_2) 0.91, 1.48	(**0.08**, 0.22, 0.36) 0.79, 0.93, 1.08, 1.23, 1.37, **1.51**
4	3846.56	1		25989.89	$b^4F_{1½}-t^4G_{1½}$		
4	3845.96	3	II	25993.95			
6	3844.888	4	II	26001.22	$a^4D_{1½}-v^4D_{½}$	(0.58) 0.57, 1.72	(0.60) 0.60, **1.79**
6	3844.442	20	I	26004.23	$a^4F_{1½}-y^4F_{2½}$	(**0.30**, 0.91) 0, 0.66, 1.27, **1.93**	(**0.29**, 0.87) 0.11, 0.69, 1.27, **1.85**
6	3843.502	4	II	26010.59	$a^4D_{1½}-y^3D_{1½}$	(0) 1.15	(0) 1.17*b*
7	3843.001	2	II	26013.98			
4	3842.70	3	II	26016.02	$a^4D_{0½}-y^3D_{1½}$	(0.38) 0.38, 1.11	(0.36) 0.36, **1.09**
6	3841.892	5	I A	26021.50	$a^4F_{3½}-z^3G_{3½}$	(0) 1.03	(0) 1.01*b*
6	3840.757	60*r*	I	26029.19	$a^4F_{2½}-y^4D_{2½}$	(0w_1 D) 1.13w_1 C	(0) 1.02*b*
	[c]3840.443	80*r* Fe	II	26031.57	$a^4D_{3½}-v^4D_{3½}$		
6	3840.136	4	I	26033.38	$a^2G_{3½}-x^2F_{3½}$	(0.49) ?w_2 C	(0.50) 0.96*b*
6	[b]3839.379	8	II	26038.52	$a^2D_{2½}-s^2F_{3½}$	(0) 0.99	(0) 0.81*b*
6	3839.001	10	I	26041.09	$a^4D_{2½}-y^4D_{3½}$	(0) 1.31	(0.15) 1.32*b*
4	3837.75	1*hd*		26049.61	$b^4D_{1½}-t^4P_{1½}$		
5	3837.427	1		26051.76	$a^4F_{4½}-y^4D_{3½}$		
4	3836.48	1	IV	26058.22		(0) 1.28	
6	[b]3836.056	5	I	26061.08	$a^4D_{1½}-v^4D_{1½}$	(0. 44) 1.10)	(0.20) 1.12*b*
6	3835.563	4	II	26064.43	$a^4D_{0½}-v^4D_{½}$	Unaffected	(0) 0
5	3835.180	[3*p*?]		26067.03	$\{a^2F_{2½}-r^4F_{1½}$, $a^2P_{0½}-s^4D_{½}$		
4	3834.80	*tr*	IV	26069.64	$b^4F_{3½}-t^4G_{3½}$	(0) 0.97	(0) **0.98***s*
	[c]3834.227	100*r* Fe	II	26073.49	$a^2P_{0½}-v^2D_{1½}$		
5	3834.147	[4]		26074.05	$a^3G_{4½}-s^3G_{3½}$		
4	3833.80	1		26076.44	$a^2P_{1½}-s^4D_{2½}?$		
6	3833.223	3	III	26080.34	$a^2G_{4½}-y^2H_{5½}$		
6	3832.836	4	III	26082.97	$a^2P_{1½}-s^2D_{1½}$	(0.45) 1.05w_1 C	(0.39) 1.06*b*
4	[b]3831.84	3	II	26089.77	$b^4F_{4½}-t^4G_{4½}$	(0.59) 1.48w_2 diffuse	(0.41) 1.26*b*
4	3830.59	1		26098.28	$b^2G_{4½}-s^2H_{5½}$		
4	3830.29	2	III	26101.00			
6	3828.830	4	II	26110.26	$a^2G_{4½}-y^2H_{5½}$		
6	3828.562	60*r*	II	26112.09	$a^4F_{2½}-y^4D_{1½}$	(0.21) 0.92w_2 C	(**0.09**, 0.25) **0.76**, 0.92 1.09, 1.26
6	3826.770	6	II	26124.31	$a^4D_{0½}-v^4D_{1½}$		
4	3825.32	4	II	26134.23	$b^2H_{4½}-q^4F_{3½}$		
4	3825.03	1	III	26136.20	$b^4F_{3½}-t^4G_{4½}$		
6	3823.977	5	II	26143.40	$a^4D_{1½}-v^4D_{½}$	(0) 1.40	(0) **1.42***s*
4	3823.77	4	II	26144.82	$a^2D_{2½}-w^2P_{1½}$		
4	3823.40	1	III A	26147.35	$b^4F_{4½}-t^4G_{4½}$		
6	3823.212	15	I	26148.63	$\{a^6D_{2½}-z^6D_{1½}$, $(a^2F_{3½}-r^2G_{3½})\}$	(?) 1.43w_2 A	(0) 1.45*b*
6	3822.890	15	I	26150.83	$a^6D_{3½}-z^6D_{3½}$	(0) 1.43	(0) **1.40***s*
4	3822.70	1	III	26152.14			
6	3822.008	30	I	26156.86	$a^4F_{3½}-y^4D_{3½}$	(0.54w_1) 1.25C	(0.56) 1.30*b*

TABLE 1.—*Arc spectrum of vanadium* (V I)—Continued

(1)	(2)	(3)	(4)	(5)	(6)	(7)	(8)
Ref.	λ_{air} A	Int. arc	Temp. class	ν_{vac} cm^{-1}	Term combinations	Zeeman effect	
						Observed	Computed
6	3821.485	15	I	26160.45	$a^6D_{1\frac{1}{2}}-z^6D^0_{1\frac{1}{2}}$	(0.70) 1.13, 2.52	(0.71) **1.11**, 2.53
5	3820.299	4		26168.56	$a^4D_{2\frac{1}{2}}-v^4D^0_{1\frac{1}{2}}$		
6	3819.967	15	I	26170.84	$a^6D_{4\frac{1}{2}}-z^6D^0_{3\frac{1}{2}}$	(0) 1.44	(0) 1.54*b*
4	3818.76	1	III	26179.10	$a^2D_{1\frac{1}{2}}-w^2P^0_{1\frac{1}{2}}$		
6	3818.241	60	II	26182.67	$a^4F_{1\frac{1}{2}}-y^4D^0_{0\frac{1}{2}}$; $(a^4F_{3\frac{1}{2}}-y^6D^0_{3\frac{1}{2}})$	(0.28) 0.22, **0.62**	(0.23) 0.17, **0.63**
6	3817.978	4	II	26184.48	$a^2G_{4\frac{1}{2}}-z^4I^0_{5\frac{1}{2}}$		
6	3817.847	8	I A	26185.38	$a^4F_{4\frac{1}{2}}-y^6D^0_{3\frac{1}{2}}$		
6	3815.514	10	I	26201.39	$a^6D_{0\frac{1}{2}}-z^6D^0_{0\frac{1}{2}}$	(0) 3.27	(0.03) 3.26*b*
6	3813.499	60*a*	II	26215.23	$a^4F_{2\frac{1}{2}}-y^4D^0_{2\frac{1}{2}}$; $(a^6D_{1\frac{1}{2}}-z^6D^0_{1\frac{1}{2}})$	(0.48, **0.90**) 0.42, 0.82, **1.16**, 1.49, 1.85	(0.17, 0.50, **0.83**) 0.51, 0.84, **1.17**, 1.51, 1.84
5	3813.347	1*p*?		26216.27	$b^2H_{3\frac{1}{2}}-r^2G^0_{4\frac{1}{2}}$		
4	3811.32	2	III	26230.20	$z^6D^0_{3\frac{1}{2}}-f^6P^0_{2\frac{1}{2}}$		
6	3809.599	15	I	26242.07	$a^6D_{2\frac{1}{2}}-z^6D^0_{2\frac{1}{2}}$	(0) 1.58	(0.07) 1.60*b*
4	3809.08	1	III	26245.62	$z^6D^0_{2\frac{1}{2}}-f^6P^0_{1\frac{1}{2}}$		
6	3808.521	40	II	26249.49	$a^4F_{1\frac{1}{2}}-y^4D^0_{1\frac{1}{2}}$	(0.38, **1.15**) **0.00**, 0.76, 1.52	(0.38, **1.15**) 0.02, **0.78**, 1.55
4	3808.11	3	III	26252.30	$z^6D^0_{1\frac{1}{2}}-f^6P^0_{2\frac{1}{2}}$		
6	3807.506	20*a*	I	26256.49	$a^6D_{0\frac{1}{2}}-x^6D^0_{1\frac{1}{2}}$	(0.70) 1.08, 2.48	(0.74) **1.08**, 2.56
6	3806.798	8	II	26261.37	$a^2G_{4\frac{1}{2}}-v^2G^0_{4\frac{1}{2}}$	(0.23) 1.04	(0.30) 1.09*b*
4	3806.44	1		26263.81	$b^4F_{1\frac{1}{2}}-r^4D^0_{0\frac{1}{2}}$		
6	3804.917	2	III	26274.35	$a^2H_{3\frac{1}{2}}-t^2G^0_{4\frac{1}{2}}$		
6	3804.599	3	III	26276.55	$b^4P_{2\frac{1}{2}}-v^4P^0_{1\frac{1}{2}}$	(0) 1.49	(0) 1.48*b*
6	3803.901	6	I A	26281.37	$a^4F_{2\frac{1}{2}}-y^6D^0_{2\frac{1}{2}}$		
6	3803.782	6	II	26282.19	$a^2G_{3\frac{1}{2}}-v^2G^0_{3\frac{1}{2}}$	(0.31) 0.93w_1C	(0.32) 0.94*b*
5	3803.487	25	I	26284.23	$a^6D_{2\frac{1}{2}}-z^6D^0_{2\frac{1}{2}}$; $(a^2F_{2\frac{1}{2}}-r^2G^0_{3\frac{1}{2}})$	(0) 1.51	(0.03) 1.52*b*
6	3802.884	2	III	26288.41	$a^2G_{3\frac{1}{2}}-y^2H^0_{4\frac{1}{2}}$	(0) 0.59 diffuse	(0) 0.47*b*
5	3801.158	[4]		26300.33	$a^4F_{2\frac{1}{2}}-y^6D^0_{1\frac{1}{2}}$		
5	3799.922	25	I	26308.89	$a^6D_{1\frac{1}{2}}-z^6D^0_{2\frac{1}{2}}$	(0w_2D) 1.40w_1 A?	(0) 1.40*b*
5	3799.704	[0]		26310.40	$b^4F_{2\frac{1}{2}}-r^4D^0_{1\frac{1}{2}}$		
6	3799.284	1	IV	26313.31	$b^2G_{3\frac{1}{2}}-q^2G^0_{3\frac{1}{2}}$	(0) 0.85	(0.09) 0.88*b*
6	3798.660	2	III A	26317.63	$a^2P_{1\frac{1}{2}}-v^2D^0_{2\frac{1}{2}}$; $z^6D^0_{1\frac{1}{2}}-f^6P^0_{1\frac{1}{2}}$	(0) 1.16	(0) 1.10*b*
6	3798.260	4	I	26320.40			
6	3796.465	3	II	26332.84	$a^2H_{4\frac{1}{2}}-t^2G^0_{3\frac{1}{2}}$	(0) 0.90	(0) 0.90*b*
4	3796.21	1		26334.64	$z^6D^0_{3\frac{1}{2}}-f^6P^0_{2\frac{1}{2}}$; $a^2H_{5\frac{1}{2}}-t^4F^0_{4\frac{1}{2}}$		
6	3794.962	50*a*	II	26343.28	$a^6D_{4\frac{1}{2}}-x^6D^0_{4\frac{1}{2}}$; $a^4F_{2\frac{1}{2}}-y^4D^0_{2\frac{1}{2}}$	(0w_1?) 1.48w_1?	(0.20) 1.50*b*; (0) 1.86*b*
6	3793.614	8	I A	26352.63	$a^4F_{1\frac{1}{2}}-y^4D^0_{0\frac{1}{2}}$	(0.47, 1.41) 0.96, 1.81, **2.76**	(**0.47**, 1.41) −0.07, 0.87, 1.81, **2.75**
5	3792.853	1hp?		26357.92	$z^6D^0_{3\frac{1}{2}}-f^6P^0_{1\frac{1}{2}}$		
6	3791.331	2	I A	26368.51	$a^4F_{2\frac{1}{2}}-y^6D^0_{3\frac{1}{2}}$	(**0.85**, 1.51) 0?, 0.70, 1.30, 1.91	(0.30, 0.88, **1.46**) 0.13, 0.71, **1.30**, 1.89, 2.47
6	3790.467	8	II	26374.52	$a^2G_{4\frac{1}{2}}-w^2F^0_{3\frac{1}{2}}$	(0) 1.14	(0) 1.22*b*
6	3790.331	20	I	26375.46	$a^6D_{3\frac{1}{2}}-z^6D^0_{3\frac{1}{2}}$	(0) 1.41	(0) 1.41*b*
4	3788.78	1	III	27386.25			
5	3788.496	1p?		26388.23	$z^6D^0_{2\frac{1}{2}}-f^6P^0_{2\frac{1}{2}}$		
6	3787.545	3	II	26394.85	$a^2H_{5\frac{1}{2}}-p^2H^0_{5\frac{1}{2}}$	(0) 1.06	(0.09) 1.06*b*
6	3787.148	5	II	26397.62	$a^2H_{4\frac{1}{2}}-p^2H^0_{4\frac{1}{2}}$		
5	3784.822	1	III	26413.85	$b^4F_{2\frac{1}{2}}-r^4D^0_{2\frac{1}{2}}$		
6	3784.676	2	I A	26414.87	$a^4F_{2\frac{1}{2}}-y^6D^0_{2\frac{1}{2}}$		
4	3782.93	1	III	26427.06	$b^4P_{2\frac{1}{2}}-r^4D^0_{1\frac{1}{2}}$		
6	3782.555	3	II	26429.68	$a^2G_{4\frac{1}{2}}-z^2I^0_{5\frac{1}{2}}$		
4	3781.74	1	III	26435.37	$a^2H_{4\frac{1}{2}}-t^2G^0_{3\frac{1}{2}}$		
6	3781.398	3	II	26437.76	$b^4P_{2\frac{1}{2}}-p^4P^0_{2\frac{1}{2}}$; $a^4F_{1\frac{1}{2}}-y^6D^0_{1\frac{1}{2}}$	(0) 1.45	(0.13) 1.51*b*; (2.05) 1.13*b*
5	3779.764	2p?		26449.19	$b^4F_{2\frac{1}{2}}-r^4D^0_{3\frac{1}{2}}$		
6	3779.646	4	II	26450.02	$a^2G_{3\frac{1}{2}}-w^2F^0_{3\frac{1}{2}}$	(0) 0.91	(0) 0.93*b*
6	3778.683	25	I	16456.76	$a^6D_{2\frac{1}{2}}-z^6D^0_{1\frac{1}{2}}$	(0) 1.43	(0) 1.36*b*
6	3777.492	1	III	26465.10	$b^2P_{1\frac{1}{2}}-t^2P^0_{1\frac{1}{2}}$; $a^2G_{4\frac{1}{2}}-y^4H^0_{3\frac{1}{2}}$	(0) 0.85	(0.18) 1.30*b*; (0) **0.91***a*
6	3777.168	2	I A	26467.37	$a^4F_{2\frac{1}{2}}-y^6D^0_{3\frac{1}{2}}$		
6	3776.881	2	III	26469.38	$a^2G_{3\frac{1}{2}}-z^2G^0_{4\frac{1}{2}}$		
6	3776.171	4	II	26474.36	$b^4F_{4\frac{1}{2}}-r^4D^0_{3\frac{1}{2}}$	(0) 1.11	(0) **1.14***a*

TABLE 1.—*Arc spectrum of vanadium* (V I)—Continued

(1)	(2)	(3)	(4)	(5)	(6)	(7)	(8)
Ref.	λ_{air} A	Int. arc	Temp. class	ν_{vac} cm^{-1}	Term combinations	Zeeman effect: Observed	Zeeman effect: Computed
6	3775.711	4	III	26477.58	$z^6F^0_{3/2}-g^6D_{1/2}$	(0) 1.22	(0) 1.46*b*
6	3775.193	3	II	26481.22	$b^4P_{1/2}-z^4P^0_{3/2}$	(0.43) 1.27w_1 C?	(0.44) **1.24**, 2.12
6	3774.116	3	III	26488.77	$a^2P_{3/2}-x^2S^0_{1/2}$		
6	3772.755	2	III	26498.33	$a^3F_{1/2}-x^2S^0_{1/2}$		
5	3772.472	0*h*		26500.32	$a^4H_{3/2}-v^2H^0_{1/2}$		
6	3772.157	2	III	26502.52			
4	3771.66	1	I A	26506.01	$a^4F_{1/2}-y^6D^0_{3/2}$		
4	3771.17	1	II A	26509.45	$a^4D_{3/2}-u^4D^0_{3/2}$		
6	3770.529]	3	II A	26513.99	$a^4D_{3/2}-u^4D^0_{1/2}$	(0) 1.52	(0) 1.52*b*
6	3769.996	2	III	26517.72	$a^3P_{0/2}-x^2P^0_{1/2}$		
4	3769.83	1	III	26518.87	$a^4H_{3/2}-t^4F^0_{3/2}$		
6	3769.072	4	II	26524.23	$a^3P_{1/2}-w^2D^0_{3/2}$	(0) 1.03	(0) 1.06*b*
5	3767.250	[8W]		26537.05	$a^4D_{1/2}-u^4D^0_{3/2}$?		
6	3766.405	2	II	26543.00	$a^4H_{9/2}-t^4F^0_{3/2}$ $z^6F^0_{3/2}-g^6D_{3/2}$	(?w_2 D) 0.48w_2 A? diffuse	(0) 0.57*b*
5	3765.632	1	III	26548.45	$z^6F^0_{3/2}-g^6D_{2/2}$	(0) 1.00	(0) 0.94*b*
4	3764.80	2	III	26554.29	$b^2G_{4/2}-g^2G^0_{1/2}$	(0) 1.05	(0.11) 1.10*b*
6	3763.142	6	II	26566.01	$b^4P_{2/2}-r^4D^0_{3/2}$	(0.40) 1.41	(0.46) 1.43*b*
6	3761.445	3	II	26578.00	$b^4P_{1/2}-v^4P^0_{1/2}$		
6	3760.800	3	II	26582.56	$a^2G_{3/2}-w^2F^0_{3/2}$	(0.55) ?w_2	(0.59) 0.98*b*
5	3760.643	[−1]		26583.67	$a^4P_{3/2}-y^4S^0_{1/2}$		
7	3759.319	4	II	26593.03	$b^4D_{3/2}-3^0_{1/2}$	(0) 0.63, **1.41**	
6	3758.784	1	III	26596.81	$a^4H_{3/2}-v^2H^0_{1/2}$		
6	3758.548	2	II	26598.48	$a^4H_{3/2}-t^4F^0_{1/2}$		
5	3758.293	[5*h*]		26600.29	$a^4D_{0/2}-u^4D^0_{1/2}$?		
4	3756.89	tr	IV	26610.26	$b^4D_{1/2}-3^0_{1/2}$	(0) 1.08	
6	3756.036	3	II	26616.27	$a^4D_{1/2}-u^4D^0_{1/2}$	(0) 1.12	(0.10) 1.16*b*
6	3755.699	4	II	26618.66	$z^6D^0_{1/2}-g^6D_{3/2}$ $z^6D^0_{3/2}-g^6D_{3/2}$	(0?w_2 D) 1.36w_1 A	(0) 1.58*b*
6	3753.273	4	II	26635.87	$a^2P_{1/2}-x^2P^0_{1/2}$	(0?w_2 D?) 1.36w_1 A?	(0.45) 1.36*b*
4	3752.11	1		26644.14	$z^6F^0_{1/2}-g^6D_{1/2}$		
6	3751.780	5	II A	26646.48	$a^4D_{2/2}-u^4D^0_{3/2}$	(0) 1.34	(0.07) 1.34*b*
4	3750.12	1	III	26658.28	$b^4P_{1/2}-r^4D^0_{1/2}$		
5	3750.062	1*h*		26658.68	$a^4H_{3/2}-v^2H^0_{1/2}$		
5	3749.374	[7]		26663.57	$a^4D_{3/2}-u^4D^0_{3/2}$		
6	3747.980	8*h*	II	26673.49	$b^4P_{3/2}-r^4D^0_{3/2}$ $b^4P_{0/2}-z^4P^0_{1/2}$	(0w_1) 1.08w_1	(0) 1.13*b* (0.02) 2.58*b*
6	3747.131	3	II	26679.53	$a^4D_{0/2}-u^4D^0_{1/2}$	(.58) 0.59, **1.75**	(0.56) 0.56, **1.68**
4	3743.89	1	III	26702.62			
6	3741.499	6	II	26719.68	$z^6D^0_{1/2}-g^6D_{3/2}$	(0) 1.45	(0.56) 1.48*b*
6	3740.236	6	II	26728.71	$b^4P_{1/2}-r^4D^0_{1/2}$		
6	3738.760	8	II	26739.27	$b^4P_{1/2}-v^4P^0_{1/2}$	(0w_1) 1.31w_1	(0) 1.33*b*
6	3737.992	5	II	26744.75	$a^4H_{3/2}-t^4G^0_{1/2}$	(0) 0.67	(0) 0.74
5	3737.426	1	II A	26748.80	$a^4D_{1/2}-u^4D^0_{1/2}$	(0) 1.50	(0) **1.52***a*
4	3736.00	1		26759.01	$z^6D^0_{3/2}-g^6D_{1/2}$		
6	3734.428	5	II	26770.28	$b^4P_{0/2}-v^4P^0_{1/2}$		
5	3734.286	2		26771.30	$a^4P_{1/2}-y^4S^0_{1/2}$		
6	3732.067	1	II A	26787.21	$a^4P_{2/2}-z^4P^0_{3/2}$	(0) 1.46	(0.02) 1.54*b*
4	3731.02	2	III	26794.71	$z^6D^0_{1/2}-g^6D_{3/2}$	(0w_1 D) 1.49w_1 C	(0) 1.39*b*
4	3730.18	3	II A	26800.74	$a^4D_{3/2}-u^4D^0_{3/2}$		
6	3729.034	4	II	26809.00	$a^4H_{9/2}-t^4G^0_{3/2}$	(0) 0.82	(0) 0.78*b*
4	3724.17	1		26843.98	$b^2P_{3/2}-p^4F^0_{3/2}$		
4	3723.56	1	III	26848.38	$a^4H_{3/2}-t^4G^0_{1/2}$		
6	3723.332	3	III	26850.05	$b^4P_{0/2}-r^4D^0_{1/2}$	(1.24) 1.28	(1.28) 1.32*b*
6	3722.606	3		26855.29	$a^4H_{9/2}-t^4G^0_{3/2}$ $z^6D^0_{3/2}-g^6D_{3/2}$	(0) 1.12	
7	3722.201	3	III	26858.21	$z^6D^0_{3/2}-g^6D_{3/2}$?		
6	3721.996	4	II	26859.70	$a^4H_{3/2}-t^4G^0_{1/2}$	(0) 0.93	(0) 0.87*b*
5	3721.440	1		26863.71	$a^4P_{0/2}-y^4S^0_{1/2}$		
6	3721.353	3	I A	26864.34	$a^4F_{3/2}-z^2F^0_{3/2}$	(0.38) 1.41, —	(**0.06**, 0.19, 0.32) 0.88 1.01, 1.14, 1.26, 1.39 **1.52**
4	3720.92	1	III	26867.50	$b^4P_{1/2}-r^4D^0_{3/2}$		
6	3718.913	4	III	26881.96		(0) 1.10	
4	3717.54	1	III	26891.91	$z^6G^0_{3/2}-e^6H_{3/2}$		
4	3714.85	1	III	26911.38	$a^4H_{3/2}-t^4G^0_{1/2}$		

TABLE 1.—*Arc spectrum of vanadium* (V I)—Continued

(1)	(2)	(3)	(4)	(5)	(6)	(7)	(8)
Ref.	λ_{air} A	Int. arc	Temp. class	ν_{vac} cm^{-1}	Term combinations	Zeeman effect: Observed	Zeeman effect: Computed
6	3713.955	5	I A	26917.84	$a^4F_{4½}-z^3F^0_{3½}$	(0?w_1 D) 1.73w_1 B	(0) 1.75*b*
4	3713.55	1	III	26920.80	$b^4P_{2½}-r^4D^0_{1½}$		
4	3713.31	1	III	26922.54	$a^4G_{4½}-z^4G^0_{3½}$		
4	3711.41	1	III	26936.32	$a^4G_{3½}-z^4G^0_{2½}$	(0) 1.34	(0.31) 1.30*b*
6	3708.718	6	II	26955.85	$a^3H_{5½}-u^3H^0_{5½}$	(0) 1.02	(0.04) 1.06*b*
6	3706.031	4	II	26975.39	$a^3H_{4½}-u^3H^0_{4½}$	(0) 0.85	(0.19) 0.88*b*
4	3705.82	1	III	26976.94	$z^6G^0_{3½}-e^6H_{3½}$		
6	3705.037	30	I	26982.62	$a^6D_{3½}-y^6P^0_{2½}$	(0.34, **1.05**) 0.48, **1.16**, **1.90**, 2.64	(**0.36**, 1.07) **0.54**, 1.25, 1.96, 2.68
6	3704.705	60	II	26985.06	$a^6D_{2½}-y^6P^0_{1½}$	(0?w_2 D?) 1.33w_2 A?	(0) 1.24*b*
6	3703.993	2	II	26990.24	$a^4P_{2½}-z^4P^0_{1½}$		
6	3703.566	100*a*	II	26993.36	$a^6D_{4½}-y^6P^0_{3½}$	(0?w_2 D?) 1.40w_2 A?	(0) 1.36*b*
5	3702.231	1*h*		27003.08	$z^6G^0_{3½}-f^6G_{3½}$		
4	3700.63	*tr*	III A	27014.76	$a^3G_{4½}-t^4D^0_{3½}$		
6	3699.474	3	II	27023.21	$a^2G_{4½}-z^3H^0_{4½}$	(0.77) 0.99w_2	(0.93) 1.00*b*
6	3695.867	40	II	27049.56	$a^6D_{1½}-y^6P^0_{1½}$; $(a^4F_{3½}-z^3F^0_{3½})$	(0.24, 0.80) **1.45**, 2.01, 2.55	(0.25, **0.75**) 1.57, **2.07**, 2.57
6	3695.331	30	II	27053.51	$z^6G^0_{4½}-e^6H_{3½}$	(0) 1.19 diffuse	(0) 1.22
6	3694.617	3	II	27058.73	$z^6G^0_{3½}-e^6H_{4½}$; $a^4P_{1½}-z^4P^0_{1½}$		
6	3692.224	50	II	27076.28	$a^6D_{2½}-y^6P^0_{2½}$	(0.48) 1.67w_2 C	(0.33) 1.68*b*
7	3690.277	40	II	27090.56	$a^6D_{½}-y^6P^0_{1½}$	(0.45 **1.82**, 2.71	(0.49) **1.83**, 2.81
6	3688.070	50	II	27106.77	$a^6D_{3½}-y^6P^0_{2½}$	(0.38) 1.57	(0.27) 1.58*b*
6	3687.473	12?	II?	27111.16	$z^6G^0_{1½}-e^6H_{2½}$	(0) 1.20	(0) 1.41*b*
4	3686.74	1	III	27116.51			
6	3686.259	8	I	27120.08	$a^2G_{4½}-z^3H^0_{3½}$	(0) 0.98	(0) **0.96***s*
4	3684.35	3	II	27134.17	$z^6G^0_{2½}-e^6H_{3½}$	(0.87)?w_2 C	
6	3683.114	30	I	27143.24	$a^6D_{1½}-y^6P^0_{1½}$	(0) 1.77	(0) 1.72*b*
5	3682.581	0		27147.17	$a^4F_{2½}-z^3F^0_{1½}$?		
5	3682.064	[0]		27150.98	$a^4P_{2½}-x^4P^0_{2½}$		
6	3680.103	15	II	27165.45	$z^6G^0_{1½}-e^6H_{2½}$	(0) 1.02	(0) **1.06***s*
4	3677.08	2	I A	27187.80	$a^4F_{1½}-z^3F^0_{2½}$	(**0.22**, 0.67)?	(**0.34**, 1.01) 0.06, 0.74 1.41, **2.08***
7	3676.693	10	II	27190.65	$z^6G^0_{4½}-f^6G_{3½}$	(0.43)?	(0.42) 1.39*b*
6	3675.698	20	II	27198.00	$a^6D_{3½}-y^6P^0_{3½}$	(0) 1.67	(0) **1.85***s*
4	3675.49	3	III	27199.56	$z^6G^0_{5½}-e^6H_{5½}$		
6	3673.392	12	III	27215.06	$z^6G^0_{3½}-e^6H_{4½}$	(0) 0.93	(0) 1.13*b*
6	3672.394	8	II	27222.48	$z^6G^0_{4½}-f^6G_{3½}$	(0) 1.26	(0.36) 1.30*b*
6	3671.207	10	I	27231.27	$a^3G_{3½}-z^3H^0_{4½}$	(0) 0.89	(0) 0.88*b*
6	3667.731	15	II	27257.08	$z^6G^0_{2½}-e^6H_{3½}$	(0) 0.79	(0) 1.00*b*
6	3665.137	8	II	27276.38	$z^6G^0_{3½}-f^6G_{4½}$	(0) 1.19	(0.15) 1.24*b*
6	3663.582	15	II	27287.95	$z^6G^0_{2½}-e^6H_{3½}$	(0) 0.67 diffuse	(0) 0.67*b*
4	3662.01	1	III	27299.66	$z^6F^0_{4½}-g^6F_{4½}$		
4	3661.37	2	III	27304.42	$a^3G_{4½}-x^4H^0_{4½}$	(0) 0.96 diffuse	(0) **1.02***s*
4	3659.45	2	III	27318.74			
5	3658.274	−1?		27327.54	$z^6F^0_{5½}-g^6F_{5½}$		
4	3657.47	2	I A	27333.54	$a^4F_{3½}-z^3F^0_{3½}$	(0) 1.25	(0) 1.01*b*
6	3656.689	6	II	27339.38	$z^6G^0_{4½}-f^6G_{5½}$	(0.25) 1.11	(0.06) 1.11*b*
4	3654.67	2	III	27354.46	$z^6F^0_{3½}-g^6F_{3½}$	(?) 0.48w_2 diffuse	
7	3652.453	2	III	27371.08	$z^6F^0_{2½}-g^6F_{2½}$	(0?w_2 D) 0.80 w_2 A	
6	3648.962	5	II	27397.28	$z^6G^0_{3½}-f^6G_{3½}$; $b^4P_{2½}-w^4S^0_{1½}$	(?)w_2 D) (1.17 w_2 C	(0) 0.78*b*; (0) 1.24*b*
5	3648.382	tr	IV	27401.63	$a^2D_{2½}-u^1F^0_{2½}$		
7	3647.359	3	II	27409.32	$b^4P_{2½}-z^4F^0_{1½}$	(0.63)?	
5	3647.157	Oh		27410.83	$z^6G^0_{4½}-f^6G_{5½}$		
7	3645.626	3	II	27422.34			
6	3644.709	8	II	27429.25	$a^3G_{4½}-u^3G^0_{4½}$	(0) 1.04	(0.52) 1.06*b*
4	3644.34	1	III A	27432.02			
5	3644.264	−1		27432.59	$z^6G^0_{5½}-f^6G_{4½}$		
6	3643.859	5	II	27435.64	$a^3D_{3½}-u^3F^0_{3½}$	(0) 0.73	(0) 0.74*b*
4	3643.10	1	III	27441.39	$z^6F^0_{3½}-g^6F_{2½}$; $z^6D^0_{3½}-g^6F_{3½}$		
6	3641.082	4	II	27456.57	$z^6G^0_{4½}-f^6G_{3½}$	(0.54)? w_2	(0.53) 0.19*b*
4	3640.392	15Fe	IV	27461.75	$z^6G^0_{5½}-f^6G_{5½}$		
4	3640.05	2	III	27464.38	$z^6F^0_{5½}-g^6F_{5½}$		
6	3639.023	6	II	27472.10	$a^3D_{3½}-u^3F^0_{3½}$	(0) 1.00	(0) 1.04*b*

TABLE 1.—*Arc spectrum of vanadium* (V I)—Continued

(1)	(2)	(3)	(4)	(5)	(6)	(7)	(8)
Ref.	λ_{air} A	Int. arc	Temp. class	ν_{vac}cm^{-1}	Term combinations	Zeeman effect: Observed	Zeeman effect: Computed
4	3638.35	2	III	27477.21			
6	3637.762	3	IV	27481.63		(0) 0.88	
5	3637.240	−1		27485.57	$z^6G_{13/2}-f^6G_{13/2}$		
4	3636.95	1	III	27487.78			
5	3635.873	3	III	27495.90		(0) 1.07	
4	3635.41	2		27499.43	$a^4G_{3/2}-p^4D^0_{1/2}$		
4	3633.91	3	III	27510.77	$z^6D^0_{3/2}-g^6F_{3/2}$		
5	3632.871	1		27518.62	$z^6F^0_{5/2}-g^6F_{1/2}$; $a^4G_{3/2}-p^4D^0_{3/2}$?		
4	3632.52	1		27521.29	$z^6F^0_{1/2}-g^6F_{3/2}$		
4	*3629.31	2	III	27545.63	$z^6D^0_{3/2}-g^6F_{3/2}$	(0.56) 0.85	(**0.16**, 0.48, 0.80) **0.46**, 0.78, 1.10, 1.42, 1.74, 2.06
4	3628.38	1	III	27552.68	$z^6D^0_{5/2}-g^6F_{1/2}$		
4	3625.58	1		27573.96	$z^6D^0_{1/2}-g^6F_{3/2}$		
5	3624.149	−1		27584.85	$b^4F_{1/2}-q^4D^0_{3/2}$		
4	3622.64	2	III	27596.33	$z^6D^0_{3/2}-g^6F_{3/2}$		
5	3619.529	0		27620.06	$b^4F_{3/2}-q^4D^0_{3/2}$		
4	3617.29	1	III	27637.14	$a^2G_{3/2}-u^2G^0_{3/2}$		
6	3616.727	3	III	27641.46		(0) 1.01	
5	3610.810	0		27686.75	$b^4F_{3/2}-q^4D^0_{3/2}$		
6	3609.296	3	III	27698.36	$b^4P_{1/2}-w^4S^0_{1/2}$?	(0.37) 1.72	(0.36) 1.81*b*
5	3606.694	8	II?	27718.34	$a^2G_{3/2}-u^2G^0_{3/2}$	(0) 0.86	(0) 0.88
6	d3605.578	3	III	27726.93		(0) 0.87	
4	3604.09	1	IV	27738.40			
6	3600.024	5	II	27769.69	$a^2D_{3/2}-v^2P^0_{1/2}$	(0) 0.99	(0) 1.04*b*
4	3598.11	1	III	27784.49	$b^4F_{4/2}-q^4D^0_{3/2}$		
5	3595.613	1	III	27803.77	$a_2D_{1/2}-v^2P^0_{1/2}$	(0?w_1) 1.15w_1	(0.52) 1.15*b*
6	3592.527	3	III	27827.65		(0) 0.96	
4	3592.17	1	11A	27830.43			
4	3591.08	1	III	27838.87	$b^4P_{3/2}-q^4D^0_{3/2}$		
5	3586.222	−1		27876.57	$a^4G_{3/2}-r^4F^0_{1/2}$		
5	3586.111	2	V	27877.43			
5	3584.333	[0h]		27891.26	$b^4P^0_{3/2}-w^4S^0_{3/2}$		
6	3583.706	8	II	27896.14	$a^4D_{3/2}-x^4P^0_{3/2}$	(0) 1.20	(0) 1.20*b*
6	3582.814	3	III	27903.09	$a^4G_{3/2}-r^4F^0_{3/2}$	(0) 1.18	(0) 1.29*b*
6	*3580.823	3	III	27918.60	$a^4G_{3/2}-r^4F^0_{3/2}$	(0) 0.60w_1 A	(0) 0.60*b*
4	3579.31	1	IV	27930.39			
4	3579.09	2	III	27932.10	$a^4G_{3/2}-r^4F^0_{3/2}$		
6	3577.868	4	II	27941.67	$a^4G_{3/2}-r^4F^0_{3/2}$		
6	b3575.124	3	III	27963.11	$a^4G_{3/2}-r^4F^0_{1/2}$	(0.35) 1.05	(0.44) 1.20*b*
6	3574.768	3	II	27965.90	$a^2D_{1/2}-v^2P^0_{3/2}$	(0)0.86	(0) **0.80***a*
5	3574.173	1		27970.54	$a^2F_{3/2}-s^2F^0_{3/2}$		
6	3573.506	5	II	27975.76	$a^4G_{3/2}-q^4F^0_{3/2}$	(0) 1.34	(0) 1.29*b*
6	3572.623	2	III	27982.69	$b^4P_{3/2}-q^4D^0_{3/2}$?	(0) 1.34 diffuse	(0) 1.36*b*
4	3572.30	1	III A	27985.18	$a^4D_{3/2}-z^2D^0_{3/2}$		
6	b3571.649	5	II	27990.32	$a^4G_{3/2}-q^4E^0_{3/2}$	(0) 0.87	(0) 1.00*b*
6	3571.210	2	III	27993.75			
6	3571.027	4	II	27995.19	$a^4G_{3/2}-q^4F^0_{3/2}$	(0) 1.29	(0) 1.38*b*
6	3569.081	1	II A	28010.45	$a^4P_{3/2}-t^4D^0_{3/2}$		
6	3568.929	3	III	28011.65	$a^4G_{3/2}-q^4F^0_{3/2}$	(0) 0.59	(0) 0.59*b*
4	3566.81	1		28028.32	$a^4G_{3/2}-r^4F^0_{3/2}$		
6	d3566.176	4	III	28033.29	$a^4D_{3/2}-z^4P^0_{3/2}$	(0.38, 0.87) 0.26, 0.61, 1.04, 1.49	(0.09, 0.28, **0.47**), 1.07, 1.26, **1.45**, 1.63, 1.82
5	3565.480	[−1]		28038.74	$b^4P_{1/2}-q^4D^0_{1/2}$?		
5	3564.984	1	III A	28042.64	$a^4F_{4/2}-z^4D^0_{3/2}$		
4	3563.52	1	IV	28054.19			
6	3563.394	2	III	28055.15	$a^4G_{3/2}-q^4F^0_{3/2}$	(0.21) 1.13	(0.30) 1.18*b*
6	b3562.133	2	III	28065.08	$a^2F_{3/2}-s^2F^0_{3/2}$	(0) 1.08	(0.35) 1.08*b*
4	3561.40	1	III	28070.88		(0.71) ?w_2 B	
6	3557.164	2	III	28104.29	$a^4D_{1/2}-y^4P^0_{1/2}$		
7	3556.241	4	II	28111.58		(0) 1.27	
6	3555.735	2	II	28115.57	$a^4P_{1/2}-w^4D^0_{3/2}$	(**0.17**, 0.79) **0.33**, —	(**0.26**, 0.78) **0.40**, 0.92, 1.44, 1.96
6	3555.140	3	III	28120.30	$a^4P_{1/2}-t^4D^0_{3/2}$	(0.84) 0.82, [2.49	(0.85) 0.85, **2.55**

TABLE 1.—*Arc spectrum of vanadium* (V I)—Continued

(1)	(2)	(3)	(4)	(5)	(6)	(7)	(8)
	λ_{air} A	Int. arc	Temp. class	ν_{vac} cm^{-1}	Term combinations	Zeeman effect: Observed	Zeeman effect: Computed
6	3553.274	6	II	28135.06	$a^4P_{2½}-t^4D^0_{1½}$	(0.50) 1.41w_2 C	(0.48) 1.44*b*
5	3552.814	[2]		28138.69	$a^4F_{3½}-z^6D^0_{3½}$		
5	3552.598	1	III	28140.40	$b^4P_{1½}-q^4D^0_{½}$		
6	3551.534	3	III	28148.84	$a^2P_{1½}-w^2F^0_{1½}$	(?) 0.35w_2 A	(0) **0.30***s*
5	3548.696?	0h		28171.35	$b^4P_{0½}-q^4D^0_{½}$		
4	3546.78	1		28186.56	$b^4F_{3½}-t^2F^0_{1½}$		
6	3545.339	8	II	28198.02	$a^4P_{1½}-t^4D^0_{½}$		
6	3543.498	8	II	28212.66	$a^4P_{0½}-t^4D^0_{½}$	(1.28)1.25	(1.29) 1.30*b*
5	3543.171	[1]		28215.27	$a^4F_{4½}-z^6D^0_{4½}$		
6	h3542.656	1	II A	28219.38	$a^4D_{1½}-z^4P^0_{½}$		
5	3541.239?	[−1]		28230.67	$b^4P_{0½}-q^4D^0_{1½}$		
5	3541.158	[0]		28231.37	$a^4F_{3½}-z^6D^0_{1½}$		
6	3540.534	1	II A	28236.28	$a^4D_{2½}-z^4P^0_{1½}$	(0) 0.68	(0) **0.72***s*
5	3536.096	[3]		28272.20	$a^4F_{3½}-z^6D^0_{2½}$		
7	3534.739	1	II A	28282.56	$a^4D_{0½}-z^4P^0_{½}$	(1.25) 1.24	(1.26) 1.26*b*
6	h3533.759	6	II	28290.42	$a^4P_{0½}-t^4D^0_{½}$	(0) 1.14	(0) 0.83*b*
7	3533.666	10	I	28291.16	$a^4P_{2½}-t^4D^0_{2½}$	(0) 1.14	(0) 1.10*b*
5	3530.869	−1?		28313.58	$a^4F_{4½}-z^6D^0_{3½}$		
6	3529.743	10	II	28322.62	$a^4P_{1½}-t^4D^0_{2½}$	(0.19, 0.56) **0.71**, 1.12, **1.49**	(**0.19**, 0.56) **0.77**, 1.14, 1.51, 1.89
5	3529.474	[2]		28324.77	$a^4F_{3½}-z^6D^0_{2½}$		
5	3528.198	1	III	28335.01	$b^4F_{1½}-s^4G^0_{½}$		
4	3527.74	1		28338.73	$a^4D_{1½}-z^4P^0_{½}$		
6	3525.767	1	III	28354.55	$b^4F_{2½}-s^4G^0_{½}$	(0) 0.93	(0) 0.89*b*
5	3524.009	[0]		28368.69	$a^4F_{4½}-z^6D^0_{4½}$		
6	h3522.568	3	III	28380.30	$b^4F_{3½}-s^4G^0_{½}$	(0) 1.18	(0) 1.33*b*
7	h3519.165	3	III	28407.74	$b^4F_{4½}-s^4G^0_{½}$	(0) 1.23	(0) 1.41*b*
4	3518.12	*tr*	IV	28416.20	$b^4P_{2½}-z^6P^0_{3½}$?		
4	3516.20	1	IV	28431.71	$b^4F_{4½}-z^6F^0_{4½}$		
5	3514.629	−1		28444.40	$a^4F_{3½}-z^6D^0_{4½}$		
4	3511.87	1		28466.75	$b^2H_{5½}-s^2H^0_{4½}$		
6	3506.845	3	III	28507.55	$a^2P_{0½}-v^2P^0_{½}$	(0.35) 0.99, 1.65	(0.35) 0.99, **1.69**
6	3505.694	6	III	28516.90	$a^2P_{1½}-v^2P^0_{½}$	(0.30) 1.20	(0.20) 1.27*b*
4	3505.24	1	IV	28520.59		(0?w_1D) 0.80w_1 B	
6	3503.181	1	III	28537.35		(0.39) 1.02	(0.43) 1.07*b*
6	3501.489	4	III	28551.21	$a^2P_{0½}-w^2S^0_{½}$		
6	h3500.818	3	III	28556.61	$b^2H_{5½}-s^2H^0_{5½}$	(0) 1.01	(0.63) 1.01*b*
4	h3500.32	1	IV	28560.66	$a^2P_{1½}-w^2S^0_{½}$	(0) 0.95	(0) 1.12*b*
4	3499.00	1		28571.43	$a^4G_{2½}-p^4F^0_{1½}$	(0) 0.65	
6	h3498.198	3	III	28578.00	$a^4G_{4½}-p^4F^0_{3½}$	(0w_1 D) 0.94w_1 A	(0) 1.35*b*
6	h3496.939	3	III	28588.28	$b^2H_{4½}-s^2H^0_{4½}$	(0) 0.96	(0.37) 0.96*b*
4	3496.25	1	IV	28593.90	$a^4G_{3½}-p^4F^0_{1½}$	(0) 0.56	(0) 0.58*b*
4	3491.39	*tr*	IV	28633.68	$a^4G_{3½}-p^4F^0_{2½}$		
4	3490.25	1	IV	28643.04	$a^4G_{3½}-p^4F^0_{3½}$		
6	3489.466	4	III	28649.51	$a^4G_{5½}-p^4F^0_{4½}$	(0) 1.07	(0) **1.04***s*
6	3487.008	2	III	28669.70	$a^2P_{0½}-v^2P^0_{½}$	(0.23) 0.88	(0.25) 0.89*b*
5	3485.867	6	III	28679.09	$a^2P_{1½}-v^2P^0_{½}$		
7	3482.188	1	IV	28709.40	$a^4G_{4½}-p^4F^0_{4½}$	(0.59) 1.16w_2	(0.67) 1.23*b*
4	3480.78	1		28721.03	$a^4G_{3½}-o^4D^0_{2½}$		
5	3465.243	*tr*	IV	28849.77	$b^4F_{3½}-p^4D^0_{3½}$		
6	3463.393	2	II A	28865.19	$a^4F_{4½}-y^6P^0_{3½}$ $b^4F_{2½}-p^4D^0_{1½}$		
	f3461.66	125*R* Ni	II	28879.63	$(a^4D_{2½}-w^2D^0_{1½})$		
5	3460.099	1	III A	28892.66	$b^4F_{3½}-p^4D^0_{2½}$ $a^6D_{4½}-z^4F^0_{4½}$		
6	3456.917	4	III	28919.26	$a^2H_{5½}-t^2H^0_{4½}$		
4	3455.80	*tr*	IV	28928.57	$a^2D_{1½}-u^4P^0_{½}$ $a^4D_{2½}-p^4G^0_{2½}$		
5	3455.585	1	IV	28930.40	$b^4F_{4½}-p^4D^0_{3½}$?		
6	3455.211	1	IV	28933.54	$a^2F_{2½}-q^2G^0_{3½}$	(0) 1.05	(0) **0.97***s*
6	3454.881	3	IV	28936.30	$b^2H_{4½}-q^2G^0_{4½}$	(0) 0.88	(0) 0.95*b*
4	3453.51	1	IV	28947.75			
4	3452.98	*tr*	IV	28952.23			
5	3450.504	1		28973.00	$a^4F_{3½}-y^6P^0_{2½}$		

TABLE 1.—*Arc spectrum of vanadium* (V I)—Continued

(1)	(2)	(3)	(4)	(5)	(6)	(7)	(8)
Ref.	λ_{air} A	Int. arc	Temp. class	ν_{vac}cm^{-1}	Term combinations	Zeeman effect	
						Observed	Computed
5	3449.511	0h		28981.34	$a^4D_{1½}-w^2D^0_{1½}$		
4	3447.09	*tr*	IV	29001.73	$a^4G_{3½}-r^4G^0_{3½}$		
6	3445.812	2	IV	29012.46	$b^3H_{3½}-q^2G^0_{4½}$	(0) 0.99	(0) 1.08*b*
4	3444.86	1	IV	29020.50			
4	3443.55	1	IV	29031.54		(0) 0.99	
5	3442.927	1		29036.76	$a^4D_{3½}-w^2D^0_{3½}$		
6	3442.317	2	III	29041.92	$a^2D_{2½}-t^2H^0_{3½}$	(0) 0.91	(0) 0.90*b*
6	3442.006	2	IV	29044.54	$a^4D_{0½}-w^2D^0_{1½}$ $b^4P_{2½}-p^4D^0_{3½}$		
5	3439.659	[−1h*p*?]		29064.35	$a^4F_{2½}-y^6P^0_{3½}$		
4	3438.99	*tr*	IV	29070.02			
5	3437.876	2		29079.42	$a^3F_{3½}-q^2G^0_{4½}$		
6	3437.779	1	IV	29080.25	$a^2H_{4½}-t_2H^0_{5½}$		
5	3436.080	1		29094.62	$a^4F_{3½}-y^6P^0_{3½}$		
4	3432.05	1	IV	29128.78	$b^4P_{2½}-p^4D^0_{3½}$		
5	3428.490	−1		29159.03	$a^4F_{3½}-y^6P^0_{2½}$		
5	3427.486	1	IV	29167.57			
4	3427.09	1		29170.96	$z^6G^0_{3½}-g^6F_{3½}$		
4	3426.73	1	III A	29174.08	$a^4D_{2½}-w^2D^0_{2½}$		
6	3425.958	1	II A	29180.58			
6	3425.287	1	IV	29186.30		(0) 0.87	
6	3425.072	6	II	29188.14		(0) 0.96	
6	3423.867	3	III	29198.42	$a^2H_{4½}-s^2G^0_{4½}$	(0) 1.02	(0) 1.03*b*
5	3423.328	−1h		29203.00	$a^4F_{1½}-y^6P^0_{2½}$		
6	3418.517	5	II	29244.10	$a^4D_{3½}-t^4D^0_{3½}$	(0) 1.42	(0) 1.46*b*
6	3417.069	5	II	29256.50	$a^4D_{2½}-t^4D^0_{1½}$	(0) 1.43	(0) 1.48*b*
6	3416.541	2	II A	29261.04	$a^3G_{3½}-v^3F^0_{3½}$		
	3414.77	150*R* Ni	II	29276.18	$(a^4D_{1½}-w^2D^0_{2½})$		
6	3414.201	5	II	29281.06	$a^4D_{1½}-t^4D^0_{2½}$	(0.56) 0.58, **1.71**	(0.60) 0.60, **1.79**
4	3413.76	1	IV	29284.81	$b^4F_{3½}-r^4F^0_{3½}$		
4	3410.96	1	IV	29308.92	$b^4F_{1½}-r^4F^0_{1½}$	(0) 0.77	(0.27) 0.49*b*
6	3409.098	4	III	29324.89	$a^2D_{2½}-t^2F^0_{3½}$ $b^4F_{3½}-r^4F^0_{3½}$		
4	3408.46	1	II A	29330.41			
6	3408.001	3	III	29334.34	$b^4F_{3½}-r^4F^0_{4½}$	(0.63) 1.07w_1 C	(0.74) 1.09*b*
6	3406.838	6	III	29344.35	$a^4D_{0½}-t^4D^0_{1½}$	Unaffected	(0.12) 0.12
5	3406.617	2		29346.24	$b^4P_{1½}-p^4D^0_{2½}$		
6	3405.160	6	II	29358.80	$a^4D_{1½}-t^4D^0_{1½}$	(0) 1.14	(0) 1.18*b*
6	3404.964	2	IV	29360.49	$a^2D_{1½}-t^2F^0_{2½}$ $b^4F_{2½}-r^4F^0_{2½}$	(0) 0.76	(0) 0.78*b*
6	3403.364	5	IIII	29374.29	$b^4F_{4½}-r^4F^0_{4½}$	(0.23) 1.23	(0.19) 1.28*b*
5	3402.977	0		29377.63	$b^4F_{3½}-q^4F^0_{3½}$		
6	3402.572	9	II	29381.13	$a^4D_{2½}-t^4D^0_{2½}$	(0) 1.29	(0.04) 1.34*b*
5	3402.367	−1		29382.90	$b^4F_{2½}-q^4F^0_{2½}$		
5	3401.894	−1		29386.99	$b^4F_{4½}-q^4F^0_{4½}$		
6	3401.345	2	III	29391.73	$a^2H_{4½}-s^2G^0_{3½}$	(0) 0.87	(0) 0.88*b*
6	3400.396	12	II	29399.94	$a^4D_{3½}-t^4D^0_{3½}$	(0) 1.34	(0.12) 1.37*b*
5	3400.200	1		29401.63	$b^4F_{1½}-q^4F^0_{1½}$		
6	3398.272	1	IV	29418.30	$b^4F_{3½}-q^4F^0_{3½}$	(0) 0.95	(0.26) 0.99*b*
6	3397.845	4	III	29422.00	$a^4D_{0½}-t^4D^0_{1½}$	(0.56) 0.56, **1.69**	(0.59) 0.59, **1.77**
6	3397.583	6	III	29424.28	$a^4P_{2½}-w^4P^0_{1½}$	(0) 1.48	(0) **1.48***s*
6	3396.514	3	IV	29433.54	$b^4F_{3½}-q^4F^0_{3½}$	(0.34) 1.13w_1	(0.50) 1.14*b*
5	3396.224	−1		29436.05	$b^4P_{0½}-p^4D^0_{1½}$		
5	3395.524	3	III	29442.11	$b^4F_{1½}-q^4F^0_{2½}$ $a^4P_{2½}-t^4F^0_{3½}$		
4	3394.76	2	IV	29448.75			
5	3392.729	1		29466.37	$b^4F_{4½}-q^4F^0_{4½}$		
4	3392.45	1		29468.80	$b^4F_{3½}-q^4F^0_{3½}$		
5	3391.614	0h		29476.06	$a^4P_{2½}-u^4F^0_{3½}$ $b^4P_{0½}-p^4D^0_{1½}$		
6	3390.767	6	III	29483.42	$a^4D_{1½}-t^4D^0_{2½}$	(0) 1.44	(0) 1.44*b*
7	3390.388	2	III	29486.72	$a^2G_{4½}-v^2F^0_{3½}$	(0) 0.95	(0) 1.34*b*
4	3389.50	*tr*	IV	29494.43	$b^4F_{1½}-u^2F^0_{1½}$ $a^2D_{2½}-s^4G^0_{3½}$		
6	3387.386	2	IV	29512.85	$b^4F_{3½}-q^4F^0_{4½}$	(0) 1.14	(0) 1.22*b*
5	3386.910	0h		29516.99	$a^4P_{2½}-u^4F^0_{2½}$		

TABLE 1.—*Arc spectrum of vanadium* (V I)—Continued

(1)	(2)	(3)	(4)	(5)	(6)	(7)	(8)
Ref.	λ_{air} A	Int. arc	Temp. class	ν_{vac} cm^{-1}	Term combinations	Zeeman effect: Observed	Zeeman effect: Computed
6	3384.602	5	III	29537.12	$a^4D_{3/2}-t^4D_{1/2}$	(0) 1.42	(0) 1.35*b*
4	3379.35	2	IV	29583.00		(0) 1.08	
6	3377.629	15	II	29598.10	$a^4P_{3/2}-w^4P_{3/2}$	(0) 1.49	(0.07) 1.54*b*
6	3377.398	10	II	29600.12	$a^4P_{1/2}-w^4P_{1/2}$	(0.45) **1.21**, 2.11	(0.43) **1.37**, 2.13
6	3376.059	8	II	29611.86	$a^4P_{1/2}-w^4P_{1/2}$	(0) 1.59	(0.14) 1.65*b*
6	3374.036	3	III	29629.62	$a^4P_{1/2}-u^4F_{1/2}$	(1.70) **0**, 1.06, 2.21	(0.58, **1.74**) −0.04, **1.12**, 2.28
4	3372.80	*tr*	IV A	29640.52			
6	3371.118	3	IV	29655.27	$b^4P_{1/2}-z^2S_{1/2}$	(0.29, —) **0.94**, 1.63	(0.34) **1.03**, 1.70.
5	3370.196	1		29663.37	$a^4P_{1/2}-u^4F_{1/2}$		
4	3369.0	1	IV	29673.90	$a^4D_{3/2}-z^2S_{1/2}$		
4	3367.04	1	IV	29691.21			
6	3366.875	4	II	29692.64	$a^4P_{3/2}-w^4P_{3/2}$	(0) 2.54	(0.01) 2.58*b*
6	3365.556	10	II	29704.27	$a^4P_{3/2}-w^4P_{1/2}$	(0.46) **1.07**, 2.05	(0.50) **1.10**, 2.10
6	*b*3363.551	4	III	29721.97	$a^4P_{3/2}-u^4F_{1/2}$	(1.07) **1.07**, 1.56	(1.02) **0.48**, 1.56
4	3362.1	1	IV	29734.80			
6	3356.358	10	II	29785.67	$a^4P_{1/2}-w^4P_{1/2}$	(0) 1.38	(0) 1.38*b*
4	3345.01	*tr*	IV	29886.70			
4	3342.28	2	IV	29911.10			
4	3340.17	1	IV	29929.99			
4	3336.79	2	IV	29960.30	$b^4F_{1/2}-p^4F_{1/2}$	(?w_2) 1.40	(0) 1.39*b*
4	3336.350	2	IV	29964.29	$b^4F_{3/2}-p^4F_{3/2}$	(0) 1.01	
5	3336.212	1	IV	29965.53	$b^4F_{3/2}-t^2P_{1/2}$?		
4	3334.14	*tr*	IV	29984.11	$b^4F_{1/2}-p^4F_{1/2}$		
4	3333.573	2	III	29989.24	$b^4F_{5/2}-p^4F_{3/2}$		
5	3332.449	*tr*	IV	29999.36	$b^4F_{3/2}-p^4F_{3/2}$		
6	*b*3329.858	12	II	30022.71	$a^4P_{3/2}-x^4S_{1/2}$	(?w_2D) 1.02w_2 A	(0) **0.88***s*
6	*b*3328.404	2	IV	30035.82	$b^4F_{3/2}-p^4F_{3/2}$	(0) 1.17	(0.59) 1.12*b*
6	3327.983	2	IV	30039.62	$b^4P_{3/2}-v^2S_{1/2}$	(0.67) 1.36w_1 A	(0.68) 1.35*b*
4	3327.14	*tr*	IV	30047.26		(0) 1.06	
4	3326.38	1	IV	30054.13	$a^2H_{5/2}-q^4F_{3/2}$		
5	3324.489	1		30071.19	$b^4F_{3/2}-p^4F_{5/2}$		
6	3324.393	3	III	30072.05	$a^2H_{9/2}-r^2G_{9/2}$	(0) 0.77	(0) 0.76*b*
5	3324.208	1	IV	30073.73	$a^2P_{1/2}-t^2F_{3/2}$		
6	3321.684	5	III	30096.58	$a^2H_{11/2}-r^2G_{9/2}$	(0) 0.91	(0) 0.91*b*
6	3320.140	3	III	30110.58	$a^4P_{3/2}-s^4D_{1/2}$	(0.23, 0.66) ?w_3 B	(**0.23**, 0.68) 0.87, 1.33, 1.78, **2.23**
4	3319.77	1	IV	30113.95	$b^4F_{3/2}-o^4D_{3/2}$		
6	3319.010	4	III	30120.82	$b^4F_{4/2}-p^4F_{3/2}$	(0) 1.19	(0.04) 1.32*b*
4	3315.87	1	IV	30149.36	$b^4F_{3/2}-o^4D_{3/2}$		
4	3313.97	3	IV	30166.64	$b^4F_{4/2}-o^4D_{3/2}$	(0?w_1) 1.14	(0) 1.06*b*
4	3313.00	2	III	30175.48	$a^4P_{3/2}-s^4D_{3/2}$	(0.48) 1.37w_1	(0.48) 1.44*b*
6	3309.179	8	II	30210.31	$a^4P_{1/2}-x^4S_{1/2}$	(0.32) 1.75	(0.42) 1.85*b*
4	3308.89	1	IV	30212.95	$b^4F_{3/2}-o^4D_{3/2}$		
6	3308.250	3	III	30218.79	$a^4F_{4/2}-y^4G_{3/2}$		
5	3305.101	0h		30247.58	$a^4P_{1/2}-s^2D_{3/2}$		
5	3299.972	2	III	30294.59	$a^4P_{3/2}-s^2D_{3/2}$	(0.96)?w_2	(0.90) 1.34*b*
5	3299.588	0		30298.12	$a^4P_{1/2}-s^4D_{1/2}$		
5	3299.256	1	IV	30301.17	$a^4P_{3/2}-s^4D_{3/2}$		
6	3299.089	3	III	30302.69	$a^4P_{1/2}-x^4S_{1/2}$		
6	3298.147	15	II	30311.37	$a^4F_{4/2}-y^4G_{3/2}$	(0) 1.07	(0) 1.05*b*
5	3295.788	0		30333.05	$a^4P_{1/2}-s^4D_{1/2}$		
5	*b*3295.465	1	IV	30336.02	$a^2G_{9/2}-t^2G_{7/2}$	(0?) 1.17	(0) 1.53*b*
5	3292.561	0h		30362.78	$a^4P_{1/2}-s^4D_{3/2}$		
6	3291.678	4	I	30370.93	$a^4F_{3/2}-y^4G_{3/2}$		
5	3289.525	−1		30390.80	$a^4P_{1/2}-s^4D_{1/2}$?		
6	*b*3288.435	2	III	30400.88	$a^2G_{7/2}-z^2H_{9/2}$	(0) 1.00	(0.96) 1.00*b*
6	3284.361	6	III	30438.58	$a^2G_{9/2}-t^2G_{7/2}$	(0) 1.06	(0.33) 1.08*b*
6	3283.311	15	II	30448.32	$a^4F_{3/2}-y^4G_{3/2}$	(0) 1.01	(0) 1.01*b*
6	3277.939	5	II A	30498.22	$a^4F_{3/2}-y^4G_{3/2}$		
5	3277.791	0		30499.59	$b^2P_{1/2}-z^2D_{3/2}$		
7	3273.025	7	II	30544.00	$a^2G_{9/2}-t^2G_{9/2}$	(0) 0.86	(**0.07**) **0.89***s*
5	3272.188	1	III	30551.82	$a^2D_{3/2}-q^4F_{3/2}$		
6	3271.635	12	II	30556.98	$a^4F_{3/2}-y^4G_{3/2}$		
4	3271.39	3	III	30559.27	$a^2G_{9/2}-z^2H_{9/2}$		

TABLE 1.—*Arc spectrum of vanadium* (V I)—Continued

(1)	(2)	(3)	(4)	(5)	(6)	(7)	(8)
Ref.	λ_{air} A	Int. arc	Temp. class	ν_{vac} cm^{-1}	Term combinations	Zeeman effect: Observed	Zeeman effect: Computed
6	3266.078	4	III	30608.97	$a^3D_{2½}-g^4F_{3½}$ / $a^3G_{3½}-y^3H_{3½}$		
6	3265.887	5	IV	30610.76	$a^3F_{3½}-f^3D_{3½}$	(0) 1.00	(0) 1.00*b*
6	3263.238	15	II	30635.62	$a^4F_{1½}-g^4G_{2½}$		
6	3262.063	5	III	30646.64	$a^3G_{3½}-f^3G_{3½}$		
6	3261.080	6	III	30655.88		(0) 1.15	
5	3260.889?	−1		30657.67	$a^3G_{4½}-t^4G_{4½}$		
5	3260.382	−1		30662.44	$a^3F_{2½}-f^3D_{2½}$?		
6	3259.531	5	III	30670.44	$a^4D_{2½}-w^4P_{1½}$	(0) 1.02	(0) 0.98*s*
5	3256.779	1	IV	30696.36	$a^3F_{2½}-f^3D_{1½}$		
4	3256.46	1	IV	30699.33		(0) 1.13	
6	3255.649	9	III	30707.02	$a^4D_{2½}-w^4P_{2½}$	(0?w_2D) 1.15w_2A	(0) 1.23*b*
5	d3254.783	10	II	30715.18	$a^4F_{4½}-x^4F_{3½}$	(0w^4D) 0.90w^4A diffuse	(0) 1.40*b*
4	3252.86	1	IV	30733.30			
6	3250.033	2	III	30760.08	$a^3G_{4½}-t^4G_{3½}$		
5	3249.930	3		30761.05	$a^4D_{1½}-w^4P_{0½}$		
5	3249.790	0*h*		30762.38	$a^3G_{3½}-t^4G_{2½}$		
6	d3249.567	10	II	30764.49	$a^4F_{4½}-x^4F_{3½}$	(0.61) 1.11w_2C	(0.15) 1.30*b*
6	3248.696	3	III	30772.73	$a^4D_{1½}-w^4P_{1½}$ / $b^4P_{2½}-t^4P_{3½}$		
4	3246.83	1	IV	30790.42	$a^4D_{1½}-u^4F_{1½}$?		
5	3243.957	1		30817.69	$a^3G_{4½}-t^4G_{3½}$		
6	3243.274	3	III	30824.17	$a^4D_{0½}-w^4P_{0½}$	(1.29) 1.25w_1C	(1.29) 1.29*b*
6	3242.033	1	III A	30835.98	$a^4D_{0½}-w^4P_{1½}$		
6	3241.167	4	III	30844.22	$a^4D_{3½}-w^4P_{2½}$	(0.49) 1.43w_2C	(0.37) 1.43*b*
5	3238.894	1	IV	30865.86	$a^3G_{3½}-t^4G_{3½}$		
4	3234.73	2	III	30905.59	$a^4F_{3½}-x^4F_{3½}$		
5	3233.497	1		30917.38	$b^2P_{2½}-f^2D_{2½}$		
6	d3233.183	6	III	30920.37	$a^3G_{4½}-u^3F_{3½}$	(0) 0.96	(0) 1.16*b*
6	3230.645	6	II	30944.67	$a^4F_{2½}-x^4F_{1½}$	(0) 1.18	(0.03) 1.20*b*
5	3230.441	1		30946.62	$a^4D_{1½}-w^4P_{1½}$		
5	3229.604	4	IV	30954.64	$b^2H_{4½}-z^2I_{4½}$	(0) 0.90	(0) 0.91*b*
5	3228.182	3	III	30968.28	$a^3G_{3½}-t^4G_{4½}$	(0) 1.86	(0) 1.76*b*
6	3227.408	4	IV	30975.71	$b^2H_{5½}-z^2I_{6½}$	(0) 0.99	(0) 1.00*b*
6	3227.117	3	III	30978.50	$a^3G_{4½}-u^3H_{5½}$		
6	3226.106	4	II	30988.20	$a^4F_{4½}-x^4G_{5½}$		
4	3225.63	1	III A	30992.76			
5	3225.490	1		30994.12	$a^4F_{3½}-x^4F_{4½}$		
6	3218.874	5	III	31057.83	$a^3G_{3½}-u^3F_{3½}$	(0) 0.89	(0) 0.93*b*
5	3218.355	1	III A	31062.84	$a^4F_{2½}-x^4F_{2½}$		
6	d3217.113	10	II?	31074.82	$a^4F_{2½}-x^4G_{3½}$	(0) 1.08 diffuse	(0) 2.04*b*
6	3215.379	4	II	31091.59	$a^4F_{3½}-x^4F_{3½}$	(0) 0.98	(0) 1.01*b*
6	d3213.939	2	III	31105.52	$a^4D_{3½}-f^2P_{1½}$	(0) 1.12	(0) 1.12*b*
6	3212.437	15	II	31120.06	$a^3G_{4½}-u^3H_{5½}$	(0) 1.02	(0) 0.90*b*
5	3211.569	1	III	31128.47	$a^3G_{3½}-u^3F_{3½}$		
5	3211.323	0		31130.85	$a^4F_{3½}-x^4F_{4½}$		
5	3210.427	2	IV	31139.54	$a^2D_{1½}-f^2P_{1½}$ / $a^2D_{2½}-p^4F_{2½}$	(0) 1.12	(0.38) 1.10*b*
5	3210.096	4	III	31142.75	$a^4H_{3½}-r^4G_{3½}$	(0) 0.76	(0) 0.76*b*
6	3207.415	20	II	31168.79	$a^4F_{4½}-x^4G_{5½}$	(0.58) 1.16w_2 C	(0.59) 1.20*b*
5	3206.923	1	IV	31173.56	$a^2D_{1½}-p^4F_{2½}$		
6	b3205.581	15	II	31186.61	$a^2G_{3½}-u^3H_{4½}$	(0) 0.93	(0) 0.80*b*
5	3205.257	5	III	31189.76	$a^4H_{4½}-r^4G_{5½}$	(0) 0.90	(0) 0.90*b*
6	3204.193	3	I	31200.12	$a^4F_{1½}-x^4F_{1½}$	(0) 0.36	(0.03) 0.39*b*
6	3202.383	25	II	31217.76	$a^4F_{2½}-x^4G_{3½}$	(0.55) 1.04w_2 C	(0.74) 1.06*b*
7	3201.227	2	III A	31229.03	$a^4F_{1½}-x^4F_{2½}$ / $a^4H_{5½}-r^4G_{5½}$		
6	3199.819	6	III	31242.77	$a^4H_{5½}-r^4G_{4½}$	(0) 0.99	(0) 0.99*b*
6	3198.012	20	II	31260.43	$a^4F_{3½}-x^4G_{3½}$	(0.62, **1.17**) 0.22, 0.73, 1.17, 1.68	(0.23, 0.71, **1.19**) −0.18, 0.30, **0.77**, 1.24, 1.72
4	3194.92	1	IV	31290.67	$b^4P_{2½}-t^4P_{1½}$		
4	3194.57	1	IV	31294.11	$a^4H_{4½}-r^4G_{3½}$?		

TABLE 1.—*Arc spectrum of vanadium* (V I)—Continued

(1)	(2)	(3)	(4)	(5)	(6)	(7)	(8)
Ref.	λ_{air} A	Int. arc	Temp. class	ν_{vac} cm^{-1}	Term combinations	Zeeman effect: Observed	Zeeman effect: Computed
4	3194.40	2	IV	31295.77	$a^4H_{3½}-r^4G^0_{3½}$		
6	3193.919	6	II	31300.48	$a^4F_{4½}-x^4G^0_{5½}$	(0) 1.15	(0) 1.16*b*
7	3189.078	1	IV	31347.99	$a^2P_{0½}-u^2P^0_{1½}$		
6	3188.096	3	IV	31357.64	$a^2P_{1½}-u^2P^0_{1½}$	(0.67)? w_1	(0.65) 1.43
6	°3185.404	40R*a*	II	31384.17	$a^4F_{1½}-x^4G^0_{2½}$	(0.45) 0.68, **1.50**?	(0.12) 1.02*b*
6	°3183.995	(150R)*a*	II	31398.03	$a^4F_{1½}-x^4G^0_{2½}$	(0.59) 0, 0.62, 1.33	(**0.06**, 0.19) 0.34, 0.46, 0.59, **0.72**
8	3183.96	(125R)*a*	II	31398.38	$a^4F_{2½}-x^4F^0_{1½}$		
6	°3183.415	150*Ra*	II	31403.78	$a^4F_{2½}-x^4G^0_{3½}$	(0.34) 0.55, **1.15**	(0.05) 0.88*b*
8	3182.76	1	IV	31410.19	$a^4D_{2½}-s^4D^0_{1½}$		
8	3181.63	1	IV	31421.35	$a^4D_{2½}-s^4D^0_{2½}$		
4	3180.56	1	IV	31431.91	$a^2D_{1½}-t^2P^0_{0½}$		
4	3180.09	1	IV	31436.56			
8	3177.83	1	IV	31458.90	$a^4D_{1½}-s^4D^0_{1½}$		
8	3169.6	1	IV	31540.77	$a^4D_{2½}-s^4D^0_{2½}$		
4	3165.59	3	IV	31580.61	$b^4P_{1½}-t^4P^0_{0½}$		
8	3164.5	1	IV	31591.46			
4	3163.89	4	IV	31597.57	$b^4P_{1½}-t^4P^0_{1½}$		
8	3161.9	3*H*	IV	31617.55			
4	3159.87	2	V	31637.76			
8	3158.77	[1]	IV	31648.77			
8	3156.89	2*h*	IV	31667.62	$a^4P_{2½}-t^4F^0_{1½}$		
4	3156.19	10	IV	31674.64		(8) 1.15	
8	3153.54	5*H*	IV	31701.25			
8	3152.75	2*H*	IV	31709.19			
4	3150.59	5	IV	31730.92		(0) 0.83	
8	3150.03	2*H*	IV	31736.56			
8	3147.97	3*H*	IV	31757.32			
6	3147.255	8	IV	31764.56		(0) 0.65	
8	3146.8	1*H*	IV	31769.23			
8	3145.65	[1]	IV	31780.73			
8	3143.2	1	IV	31805.60			
4	3139.97	4	IV	31838.21	$a^2P_{0½}-p^4F^0_{1½}$?		
4	3139.04	3	IV	31847.64	$a^2P_{1½}-p^4F^0_{1½}$		
4	3138.50	3	IV	31853.12	$a^2P_{1½}-t^2P^0_{1½}$		
8	3135.17	2	IV	31886.94	$a^2P_{1½}-p^4F^0_{2½}$ $a^4D_{0½}-z^4S^0_{0½}$		
8	3134.54	1	IV	31893.45			
8	3133.0	1*H*	IV	31909.12			
8	3131.9	1*H*	IV	31920.33			
8	3131.3	1	IV	31926.44			
8	3123.25	1	V	32008.71	$a^4D_{2½}-b^2F^0_{3½}$		
4	3121.78	4	III*A*	32023.78	$a^4P_{2½}-v^4P^0_{1½}$		
8	3116.35	1	IV	32079.56			
4	3112.93	8	III	32114.79	$a^4P_{1½}-v^4P^0_{0½}$		
8	3112.13	3	IV	32123.04			
8	3110.9	1	IV	32135.74	$a^2P_{0½}-t^2P^0_{0½}$		
8	3108.56	[1]	IV	32159.92			
5	3107.142	5	IV	32174.61	$a^4P_{2½}-r^4D^0_{1½}$		
4	3106.12	5	IV	32185.18	$a^4P_{2½}-v^4P^0_{2½}$		
4	3103.99	6	IV	32207.26	$a^4P_{0½}-v^4P^0_{0½}$		
8	3103.60	1	IV	32211.31	$a^4P_{1½}-v^4P^0_{1½}$		
8	3101.4	1	IV	32234.15			
8	3099.59	2*h*	IV	32252.96			
5	3096.763	−1		32282.44	$z^6F^0_{3½}-h^6G_{2½}$		
8	3096.04	2	IV	32289.93			
4	3095.90	5	III	32291.40	$a^4P_{1½}-r^4D^0_{0½}$		
6	3094.699	20	III	32303.98	$a^4P_{0½}-v^4P^0_{1½}$		
4	3093.79	25	III	32313.41	$a^4P_{2½}-r^4D^0_{1½}$		
8	3093.24	6?	III	32319.16	$a^4F_{2½}-x^4D^0_{1½}$		
8	3092.85	1	IV	32323.33			
4	3092.72	8	III	32324.64			
6	3091.552	15	II	32336.85	$a^4F_{3½}-x^4D^0_{2½}$		
8	3091.42	20	II	32338.28	$a^4F_{4½}-x^4D^0_{3½}$		
4	3090.81	4	III A	32344.66	$a^4F_{4½}-x^4H^0_{5½}$		

TABLE 1.—*Arc spectrum of vanadium* (V I)—Continued

(1)	(2)	(3)	(4)	(5)	(6)	(7)	(8)
Ref.	λ_{air} A	Int. arc	Temp. class	ν_{vac} cm^{-1}	Term combinations	Zeeman effect: Observed	Zeeman effect: Computed
5	3090.538	3*h*	III	32347.46			
8	3090.40	[1]	IV	32348.96	$a^4F_{1½}-x^4D_{½}^{0}$		
6	3089.134	25	III	32362.16	$a^4P_{1½}-r^4D_{½}^{0}$; $(z^6F_{½}^{0}-h^6G_{½})$	(0.68)w_3	
6	3088.119	30	III	32372.81	$a^4P_{1½}-v^4P_{½}^{0}$		
4	3087.49	2*h*	IV	32379.44	$z^6F_{½}^{0}-h^6G_{½}$		
6	3087.072	15	III	32383.79	$a^4P_{½}-r^4D_{½}^{0}$	(1.25) 1.28	(1.28) 1.32*b*
5	3085.923	1*h*	IV	32395.84	$z^6F_{½}^{0}-h^6G_{½}$		
6	3084.384	20	III	32412.01	$a^4P_{½}-z_{½}^{0}$		
6	3083.542	30	III	32420.87	$a^4P_{½}-r^4D_{½}^{0}$		
5	3082.109	50*r*	II	32435.92	$a^4F_{½}-w^4F_{½}^{0}$		
5	3082.010	6	IV	32436.96	$a^2H_{½}-s^2H_{½}^{0}$		
4	3080.34	12	III	32454.57	$a^4P_{½}-r^4D_{½}^{0}$	(0.65) 0.54, —	(0.70) **0.50**, 1.90
4	3080.16	6	III	32456.46	$a^4F_{1½}-x^4D_{½}^{0}$		
5	3079.365	4	III A	32464.83	$a^4F_{½}-z^4H_{½}^{0}$		
8	3077.86	5*h*	IV	32480.71	$z^6F_{½}^{0}-h^6G_{½}$		
4	3077.73	6	IV	32482.09	$a^2D_{1½}-s^2F_{½}^{0}$	(w_1 D) 0.72 w_1 A	
8	3076.69	5*h*	IV	32493.06	$z^6F_{½}^{0}-h^6G_{½}$		
8	3076.63	4	III	32493.70	$a^4P_{½}-v^2P_{½}^{0}$		
6	3075.935	8	III	32501.04	$a^4P_{1½}-r^4D_{½}^{0}$; $(z^6F_{½}^{0}-h^6G_{4½}?)$		
6	3075.269	10	III	32508.08	$a^2H_{4½}-s^2H_{½}^{0}$	(0) 0.84	(**0.45**) **0.95***s*
8	3074.83	8*h*	IV	32512.71	$z^6F_{½}^{0}-h^6G_{½}$		
8	3074.06	10*h*	IV	32520.85	$z^6F_{½}^{0}-h^6G_{½}$		
6	3073.825	60*r*	II	32523.35	$a^4F_{3½}-w^4F_{½}^{0}$; $a^4F_{2½}-x^4D_{½}^{0}$	(w_2 D) 1.00w_2 B	(0) **1.68***s*; (0.61) 1.15*b*
8	3072.73	2*h*	IV	32534.93			
8	3070.88	2	III A	32554.52	$a^4F_{3½}-z^4H_{½}^{0}$		
6	3069.648	30*r*	I	32567.60	$a^4F_{3½}-x^4D_{½}^{0}$	(0.52) 1.22w_2 C	(**0.52**) **1.28***s*
5	3067.117	6	IV E	32594.46	$a^2D_{2½}-s^2F_{½}^{0}$		
8	3066.51	20	I	32600.90	$a^4F_{2½}-w^4F_{½}^{0}$		
6	3066.373	125*R*	II	32602.38	$a^4F_{4½}-w^4F_{½}^{0}$	(0.30) 1.05, 1.41	(0.07), 1.29*b*
6	3063.725	12	II	32630.57	$a^4F_{2½}-z^2P_{½}^{0}$		
4	3060.93	2	III A	32660.32	$a^4F_{1½}-x^4D_{½}^{0}$		
6	3060.457	125R	II	32665.40	$a^4F_{3½}-w^4F_{½}^{0}$		
8	3056.59	[1]	IV	32706.67			
6	3056.339	100*R*	II	32709.42	$a^4F_{3½}-w^4F_{½}^{0}$	(0) 0.87	(0) 1.01*b*
8	3054.89	1	IV A	32724.86	$a^4F_{1½}-z^2P_{½}^{0}$; $a^4P_{1½}-w^2S_{½}^{0}$		
8	3053.65	80*R*	II	32738.26	$a^4F_{1½}-w^4F_{½}^{0}$		
6	3052.195	20	II	32753.81	$a^4F_{2½}-x^4D_{½}^{0}$; $(a^4F_{4½}-y^4G_{4½}^{0})$	(0.92w_2 B) 1.56w_2 C	(0.34) 1.78*b*; (0.88) 1.16*b*
8	3051.39	*tr*	IV A	32762.45			
6	3050.883	35*r*	II	32767.90	$a^4F_{1½}-z^2P_{½}^{0}$	(0) 1.13	(1.15) 0.81*b*
6	3050.396	25	IV	32773.13	$a^2G_{4½}-t^2F_{3½}^{0}$		
8	3050.33	1	IV	32773.88	$a^4P_{½}-v^2P_{½}^{0}$		
8	3047.21	[1]	IV	32807.43			
6	3044.938	50*r*	II	32831.87	$a^4F_{3½}-w^4F_{½}^{0}$	(0) 1.39	(0) 1.48*b*
6	3043.553	50*r*	II	32846.80	$a^4F_{1½}-w^4F_{½}^{0}$	(0.54w_2 B) 1.14w_2 C	(**0.30**, 0.91) 0.10, 0.70, 1.31, **1.02**
6	3043.123	50*r*	II	32851.44	$a^4F_{3½}-w^4F_{½}^{0}$	(w_1 D) 1.58w_1 B	(0) **1.61***s*
	(3042.672	15*Fe*	III	32856.31)	$(a^2H_{4½}-q^2G_{4½}^{0})$		
4	3041.83	8	IV	32865.44			
8	3040.13	1	IV	32883.81	$a^4D_{3½}-t^4F_{3½}^{0}$		
8	3039.46	[1]	IV	32891.06			
5	3039.305	1		32892.72	$a^2H_{3½}-q^2G_{4½}^{0}$		
6	3038.710	10	IV	32899.16			
8	3038.06	[1]	IV	32906.21			
5	3037.372	2		32913.65	$a^4D_{2½}-t^4F_{3½}^{0}$; $a^6D_{3½}-u^4D_{½}^{0}$		
8	3033.75	[1]	IV	32952.94	$a^4D_{1½}-t^4F_{2½}^{0}$		
6	3031.009	10?	III	32982.75	$a^2G_{3½}-t^2F_{3½}^{0}$	(0) 0.86	(0) **0.93***s*
8	3030.93	5?	III A	32983.60	$a^4F_{3½}-y^2G_{4½}^{0}$		
4	3027.07	2	IV	33025.64			

TABLE 1.—*Arc spectrum of vanadium* (V I)—Continued

(1)	(2)	(3)	(4)	(5)	(6)	(7)	(8)
Ref.	λ_{air} A	Int. arc	Temp. class	ν_{vac} cm^{-1}	Term combinations	Zeeman effect: Observed	Zeeman effect: Computed
8	3022.77	10*H*	IV	33072.61	$z^6G_{13/2}-g^6G_{11/2}$		
4	3021.78	6	IV	33083.45	$a^2G_{9/2}-f^2H_{11/2}$		
5	3016.392	1	IV A	33142.56	$a^4F_{9/2}-z^2H_{11/2}$?		
4	3016.17	20	III	33144.96	$a^4P_{3/2}-w^4S_{3/2}$		
5	3014.972	1	IV A	33158.17	$a^4F_{3/2}-y^2F_{5/2}$		
4	3014.33	15*H*	IV	33165.19	$z^6G_{11/2}-f^5H_{7/2}$		
8	3014.19	[4]	IV A	33166.73			
8	3011.58	1	IV	33195.46	$a^3P_{1/2}-s^3F_{3/2}$		
8	3011.40	[2]	IV	33197.44	$z^6G_{13/2}-g^6G_{13/2}$		
8	3010.84	[1]	IV	33203.62	$z^6G_{13/2}-g^6G_{11/2}$		
8	3009.66	[1]	IV	33216.63	$z^6G_{13/2}-g^6G_{13/2}$		
8	3006.90	5 H	IV	33247.11	$z^6G_{13/2}-f^5H_{9/2}$		
4	3006.34	6	IV	33253.30	$a^3G_{3/2}-z^3H_{1/2}$		
8	3006.24	5 H	IV	33254.41	$z^6G_{13/2}-f^5H_{5/2}$		
4	3004.82	10	IV	33270.12	$a^4D_{3/2}-v^4P_{1/2}$		
4	3004.33	4	IV A	33275.55	$a^4D_{1/2}-v^4P_{3/2}$		
6	3003.288	5	IV	33287.16			
4	3002.65	8	III	33294.27	$a^4D_{3/2}-v^4P_{1/2}$		
6	3002.450	6	IV	33296.47			
8	3001.90	10 H	IV	33302.58	$z^6G_{13/2}-f^5H_{11/2}$		
8	3001.05	1 h	IV	33312.02			
5	3000.566	*tr*	IV A	33317.36			
4	2999.20	12	III	33332.55	$a^4P_{1/2}-w^4S_{1/2}$	(?) 1.74	(0.36) 1.82*s*
4	2998.62	4	IV	33339.00	$a^4D_{5/2}-v^4P_{5/2}$		
8	2997.87	5 H	IV	33347.33	$z^6G_{1/2}-f^5H_{3/2}$		
8	2997.08	3 H	IV	33356.12	$z^6G_{1/2}-f^5H_{3/2}$		
4	2996.48	6	IV	33362.80	$a^3G_{4/2}-s^3G_{3/2}$		
6	2995.617	4	IV	33372.40	$a^4D_{1/2}-v^4P_{1/2}$		
8	2994.61	2 h	IV	33383.63			
8	2994.50	1	IV	33384.86			
8	2994.01	1	IV A	33390.32	$a^4F_{3/2}-y^2F_{3/2}$		
8	2992.79	[*tr*]	IV	33403.93			
8	2991.14	2	IV	33422.35	$a^4D_{3/2}-r^4D_{3/2}$		
4	2990.93	8	III	33424.69	$a^4P_{3/2}-w^4S_{3/2}$		
8	2990.31	1	IV	33431.62	$a^4D_{3/2}-v^4P_{3/2}$		
4	2982.18	2	IV	33522.74	$a^4D_{1/2}-r^4D_{1/2}$		
5	2981.537	0		33529.99	$a^4D_{3/2}-r^4D_{1/2}$		
8	2979.21	2	IV	33556.15			
6	2978.936	4	IV	33559.27	$a^4D_{3/2}-r^4D_{3/2}$		
6	2977.550	25*r*	I	33574.90	$a^4F_{4/2}-w^4D_{3/2}$	(?) 1.12	(0.93) 1.04*s*
6	*d*2976.527	8	IV E	33586.43	$a^4P_{3/2}-q^4D_{3/2}$		
6	2975.077	8	IV	33602.80	$a_2G_{3/2}-s^2G_{3/2}$		
5	2974.217	8	IV	33612.51	$a^4P_{1/2}-q^4D_{3/2}$		
5	2969.868	0		33661.73	$a^4D_{1/2}-r^4D_{3/2}$		
5	2969.363	1		33667.45	$a^4D_{3/2}-r^4D_{3/2}$?		
6	2968.981	3	IV	33671.79	$a^4P_{1/2}-q^4D_{1/2}$		
8	2968.29	5	IV A	33679.67	$a^4P_{3/2}-u^4P_{1/2}$		
5	2966.079	0		33704.73	$a^4P_{3/2}-q^4D_{3/2}$		
6	2963.818	6	IV	33730.56	$a^4P_{3/2}-q^4D_{3/2}$		
6	2962.784	30*r*	II	33742.22	$a^4F_{3/2}-w^4D_{3/2}$		
4	2962.07	1	V	33750.38	$b^3H_{4/2}-p^3G_{3/2}$?		
6	2961.127	10	III	33761.09	$a^4P_{3/2}-u^4P_{3/2}$		
5	2960.849?	−1		33764.26	$a^4P_{3/2}-q^4D_{3/2}$		
8	2959.99	2	IV	33774.09	$a^4P_{1/2}-q^4D_{3/2}$		
	*(2957.520	10	V E	33802.27)	($b^3H_{13/2}-p^3G_{13/2}$)		
4	2957.30	10?	II	33804.80	$a^4F_{3/2}-w^4D_{1/2}$		
5	2957.176	8h	IV	33806.20	$a^4P_{1/2}-u^4P_{3/2}$		
8	2956.57	1h	V	33813.14			
5	2956.142	1	IV A	33818.02			
6	2955.806	15	II	33821.87	$a^4F_{4/2}-v^4F_{3/2}$		
4	2954.33	20	II	33838.77	$a^4F_{3/2}-w^4D_{1/2}$		
	*(2953.943	50*R* Fe	II	33843.19)	($a^4F_{3/2}-v^4F_{3/2}$)		
8	2951.84	2h	IV	33867.31	$a^4P_{1/2}-u^4P_{1/2}$		
8	2949.91	2h	IV	33889.46	$z^6G_{1/2}-A^6G_{3/2}$?		
4	2949.62	25	II	33892.79	$a^4F_{3/2}-v^4F_{1/2}$		

TABLE 1.—*Arc spectrum of vanadium* (V I)—Continued

(1)	(2)	(3)	(4)	(5)	(6)	(7)	(8)
						Zeeman effect	
Ref.	λ_{air} A	Int. arc	Temp. class	ν_{vac} cm^{-1}	Term combinations	Observed	Computed
8	2949.09	1	IV A	33898.87	$a^4P_{5/2}-w^4P_{3/2}$		
4	2946.54	15	II	33928.21	$a^4F_{3/2}-w^4D_{3/2}$		
4	2944.76	10h	IV	33948.71	$a^4P_{1/2}-w^4P_{3/2}$		
8	2943.84	12h	IV	33959.32	$a^4P_{3/2}-w^4P_{3/2}$ $(z^6G_{3/2}-h^6G_{1/2})$		
6	2943.197	30r	II	33966.76	$a^4F_{1/2}-w^4D_{3/2}$		
6	2942.354	10	I	33976.49	$a^4F_{1/2}-w^4D_{1/2}$		
8	2942.33	10	I	33976.74	$a^4F_{1/2}-z^4F_{1/2}$		
4	2942.02	tr	III A	33980.32			
8	2941.11	1	III A	33990.83	$a^4F_{3/2}-w^4D_{3/2}$		
8	2939.26	2h	V	34012.22			
8	2938.67	6	II	34019.04	$a^4F_{1/2}-1^o$		
8	2938.30	5h	IV	34023.32	$z^6G_{1/2}-h^6G_{1/2}$		
6	2937.696	15	I	34030.35	$a^4F_{3/2}-z^4F_{3/2}$ $a^4F_{1/2}-z^4F_{1/2}$		
6	2935.880	15	I	34051.41	$a^4F_{3/2}-z^4F_{3/2}$		
8	2934.72	20h	IV	34064.82	$z^6G_{3/2}-h^6G_{3/2}$		
5	2934.646	2	III A	34065.72	$a^4F_{1/2}-w^4D_{1/2}$		
5	2933.234	3h	IV	34082.12	$z^6G_{1/2}-h^6G_{3/2}$		
8	2930.89	15h	IV	34109.32	$z^6G_{1/2}-h^6G_{3/2}$		
8	2928.74	1h	IV	34134.47	$z^6G_{1/2}-h^6G_{1/2}$		
4	2928.62	2	IV	34135.87			
6	2927.646	10h	IV	34147.17	$z^6G_{1/2}-h^6G_{1/2}$		
5	2926.258	12	I	34163.37	$a^4F_{3/2}-y^4D_{3/2}$		
6	2925.880	4	III A	34167.78	$a^4F_{1/2}-z^4F_{3/2}$		
8	2924.92	5h	IV	34179.04	$z^6G_{1/2}-h^6G_{3/2}$		
6	2923.627	70Ra	II	34194.11	$a^4F_{3/2}-z^4D_{3/2}$		
8	2923.41	2h	V	34196.69			
5	2922.715	5h	IV	34204.78	$z^6G_{1/2}-h^6G_{3/2}$		
6	2922.582	4	III A	34206.34	$a^4F_{3/2}-z^4F_{1/2}$		
8	2921.18	6h	IV	34222.78	$z^6G_{1/2}-h^6G_{3/2}$		
5	2919.931	6	III A	34237.39	$a^4F_{3/2}-z^4F_{3/2}$		
4	2917.94	8	IV	34260.78	$a^6G_{3/2}-r^6G_{1/2}$		
4	2917.52	4	IV	34265.70			
4	2916.00	8	IV	34283.56	$a^6G_{3/2}-r^6G_{3/2}$ $(z^6G_{3/2}-h^6G_{3/2})$		
4	2915.33	10	II	34291.44	$a^4F_{3/2}-y^4D_{3/2}$		
6	2914.924	50Ra	II	34296.21	$a^4F_{3/2}-z^4D_{3/2}$ $(z^6G_{1/2}-h^6G_{3/2})$ $(z^6G_{1/2}-h^6G_{3/2})$		
8	2914.43	2h	IV	34302.03	$z^6G_{1/2}-h^6G_{3/2}$		
6	d2914.290	2h	IV	34303.55	$z^6G_{3/2}-h^6G_{3/2}$		
5	d2910.435	5?	II A	34349.09	$a^4F_{3/2}-y^4D_{3/2}$		
6	2906.134	40r	II	34399.92	$a^4F_{3/2}-z^4D_{3/2}$		
6	2904.126	20	II	34423.71	$a^4F_{3/2}-z^4D_{3/2}$		
6	2903.700	12	II	34428.75	$a^4F_{1/2}-y^4D_{1/2}$		
8	2900.86	5H	IV	34462.44			
6	2899.602	30	II	34477.40	$a^4F_{1/2}-z^4D_{3/2}$		
6	2899.207	20	II	34482.11	$a^4F_{3/2}-z^4D_{3/2}$		
6	2898.822	5	III A	34486.69	$a^4F_{1/2}-y^4D_{3/2}$		
8	2895.16	4h	V	34530.27			
6	2894.583	8	III	34537.19	$a^4F_{1/2}-z^4D_{1/2}$		
8	2893.47	4h	IV	34550.43	$a^4D_{3/2}-z^4F_{3/2}$		
5	2891.977	2h	IV	34568.31	$a^4D_{3/2}-z^4F_{3/2}$ $a^4D_{1/2}-z^4F_{1/2}$		
5	2891.430	2h	IV	34574.85	$a^4D_{1/2}-z^4F_{3/2}$		
8	2890.56	5H	IV	34585.26			
6	2888.523	2	III A	34609.64	$a^4F_{3/2}-z^4D_{1/2}$		
6	2887.707	2	III A	34619.43	$a^4F_{1/2}-z^4D_{3/2}$		
6	2873.378	2		34792.06	$a^4F_{3/2}-z^4D_{3/2}$		
6	2870.575	35r	II	34826.04	$a^4F_{3/2}-w^4D_{3/2}$		
4	2870.04	5	IV	34832.52	$a^4D_{3/2}-g^4D_{3/2}$ $a^4D_{1/2}-g^4D_{1/2}$		
6	2869.484	3	IV	34839.27	$a^4D_{3/2}-g^4D_{3/2}$		
5	2868.130	20	IV	34855.71	$a^4H_{5/2}-z^4H_{5/2}$		
6	2866.971	10	IV	34869.82	$a^4D_{3/2}-w^4P_{3/2}$		
6	2866.620	15	IV	34874.07	$a^4H_{3/2}-z^4H_{3/2}$		

TABLE 1.—*Arc spectrum of vanadium* (V I)—Continued

(1)	(2)	(3)	(4)	(5)	(6)	(7)	(8)
Ref.	λ_{air} A	Int. arc	Temp. class	ν_{vac} cm^{-1}	Term combinations	Zeeman effect: Observed	Zeeman effect: Computed
6	2866.447	20	IV	34876.19	$a^4P_{3/2}-p^4D^\circ_{3/2}$		
5	2864.386	30r	II	34901.27	$a^4F_{3/2}-u^4D^\circ_{3/2}$		
6	2863.076	12	IV	34917.25	$a^4P_{1/2}-p^4D^\circ_{1/2}$		
6	2862.418	10	IV	34925.28	$a^4D_{3/2}-u^4P^\circ_{1/2}$		
5	2861.677	1	IV	34934.31			
6	2859.997	25	II	34954.84	$a^4F_{3/2}-u^4D^\circ_{1/2}$		
6	2859.001	4h	IV	34967.00	$a^4D_{1/2}-u^4P^\circ_{3/2}$		
6	2858.787	10	IV	34969.63	$a^4P_{3/2}-p^4D^\circ_{3/2}$		
6	2857.972	20	IV	34979.59	$a^4P_{1/2}-p^4D^\circ_{3/2}$		
6	2855.739	2	IV	35006.95	$a^4D_{3/2}-u^4P^\circ_{3/2}$		
6	2855.518	6	IV	35009.65	$a^4P_{3/2}-p^4D^\circ_{1/2}$		
6	2855.252	20	II	35012.91	$a^4F_{1/2}-u^4D^\circ_{3/2}$		
6	2854.057	4h	IV	35027.57	$a^4D_{1/2}-u^4P^\circ_{1/2}$; $a^4H_{3/2}-x^3I^\circ_{1/2}$?		
4	2853.82	3h	IV	35030.44	$a^4D_{3/2}-u^4P^\circ_{5/2}$		
6	2853.579	2	V	35033.88	$a^3P_{2/2}-p^3S^\circ_{1/2}$		
6	2852.899	25	IV	35041.80	$a^3P_{1/2}-p^3S^\circ_{1/2}$		
6	2851.784	20	II	35055.49	$a^4F_{3/2}-u^4D^\circ_{1/2}$		
5	2849.197	15	II	35087.32	$a^4F_{3/2}-u^4D^\circ_{3/2}$		
5	2849.086	4		35088.69			
6	2848.807	15	II	35092.11	$a^4F_{1/2}-u^4D^\circ_{1/2}$		
6	2846.600	20	IV	35120.01			
4	2844.92	2	IV	35140.12	$a^2D_{2/2}-f^2D^\circ_{3/2}$		
4	2839.43	4	IV	35208.05	$a^2D_{1/2}-f^2D^\circ_{1/2}$		
4	2838.06	5	III	35225.03	$a^4F_{1/2}-u^4D^\circ_{1/2}$		
6	2836.714	3	IV	35241.72	$a^4F_{3/2}-u^4D^\circ_{3/2}$		
6	2835.660	5	V	35254.82	$a^6D_{2/2}-w^5F^\circ_{1/4}$?		
4	2834.88	3	V	35264.54			
6	2815.994	5h	V	35501.02			
6	2799.229	3		35713.61			
6	2798.526	2		35722.57	$a^6D_{9/2}-t^4D^\circ_{1/2}$		
4	2788.16	2	V	35855.41			
4	2785.66	10r	IV	35887.57	$a^3P_{1/2}-f^3D^\circ_{3/2}$		
4	2785.52	8	IV	35889.37			
6	2785.216	3		35893.28			
4	2783.76	7	IV	35912.06	$a^3P_{2/2}-f^3D^\circ_{1/2}$		
5	2778.058	4	IV	35985.77	$a^4D_{3/2}-p^4D^\circ_{1/2}$?; $a^4F_{3/2}-z^4G^\circ_{1/2}$?		
4	*2777.70	8h	IV	35990.41			
6	2777.157	5		35997.43			
8	2776.67	2h	V	36003.73			
4	2776.47	6h	IV	36006.35			
6	2775.911	2		36013.59	$a^4P_{3/2}-o^4D^\circ_{3/2}$		
4	2774.01	3	IV	36038.24	$a^4D_{2/2}-p^4D^\circ_{3/2}$; $a^4D_{1/2}-p^4D^\circ_{1/2}$		
4	2773.66	8	IV	36042.79	$a^3G_{4/2}-s^3F^\circ_{3/2}$		
4	2770.94	2d	IV	36078.16	$a^4D_{1/2}-p^4D^\circ_{1/2}$		
4	2768.93	6	IV	36104.34	$a^3G_{3/2}-s^3F^\circ_{3/2}$		
4	2768.30	3	IV	36112.56	$a^4P_{3/2}-o^4D^\circ_{3/2}$		
4	2766.10	1	V	36141.27	$a^4D_{3/2}-p^4D^\circ_{1/2}$		
4	2757.75	2	V	36250.79	$a^3G_{3/2}-s^3F^\circ_{1/2}$		
1	2755.653	(10)	V	36278.34			
1	2753.084	(8)	V	36312.19			
1	*2747.534	(6)	III	36385.54	$a^4F_{3/2}-w^4G^\circ_{3/2}$		
1	2738.075	5		36511.22	$a^3G_{4/2}-s^3H^\circ_{3/2}$		
1	2733.334	(8)	IV	36574.55	$a^4F_{3/2}-w^4G^\circ_{1/2}$		
1	2731.518	(20h?)	IV	36598.86			
1	2731.347	(80r?)	IV	36601.16	$a^3G_{4/2}-s^3H^\circ_{3/2}$		
1	2729.807	2		36621.80	$a^4F_{4/2}-s^3G^\circ_{3/2}$		
1	2729.120	2		36631.02	$a^4D_{3/2}-q^4F^\circ_{3/2}$		
1	2727.440	1		36653.58	$a^4D_{2/2}-q^4F^\circ_{1/2}$		
1	2727.124	1		36657.83	$a^4F_{4/2}-y^3H^\circ_{3/2}$		
1	2725.062	4		36685.57	$a^4F_{2/2}-w^4G^\circ_{1/2}$		

TABLE 1.—*Arc spectrum of vanadium* (V I)—Continued

(1)	(2)	(3)	(4)	(5)	(6)	(7)	(8)
						Zeeman effect	
Ref.	λ_{air} A	Int. arc	Temp. class	ν_{vac} cm^{-1}	Term combinations	Observed	Computed
1	2723.925	2		36700.88	$a^4F_{1½}-x^2D^0_{1½}$		
1	2722.560	(60r)	IV	36719.28	$a^3G_{3½}-s^3H^0_{4½}$		
1	2721.139	(20)	IV	36738.45			
1	2717.433	3		36788.56	$a^4F_{2½}-x^2F^0_{3½}$		
1	2716.689	3		36798.63			
1	2715.025	(7)	V	36821.18			
1	2712.217	4		36859.30	$a^3G_{4½}-q^3G^0_{4½}$		
1	2707.589	3		36922.30	$a^4F_{1½}-w^2F^0_{1½}$		
1	2703.904	1		36972.61	$a^4D_{3½}-p^4F^0_{3½}$		
1	2701.266	(7)	IV	37008.72			
1	2700.506	1		37019.13	$a^4F_{3½}-w^2F^0_{3½}$		
1	2700.046	4		37025.44			
1	2699.12	(20)	IV	37038.14	$a^4P_{2½}-t^4P^0_{1½}$		
1	2698.724	(40)	IV	37043.58	$a^4P_{2½}-t^4P^0_{2½}$ $(a^4D_{3½}-p^4F^0_{3½})$		
1	2697.744	(50r?)	IV	37057.03	$a^3G_{4½}-q^3G^0_{4½}$		
1	2696.996	(40r?)	IV	37067.31	$a^3G_{3½}-q^3G^0_{3½}$		
1	2696.760	(6)	IV	37070.55	$a^4D_{2½}-p^4F^0_{1½}$		
1	2696.376	1		37075.83	$a^4D_{2½}-t^3P^0_{1½}$		
1	2696.222	(5)	V	37077.95			
1	2695.235	4		37091.53	$a^4F_{4½}-v^4G^0_{4½}$		
1	2694.102	3		37107.12			
1	2693.918	6		37109.66	$a^4D_{2½}-p^4F^0_{2½}$		
1	2693.00	2		37122.31	$a^4D_{3½}-o^4D^0_{3½}$		
1	2689.350	2		37172.69	$a^4D_{1½}-p^4F^0_{1½}$		
1	2689.114	3		37175.95	$a^4D_{3½}-p^4F^0_{4½}$		
1	2688.942	4		37178.33	$a^4D_{1½}-t^3P^0_{1½}$		
	*(2688.719	(60)	V E	37181.41)	$(a^4D_{2½}-p^4F^0_{2½})$		
1	2688.55	1		37183.75	$a^4D_{2½}-o^4D^0_{1½}$		
1	2687.408	5		37199.55			
1	2687.001	1		37205.18	$a^4F_{2½}-w^2F^0_{2½}$		
1	2686.512	(10)	III	37211.96	$a^4F_{4½}-p^4G^0_{3½}$ $(a^4D_{1½}-p^4F^0_{2½})$		
1	2686.356	9		37214.11	$a^4P_{1½}-t^4P^0_{2½}$		
1	2685.843	4		37221.22	$a^4D_{2½}-o^4D^0_{2½}$		
1	2685.515	4		37225.77	$a^4P_{1½}-t^4P^0_{1½}$ $a^4P_{1½}-t^4P^0_{1½}$ $a^4D_{1½}-o^4D^0_{2½}$		
1	2685.14	(15)	III	37230.96	$a^4P_{1½}-t^4P^0_{2½}$		
1	2685.018	5		37232.66	$a^4F_{3½}-v^4G^0_{3½}$		
	*(2683.092	(80)	V E	37259.38	$(a^4D_{2½}-o^4D^0_{2½})$		
1	2682.682	1		37265.08	$a^3G_{3½}-q^3G^0_{3½}$		
1	2681.17	2		27286.09	$a^4D_{1½}-o^4D^0_{1½}$		
1	2680.939	2		37289.30	$a^4D_{3½}-o^4D^0_{3½}$		
1	2679.707	5		37306.45	$a^4P_{1½}-t^4P^0_{0½}$		
1	2678.878	10		37317.99	$a^4P_{½}-t^4P^0_{1½}$		
1	2678.674	(5)	III	37320.83	$a^4F_{3½}-v^4G^0_{4½}$		
1	2677.472	1		37337.59	$a^4F_{3½}-w^2F^0_{3½}$		
1	2677.117	(4)	III	37342.54	$a^4F_{1½}-w^2F^0_{2½}$		
1	2676.636	3		37349.25	$a^4D_{½}-o^4D^0_{1½}$		
1	2675.977	4		37358.44	$a^4D_{2½}-o^4D^0_{1½}$		
1	2675.753	(8)	III	37361.57	$a^4F_{3½}-v^4G^0_{3½}$ $a^4D_{1½}-o^4D^0_{2½}$		
1	2671.669	(10)	III	37418.68	$a^4F_{2½}-v^4G^0_{3½}$		
1	2670.918	(7)	III	37429.20	$a^4F_{3½}-w^2D^0_{3½}$		
1	2668.894	3		37457.58	$a^4F_{1½}-w^2D^0_{1½}$		
1	2665.958	(20)	III	37498.83	$a^4F_{1½}-v^4G^0_{2½}$		
1	2661.424	(7OR)	III	37562.71	$a^4F_{½}-t^4D^0_{1½}$		
1	2657.708	5		37615.23	$a^4F_{2½}-w^2D^0_{2½}$		
1	2656.55	10		37631.62			
1	2656.224	(6OR)	III	37636.24	$a^4F_{1½}-t^4D^0_{½}$		
1	2654.005	2		37667.71	$a^4F_{4½}-x^2H^0_{5½}$		
1	2653.824	(25)	IV	37670.28	$a^2H_{4½}-p^2G^0_{3½}$		
1	2652.919	(20)	IV	37683.12	$a^2H_{5½}-p^2G^0_{4½}$		
1	2651.896	(5OR)	III	37697.66	$a^4F_{2½}-t^4D^0_{1½}$		

TABLE 1.—*Arc spectrum of vanadium* (V I)—Continued

(1)	(2)	(3)	(4)	(5)	(6)	(7)	(8)
						Zeeman effect	
Ref.	λ_{air} A	Int. arc	Temp. class	ν_{vac} cm^{-1}	Term combinations	Observed	Computed
1	d2650.608	3		37715.98			
1	2648.891	6		37740.42			
1	2647.710	(40R)	III	37757.26	$a^4F_{1\frac{1}{2}}-t^4D^0_{0\frac{1}{2}}$		
1	2645.990	2		37781.80	$a^6D_{1\frac{1}{2}}-s^4D^0_{1\frac{1}{2}}$?		
1	2645.343	5		37791.04			
1	2645.256	(10)	III	37792.28	$a^4F_{2\frac{1}{2}}-t^4D^0_{2\frac{1}{2}}$		
1	2644.690	1		37800.37	$a^4F_{2\frac{1}{2}}-z^4H^0_{3\frac{1}{2}}$		
1	2643.19	5		37821.82			
1	2643.14	(5)	III	37822.53	$a^4F_{2\frac{1}{2}}-t^4D^0_{2\frac{1}{2}}$		
1	2642.289	(4)	III	37834.71	$a^4F_{1\frac{1}{2}}-t^4D^0_{1\frac{1}{2}}$		
1	2640.684	(6)	III	37857.71			
1	2640.267	(7)		37863.69			
1	d2637.222	(20H)	III	37907.40			
1	2634.864	8H?		37941.33			
1	2633.588	4		37959.71	$a^4F_{1\frac{1}{2}}-t^4D^0_{0\frac{1}{2}}$		
1	2632.398	2		37976.87	$a^4F_{4\frac{1}{2}}-u^2G^0_{4\frac{1}{2}}$		
1	2632.300	(2)	III	37978.28	$a^4F_{2\frac{1}{2}}-t^4D^0_{1\frac{1}{2}}$		
1	2629.094	5		38024.59			
1	2620.284	(20)	III	38152.43	$a^4D_{2\frac{1}{2}}-t^4P^0_{1\frac{1}{2}}$		
1	2618.908	5		38172.47	$a^6D_{1\frac{1}{2}}-u^4_{\frac{1}{2}}D^0_{2\frac{1}{2}}$		
8	2614.90	2	III	38230.98			
8	2611.75	1	III	38277.09			
1	2611.255	8		38284.34	$a^4D_{2\frac{1}{2}}-t^4P^0_{1\frac{1}{2}}$		
1	2611.031	1?		38287.62	$a^4F_{3\frac{1}{2}}-u^2G^0_{3\frac{1}{2}}$		
1	2610.891	6		38289.68	$a^4D_{2\frac{1}{2}}-t^4P^0_{2\frac{1}{2}}$		
1	2607.752	(10)	III	38335.76			
1	2607.12	7		38345.06			
1	2605.084	4		38375.02	$a^4D_{1\frac{1}{2}}-t^4P^0_{0\frac{1}{2}}$		
1	2604.294	5		38386.66	$a^4D_{1\frac{1}{2}}-t^4P^0_{1\frac{1}{2}}$		
1	2603.932	1		38392.00	$a^4D_{1\frac{1}{2}}-t^4P^0_{2\frac{1}{2}}$		
8	2602.7	1	III	38410.17			
1	2600.798	5		38438.26	$a^4D_{0\frac{1}{2}}-t^4P^0_{1\frac{1}{2}}$		
1	2600.01	2		38449.91	$a^4D_{2\frac{1}{2}}-t^4P^0_{2\frac{1}{2}}$		
1	2586.242	5h		38654.58			
1	2577.292	(20r?)	III	38788.81	$a^4F_{4\frac{1}{2}}-u^4F^0_{4\frac{1}{2}}$		
1	2574.866	3h		38825.35			
1	2574.020	(50R)	III	38838.11	$a^4F_{4\frac{1}{2}}-u^4F^0_{4\frac{1}{2}}$		
1	2570.268	4h		38894.80			
1	2568.376	30h		38923.45			
1	2564.817	(40r?)	III	38977.46	$a^4F_{3\frac{1}{2}}-u^4F^0_{3\frac{1}{2}}$ $a^2H_{4\frac{1}{2}}-r^2H^0_{4\frac{1}{2}}$		
1	2564.348	(4h)	III	38984.59			
1	2564.228	(20h)		38986.42	$a^2H_{3\frac{1}{2}}-r^2H^0_{3\frac{1}{2}}$		
1	2562.125	(60R)	III	39018.41	$a^4F_{3\frac{1}{2}}-u^4F^0_{3\frac{1}{2}}$		
1	2558.893	(15)	III	39067.69	$a^4F_{3\frac{1}{2}}-u^4F^0_{4\frac{1}{2}}$		
1	2556.815	(6)	III	39099.44	$a^4F_{3\frac{1}{2}}-w^4P^0_{2\frac{1}{2}}$		
1	2556.016	(9)	III	39111.66	$a^4F_{3\frac{1}{2}}-w^4P^0_{1\frac{1}{2}}$		
1	2554.856	(15)	III	39129.42	$a^4F_{2\frac{1}{2}}-u^4F^0_{1\frac{1}{2}}$		
1	2552.648	(50r)	III	39163.26	$a^4F_{2\frac{1}{2}}-u^4F^0_{2\frac{1}{2}}$		
1	2549.965	12		39204.46	$a^4F_{2\frac{1}{2}}-u^4F^0_{3\frac{1}{2}}$		
1	2549.834	4		39206.48			
		5					
1	2547.832	1		39237.28	$a^4F_{1\frac{1}{2}}-w^4P^0_{0\frac{1}{2}}$		
1	2547.073	6		39248.98	$a^4F_{1\frac{1}{2}}-w^4P^0_{1\frac{1}{2}}$		
1	2545.981	(30r?)	III	39266.78	$a^4F_{1\frac{1}{2}}-u^4F^0_{1\frac{1}{2}}$		
1	2543.723	(20)	III	39300.66	$a^4F_{1\frac{1}{2}}-u^4F^0_{2\frac{1}{2}}$		
1	2541.765	7		39330.93			
1	2536.932	8		39405.86			
1	2535.835	1		39422.90	$a^4F_{1\frac{1}{2}}-w^4P^0_{2\frac{1}{2}}$?		
1	2534.825	15h		39438.61			
1	2534.206	3		39448.24	$a^4F_{4\frac{1}{2}}-u^4G^0_{4\frac{1}{2}}$?		
1	2533.800	10h		39454.56			
1	2532.280	5		39478.24			
1	2531.778	3		39486.07			
1	2531.20	4h		39495.08			
1	2530.174	(80R)	III	39511.10	$a^4F_{4\frac{1}{2}}-u^4G^0_{5\frac{1}{2}}$		
1	2526.213	(100R)	III	39573.04	$a^4F_{4\frac{1}{2}}-s^4D^0_{3\frac{1}{2}}$		

TABLE 1.—*Arc spectrum of vanadium* (V I)—Continued

(1)	(2)	(3)	(4)	(5)	(6)	(7)	(8)
Ref.	λ_{air} A	Int. arc	Temp. class	ν_{vac} cm^{-1}	Term combinations	Zeeman effect: Observed	Zeeman effect: Computed
1	2523.505	5h		39615.51			
1	2522.024	1		39638.77	$a^4F_{3/2}-u^4G^0_{3/2}$		
1	2521.615	(3h)	III	39645.20			
1	2521.512	6h		39646.82			
1	2520.31	10h		39665.73			
1	2519.622	(100*R*)	III	39676.56	$a^4F_{3/2}-s^4D^0_{3/2}$ ($a^4F_{3/2}-u^4G^0_{3/2}$)		
1	2517.500	8		39710.00	$a^4F_{3/2}-z^4S^0_{3/2}$		
1	2517.142	(80*R*)	III	39715.64	$a^4F_{3/2}-u^4G^0_{3/2}$		
1	2515.649	6h		39739.22			
1	2515.145	(30*r*)	III	39747.18	$a^4F_{3/2}-p^2D^0_{3/2}$		
1	2514.41	10h		39758.79			
1	2514.322	15h		39760.18			
1	2511.940	(100*r*)	III	39797.88	$a^4F_{3/2}-s^4D^0_{3/2}$		
1	2511.642	(80*r*)	III	39802.61	$a^4F_{3/2}-s^4D^0_{5/2}$		
1	2511.182	20h		39809.90			
1	2510.242	(8)	III	39824.80	$a^4F_{3/2}-u^4G^0_{3/2}$		
1	2510.18	1		39825.79	$a^4F_{5/2}-w^4H^0_{5/2}$		
1	2508.822	5		39847.34	$a^4F_{3/2}-z^4S^0_{3/2}$		
1	2507.777	(100*R*)	III	39863.95	$a^4F_{3/2}-u^4G^0_{3/2}$ $a^4F_{3/2}-s^4D^0_{3/2}$		
1	2506.902	150*R*		39877.86	$a^4F_{3/2}-s^4D^0_{5/2}$		
1	2506.482	6		39884.54	$a^4F_{3/2}-p^2D^0_{3/2}$		
1	2505.540	(15)	III	39899.54	$a^4F_{5/2}-w^4H^0_{5/2}$		
1	2504.382	1		39917.98	$a^6D_{3/2}-r^4D^0_{3/2}$		
1	2503.912	2		39925.47	$a^6D_{3/2}-2^0_{3/2}$		
1	2503.300	(50*r*)	III	39935.24	$a^4F_{3/2}-s^4D^0_{3/2}$		
1	2501.608	(60*R*)	III	39962.25	$a^4F_{3/2}-u^4G^0_{3/2}$		
1	2500.382	5		39981.84	$a^4F_{3/2}-p^2D^0_{3/2}$		
1	2499.959	8		39988.60	$a^4F_{3/2}-s^4D^0_{3/2}$		
1	2499.778	2		39991.50	$a^4F_{3/2}-w^4H^0_{3/2}$		
1	2499.244	(12)	III	40000.05	$a^4H_{3/2}-s^4D^0_{3/2}$		
1	2499.094	15		40002.44	$a^4F_{3/2}-u^2D^0_{3/2}$		
1	2498.232	(20h)	III	40016.25	$a^4F_{3/2}-p^2F^0_{3/2}$		
1	2498.024	(10h)	III	40019.58			
1	2497.655	6h		40025.49	$a^6D_{3/2}-r^4D^0_{5/2}$		
1	2497.099	2		40034.40	$a^4F_{5/2}-p^2F^0_{5/2}$		
1	2495.787	20		40055.44	$a^4F_{3/2}-w^4H^0_{5/2}$		
1	2491.815	2		40119.29	$a^4F_{3/2}-p^2D^0_{3/2}$		
1	2489.13	4h		40162.56	$a^6D_{4/2}-w^6D^0_{3/2}$?		
1	2488.737	4h		40168.90	$a^6D_{3/2}-w^6D^0_{3/2}$?		
1	2488.203	5		40177.52	$a^4F_{3/2}-w^4H^0_{3/2}$		
1	2487.528	10		40188.43	$a^4F_{3/2}-u^2D^0_{3/2}$		
1	2483.636	(7h)	III	40251.40			
1	2482.864	2		40263.91	$a^4F_{3/2}-p^2F^0_{3/2}$		
1	2482.711	(15h)	III	40266.39			
1	2482.115	(20h)	III	40276.06	$a^6D_{3/2}-w^6D^0_{3/2}$?		
1	2481.28	3h		40289.61			
1	2481.11	10h		40292.37			
1	2480.606	(30h)	III	40300.56	$a^6D_{4/2}-w^6D^0_{3/2}$?		
1	2478.97	5h		40327.15	$a^6D_{1/2}-w^6D^0_{3/2}$?		
1	2476.510	8h		40367.21	$a^6D_{2/2}-w^6D^0_{3/2}$?		
1	2475.178	10		40388.93			
1	2473.652	5h		40413.84	$a^6D_{2/2}-w^6D^0_{3/2}$?		
1	2473.527	6		40415.89			
1	2471.443	10		40449.96	$a^4F_{3/2}-p^2F^0_{3/2}$		
1	2468.138	3		40504.13			
1	2465.664	10h		40544.76			
1	2464.953	2		40556.46	$a^4F_{3/2}-w^2P^0_{3/2}$		
1	2445.224	3		40883.66	$a^4F_{5/2}-t^2G^0_{7/2}$		
1	2441.892	(30)	III	40939.44	$a^4F_{5/2}-t^4F^0_{7/2}$		
1	2441.352	(15)	III	40948.49	$a^4F_{5/2}-s^2H^0_{5/2}$		
1	2439.102	(50*r*)	III	40986.26	$a^4F_{5/2}-t^2G^0_{7/2}$		
1	2435.518	(100*R*)	III	41046.57	$a^4F_{5/2}-t^4F^0_{7/2}$		
1	2432.014	(25r?)	III	41105.71	$a^4F_{3/2}-t^4F^0_{5/2}$		
1	2431.940	20r?		41106.96	$a^4F_{5/2}-s^2H^0_{5/2}$		
1	2431.568	10		41113.24	$a^4F_{3/2}-t^2G^0_{5/2}$		

TABLE 1.—*Arc spectrum of vanadium* (V I)—Continued

(1)	(2)	(3)	(4)	(5)	(6)	(7)	(8)
						Zeeman effect	
Ref.	λ_{air} A	Int. arc	Temp. class	ν_{vac} cm^{-1}	Term combinations	Observed	Computed
1	2428.269	(100*R*)	III	41169.09	$a^4F_{3\frac{1}{2}}-t^4F_{3\frac{1}{2}}$		
1	2427.735	20		41178.15	$a^4F_{2\frac{1}{2}}-z^2H_{3\frac{1}{2}}$		
1	2426.126	15		41205.46	$a^4F_{4\frac{1}{2}}-t^4G_{5\frac{1}{2}}$		
1	2423.370	40r?		41252.31	$a^4F_{2\frac{1}{2}}-t^4F_{1\frac{1}{2}}$		
1	2421.976	(140*R*)	III	41276.05	$a^4F_{3\frac{1}{2}}-t^4F_{4\frac{1}{2}}$		
1	2421.058	(120*R*)	III	41291.70	$a^4F_{2\frac{1}{2}}-t^4F_{2\frac{1}{2}}$		
1	2420.614	3		41299.28	$a^4F_{2\frac{1}{2}}-t^4G_{3\frac{1}{2}}$		
1	2420.221	8		41305.98			
1	2420.115	(100*R*)	III	41307.79	$a^4F_{4\frac{1}{2}}-t^4G_{4\frac{1}{2}}$		
1	2418.738	15		41331.31	$a^4F_{3\frac{1}{2}}-t^4G_{3\frac{1}{2}}$		
1	2417.351	(100*R*)	III	41355.02	$a^4F_{2\frac{1}{2}}-t^4F_{1\frac{1}{2}}$		
1	2416.748	(150*R*)	III	41365.34	$a^4F_{4\frac{1}{2}}-t^4G_{4\frac{1}{2}}$		
1	2415.326	(110*R*)	III	41389.69	$a^4F_{1\frac{1}{2}}-t^4F_{1\frac{1}{2}}$		
1	2413.031	(60*R*)	III	41429.05	$a^4F_{1\frac{1}{2}}-t^4F_{2\frac{1}{2}}$		
1	2412.686	(80*R*)	III	41434.97	$a^4F_{2\frac{1}{2}}-t^4G_{3\frac{1}{2}}$		
1	2411.590	5*h*		41453.80			
1	2410.768	2		41467.94	$a^4F_{4\frac{1}{2}}-u^2F_{3\frac{1}{2}}$		
1	2409.721	7		41485.95			
1	2407.900	(40*R*)	III	41517.32	$a^4F_{2\frac{1}{2}}-t^4G_{3\frac{1}{2}}$		
1	2407.517	5		41523.93			
1	2407.389	2		41526.14	$a^4F_{1\frac{1}{2}}-u^2H_{3\frac{1}{2}}$		
1	2406.748	(50*R*)	III	41537.20	$a^4F_{3\frac{1}{2}}-t^4G_{4\frac{1}{2}}$		
1	2405.733	6		41554.72	$a^6D_{1\frac{1}{2}}-x^6F_{2\frac{1}{2}}$?		
1	2405.494	8		41558.85			
1	2405.245	10*h*		41563.15	$a^6D_{4\frac{1}{2}}-x^6P_{3\frac{1}{2}}$?		
1	2404.544	5*h*		41575.26			
1	2403.362	5*h*		41595.71	$a^6D_{5\frac{1}{2}}-x^6F_{5\frac{1}{2}}$?		
1	2403.029	10*h*		41601.47	$a^6D_{4\frac{1}{2}}-x^6F_{3\frac{1}{2}}$?		
1	2401.901	(60*R*)	IV	41621.01	$a^4F_{2\frac{1}{2}}-t^4G_{3\frac{1}{2}}$		
1	2401.555	1		41627.00	$a^4F_{3\frac{1}{2}}-u^2F_{3\frac{1}{2}}$		
1	2401.450	3		41628.83			
1	2399.954	(50*R*)	IV	41654.77	$a^4F_{1\frac{1}{2}}-t^4G_{2\frac{1}{2}}$		
1	2398.877	4		41673.47	$a^2G_{4\frac{1}{2}}-p^2G_{3\frac{1}{2}}$		
1	2398.697	10*h*		41676.60	$a^6D_{3\frac{1}{2}}-x^6P_{2\frac{1}{2}}$?		
1	2398.277	20*h*		41683.89	$a^4F_{4\frac{1}{2}}-2_{3\frac{1}{2}}$		
1	2398.134	20		41686.38	$a^4F_{3\frac{1}{2}}-s^4P_{2\frac{1}{2}}$		
1	2397.775	40*h*		41692.62	$\begin{cases} a^4F_{4\frac{1}{2}}-r^4D_{3\frac{1}{2}} \\ a^6D_{1\frac{1}{2}}-x^6F_{1\frac{1}{2}}? \end{cases}$		
1	2397.496	4		41697.48	$a^4F_{2\frac{1}{2}}-u^2F_{2\frac{1}{2}}$		
1	2396.706	8		41711.22	$a^4F_{2\frac{1}{2}}-s^4P_{1\frac{1}{2}}$		
1	2396.492	15*h*		41714.94	$a^6D_{2\frac{1}{2}}-x^6F_{3\frac{1}{2}}$?		
1	2396.089	1		41721.96	$a^6D_{1\frac{1}{2}}-t^2F_{2\frac{1}{2}}$		
1	2395.429	10*h*		41733.45	$a^6D_{4\frac{1}{2}}-x^6F_{4\frac{1}{2}}$?		
1	2395.104	30*h*		41739.11	$a^6D_{2\frac{1}{2}}-x^6F_{2\frac{1}{2}}$?		
1	2394.270	10		41753.65	$a^6D_{4\frac{1}{2}}-s^4G_{3\frac{1}{2}}$		
1	2394.152	2		41755.71	$a^4F_{3\frac{1}{2}}-u^2H_{4\frac{1}{2}}$		
1	2392.898	40*h*		41777.59	$a^6D_{4\frac{1}{2}}-x^6F_{4\frac{1}{2}}$ 4½?		
1	2392.00	1		41793.27	$a^6D_{3\frac{1}{2}}-s^4G_{4\frac{1}{2}}$		
1	2391.268	30*h*		41806.07	$\begin{cases} a^6D_{3\frac{1}{2}}-x^6F_{3\frac{1}{2}}? \\ a^6D_{1\frac{1}{2}}-x^6F_{2\frac{1}{2}}? \end{cases}$		
1	2390.868	4		41813.06	$a^4F_{2\frac{1}{2}}-u^2F_{2\frac{1}{2}}$		
1	2390.774	30		41814.70	$a^4F_{3\frac{1}{2}}-r^4D_{2\frac{1}{2}}$		
1	2388.910	40		41847.33	$a^2G_{4\frac{1}{2}}-p^2G_{3\frac{1}{2}}$		
1	2388.084	35		41861.80	$a^4F_{2\frac{1}{2}}-r^4D_{1\frac{1}{2}}$		
1	2387.780	8		41867.13			
1	2387.475	5		41872.48	$a^4F_{3\frac{1}{2}}-s^4P_{2\frac{1}{2}}$		
1	2386.956	40		41881.58	$a^2G_{4\frac{1}{2}}-p^2G_{3\frac{1}{2}}$		
1	2386.409	20*h*		41891.18	$a^6D_{2\frac{1}{2}}-x^6F_{3\frac{1}{2}}$?		
1	2385.14	2*h*		41913.47	$a^4F_{3\frac{1}{2}}-2_{2\frac{1}{2}}$		
1	2384.64	5		41922.25	$a^4F_{3\frac{1}{2}}-r^4D_{2\frac{1}{2}}$		
1	2384.286	20		41928.48	$a^4F_{1\frac{1}{2}}-r^4D_{2\frac{1}{2}}$		
1	2383.038	3		41950.43	$a^4F_{1\frac{1}{2}}-u^2F_{2\frac{1}{2}}$		

TABLE 1.—*Arc spectrum of vanadium* (V I)—Continued

(1)	(2)	(3)	(4)	(5)	(6)	(7)	(8)
Ref.	λ_{air} A	Int. arc	Temp. class	ν_{vac} cm^{-1}	Term combinations	Zeeman effect	
						Observed	Computed
1	2380.266	8		41999.28	$a^4F_{1½}-r^4D_{1½}$		
1	2380.178	5		42000.83	$a^4F_{2½}-r^4D_{2½}$		
1	2378.262	4		42034.67			
1	2377.083	3		42055.52	$a^3G_{3½}-p^3G_{3½}$		
1	2372.43	1?		42137.99	$a^4F_{1½}-r^4D_{½}$		
1	2370.00	1?		42181.19	$a^4F_{3½}-z^3P_{1½}$		
1	2355.441	1		42441.89	$a^5D_{0½}-p^4D_{½}$		
1	2347.026	10		42594.05	$a^4F_{4½}-s^4F_{3½}$		
1	2340.479	(50 r)	IV	42713.19	$a^4F_{4½}-s^4F_{4½}$		
1	2339.673	20		42727.90	$a^4F_{3½}-s^4F_{3½}$		
1	2334.434	40 r		42823.78	$a^4F_{3½}-s^4F_{3½}$		
1	2333.33	20		42844.04	$a^4F_{2½}-s^4F_{2½}$		
1	2329.529	30		42913.94	$a^4F_{2½}-s^4F_{1½}$		
1	2327.970	10		42942.68	$a^4F_{3½}-s^4F_{4½}$		
1	2325.873	30		42981.39	$a^4F_{1½}-s^4F_{1½}$		
1	2324.748	40		43002.19	$a^4F_{4½}-q^4D_{3½}$		
1	2324.347	6		43009.61	$a^4F_{3½}-s^4F_{3½}$		
1	2324.189	10		43012.53	$a^3D_{3½}-s^3P_{1½}$?		
1	2322.096	15		43051.30	$a^4F_{1½}-s^4F_{1½}$		
1	2321.072	5		43070.29			
1	2320.156	25		43087.29	$a^4F_{3½}-q^4D_{3½}$		
1	2316.751	25		43150.61	$a^3G_{4½}-r^3H_{3½}$		
1	2315.634	30		43171.43	$a^4F_{2½}-q^4D_{1½}$		
1	2314.691	20		43189.01	$a^3G_{3½}-r^3H_{3½}$		
1	2312.531	10		43229.34	$a^3D_{1½}-s^3P_{0½}$?		
1	2312.410	8		43231.61	$a^4F_{2½}-q^4D_{2½}$		
1	2311.465	30		43249.28	$a^4F_{1½}-q^4D_{½}$		
1	2310.958	5		43258.77			
1	2310.180	20		43273.33	$a^4F_{2½}-q^4D_{1½}$		
1	2308.287	15		43308.82	$a^4F_{1½}-q^4D_{1½}$		
1	2307.66	1?		43320.59	$a^4F_{4½}-t^3F_{3½}$		
1	2304.349	4		43382.83			
1	2302.87	1		43410.68	$a^4F_{1½}-q^4D_{2½}$		
1	2302.531	4		43417.08	$a^4F_{2½}-q^4D_{2½}$?		
1	2299.544	3		43473.47	$a^4F_{4½}-x^4F_{3½}$?		
1	2299.337	5		43477.38			
1	2295.414	4		43551.68	$a^4F_{3½}-t^3F_{3½}$ $a^4F_{4½}-s^4G_{4½}$?		
1	2293.243	2		43592.90	$a^4F_{4½}-t^3H_{4½}$		
1	2291.527	10		43625.54	$a^4F_{4½}-s^4G_{3½}$		
1	2290.263	2		43649.62	$a^4F_{4½}-x^4F_{4½}$, $_{3½}$? $a^5D_{0½}-o^4D_{1½}$?		
1	2286.581	8		43719.90	$a^4F_{3½}-s^4G_{3½}$		
1	2284.982	3		43750.49	$a^3P_{0½}-s^3P_{1½}$?		
1	2284.494	20		43759.84	$a^3P_{1½}-s^3P_{0½}$?		
1	2283.382	10		43781.14	$a^4F_{3½}-s^4G_{4½}$		
1	2279.92	4		43847.62			
1	2279.152	4		43862.39	$a^4F_{3½}-s^4G_{2½}$		
1	2276.889	6		43905.98	$a^4F_{2½}-s^4G_{3½}$		
1	2276.661	3		43910.38	$a^4F_{4½}-s^4G_{4½}$		
1	2275.475	3		43933.26	$a^3P_{1½}-s^3P_{0½}$?		
1	2272.048	4		43999.51	$a^4F_{1½}-s^4G_{2½}$		
1	[c]2264.39	30? Fe?		44148.31	$a^4F_{4½}-p^4D_{3½}$		
1	2263.17	1		44172.11	$a^4F_{3½}-s^3G_{3½}$		
1	[c]2258.805	9		44251.46			
1	[c]2256.968	50r		44293.48	$a^4F_{3½}-p^4D_{3½}$		
1	2252.681	5		44377.76	$a^4F_{3½}-p^4D_{2½}$		
1	2250.672	30r?		44417.37	$a^4F_{3½}-p^4D_{1½}$		
1	2247.520	0		44479.66	$a^4F_{2½}-p^4D_{2½}$		
1	2246.204	1		44505.71	$a^4F_{4½}-r^4F_{3½}$		
1	2245.756	30		44514.59	$a^4F_{1½}-p^4D_{2½}$		
1	2243.742	8h		44554.54	$a^4F_{1½}-p^4D_{1½}$		

TABLE 1.—*Arc spectrum of vanadium* (V I)—Continued

(1)	(2)	(3)	(4)	(5)	(6)	(7)	(8)
Ref.	λ_{air} A	Int. arc	Temp. class	ν_{vac} cm^{-1}	Term combinations	Zeeman effect: Observed	Zeeman effect: Computed
1	2243.258	6		44564.16			
1	2242.614	5		44576.95			
1	2241.846	40r		44592.21	$a^4F_{4½}-r^4F_{3½}$		
1	2241.213	7		44604.81	$a^4F_{4½}-q^4F_{3½}$		
1	2240.302	2		44622.95	$a^4F_{4½}-r^2G_{3½}$		
1	2237.228	50r		44684.26	$a^4F_{4½}-q^4F_{4½}$		
1	2234.680	10		44735.20	$a^4F_{3½}-r^4F_{3½}$		
1	2232.252	8		44783.85	$a^4F_{3½}-q^4F_{3½}$		
1	2231.412	30		44800.71			
1	2230.362	20		44821.80	$a^4F_{3½}-r^4F_{3½}$		
1	[d]2229.734	25r?		44834.42	$a^4F_{3½}-q^4F_{3½}$		
1	2228.835	15		44852.51	$a^4F_{3½}-r^2G_{3½}$		
1	2227.398	3		44881.44			
1	2225.787	10		44913.92	$a^4F_{2½}-q^4F_{3½}$; $a^4F_{2½}-r^4F_{2½}$		
1	2225.422	30		44921.29	$a^4F_{3½}-r^4F_{3½}$		
1	2225.029	8		44929.42	$a^4F_{3½}-q^4F_{4½}$		
1	2223.014	20		44969.94	$a^4F_{2½}-q^4F_{3½}$		
1	2222.834	15		44973.58	$a^4F_{3½}-r^4F_{4½}$		
1	2220.450	3		45021.86	$a^4F_{3½}-u^2P_{1½}$		
1	2219.652	3		45038.04	$a^4F_{3½}-r^2G_{4½}$		
1	2218.238	25r		45066.75	$a^4F_{1½}-q^4F_{2½}$		
1	2216.666	10		45098.71			
1	2216.245	4		45107.27	$a^4F_{1½}-q^4F_{2½}$		
1	2216.054	3		45111.16			
1	2213.692	10		45159.29	$a^4F_{1½}-u^2P_{1½}$		
1	2211.350	3		45207.11	$a^4F_{4½}-p^4F_{3½}$		
1	2210.878	5		45216.76			
1	2207.976	3		45276.18			
1	2204.930	12		45338.72	$a^4F_{4½}-p^4F_{4½}$		
1	2203.658	4		45364.89	$a^4F_{3½}-p^4F_{3½}$		
1	2202.724	60r		45384.13	$a^4F_{4½}-o^4D_{3½}$		
1	2200.174	15		45436.72	$a^4F_{3½}-p^4F_{3½}$		
1	2196.56	2?		45511.47	$a^4F_{3½}-p^4F_{4½}$		
1	2196.40	40r?		45514.78	$a^4F_{3½}-o^4D_{3½}$		
1	2196.29	5		45517.06	$a^4F_{3½}-t^2P_{1½}$		
1	2194.65	10		45551.07	$a^4F_{3½}-p^4F_{2½}$		
1	2193.82	5		45568.30	$a^4F_{3½}-p^4F_{3½}$		
1	2193.47	6		45575.57			
1	2191.65	3		45613.42	$a^4F_{3½}-o^4D_{3½}$		
1	2191.10	30		45624.87	$a^4F_{3½}-o^4D_{3½}$; $(a^4F_{3½}-p^4F_{3½})$		
1	2189.95	6		45648.83	$a^4F_{1½}-p^4F_{1½}$		
1	2189.68	2?		45654.45	$a^4F_{1½}-t^2P_{1½}$		
1	2188.06	3?		45688.26	$a^4F_{1½}-p^4F_{2½}$		
1	2187.95	15		45690.55	$a^4F_{4½}-r^4G_{4½}$		
1	2187.39	10		45702.24	$a^4F_{1½}-o^4D_{2½}$		
1	2184.53	2		45762.07	$a^4F_{1½}-o^4D_{1½}$		
1	2182.22	120R		45810.50	$a^4F_{4½}-r^4G_{5½}$		
1	2181.97	20		45815.76	$a^4F_{3½}-r^4G_{4½}$		
1	2177.24	10		45915.27	$a^4F_{3½}-r^4G_{3½}$		
1	2177.00	100R		45920.33	$a^4F_{3½}-r^4G_{4½}$		
1	2173.15	80R		46001.68	$a^4F_{3½}-r^4G_{3½}$		
1	2172.75	7		46010.14			
1	2170.74	60R		46052.75	$a^4F_{1½}-r^4G_{2½}$		
1	2169.85	8		46071.63			
1	2164.88	5		46177.39			
1	2158.12	6		46322.01			
1	2147.58	5h		46549.33			
1	2146.64	3		46569.71			
1	2138.60	3		46744.77			
1	2132.89	4		46869.89			

TABLE 1.—*Arc spectrum of vanadium* (V I)—Continued

(1)	(2)	(3)	(4)	(5)	(6)	(7)	(8)
						Zeeman effect	
Ref.	λ_{air} A	Int. arc	Temp. class	ν_{vac} cm^{-1}	Term combinations	Observed	Computed
1	2125.83	3		47025.53			
1	2106.32	3		47461.05			
1	2104.56	3		47500.75			
1	2102.21	3		47553.83			
1	2100.75	6		47586.88	$a^4F_{4½}-o^4F_{3½}$		
1	2100.51	8		47592.31	$a^4F_{3½}-o^4F_{3½}$		
1	2098.50	3h		47637.89			
1	2097.34	7		47664.24	$a^4F_{2½}-o^4F_{1½}$		
1	2096.16	8		47691.07			
1	2095.75	8		47700.39			
1	2094.70	25r?		47724.30			
1	2092.44	60r		47775.84	$a^4F_{4½}-o^4F_{4½}$		
1	2092.30	10r		47779.04	$a^4F_{3½}-o^4F_{3½}$		
1	2091.29	20r		47802.11	$a^4F_{1½}-o^4F_{1½}$		
1	2090.90	5		47811.03			
1	2090.64	20r		47816.97	$a^4F_{3½}-o^4F_{3½}$		
1	2089.89	2h		47834.13	$a^4F_{3½}-g^2G_{4½}$		
1	2088.56	15r?		47864.59			
1	2086.55	3		47910.69			
1	2086.31	8		47916.20	$a^4F_{1½}-o^4F_{3½}$		
1	2082.49	20r?		48004.08	$a^4F_{2½}-o^4F_{2½}$ $a^4F_{1½}-o^4F_{1½}$		

NOTES TO TABLE 1

a=*g* for higher level calculated from this line.
b=Observed and calculated Zeeman effects discordant.
c=Fe masks V line.
d=Blend with V II line.
e=Masked by V II line.
f=Ni masks V line.
g=Zeeman effect changed by self-reversal.

The total number of lines appearing in table 1 is 2,525; it includes all classified lines, and practically all unclassified lines since the latter are omitted only when they are suspected of molecular origin or rest on a single observer and have low intensity (2 or less). This list may, therefore, be regarded as a complete compilation of all data pertaining to spectral lines characteristic of neutral vanadium atoms, in the wave-length interval 2000 to 12000 A or, in other words, the entire range observable photographically with large-scale spectrographs in air. Since only 87 percent of the total number of lines are classified, this analysis, strictly speaking, is still incomplete. However, the main features of the V I spectrum are now revealed, and further efforts at analysis are deemed unprofitable without considerable additions to the observational material.

2. TERMS OF THE V I SPECTRUM

The established terms of the V I spectrum are collected in table 2 in order of increasing magnitude beginning with the normal state $a^4F_{1½}=0.00$. Successive columns contain the electron configuration responsible for the term, term symbols, level values, level separations, or intervals, *g*-values derived from observed Zeeman effects and

observed combinations. The total number of levels is 453, comprising 148 terms. These numbers are divided among multiplicities as follows: 113 doublet levels or 60 terms; 219 quartet levels or 60 terms; 118 sextet levels or 28 terms; 3 levels remaining unassigned to terms; and 10 terms lacking their full quota of levels. A large majority of the terms are regular, only 14 being wholly or partially inverted. Landé's interval rules are reasonably well obeyed, as is shown by the examples in table 3, but there are noteworthy exceptions, such as $z^4H°$, $w^4D°$, $v^4F°$, $w^4G°$, $x^4H°$, $u^4G°$, $t^4G°$, g^6F, etc. In some cases (e. g., $w^4D°$, $v^4F°$, $w^4P°$), the deviations are apparently the result of perturbations also accounting for anomalous g values, but there are other cases of g-sharing (e. g., $z^6D°$, $z^6F°$) unaccompanied by any marked distortion of intervals.

Magnetic splitting factors (g-values) for 346 levels are entered in column (5) of table 2. These may readily be compared with Landé values by referring to the tables cited above [34] or to the paper [25] in which observed values of g, g-sums and anomalies for V I levels have been discussed in detail.

All of the observed combinations of each term are indicated in the final column of table 2, which may serve to exhibit the combining properties in lieu of a diagram of transitions. The total number of multiplets is 634, the combinations of various types being as follows: doublet 174; quartet 210; sextet 52; doublet-quartet 156; quartet-sextet 34; and doublet-sextet 8. In addition, there are 10 combinations with the 3 miscellaneous odd levels, and 4 combinations in which the observed lines of V I are believed to mask those of the multiplet in question. Combinations in parentheses have their lines masked.

TABLE 2.—*Terms of the* V I *spectrum*

Electron configuration	Term symbol	Level	Difference	Observed g	Combinations
					($x^4S°$, $z^4P°$, $w^4P°$, $s^4P°$, $z^4D°$, $y^4D°$, $z^4D°$, $w^4D°$, $v^4D°$, $u^4D°$, $t^4D°$, $s^4D°$, $r^4D°$, $q^4D°$, $p^4D°$, $o^4D°$, $z^4F°$, $y^4F°$, $x^4F°$, $w^4F°$, $s^4F°$, $u^4F°$, $t^4F°$, $s^4F°$, $r^4F°$, $q^4F°$, $p^4F°$, $o^4F°$, $z^4G°$, $y^4G°$, $x^4G°$, $w^4G°$, $v^4G°$, $u^4G°$, $t^4G°$, $s^4G°$, $r^4G°$, $z^4H°$, $w^4H°$, $z^2P°$, $w^2P°$, $v^2P°$, $u^2P°$, $t^2P°$, $z^2D°$, $y^2D°$, $x^2D°$, $w^2D°$, $v^2D°$, $u^2D°$, $z^2F°$, $y^2F°$, $x^2F°$, $w^2F°$, $v^2F°$, $u^2F°$, $t^2F°$, $z^2G°$, $y^2G°$, $x^2G°$, $v^2G°$, $u^2G°$, $t^2G°$, $s^2G°$, $r^2G°$, $q^2G°$, $z^2H°$, $y^2H°$, $x^2H°$, $v^2H°$, $u^2H°$, $t^2H°$, $z^2P°$, $y^2P°$, $z^2D°$, $y^2D°$, $x^2D°$, $z^2F°$, $y^2F°$, $x^2F°$, $z^2G°$, 1°, 2°.
d^2s^2	$a^4F_{1½}$	0.00	137.38	0.40	
	$a^4F_{2½}$	137.38	186.04	1.01	
	$a^4F_{3½}$	323.42	229.60	1.20	
	$a^4F_{4½}$	553.02		1.28	
$d^4s(^5D)$	$a^6D_{0½}$	2112.32	40.88	3.29	($z^6P°$, $y^6P°$, $x^6P°$, $z^6D°$, $y^6D°$, $x^6D°$, $w^6D°$, $z^6F°$, $y^6F°$, $x^6F°$, $z^6S°$, $u^6D°$, $w^2F°$, $t^2F°$, $z^2G°$, $z^4P°$, $y^4D°$, u^6D^c, t^6D^c, $s^6D°$, $r^6D°$, $p^6D°$, o^6D^c, $z^6F°$, $y^6F°$, $x^6F°$, $s^4G°$, $2°$.
	$a^6D_{1½}$	2153.20	66.93	1.82	
	$a^6D_{2½}$	2220.13	91.24	1.61	
	$a^6D_{3½}$	2311.37	113.52	1.53	
	$a^6D_{4½}$	2424.89		1.52	
$d^4s(^5D)$	$a^4D_{0½}$	8412.94	63.26	0.00	($z^4P°$, $y^4P°$, $x^4P°$, $w^4P°$, $s^4P°$, $u^4P°$, $t^4P°$, $z^4D°$, $y^4D°$, $x^4D°$, $w^4D°$, $s^4D°$, $u^4D°$, $t^4D°$, $s^4D°$, $r^4D°$, $q^4D°$, $p^4D°$, $o^4D°$, $z^4F°$, $y^4F°$, $x^4F°$, $w^4F°$, $s^4F°$, $u^4F°$, $t^4F°$, $s^4F°$, $q^4F°$, $p^4F°$, $s^4G°$, $z^2S°$, z^2S^c, $z^2P°$, $y^2P°$, z^2P^c, y^2D^c, $x^2D°$, $w^2D°$, $s^2D°$, $z^2F°$, $y^2F°$, $z^2G°$, $z^2S°$, $x^2P°$, $x^2D°$, $y^2D°$, $y^2F°$, $1°$.
	$a^4D_{1½}$	8476.20	102.32	1.19	
	$a^4D_{2½}$	8578.52	137.20	1.35	
	$a^4D_{3½}$	8715.72		1.39	
d^2s^2	$a^4P_{0½}$	9544.54	92.42	2.59	($y^4S°$, $x^4S°$, $w^4S°$, $z^4P°$, $y^4P°$, $x^4P°$, $w^4P°$, $s^4P°$, $u^4P°$, $t^4P°$, $z^4D°$, $y^4D°$, $x^4D°$, $w^4D°$, $s^4D°$, $t^4D°$, $s^4D°$, $r^4D°$, $q^4D°$, $p^4D°$, $o^4D°$, $z^4F°$, $w^4F°$, $v^4F°$, $u^4F°$, $t^4F°$, $w^2S°$, $v^2P°$, $y^2D°$, $w^2D°$, $v^2D°$, $z^2F°$, $z^2S°$, $x^2P°$, $1°$, $2°$.
	$a^4P_{1½}$	9636.96	187.02	1.70	
	$a^4P_{2½}$	9824.58		1.55	
d^2s^2	$a^2G_{3½}$	10892.50	208.15	0.88	($x^2D°$, $z^2F°$, $y^2F°$, $x^2F°$, $w^2F°$, $v^2F°$, $u^2F°$, $t^2F°$, $s^2F°$, $z^2G°$, $y^2G°$, $x^2G°$, $w^2G°$, $v^2G°$, $u^2G°$, $t^2G°$, $s^2G°$, $r^2G°$, $q^2G°$, $p^2G°$, $z^2H°$, $y^2H°$, $x^2H°$, $v^2H°$, $u^2H°$, $t^2H°$, $s^2H°$, $r^2H°$, $z^2I°$, $t^2D°$, $y^4F°$, $x^4F°$, $w^4G°$, $t^4G°$, $x^4H°$, $y^4H°$, $x^4H°$, $x^4I°$, $y^4F°$.
	$a^2G_{4½}$	11100.65		1.13	

TABLE 2.—*Terms of the* V I *spectrum*—Continued

Electron configuration	Term symbol	Level	Difference	Observed g	Combinations
d^3s^2	$a^2P_{1½}$	13801.53	−9.37	1.20	$z^2S°$, $y^2S°$, $z^2S°$, $w^2S°$, $v^2S°$, $z^2P°$, $y^2P°$, $x^2P°$, $s^2P°$, $u^2P°$, $t^2P°$, $s^2P°$, $z^2D°$, $y^2D°$, $x^2D°$, $w^2D°$, $v^2D°$, $u^2D°$, $t^2D°$, $x^2F°$, $w^2F°$, $u^2F°$, $t^2F°$, $s^2F°$, $(y^4S°)$, $w^4D°$, $v^4D°$, $s^4D°$, $v^4F°$, $p^4F°$, $z^6P°$, $x^6D°$.
	$a^4P_{0½}$	13810.90		0.64	
d^3s^2	$a^2D_{1½}$	14514.75	34.08	0.97	$y^2S°$, $z^2P°$, $y^2P°$, $x^2P°$, $w^2P°$, $s^2P°$, $t^2P°$, $s^2P°$, $y^2D°$, $x^2D°$, $w^2D°$, $v^2D°$, $u^2D°$, $t^2D°$, $z^2F°$, $y^2F°$, $x^2F°$, $w^2F°$, $v^2F°$, $u^2F°$, $t^2F°$, $s^2F°$, $y^2G°$, $v^2G°$, $y^4P°$, $u^4P°$, $x^4D°$, $t^4D°$, $v^4F°$, $q^4F°$, $p^4F°$, $s^4G°$.
	$a^2D_{2½}$	14548.83		1.17	
$d^4s(^3H)$	$a^4H_{3½}$	14910.04	39.26	0.65	$y^4F°$, $u^4F°$, $t^4F°$, $y^4G°$, $x^4G°$, $w^4G°$, $v^4G°$, $u^4G°$, $t^4G°$, $r^4G°$, $z^4H°$, $y^4H°$, $x^4H°$, $w^4H°$, $z^4I°$, $v^2G°$, $z^2H°$, $y^2H°$, $x^2H°$, $v^2H°$, $z^2I°$, $y^2I°$, $x^2I°$.
	$a^4H_{4½}$	14949.30	51.54	0.94	
	$a^4H_{5½}$	15000.84	62.10	1.10	
	$a^4H_{6½}$	15062.94		1.18	
$d^4s(^3P)$	$b^4P_{0½}$	15078.25	192.17	2.60	$z^4S°$, $y^4S°$, $x^4S°$, $w^4S°$, $z^4P°$, $y^4P°$, $x^4P°$, $w^4P°$, $v^4P°$, $t^4P°$, $y^4D°$, $x^4D°$, $w^4D°$, $v^4D°$, $u^4D°$, $t^4D°$, $s^4D°$, $r^4D°$, $q^4D°$, $p^4D°$, $y^4F°$, $v^4F°$, $s^4F°$, $z^2P°$, $x^2P°$, $x^2D°$, $v^2D°$, $w^2F°$, $z^6P°$, $x^6D°$.
	$b^4P_{1½}$	15270.42	301.48	1.68	
	$b^4P_{2½}$	15571.90		1.54	
d^3s^2	$a^2H_{4½}$	15103.77	161.06	0.90	$x^2F°$, $w^2F°$, $z^2G°$, $x^2G°$, $w^2G°$, $v^2G°$, $u^2G°$, $t^2G°$, $s^2G°$ $r^2G°$, $q^2G°$, $p^2G°$, $(z^2H°)$, $y^2H°$, $x^2H°$, $w^2H°$, $v^2H°$, $u^2H°$, $t^2H°$, $s^2H°$, $r^2H°$, $z^2I°$, $y^2I°$, $x^2I°$, $y^4F°$, $t^4F°$, $q^4F°$, $w^4G°$, $u^4G°$, $x^4H°$, $z^4I°$.
	$a^2H_{5½}$	15264.83		1.07	
$d^4s(^3F)$	$b^4F_{1½}$	15664.75	24.05	0.39	$x^4P°$, $y^4D°$, $x^4D°$, $w^4D°$, $t^4D°$, $s^4D°$, $r^4D°$, $q^4D°$, $p^4D°$, $o^4D°$, $y^4F°$, $x^4F°$, $w^4F°$, $v^4F°$, $u^4F°$, $t^4F°$, $r^4F°$, $q^4F°$, $p^4F°$, $y^4G°$, $x^4G°$, $w^4G°$, $v^4G°$, $u^4G°$, $t^4G°$, $s^4G°$, $u^2P°$, $t^2P°$, $u^2D°$, $y^2F°$, $x^2F°$, $w^2F°$, $t^2F°$, $z^2G°$, $y^2G°$, $x^2G°$, $v^2G°$, $t^2G°$, $x^2H°$, $v^2H°$, $z^6F°$.
	$b^4F_{2½}$	15688.80	35.42	1.05	
	$b^4F_{3½}$	15724.22	46.50	1.22	
	$b^4F_{4½}$	15770.72		1.31	
$d^3sp(^4F)$	$z^6G_{1½}^{1}$	*16361.45*	88.40	0.00	e^6F, f^6F, g^6F, e^6G, g^6G, h^6G, e^6H, f^6H, a^4F.
	$z^6G_{2½}^{2}$	*16449.85*	122.69	0.78	
	$z^6G_{3½}^{3}$	*16572.54*	156.21	1.10	
	$z^6G_{4½}^{4}$	*16728.75*	188.40	1.22	
	$z^6G_{5½}^{5}$	*16917.15*	219.29	1.26	
	$z^6G_{6½}^{6}$	*17136.44*		1.43	
$d^4s(^3G)$	$a^4G_{2½}$	17054.87	62.05	0.59	$s^4D°$, $p^4D°$, $o^4D°$, $y^4F°$, $x^4F°$, $w^4F°$, $v^4F°$, $u^4F°$, $t^4F°$, $r^4F°$, $q^4F°$, $p^4F°$, $y^4G°$, $w^4G°$, $v^4G°$, $u^4G°$, $t^4G°$, $s^4G°$, $r^4G°$, $z^4H°$, $y^4H°$, $x^4H°$, $w^4H°$, $x^2F°$, $w^2F°$, $u^2F°$, $z^2G°$, $t^2G°$, $y^2H°$, $x^2H°$, $v^2H°$, $z^2I°$, $y^2I°$.
	$a^4G_{3½}$	17116.92	65.06	0.96	
	$a^4G_{4½}$	17181.98	60.07	1.14	
	$a^4G_{5½}$	17242.05		1.27	
$d^3sp(^4F)$	$z^6D_{0½}^{0}$	*18085.82*	40.45	3.20	f^6P, a^6D, e^6D, f^6D, g^6D, e^6F, f^6F, g^6F, a^4D, a^4F.
	$z^6D_{1½}^{1}$	*18126.27*	71.81	1.76	
	$z^6D_{2½}^{2}$	*18198.08*	104.19	1.58	
	$z^6D_{3½}^{3}$	*18302.27*	135.80	1.56	
	$z^6D_{4½}^{4}$	*18438.07*		1.55	
$d^3sp(^4F)$	$z^6F_{0½}^{0}$	*18120.12*	53.94	−0.44	a^6D, e^6D, g^6D, e^6F, f^6F, g^6F, e^6G, f^6G, h^6G, e^5H, a^4F.
	$z^6F_{1½}^{1}$	*18174.06*	84.83	1.14	
	$z^6F_{2½}^{2}$	*18258.89*	113.57	1.28	
	$z^6F_{3½}^{3}$	*18372.46*	141.00	1.28	
	$z^6F_{4½}^{4}$	*18513.46*	166.66	1.38	
	$z^6F_{5½}^{5}$	*18680.12*		1.42	
$d^4s(^3P)$	$b^2P_{0½}$	18805.05	384.23	0.67	$z^2S°$, $y^2S°$, $x^2S°$, $z^2P°$, $y^2P°$, $w^2P°$, $v^2P°$, $t^2P°$, $x^2D°$, $v^2D°$, $u^2D°$, $t^2D°$, $x^2F°$, $x^4D°$, $s^4D°$, $p^4F°$.
	$b^2P_{1½}$	19189.28		1.37	
$d^4s(^3H)$	$b^2H_{4½}$	19023.47	121.66	0.91	$w^2F°$, $x^2G°$, $v^2G°$, $t^2G°$, $r^2G°$, $q^2G°$, $p^2G°$, $z^2H°$, $y^2H°$, $x^2H°$, $w^2H°$, $v^2H°$, $u^2H°$, $t^2H°$, $s^2H°$, $z^2I°$, $y^2I°$, $x^2I°$, $q^4F°$, $w^4G°$, $v^4G°$, $u^4G°$, $x^4H°$, $x^4H°$, $w^4H°$, $z^4I°$.
	$b^2H_{5½}$	19145.13		1.08	
$d^4s(^3F)$	$a^2F_{2½}$	19026.34	51.81	0.86	$w^2P°$, $y^2D°$, $x^2D°$, $w^2D°$, $s^2D°$, $u^2D°$, $t^2D°$, $z^2F°$, $y^2F°$, $x^2F°$, $w^2F°$, $v^2F°$, $u^2F°$, $t^2F°$, $s^2F°$, $y^2G°$, $x^2G°$, $v^2G°$, $u^2G°$, $t^2G°$, $s^2G°$, $(r^2G°)$, $q^2G°$, $v^2H°$, $t^2H°$, $u^4P°$, $s^4D°$, $s^4D°$, $p^4D°$, $w^4F°$, $u^4F°$, $t^4F°$, $s^4P°$, $w^4G°$, $t^4G°$, $x^4H°$.
	$a^2F_{3½}$	19078.15		1.14	
d^5	$a^6S_{2½}$	20202.49			$y^6P°$.
$d^4sp(^3F)$	$z^4D_{½}^{½}$	*20606.43*	81.32	−0.04	a^4P, a^4D, a^4F, f^4F.
	$z^4D_{1½}^{1½}$	*20687.75*	140.73	1.21	
	$z^4D_{2½}^{2½}$	*20828.48*	204.04	1.35	
	$z^4D_{3½}^{3½}$	*21032.52*		1.45	

TABLE 2.—*Terms of the* V I *spectrum*—Continued

Electron configuration	Term symbol	Level	Difference	Observed g	Combinations
$d^4s(^3D)$	$b^4D_{3/2}$	20767.57	−21.56	1.45	$x^4P°$, $v^4P°$, $u^4P°$, $t^4P°$, $x^4D°$, $v^4D°$, $r^4D°$, $q^4D°$, $p^4D°$, $o^4D°$, $z^4F°$, $w^4F°$, $v^4F°$, $t^4F°$, $r^4F°$, $q^4F°$, $p^4F°$, $t^4G°$, $w^2P°$, $s^2P°$, $t^2P°$, $x^2D°$, $s^2F°$, 1^5, $2°$, $3°$.
	$b^4D_{1/2}$	20789.13	−23.86	1.25	
	$b^4D_{1/2}$	20812.99	−17.21	1.20	
	$b^4D_{5/2}$	20830.20		0.10	
$d^4s(^3G)$	$b^4G_{5/2}$	21603.17	−43.22	1.11	$y^2F°$, $w^2F°$, $p^2F°$, $u^2F°$, $t^2F°$, $y^2G°$, $x^2G°$, $s^2G°$, $t^2G°$ $s^2G°$, $q^2G°$, $z^2H°$, $x^2H°$, $p^2H°$, $u^2H°$, $t^2H°$, $s^2H°$ $u^4D°$, $t^4D°$, $(r^4D°)$, $u^4F°$, $q^4F°$, $x^4G°$, $w^4G°$, $t^4G°$
	$b^3G_{3/2}$	21646.39		0.86	
$d^3sp(^3F)$	$z^4G^\circ_{11/2}$	21841.45	122.05	0.55	a^4F, f^4F.
	$z^4G^\circ_{9/2}$	21963.50	157.67	0.96	
	$z^4G^\circ_{7/2}$	22121.17	192.82	1.16	
	$z^4G^\circ_{5/2}$	22313.99		1.24	
$d^3sp(^3F)$	$z^4F^\circ_{9/2}$	23088.06	122.50	0.39?	a^4D, a^4F, e^4F, f^4F, a^6D.
	$z^4F^\circ_{7/2}$	23210.56	142.53	0.98?	
	$z^4F^\circ_{5/2}$	23353.09	166.75	1.23	
	$z^4F^\circ_{3/2}$	23519.84		1.31	
$d^3sp(^3F)$	$z^2D^\circ_{5/2}$	23608.80	326.35	0.76	a^2P, e^2F, a^4D, a^4F.
	$z^2D^\circ_{3/2}$	23935.15		1.32?	
$d^4p(^5D)$	$z^6P^\circ_{7/2}$	24648.10	79.75	2.34	e^6P, a^6D, e^6D, f^6D, f^6F, a^4P, a^4P, a^4D, a^4F.
	$z^6P^\circ_{5/2}$	24727.85	110.71	1.85	
	$z^6P^\circ_{3/2}$	24838.56		1.67	
$d^4p(^5D)$	$z^4P^\circ_{5/2}$	24770.62	144.54	2.54	a^4P, b^4P, a^4D, e^4D, a^4F, a^6D.
	$z^4P^\circ_{3/2}$	24915.16	215.80	1.71	
	$z^4P^\circ_{1/2}$	25130.96		1.59	
$d^4p(^5D)$	$y^6F^\circ_{11/2}$	24789.36	40.82	−0.58	a^6D, e^6D, f^6F, e^6G, h^6G, a^4G, a^4D, e^4D, a^4F.
	$y^6F^\circ_{9/2}$	24830.18	68.55	1.02	
	$y^6F^\circ_{7/2}$	24898.73	94.15	1.23	
	$y^6F^\circ_{5/2}$	24992.88	118.62	1.37	
	$y^6F^\circ_{3/2}$	25111.50	142.03	1.41	
	$y^6F^\circ_{1/2}$	25253.53		1.41	
$d^4p(^5D)$	$y^4F^\circ_{9/2}$	25930.51	73.71	0.42	b^4P, a^4D, e^4D, a^4F, b^4F, e^4F, a^4G, a^4H, a^2G, a^2H, a^6D
	$y^4F^\circ_{7/2}$	26004.22	117.82	0.98	
	$y^4F^\circ_{5/2}$	26122.04	49.92	1.15	
	$y^4F^\circ_{3/2}$	26171.96		1.23	
$d^3sp(^3F)$	$z^2G^\circ_{9/2}$	26021.89	323.05	0.92	a^2G, a^2H, a^4D, a^4F, b^4F, e^4F, a^4G, a^6D.
	$z^2G^\circ_{7/2}$	26344.94		1.13	
$d^4p(^5D)$	$y^4D^\circ_{5/2}$	26182.60	66.88	−0.06	a^4P, b^4P, a^4D, e^4D, a^4F, b^4F, e^4F, f^4F, a^6D.
	$y^4D^\circ_{3/2}$	26249.48	103.11	1.17	
	$y^4D^\circ_{1/2}$	26352.59	127.09	1.34	
	$y^4D^\circ_{7/2}$	26480.88		1.39	
$d^4p(^5D)$	$y^6D^\circ_{9/2}$	26397.86	40.32	3.25	e^6P, a^6D, e^6D, f^6F, e^6F, f^6F, a^4D, a^4F, e^4F.
	$y^6D^\circ_{7/2}$	26437.68	68.20	1.86	
	$y^6D^\circ_{5/2}$	26505.88	98.89	1.59	
	$y^6D^\circ_{3/2}$	26604.77	133.54	1.58	
	$y^6D^\circ_{1/2}$	26738.31		1.50	
$d^3sp(^3F)$	$z^2F^\circ_{7/2}$	27187.77	283.11	1.07?	a^2D, a^2F, a^2G, e^2F, a^4P, a^4D, a^4F, e^4F, f^4F.
	$z^2F^\circ_{5/2}$	27470.88		1.01	
$d^3sp\ (^1P)$	$x^2D^\circ_{5/2}$	28313.68	55.08	3.23	f^6P, a^6D, f^6F, h^6G, a^2P, b^4P, a^2_2F.
	$x^2D^\circ_{3/2}$	28368.76	93.39	1.82	
	$x^2D^\circ_{5/2}$	28462.15	133.49	1.55	
	$x^2D^\circ_{3/2}$	28595.64	172.49	1.52	
	$x^2D^\circ_{1/2}$	28768.13		1.47	
	$x^4S^\circ_{1/2}$	28621.27			b^4P.
$d^3sp(^1P)$	$y^6P^\circ_{7/2}$	29202.80	93.63	2.32	a^6S, a^6D, a^6F.
	$y^6P^\circ_{5/2}$	29296.43	121.74	1.76	
	$y^6P^\circ_{3/2}$	29418.17		1.62	
$d^3sp(^3P)$	$y^4P^\circ_{5/2}$	30021.67	72.95	2.67	a^4P, b^4P, a^4D, a^2D.
	$y^4P^\circ_{3/2}$	30094.62	26.26	1.74	
	$y^4P^\circ_{1/2}$	30120.78		1.67	
$d^3sp(^3G)$?	$y^4G^\circ_{11/2}$	30635.60	58.74	0.53	a^4F, b^4F, a^4G, a^4H.
	$y^4G^\circ_{9/2}$	30694.34	77.38	0.93	
	$y^4G^\circ_{7/2}$	30771.12	92.62	1.13	
	$y^4G^\circ_{5/2}$	30864.34		1.21	

TABLE 2.—*Terms of the* V I *spectrum*—Continued

Electron configuration	Term symbol	Level	Difference	Observed g	Combinations
$d^3sp(^1P)$	$z^6Si_{3/2}$	*30832.58*			a^4P, a^4D.
$d^3sp(^3G)$	$x^4F_{11/2}$	*31200.12*		0.38	
	$x^4F_{9/2}$	*31228.98*	28.86	1.01	a^4P, a^4D, b^4D, a^4F, b^4F, a^4G, e^2F, a^2G, a^6D
	$x^4F_{7/2}$	*31268.15*	39.17	1.21	
	$x^4F_{5/2}$	*31317.50*	49.35	1.32	
$d^3sp(^1F)$	$x^4G_{11/2}$	*31398.09*		0.53	
	$x^4G_{9/2}$	*31541.18*	143.09	0.95	a^4F, b^4F, a H, b^2G.
	$x^4G_{7/2}$	*31721.73*	180.55	1.12	
	$x^4G_{5/2}$	*31937.18*	215.45	1.20	
	$z^2Si_{3/2}$	*31786.19*		2.30	a^2P, b^2P, a^4D, a^6D.
	$y^2Si_{1/2}$	*31962.30*		2.21	a^2P, b^2P, a^2D.
	$x^4D_{3/2}$	*32348.89*		0.08	
	$x^4D_{1/2}$	*32456.45*	107.56	1.17	a^4P, b^4P, a^4D, b^4D, a^4F, b^4F, b^2P, a^2D.
	$x^4D_{3/2}$	*32660.26*	203.81	1.29	
	$x^4D_{5/2}$	*32891.06*	230.80	1.35	
$d^3sp(^3G)$	$z^4H_{13/2}$	*32692.09*		0.68	
	$z^4H_{11/2}$	*32788.22*	96.13	0.98	a^4F, a^4G, a^4H, a^2F, a^2G, b^2H.
	$z^4H_{9/2}$	*32897.81*	109.59	1.11	
	$z^4H_{7/2}$	*32963.90*	66.09	1.21	
	$z^2P_{3/2}$	*32724.86*	43.02	0.73?	a^2P, b^2P, a^2D, b^4P, a^4D, a^4F.
	$z^2P_{1/2}$	*32767.88*		1.22	
$d^3sp(^1F)$	$w^4F_{11/2}$	*32738.14*		0.52	
	$w^4F_{9/2}$	*32846.74*	108.60	1.01	a^4P, a^4D, b^4D, a^4F, b^4F, a^4G, a^2F.
	$w^4F_{7/2}$	*32988.82*	142.08	1.18	
	$w^4F_{5/2}$	*33155.30*	166.48	1.30	
	$y^2G_{9/2}$	*33306.96*	−53.35	1.03	a^2D, a^2F, a^2G, b^2G, a^4F, b^4F.
	$y^2G_{7/2}$	*33360.31*		0.91	
	$y^4F_{9/2}$	*33481.45*	−46.19	1.11	a^2D, a^2F, a^2G, b^2G, a^4D, a^4F, b^4F.
	$y^4F_{3/2}$	*33527.64*		0.85	
	$z^2H_{11/2}$	*33640.18*	55.14	0.92	a^2G, b^2G, (a^2H^6), b^2H^6, a^4F, a^4H.
	$z^2H_{9/2}$	*33695.32*		1.09	
$d^3sp(^3P)$	$w^4D_{3/2}$	*33966.72*	9.30	0.09	
	$w^4D_{1/2}$	*33976.02*	89.59	0.80	a^4P, b^4P, a^4D, a^4F, b^4F, a^2P.
	$w^4D_{3/2}$	*34065.61*	62.43	1.30	
	$w^4D_{5/2}$	*34128.04*		1.35	
	1°	*34019.12*			a^4P, a^4D, b^4D, a^4F, f^2P.
	$v^4F_{11/2}$	*34030.04*	137.80	0.86	
	$v^4F_{9/2}$	*34167.84*	206.97	1.32?	a^4P, b^4P, a^4D, b^4D, a^4F, b^4F, a^4G, a^2P, a^2D.
	$v^4F_{7/2}$	*34374.81*	155.00	1.21	
	$v^4F_{5/2}$	*34529.81*		1.41	
	$y^2D_{5/2}$	*34428.76*	58.04	0.73	a^2P, a^2D, a^2F, a^4P, a^4D, a^4F.
	$y^2D_{3/2}$	*34486.80*		1.18	
$d^3sp(^1F)$	$v^4D_{3/2}$	*34477.40*		0.00	
	$v^4D_{1/2}$	*34537.21*	59.81	1.05	a^4P, b^4P, a^4D, b^4D, a^4F, a^4G, a^2P, a^2F.
	$v^4D_{3/2}$	*34619.52*	82.31	1.28	
	$v^4D_{5/2}$	*34747.06*	127.54	1.35	
	$u^4D_{3/2}$	*35012.91*			
	$u^4D_{1/2}$	*35092.36*	79.45	1.12	b^4P, a^4D, a^4F, b^2G, a^6D.
	$u^4D_{3/2}$	*35225.04*	132.68	1.32	
	$u^4D_{5/2}$	*35379.11*	154.07	1.33	
$d^4p(^3P)$?	$y^4Si_{3/2}$	*36408.23*		1.85	a^4P, b^4P, (a^2P).
	$x^2D_{5/2}$	*36416.49*	284.29	0.89	a^2P, b^2P, a^2D, a^2F, a^2G, b^4P, a^4D, b^4D, a^4F.
	$x^2D_{3/2}$	*36700.78*		1.13	
$d^4p(^3F)$	$x^2G_{9/2}$	*36461.26*	77.32	0.85	a^2F, a^2G, b^2G, a^2H, b^2H, a^4F, b^4F.
	$x^2G_{7/2}$	*36538.58*		1.05	
$d^3sp(^1D)$	$y^2P_{3/2}$	*36477.75*	102.71	0.74	a^2P, b^2P, a^2D, a^4D.
	$y^2P_{1/2}$	*36580.46*		1.17	
$d^4p(^3P)$?	$x^4P_{1/2}$	*36611.81*	−83.68	1.54	
	$x^4P_{3/2}$	*36695.49*	119.31	2.51	a^4P, b^4P, a^4D, b^4D, b^4F.
	$x^4P_{5/2}$	*36814.80*		1.77	

TABLE 2.—*Terms of the* V I *spectrum*—Continued

Electron configuration	Term symbol	Level	Difference	Observed g	Combinations
	$w^3G_{3\frac{1}{2}}$	*36828.83*	199.51	0.65?	a^3G, a^3H.
	$w^3G_{4\frac{1}{2}}$	*36828.33*			
$d^3sp(^3H)$?	$w^4G_{2\frac{1}{2}}$	*36763.41*			
	$w^4G_{3\frac{1}{2}}$	*36822.86*	59.45	1.06	a^4F, b^4F, a^4G, a^4H, a^3F, a^3G, b^3G, a^3H, b^3H.
	$w^4G_{4\frac{1}{2}}$	*36897.88*	75.02	1.17	
	$w^4G_{5\frac{1}{2}}$	*36938.42*	40.54	1.26	
	$x^3F_{3\frac{1}{2}}$	*36766.00*	159.88	0.89	a^3P, b^3P, a^3D, a^3F, a^3G, a^3H, a^4F, b^4F, a^4G.
	$x^3F_{4\frac{1}{2}}$	*36925.88*		1.05	
d^3	$e^4F_{1\frac{1}{2}}$	36983.63			
	$e^4F_{2\frac{1}{2}}$	36989.20	5.57		y^4D°, z^4F°, y^4F°, z^2F°, z^2G°, y^2D°.
	$e^4F_{3\frac{1}{2}}$	37025.60	36.40		
	$e^4F_{4\frac{1}{2}}$	37075.64	50.04		
$d^4s(^5D)$	$e^6D_{0\frac{1}{2}}$	37116.68		3.08	
	$e^6D_{1\frac{1}{2}}$	37158.36	41.68	1.87	z^6P°, z^6D°, y^6D°, z^6F°, y^6F°.
	$e^6D_{2\frac{1}{2}}$	37227.44	69.08	1.61	
	$e^6D_{3\frac{1}{2}}$	37322.09	94.65	1.64	
	$e^6D_{4\frac{1}{2}}$	37440.74	118.65	1.48	
$d^4p(^3H)$	$z^3G_{3\frac{1}{2}}$	*37174.68*	187.27	0.99	a^3D, a^1F, a^3G, b^3G, a^3H, b^3H, a^4F, b^4F, a^4H.
	$z^3G_{4\frac{1}{2}}$	*37361.95*		1.05	
	$y^3H_{4\frac{1}{2}}$	*37180.90*	29.95	0.73	a^3G, a^3H, b^3H, a^4F, a^4G, a^4H.
	$y^3H_{5\frac{1}{2}}$	*37210.85*		1.08	
$d^4p(^3H)$	$z^4I_{3\frac{1}{2}}$	*37285.03*	30.80	0.87	a^4H, a^3G, a^3H, b^3H.
	$z^4I_{4\frac{1}{2}}$	*37315.83*	88.42	0.96	
	$z^4I_{5\frac{1}{2}}$	*37404.25*	114.11	1.08	
	$z^4I_{6\frac{1}{2}}$	*37518.36*		1.15	
$d^4p(^3F)$?	$w^2F_{2\frac{1}{2}}$	*37342.66*	132.42	0.84	a^2P, a^2D, a^2F, a^2G, b^2G, a^2H, b^2H, b^4P, a^4F, b^4F, a^4G, a^6D.
	$w^2F_{3\frac{1}{2}}$	*37475.08*		1.08	
$d^3s.s(^5F)$	$e^6F_{0\frac{1}{2}}$	37374.98	48.19	−0.72	z^6D°, y^6D°, z^6F°, z^6G°.
	$e^6F_{1\frac{1}{2}}$	37423.17	79.97	1.05	
	$e^6F_{2\frac{1}{2}}$	37503.14	111.83	1.30	
	$e^6F_{3\frac{1}{2}}$	37614.97	143.10	1.33	
	$e^6F_{4\frac{1}{2}}$	37758.07	173.34	1.43	
	$e^6F_{5\frac{1}{2}}$	37931.41		1.52	
$d^4p(^3F)$	$w^2D_{1\frac{1}{2}}$	*37457.50*	295.04	0.80	a^2P, a^2D, a^2F, a^4P, a^4D, a^4F.
	$w^2D_{2\frac{1}{2}}$	*37752.54*		1.18	
$d^3sp(^3H)$?	$y^4H_{3\frac{1}{2}}$	*37481.36*	35.59	0.76	a^4G, a^4H, a^2G.
	$y^4H_{4\frac{1}{2}}$	*37516.95*	48.93	1.05	
	$y^4H_{5\frac{1}{2}}$	*37565.88*	60.56	1.09	
	$y^4H_{6\frac{1}{2}}$	*37626.44*		1.24	
$d^4p(^3F)$	$v^4G_{2\frac{1}{2}}$	*37498.76*	57.24	0.60	a^4D, a^4F, b^4F, a^4G, a^4H, b^2H.
	$v^4G_{3\frac{1}{2}}$	*37556.00*	88.41	1.02	
	$v^4G_{4\frac{1}{2}}$	*37644.41*	120.48	1.15	
	$v^4G_{5\frac{1}{2}}$	*37764.89*		1.22	
$d^4p(^3H)$?	$z^2I_{5\frac{1}{2}}$	*37530.29*	76.03	0.94	a^2G, a^2H, b^2H, a^4G, a^4H.
	$z^2I_{6\frac{1}{2}}$	*37606.32*		1.06	
$d^4p(^3F)$	$t^4D_{1\frac{1}{2}}$	*37757.24*	77.74	0.01	a^4P, b^4P, a^4D, a^4F, b^4F, a^2D, a^2G, b^2G, a^6D.
	$t^4D_{2\frac{1}{2}}$	*37834.98*	124.68	1.18	
	$t^4D_{3\frac{1}{2}}$	*37959.66*	155.99	1.33	
	$t^4D_{4\frac{1}{2}}$	*38115.65*		1.35	
$d^4s(^5D)$	$e^4D_{0\frac{1}{2}}$	37940.08	63.85		z^4P°, y^4D°, y^4F°, y^6F°.
	$e^4D_{1\frac{1}{2}}$	38003.93	102.39		
	$e^4D_{2\frac{1}{2}}$	38106.32	136.14		
	$e^4D_{3\frac{1}{2}}$	38242.46			
	$x^3H_{4\frac{1}{2}}$	*38123.76*	96.87	0.88	a^3G, b^3G, a^3H, b^3H, a^4F, b^4F, a^4G, a^4H.
	$x^3H_{5\frac{1}{2}}$	*38220.63*		1.10	
$d^4p(^3H)$	$x^4H_{3\frac{1}{2}}$	*38245.75*	78.12	0.67	a^4G, a^4H, a^2G, a^2H, b^2H.
	$x^4H_{4\frac{1}{2}}$	*38323.87*	81.09	0.93	
	$x^4H_{5\frac{1}{2}}$	*38404.96*	78.00	1.11	
	$x^4H_{6\frac{1}{2}}$	*38482.96*		1.22	
	$u^3G_{3\frac{1}{2}}$	38529.78	−81.16	0.99	a^2F, a^2G, a^2H, a^4F.
	$u^3G_{4\frac{1}{2}}$	*38610.94*		0.88?	

TABLE 2.—*Terms of the* V I *spectrum*—Continued

Electron configuration	Term symbol	Level	Difference	Observed g	Combinations
$d^3sp(^1H)$?	$y^1I_{5\frac{1}{2}}$	*39008.60*		0.92	a^3H, b^3H, a^4G, a^4H.
	$y^1I_{6\frac{1}{2}}$	*39081.10*	72.50	1.06	
$d^3s.s(^1F)$	$f^4F_{1\frac{1}{2}}$	39127.23		0.46?	$z^4D°$, $y^4D°$, $z^4F°$, $z^4G°$, $z^2F°$.
	$f^4F_{2\frac{1}{2}}$	39241.34	114.11	1.03	
	$f^4F_{3\frac{1}{2}}$	39398.82	157.48	1.22?	
	$f^4F_{4\frac{1}{2}}$	39597.01	198.19	1.33?	
$d^3sp(^1P)$	$w^4P_{0\frac{1}{2}}$	*39237.10*		2.57	a^4P, b^4P, a^4D, a^4F.
	$w^4P_{1\frac{1}{2}}$	*39248.90*	11.80	1.60	
	$w^4P_{2\frac{1}{2}}$	*39422.66*	173.76	1.52	
$d^4p(^3F)$	$u^4F_{1\frac{1}{2}}$	*39266.60*		0.54	a^4P, a^4D, a^4F, b^4F, a^4G, a^4H, a^2F, b^2G.
	$u^4F_{2\frac{1}{2}}$	*39300.48*	33.88	1.00	
	$u^4F_{3\frac{1}{2}}$	*39341.76*	41.28	1.21	
	$u^4F°_{4\frac{1}{2}}$	*39391.02*	49.26	1.30	
$d^3sp(^3P)$	$x^4S_{1\frac{1}{2}}$	*39847.24*		2.00	a^4P, b^4P, a^4F.
$d^4p(^3P)$	$s^4D_{0\frac{1}{2}}$	*39877.62*		0.01	a^4P, b^4P, a^4D, a^4F, b^4F, a^2P, b^2P, a^2F, a^6D.
	$s^4D_{1\frac{1}{2}}$	*39935.07*	57.45	1.10	
	$s^4D_{2\frac{1}{2}}$	*39999.89*	64.82	1.33	
	$s^4D_{3\frac{1}{2}}$	*40125.79*	125.90	1.38	
$d^4p(^3P)$	$v^2D_{1\frac{1}{2}}$	*39884.45*		0.92	a^2P, b^2P, a^2D, a^2F, a^4P, b^4P, a^4D, a^4F.
	$v^2D_{2\frac{1}{2}}$	*40119.26*	234.83	1.14	
$d^4p(^3H)$	$u^4G_{2\frac{1}{2}}$	*39968.17*		0.53	a^4F, b^4F, a^4G, a^4H, a^2H, b^2H.
	$u^4G_{3\frac{1}{2}}$	*40001.18*	39.01	0.99	
	$u^4G_{4\frac{1}{2}}$	*40038.95*	37.77	1.19	
	$u^4G_{5\frac{1}{2}}$	*40063.78*	24.83	1.23	
	$v^2F_{3\frac{1}{2}}$	*40153.51*			a^2D, a^2F, a^2G, b^2G, a^4D, a^4F.
	$v^2F_{4\frac{1}{2}}$	*40587.35*	433.84	1.01	
$d^3sp(^1P)$?	$u^2D_{1\frac{1}{2}}$	*40225.38*		0.70	a^2P, b^2P, a^2D, a^2F, a^4F, b^4F, a^6D.
	$u^2D_{2\frac{1}{2}}$	*40325.77*	100.39	1.12	
$d^3sp(^1P)$?	$x^2S_{0\frac{1}{2}}$	*40299.81*			a^2P, a^4D.
$d^4p(^3G)$	$w^4H_{3\frac{1}{2}}$	*40314.83*		0.65	a^4F, a^4G, a^4H, b^2H.
	$w^4H_{4\frac{1}{2}}$	*40378.70*	63.87	0.92	
	$w^4H_{5\frac{1}{2}}$	*40452.38*	73.68	1.08	
	$w^4H_{6\frac{1}{2}}$	*40535.62*	83.24	1.22	
	$x^4P_{0\frac{1}{2}}$	*40328.62*			a^2P, a^2D, b^4P.
	$x^4P_{1\frac{1}{2}}$	*40437.42*	108.80	1.52	
	$w^2P_{0\frac{1}{2}}$	?			b^2P, a^2D, a^2F, b^4D a^4F.
	$w^2P_{1\frac{1}{2}}$	*40693.76*			
	$w^2H_{4\frac{1}{2}}$	*40919.68*		0.96	a^2H, b^2H.
	$w^2H_{5\frac{1}{2}}$	*40980.54*	−60.86	0.99	
$d^4p(^3G)$	$t^4F_{1\frac{1}{2}}$	*41389.49*		0.42	a^4P, a^4D, b^4D, a^4F, b^4F, a^4G, a^4H, a^2F, a^2H.
	$t^4F_{2\frac{1}{2}}$	*41428.93*	39.44	0.89	
	$t^4F_{3\frac{1}{2}}$	*41492.29*	63.36	1.15	
	$t^4F_{4\frac{1}{2}}$	*41599.36*	107.07	1.23	
$d^3sp(^1G)$?	$t^2G_{3\frac{1}{2}}$	*41436.58*		0.90	a^2F, a^2G, b^2G, a^2H, b^2H, a^4F b^4F, a^4G.
	$t^2G_{4\frac{1}{2}}$	*41539.14*	102.56	1.04	
$d^3sp(^1H)$?	$v^2H_{4\frac{1}{2}}$	*41501.41*		0.87	a^2F, a^2G, b^2G, a^2H, b^2H, a^4F, b^4F, a^4G, a^4H.
	$v^2H_{5\frac{1}{2}}$	*41659.71*	158.30	1.05	
$d^4p(^3G)$	$t^4G_{2\frac{1}{2}}$	*41654.70*		0.58	b^4D, a^4F, b^4F, a^4G, a^4H, a^2F, a^2G, b^2G.
	$t^4G_{3\frac{1}{2}}$	*41758.41*	103.71	1.03	
	$t^4G_{4\frac{1}{2}}$	*41860.54*	102.13	1.20	
	$t^4G_{5\frac{1}{2}}$	*41918.24*	57.70	1.20	
	$v^4P_{0\frac{1}{2}}$	*41751.78*		2.56	a^4P, b^4P, a^4D, b^4D, a^4F.
	$v^4P_{1\frac{1}{2}}$	*41848.47*	96.69	1.62	
	$v^4P_{2\frac{1}{2}}$	*42009.93*	161.46	1.48	
$d^3sp(^1P)$	$r^4D_{0\frac{1}{2}}$	*41928.47*		0.04	a^4P, b^4P, a^4D, b^4D, a^4F, b^4F, (b^2G), a^6D.
	$r^4D_{1\frac{1}{2}}$	*41999.10*	70.63	1.20	
	$r^4D_{2\frac{1}{2}}$	*42138.00*	138.90	1.33	
	$r^4D_{3\frac{1}{2}}$	*42245.61*	107.61	1.36	
$d^3sp(^1D)$?	$u^2F_{2\frac{1}{2}}$	*41950.35*		0.84	a^2P, a^2D, a^2F, a^2G, b^2G, a^4F, a^4G.
	$u^2F_{3\frac{1}{2}}$	*42020.93*	70.58	1.11	

TABLE 2.—*Terms of the* V I *spectrum*—Continued

Electron configuration	Term symbol	Level	Difference	Observed g	Combinations
$d^4.d(^3D)$	$e^6G_{13/2}$	42033.84	36.21		
	$e^6G_{9/2}$	42070.05	44.12		
	$e^6G_{7/2}$	42114.17	63.14	1.08	$z^4F°$, $y^6F°$, $z^6G°$.
	$e^6G_{5/2}$	42177.31	80.01	1.23	
	$e^6G_{3/2}$	42257.32	96.10	1.32	
	$e^6G_{1/2}$	42353.42		1.35	
$d^3sp(^1G)$	$u^1H_{11/2}$	*42079.14*	141.55	0.85	a^1G, b^3G, a^3H, b^3H, a^1F.
	$u^1H_{9/2}$	*42220.69*		1.06	
$d^4.d(^3D)?$	$e^6P_{11/2}$	?			
	$e^6P_{9/2}$	?			$z^6P°$, $y^6D°$.
	$e^6P_{3/2}$	42164.74		1.44?	
	$2_{9/2}$	*42236.66*			a^4P, b^4D, a^4F, a^6D.
$d^3sp(^1P)?$	$v^3P_{1/2}$	*42318.42*	−162.20	1.34	a^2P, b^2P, a^2D, a^4P, b^4D, a^4F.
	$v^3P_{3/2}$	*42480.62*		1.14	
	$w^2S_{1/2}$	*42362.04*		1.50?	a^2P, a^4P.
$d^4.d(^3D)$	$f^6F_{9/2}$	?			
	$f^6F_{11/2}$	?			
	$f^6F_{13/2}$	?			$z^6P°$, $z^6D°$, $y^6D°$, $z^4D°$, $z^6F°$, y^6F, $z^6G°$.
	$f^6F_{3/2}$	42363.62	142.70		
	$f^6F_{5/2}$	42506.32	71.66		
	$f^6F_{7/2}$	42597.98		1.39	
$d^4.d(^3D)$	$f^4D_{9/2}$	?			
	$f^4D_{11/2}$	?			
	$f^4D_{13/2}$	?			$z^6P°$, $z^6D°$, $y^6D°$.
	$f^4D_{3/2}$	42404.89	148.73		
	$f^4D_{5/2}$	42553.62		1.61	
	$w^6D_{9/2}$	?			
	$w^6D_{11/2}$	?			
	$w^6D_{13/2}$	*42480.31*	107.10		a^6D.
	$w^6D_{1/2}$	*42587.41*	137.92		
	$w^6D_{7/2}$	*42725.33*			
$d^3sp(^5P)$	$w^4S_{3/2}$	*42969.49*		1.94	a^4P, b^4P.
	$z^4F_{11/2}$	*42981.54*	69.97		
	$z^4F_{9/2}$	*43051.51*	95.78		b^4P, a^4D, a^4F.
	$z^4F_{7/2}$	*43147.09*	119.06		
	$z^4F_{5/2}$	*43266.15*			
	$q^4D_{5/2}$	*43249.44*	59.39		
	$q^4D_{7/2}$	*43308.83*	101.99		a^4P, b^4P, a^4D, b^4D, a^4F, b^4F.
	$q^4D_{3/2}$	*43410.82*	144.30		
	$q^4D_{1/2}$	*43555.12*		1.46	
	$u^4P_{3/2}$	*43443.33*	60.66		
	$u^4P_{1/2}$	*43503.99*	81.60		a^4P, a^4D, b^4D, a^2D, a^2F.
	$u^4P_{5/2}$	*43585.59*			
$d^3s.d(^3F)$	$e^6H_{3/2}$	43649.40	57.42	0.38	
	$e^6H_{5/2}$	43706.82	80.78	0.88	
	$e^6H_{7/2}$	43787.60	106.55	1.11	$z^6F°$, $z^6G°$.
	$e^6H_{9/2}$	43894.15	134.18	1.18	
	$e^6H_{9/2}$	44028.33	161.62	1.30	
	$e^6H_{7/2}$	44189.95		1.38	
$d^3s.d(^3F)$	$f^6G_{13/2}$	43818.02	29.14	0.38?	
	$f^6G_{11/2}$	43847.16	64.77	0.78	
	$f^6G_{9/2}$	43911.93	93.21	1.12	$z^6F°$, $z^6G°$.
	$f^6F_{5/2}$	44005.14	134.55	1.26	
	$f^6G_{5/2}$	44139.69	187.35	1.34	
	$f^6G_{3/2}$	44327.04		1.35	
$d^3sp(^1G)$	$t^3F_{3/2}$	*43873.79*	−1.46	1.04?	a^2P, a^2D, a^2F, a^1G, b^3G, a^4F, b^4F, a^6D.
	$t^3F_{5/2}$	*43875.25*		0.86	
$d^3s.s(^3F)$	$e^2F_{7/2}$	43918.58	147.47	0.89	$z^2D°$, $z^4F°$, $z^4F°$.
	$e^2F_{5/2}$	44066.05		1.18	
	$x^6F_{9/2}$	*43707.97*	137.83		
	$x^6F_{11/2}$	*43845.80*	113.44		
	$x^6F_{7/2}$	*43959.24*	67.05		a^6D, b^4D, a^4F, b^4F.
	$x^6F_{5/2}$	*44026.29*	176.22		
	$x^6F_{3/2}$	*44202.51*	0.00		
	$x^6F_{1/2}$	*44202.51*			

TABLE 2.—*Terms of the* V I *spectrum*—Continued

Electron configuration	Term symbol	Level	Difference	Observed g	Combinations
	$x^6P_{1\frac{1}{2}}$	?			
	$x^6P_{2\frac{1}{2}}$	?			a^6D, b^4P.
	$x^6P_{3\frac{1}{2}}$	*45988.00*			
	$z^4G_{2\frac{1}{2}}$	*43999.68*	43.68		
	$z^4G_{3\frac{1}{2}}$	*44043.36*	61.19	0.98	a^4F, b^4F, a^4G, a^2D, a^6D.
	$z^4G_{4\frac{1}{2}}$	*44104.55*	73.90	1.26	
	$z^4G_{5\frac{1}{2}}$	*44178.45*		1.34	
$d^4p(^3G)$	$t^2H_{5\frac{1}{2}}$	*44145.77*	38.25	0.90	a^2F, a^2G, b^2G, a^2H, b^2H, a^2F.
	$t^2H_{4\frac{1}{2}}$	*44184.02*		1.06?	
$d^5s.d(^7F)$	$f^6P_{1\frac{1}{2}}$	44443.67	88.93		z^6D°, z^6D°, 1°.
	$f^6P_{2\frac{1}{2}}$	44532.60	157.87		
	$f^6P_{3\frac{1}{2}}$	44690.47			
$d^4p(^3G)$	$s^2G_{3\frac{1}{2}}$	*44463.28*	−32.15	1.09	a^2F, a^2G, b^2G, a^2H, a^4F.
	$s^2G_{4\frac{1}{2}}$	*44495.43*		0.91	
	$p^4D_{0\frac{1}{2}}$	*44514.34*	39.91		
	$p^4D_{1\frac{1}{2}}$	*44554.25*	62.43	1.22	a^4P, b^4P, a^4D, b^4D, a^4F, b^4F, G, a^2F, a^6D.
	$p^4D_{2\frac{1}{2}}$	*44616.68*	84.20	1.37?	
	$p^4D_{3\frac{1}{2}}$	*44700.88*		1.32?	
$d^5s.d(^7F)$	$g^6D_{0\frac{1}{2}}$	?			
	$g^6D_{1\frac{1}{2}}$	44844.83	76.25		
	$g^6D_{2\frac{1}{2}}$	44921.08	135.53	1.55?	z^6D°, z^6F°.
	$g^6D_{3\frac{1}{2}}$	45056.61	101.13		
	$g^6D_{4\frac{1}{2}}$	45157.74			
	$r^4F_{1\frac{1}{2}}$	*44973.60*	75.57	0.58?	
	$r^4F_{2\frac{1}{2}}$	*45049.17*	9.45		
	$r^4F_{3\frac{1}{2}}$	*45058.62*	86.54	0.97	b^4D, a^4F, b^4F, a^4G, a^2F.
	$r^4F_{4\frac{1}{2}}$	*45145.16*		1.26	
	$q^4F_{1\frac{1}{2}}$	*45066.56*	40.65	0.59	
	$q^4F_{2\frac{1}{2}}$	*45107.21*	50.51	0.93	a^4D, b^4D, a^4F, b^4F, a^4G, a^2D, b^2G, a^2H, b^2H.
	$q^4F_{3\frac{1}{2}}$	*45157.72*	79.44	1.05	
	$q^4F_{4\frac{1}{2}}$	*45237.16*		1.22	
	$u^2P_{0\frac{1}{2}}$	?			
	$u^2P_{1\frac{1}{2}}$	*45159.15*		1.66?	a^2P, a^4F, b^4F.
$d^3sp(^1H)?$	$r^2G_{3\frac{1}{2}}$	*45175.92*	185.50	0.98	(a^2F), a^2G, a^2H, b^2H, a^4F.
	$r^2G_{4\frac{1}{2}}$	*45361.42*		1.14	
	$g^6F_{0\frac{1}{2}}$	(?)			
	$g^6F_{1\frac{1}{2}}$	*45638.54*	61.71		
	$g^6F_{2\frac{1}{2}}$	*45700.25*	43.37		
	$g^6F_{3\frac{1}{2}}$	*45743.62*	69.23	1.26	z^6D°, z^6F°, z^6G°.
	$g^6F_{4\frac{1}{2}}$	*45813.25*	221.33		
	$g^6F_{5\frac{1}{2}}$	*46034.58*			
$d^4p(^4D)$	$p^4F_{1\frac{1}{2}}$	*45648.86*	39.55	0.60	
	$p^4F_{2\frac{1}{2}}$	*45688.41*	71.62		
	$p^4F_{3\frac{1}{2}}$	*45760.03*	131.52	1.02	a^4D, b^4D, a^4F, b^4F, a^4G, a^4P, b^2P, a^2D.
	$p^4F_{4\frac{1}{2}}$	*45891.55*		1.32	
	$t^2P_{1\frac{1}{2}}$	*45654.50*	−292.16	1.04?	a^2P, b^2P, a^2D, a^4D, b^4D, a^4F, b^4F.
	$t^2P_{2\frac{1}{2}}$	*45946.66*			
$d^4p(^2D)$	$o^4D_{0\frac{1}{2}}$	*45702.14*	60.10		
	$o^4D_{1\frac{1}{2}}$	*45762.24*	75.82	0.96?	z^4P, a^4D, b^4D, a^4F, b^4F, a^4G, a^2D.
	$o^4D_{2\frac{1}{2}}$	*45838.06*	99.01		
	$o^4D_{3\frac{1}{2}}$	*45937.07*		1.45	
	$r^4G_{2\frac{1}{2}}$	*46052.79*	86.27	0.56	
	$r^4G_{3\frac{1}{2}}$	*46139.06*	104.58	0.96	a^4F, a^4G, a^4H.
	$r^4G_{4\frac{1}{2}}$	*46243.64*	119.78	1.15	
	$r^4G_{5\frac{1}{2}}$	*46363.42*		1.19	
	$t^4P_{0\frac{1}{2}}$	*46851.10*	11.63		
	$t^4P_{1\frac{1}{2}}$	*46862.73*	5.37		a^4P, b^4P, a^4D, b^4D.
	$t^4P_{2\frac{1}{2}}$	*46868.10*			
$d^3sp(^3G)$	$s^3F_{2\frac{1}{2}}$	*46996.84*	146.40	1.02	a^2P, a^2D, a^2F, a^2G.
	$s^3F_{3\frac{1}{2}}$	*47143.24*			
	$3l_{3\frac{1}{2}}$	*47423.18*			b^4D.
$d^3sp(^3G)$	$s^3H_{4\frac{1}{2}}$	*47611.77*	89.78	1.01?	a^2G, b^2G, a^2H, b^2H.
	$s^3H_{5\frac{1}{2}}$	*47701.55*		0.94	

TABLE 2.—*Terms of the* V I *spectrum*—Continued

Electron configuration	Term symbol	Level	Difference	Observed g	Combinations
	$a^4F_{1/2}$	*47801.87*	114.44		
	$a^4F_{3/2}$	*47916.31*	223.84		a^4F.
	$a^4F_{5/2}$	*48140.15*	188.71		
	$a^4F_{7/2}$	*48328.86*			
$d^2sp(^3G)$	$q^3G_{3/2}$	*47959.82*	197.75	0.89	p^3F, a^3G, b^3G, a^3H, b^3H, a^4F.
	$q^3G_{5/2}$	*48157.57*		1.08	
$d^4p(^3P)$?	$z^6S_{5/2}$	*48844.67*		2.03	a^3P, b^3P.
$d^2sp(^3D)$	$t^3D_{3/2}$	*49689.01*	−33.87	1.25	a^3P, b^3P, a^3D, a^3F.
	$t^3D_{1/2}$	*49722.88*			
$d^2s.d(^5F)$	$f^6H_{7/2}$	49717.57	79.61		
	$f^6H_{9/2}$	49797.18	77.94		
	$f^6H_{11/2}$	49875.12	108.04		$z^6G°$.
	$f^6H_{13/2}$	49983.16	181.10		
	$f^6H_{15/2}$	50164.26	137.37		
	$f^6H_{17/2}$	50301.63			
$d^2s.d(^5F)$	$g^6G_{11/2}$	(?)			
	$g^6G_{13/2}$	(?)			
	$g^6G_{7/2}$	49789.17	143.20		$z^6G°$.
	$g^6G_{9/2}$	49932.37	182.22		
	$g^6G_{3/2}$	50114.59	94.46		
	$g^6G_{5/2}$	50209.05			
$d^2sp(^3H)$	$x^3H_{5/2}$	*49977.90*	142.79	0.91	a^3H, b^3H, a^4H.
	$x^3H_{7/2}$	*50120.69*		1.06	
d^3p^3	$h^6G_{11/2}$	50584.27	70.45		
	$h^6G_{13/2}$	50654.72	97.11		
	$h^6G_{15/2}$	50751.83	124.17		$z^4D°$, $z^4F°$, $y^4F°$, $z^4G°$.
	$h^6G_{17/2}$	50876.00	150.30		
	$h^6G_{19/2}$	51026.30	174.82		
	$h^6G_{21/2}$	51201.12			
$d^2sp(^3H)$?	$p^3G_{5/2}$	*52744.08*	173.90		a^3G, a^3H, b^3H.
	$p^3G_{3/2}$	*52947.98*			
	$r^3H_{5/2}$	*54081.51*	169.75		a^3G, a^3H.
	$r^3H_{7/2}$	*54251.26*			
	$s^1P_{1/2}$	*57561.36*	−182.76		a^2P, a^2D.
	$s^1P_{3/2}$	*57744.12*			

TABLE 3.—*Intervals of some* V I *terms*

Term	Level intervals	Interval ratios		Term	Level intervals	Interval ratios	
		Observed	Theoretical			Observed	Theoretical
a^4F	229.60	9.0	9	$z^6F°$	166.66	11.0	11
	186.04	7.3	7		141.00	9.3	9
	137.38	5.4	5		113.57	7.5	7
					84.83	5.6	5
a^6D	113.52	9.0	9		53.94	3.6	3
	91.24	7.2	7				
	66.93	5.3	5	$z^6G°$	219.29	13.0	13
	40.88	3.2	3		188.40	11.2	11
					156.21	9.2	9
a^4D	137.20	7.0	7		122.69	7.2	7
	102.32	5.2	5		88.40	5.2	5
	163.26	3.2	3				
				$z^4D°$	204.04	7.0	7
a^4P	187.62	5.0	5		140.73	4.8	5
	92.42	2.5	3		81.32	2.9	3
				$z^4F°$	166.75	9.0	9
$z^6D°$	135.80	9.0	9		142.53	7.7	7
	104.19	6.9	7		122.50	6.6	5
	71.81	4.8	5				
	40.45	3.0	3	$z^4G°$	192.82	11.0	11
					157.67	9.0	9
					122.05	7.0	7

3. ELECTRON CONFIGURATIONS, THEORETICAL AND OBSERVED TERMS

The atomic number being 23, the extra-nuclear structure of normal vanadium atoms is represented by

$$1s^2\ 2s^2\ 2p^6\ 3s^2\ 3p^6\ 3d^3\ 4s^2,$$

but only the last five electrons need be considered in the theory of the first spectrum [7]; thus the configuration $3d^3\ 4s^2$ gives rise to a group of terms including the ground state ^{4}F, while $3d^4\ 4s$ and $3d^5$ both produce larger families of metastable states. These even terms combine with a multitude of odd terms resulting from configurations involving a p electron, $3d^3\ 4s\ 4p$ or $3d^4\ 4p$, thereby accounting for a majority of the observed V I lines. These odd terms also combine with higher even ones which form series with the lower ones because they arise from similar electron configurations with augmented total quantum numbers, $3d^3\ 4s\ 5s$, $3d^4\ 5s$, $3d^3\ 4s\ 4d$. Such series converge to low states of the V^+ atom, but the structure of the V II spectrum has not been sufficiently analyzed to permit a complete correlation of terms and series. Also the identification of established terms of V I is sometimes doubtful or ambiguous because, on account of overlapping, there is little justification for ascribing to some terms a single configuration and convergence limit. However, since the V I spectrum is, for the most part, orderly and regular as indicated by intensities, intervals and Zeeman effects for LS coupling, it has been possible to find a fairly satisfactory correlation between electron configurations and the resulting terms. We now enter upon a discussion of such correlation, assisted by comparison with other spectra, under the headings (a), low terms; (b), middle odd terms; and (c), high terms.

(a) LOW TERMS

Those to be expected are:
$3d^3\ 4s^2$: ^{4}F, ^{4}P; ^{2}P, ^{2}D, ^{2}F, ^{2}G, ^{2}H; ^{2}D.
$3d^4\ 4s$: ^{6}D^{4}D; ^{4}P^{2}P, ^{4}D^{2}D, ^{4}F^{2}F, ^{4}G^{2}G, ^{4}H^{2}H; ^{4}P^{2}P, ^{4}F^{2}F.
d^5: ^{6}S; ^{4}P, ^{4}D, ^{4}F, ^{4}G, and many doublets.
The $d^3\ s^2$ terms may be identified by comparison with the d^3 configurations in the related spectra V III and Ti II. Taking the components of highest J, and temporarily measuring all levels from the lowest of these in this particular configuration, we compile [35] the data given in table 4. The overall separations of the highest and lowest levels of each term are given in parentheses.

TABLE 4.—*Comparison of spectral terms from* d^3

	d^3 V I		d^3 V III		d^3 Ti II	
a^4F	0	(553)	0	(583)	0	(308)
a^4P	9271	(280)	11188	(258)	8302	(154)
a^2P	13248	(−9)	10804	(180)	8759	(125)
a^2D	13995	(34)	15793	(147)	11542	(129)
^{2}F					19676	(−60)
a^2G	10548	(208)	11604	(221)	7902	(120)
a^2H	14711	(161)	16394	(155)	11559	(98)

This comparison settles the identification of these terms beyond doubt. The narrow separation of a^2D and inversion of a^2P may be explained by repulsion of $a^2D_{1½}$ $a^2P_{1½}$, which share their g's. The

missing ^2F level in V I is probably at about 23 000 and should, therefore, give faint lines.

A similar comparison for the d^4s configurations is given [35] in table 5. The identification is again satisfactory.

TABLE 5.—*Comparison of spectral terms from d^4s*

d^4s V I			d^4s Cr II			d^4 V II		
a^6D	0	(313)	^6D	0	(535)	^5D	0	(339)
a^4D	6290	(303)	^4D	7527	(495)			
b^4P	13147	(494)	^4P	18368	(912)	^3P	11568	(612)
b^2P	16764	(384)	^2P	22859	(697)			
b^4D	18342	(−63)	^4D			^3D		
b^4F	13345	(106)	^4F	18723	(137)	^3F	13269	(118)
a^2F	16653	(52)	^2F	23111	(39)			
a^4G	14817	(187)	^4G	21198	(276)	^3G	16193	(192)
b^2G	19178	(−43)	^2G	26066?	(54)			
a^4H	12638	(153)	^4H	17895	(234)	^3H		
b^2H	16720	(122)	^2H	22316	(182)			

The terms from the d^5 configuration should be much higher and their combinations should be in the infrared. Two have been identified, as shown [35] in table 6.

TABLE 6.—*Comparison of spectral terms from d^5*

	d^5 V I		d^5 Cr II	
a^6S	20202	-------	0	-------
^4P	----------	-------	21824	(2)
^4D	----------	-------	25035	(13)
c^4F	37075	(92)	32856	(18)
^4G	----------	-------	20514	(7)

Here the levels for V I are referred to the ground level. In configurations of this d^n type the differences between the various terms are much smaller in the arc than in the related spark spectra. It appears, therefore, that the undiscovered terms in V I are about 32000 above the bottom, which would make all their combinations of any strength lie too far in the infrared to be observed.

(b) MIDDLE ODD TERMS

The odd terms, at middle levels, arise from the configurations d^4p and d^3sp. They may be divided into families according to limit term in V II, and give numerous triads of closely related terms. Each triad should give its strongest combinations with the corresponding term of d^4s. In this way the identifications in tables 7 and 8 have been made. Terms in heavy type are regarded as securely identified; the others are doubtful. Under each term is given the wave number of the leading line of the multiplet resulting from its combination with the related d^4s term. Most of these groups lie between 20000 and 26000, and make the spectrum very rich in this region.

TABLE 7.—*Identified* V I *terms from* d^4p

V II d^4	V I d^4s		V I d^4p Predicted		Identified					
^5D	a^5D	a^3D	^6PDF	^4PDF	$z^5P°$ 22413	$y^5D°$ 24313	$y^5F°$ 22828	$z^3P°$ 16415	$y^3D°$ 17764	$y^3F°$ 17456
^3P	b^5P	b^3P	^4SPD	^2SPD	$y^3S°?$ 20836	$x^3P°?$ 21039	$s^3D°$ 24553	$v^3S°?$ 29655	-------	$v^3D°$ 20929
^3D	b^5D	----------	^4PDF	^2PDF	-------	$v^3D°$ 25169	$v^3F°$ 25123	-------	-------	------
^3F	b^5F	a^3F	^4DFG	^2DFG	$t^5D°$ 22344	$u^5F°$ 23620	$r^5G°$ 21994	$w^3D°$ 18674	$w^3F°?$ 18396	$x^3G°$ 17460
^3G	a^5G	b^3G	^4FGH	^2FGH	$t^3F°$ 24357	$t^3G°$ 24676	$w^3H°$ 23293	-------	$s^3G°$ 22859	$t^3H°$ 22580
^3H	a^5H	b^3H	^4GHI	^2GHI	$u^3G°$ 25000	$x^3H°$ 23420	$z^3I°$ 22455	$v^3G°$ 18216	$x^3H°$ 19075	$z^3I°?$ 18461

From d^3sp we obtained the results given in table 8.

TABLE 8.—*Identified* V I *terms from* d^3sp

V III d^3	V II d^3s	V I d^3s^2	V I d^3sp Predicted		V I Identified					
^4F	^5F	a^4F	^6DFG	^4DFG	$z^5D°$	$z^5F°$	$z^5G°$	$s^5D°$ 34194	$w^5F°$ 32602	$x^5G°$ 31384
	^3F		^4DFG	^2DFG	$z^3D°$ 20479	$z^3F°$ 22966	$z^3G°$ 21760	$z^3D°$	$z^3F°$	$z^3G°$
^4P	^5P	a^4P	^6SPD	^4SPD	$z^5S°$	$y^5P°$	$x^5D°$	$w^5S°$ 33144	$w^5P°$ 29598	$r^5D°$ 32420
	^3P		^4SPD	^2SPD	$x^3S°$ 30022	$y^3P°$ 20296	$w^3D°$ 24303	--	--	--
^2P	^3P	a^2P	^4SPD	^2SPD						
	^1P			^2SPD	$x^1S°?$ 26498	$z^1P°?$ 28516	$u^1D°?$ 26524			
^2D	^3D	a^2D	^4PDF	^2PDF	--	--	--	--	$t^3D°$ 35139	--
	^1D			^2PDF	$y^3P°$ 22031	--	$u^3F°?$ 27472			
^2F	^3F	^2F	^4DFG	^2DFG						
	^1F			^2DFG						
^2G	^3G	a^2G	^4FGH	^2FGH	$x^3F°$	$y^3G°?$	$z^3H°$	$s^3F°$ 36042	$q^3G°$ 37056	$s^3H°$ 36600
	^1G			^2FGH	$t^1F°$ 32773	$t^1G°?$ 30438	$u^1H°$ 31120	--	--	--
^2H	^3H	a^2H	^4GHI	^2GHI	$w^3G°?$	$y^3H°?$	--	$p^3G°?$ 37683	$r^3H°?$ 36821	$x^3I°$ 34855
	^1H			^2GHI	$r^1G°?$ 30096	$s^1H°?$ 26394	$y^1I°?$ 23816	--	--	--

Here each low term has two "proper triads" with different limits in V II, and also related triads of higher and lower multiplicity (if the latter is possible). The latter triads have no low terms closely related to them, so that no combinations are given in the table. Their

combinations with low terms of other families are not often strong. There are other terms from this configuration not likely to be observed.

The identification of many of the odd doublet and quartet combinations is practically impossible—indeed, it is probable that the configurations are so intermixed that there is little sense in ascribing to a given term a single configuration and limit term. The sextets may, however, be definitely identified as follows:

z^6D°, z^6F°, z^6G° } d^3sp (^5F). Combinations with e^6F.

z^6P°, y^6D°, y^6F° } d^4p (^5D). Combinations with a^6D.

z^6S°, y^6P°, x^6D° } d^3sp (^5P). Left over.

The assignment of z^6S° is doubtful. It is a real level and in the right position.

x^6P°, w^6D°, x^6F° } $d^4.5p$. Combinations with a^6D; no more sextets from $4p$; and these are too high. The general nature of these levels appears to be certain; some of the details are doubtful.

(c) HIGH TERMS

For the high terms, the distinctness of the various families, each with its own limit, is much sharper, and interfamily combinations are usually very weak or absent.

All the sextet configurations can be reliably assigned, the reasons being as summarized:

e^6D $d^4.s$ (^5D). Combination with z^6P°, y^6D°, y^6F°, and also series.

---
e^6P
f^6D } $d^4.d$ (^5D). Combination with same triad. (Lower members fragmentary).
f^6F
e^6G

e^6F $d^3s.s$ (^5F). Combination with z^6D°, z^6F°, z^6G°; series.

f^6P
g^6D
g^6F } $d^3s.d$ (^5F). Combination with same triad; series.
f^6G
e^6H

--- } $d^3s.d$ (^5F). Combinations; series (no satellites).
g^6G
f^6H

h^6G d^3p^2. Only chance left; also analogy with Ti I.

For the high quartets we have:

e^4D $d^4.s$ (^5D). Combinations with d^4p triad; series.
e^4F d^5 Combinations with same triad. At right level for this; not for anything else.
f^4F $d^3s.s$ (^5F). Combinations with d^3sp triad; series.

No other high even quartet terms have been found despite much searching. There should be pentads $d^4.d$ and $d^3s.d$.

The only high doublet found is e^2F, which combines with the d^3sp triad, and has obviously the limit d^3s (^3F)—the lowest triplet term in V II.

It is of interest to compare the numbers of terms predicted by Hund's theory and those found in the present work.

For the low levels we have:

Electrons		^6S	^6D	^4S	^4P	^4D	^4F	^4G	^4H	^2S	^2P	^2D	^2F	^2G	^2H	^2I
d^3s^2	Predicted				1		1				1	2	1	1	1	
	Observed				1		1				1	1		1	1	
d^4s	Predicted		1		2	2	2	1	1	2	2	3	3	3	1	1
	Observed		1		1	2	1	1	1		1		1	1	1	
d^5	Predicted	1			1	1	1	1		1	1	3	2	2	1	1
	Observed	1					1									

All the low sextet terms have been found and all of the quartets except a few which are known to lie high and must give infrared lines. Most of the doublets are still undiscovered. The missing terms are mainly those which have (probably high) singlet limits in V II. Only a small part of the high-lying d^5 group is known.

For the odd levels, involving a $4p$ electron, distinction between the origins d^3sp and d^4p is often impracticable. The two together give:

Electrons	^6S	^6P	^6D	^6F	^6G	^4S	^4P	^4D	^4F	^4G	^4H	^4I	^2S	^2P	^2D	^2F	^2G	^2H	^2I	^2K
d^3sp	1	1	2	1	1	3	5	8	6	5	2	1	3	7	10	9	7	4	2	
d^4p		1	1	1		2	4	6	5	4	2	1	2	7	8	9	7	5	2	1
Combined	1	2	3	2	1	5	9	14	11	9	4	2	5	14	18	18	14	9	4	1
Observed	1	3	4	3	1	4	7	12	12	9	4	1	5	8	7	8	11	9	3	

The number of observed terms sometimes exceeds the computed, indicating that some terms arising from a $5p$ electron have been observed. This is certain among the sextets. The doublets are far from complete.

The high levels, arising from the addition of a $4s$ or $4d$ electron to the terms of V II, are theoretically very numerous—50 in the first case and 220 in the second. Only a very few of these, arising from the lowest levels, have been detected—as is the case in all other spectra.

Table 1 contains 420 lines of intensity 15 or more. Of these only 16 remain unclassified. This, together with the results of this section, indicates that both the theoretical and practical analysis of the spectrum in the observable region is very nearly complete.

4. SERIES AND IONIZATION POTENTIALS

The foregoing analysis indicates that a considerable number of series have been identified in the V I spectrum, but in no case have they been observed beyond two members. All the observed series converge to the two lowest terms in V II, a^5D and a^5F. The series formed by addition of s-electrons to these terms, if reduced with the simple Rydberg formula, give the following values for the difference of the lowest energy levels in V I and V II (table 9).

TABLE 9—V I *series*

Electron	4s	5s	n* for 4s	Limit	V II	Ionization
$a^6D_{9/2}$	2425	37441	1.4311	56009	339	55670
$a^6D_{7/2}$	2311	37322	1.4312	55889	209	55680
$a^6D_{5/2}$	2220	37227	1.4312	55793	107	55686
$a^6D_{3/2}$	2153	37158	1.4313	55723	36	55687
$a^6D_{1/2}$	2112	37117	1.4313	55682	0	55682
Mean						55681
$a_4D_{3/2}$	8716	38242	1.5344	55327	339	54988
$a^4D_{3/2}$	8579	38106	1.5344	55191	209	54982
$a^4D_{1/2}$	8476	38004	1.5343	55089	107	54982
$a^4D_{0/2}$	8413	37940	1.5344	55025	36	54989
Mean						54985
$a^4F_{9/2}$	553	39597	1.3684	59161	3163	55998
$a^4F_{7/2}$	323	39399	1.3679	58971	2968	56003
$a^4F_{5/2}$	137	39241	1.3675	58818	2809	56009
$a^4F_{3/2}$	0	39127	1.3672	58711	2687	56024
Mean						56009

The general mean is 55558, corresponding to 6.85 volts. The agreement between the results from the various components of a term is so much better than that from terms of different types (though the latter is good), that it would have sufficed to use only the components of highest J. The mean result is, however, almost certainly too high, for a study of the spectra of elements of neighboring atomic number, for which long series and reliable values of the so-called effective quantum number n^* exist, shows that for the $4s$ and $5s$ terms Δn^* is always considerably greater than unity. The principal data are summarized in table 10, which explains itself.

This table may be applied to vanadium in two ways; by estimating the actual value of n^* by interpolation between Ti and Cr, or by a similar estimation of Δn^*.

TABLE 10.—*Denominator n* for spectra of iron group*

Configuration	$d^{n-1}s+s$			$d^{n-1}s+d$			d^n+s			d^n+d		
Electron	Term	4s	5s	Term	4d	5d	Term	4s	5s	Term	4d	5d
K I							^2S	1.771	2.802	^2D	3.798	4.771
Ca I	^1S	1.492	2.620	^1D	3.023	*4.146	^1D	1.633	(*)			
	^3S		2.485	^3D	3.083	4.091	^3D	1.604	2.657			
Ti I	^3F	1.411	2.489				^3F	1.569				
	^5F		2.392	^5H	2.870	3.885	^5F	1.489	2.545	^5H	2.997	
Cr I	^5D	1.367	2.454				^5S	1.529	2.567			
	^7D		2.338				^7S	1.418	2.494	^7D	2.989	4.008
Mn I	^6S	1.352	2.433	^6D	2.936		^6D	1.467	2.544			
	^8S		2.313	^8D	2.881	3.895	^8D	1.385	2.464			
Ni I	^3F	1.252	2.372	^3H	2.867	*3.701	^1D	1.374	2.517	^1G	3.177	
	^5F		2.259	^5H	2.896	3.907	^3D	1.337	2.411	^3G	2.972	
Cu I	^2D	1.226	2.368				^2S	1.327	2.392	^2D	2.978	3.980
	^4D		2.242	^4G	2.894	3.899						
Zn I	^1S	1.203	2.344	^1D	2.871	3.843						
	^3S		2.229	D	2.906	3.908						

* Series known to be perturbed.

It should be noted that, if we should apply a simple Rydberg series to the configurations $d^{n-1}\ 4s^2$ and $d^{n-1}4s5s$, we would do better by taking the upper term of higher multiplicity, e. g., ^{3}S in Ca I, and the lower one of lower multiplicity, as Δn^* is much nearer unity than for the two terms of the same multiplicity. (This was pointed out to one of us long ago by Shenstone.)

Estimating n^* itself for the possible series in V I, we find the value given in table 11. Each separate member of a series gives an estimate of the limit, and upon allowance for the limit-term in V II, of the ionization energy.

TABLE 11.—V I *series*

Configuration	Term	Estimated n^*	Resulting term	Observed level	Limit	Limit in V II		Ionization
						$^5F_3$	$^5D_4$	
d^3s+4s	$a^4F_{4½}$	1.387	57043	553	57596	3163		54433
d^4s+5s	$f^4F_{4½}$	2.472	17958	39597	57555	3163		54392
	$e^6F_{5½}$	2.364	19636	37931	57567	3163		54404
d^3s+4d	$e^6H_{7½}$	2.873	13295	44190	57485	3163		54322
d^4s+5d	$f^6H_{7½}$	3.888	7259	50302	57561	3163		54398
d^4+4s	$a^4D_{3½}$	1.543	46092	8716	54808		339	54469
	$a^6D_{4½}$	1.450	52194	2425	54619		339	54280
d^4+5s	$e^4D_{3½}$	2.59±	16359±	38242	54601		339	54262±
	$e^6D_{4½}$	2.520	17280	37441	54721		339	54382
d_5+4d	$e^6G_{6½}$	2.993	12250	42353	54603		339	54264

The agreement of the 10 values is extraordinary. The five with limit ^{5}F give 54390; those with limit ^{5}D give 54331.

It is evident that estimations of Δn^* would have led to almost exactly the same limit—but the present method makes more terms available. The general mean 54361 corresponds to 6.71 volts.

If these 10 values were really independent observations the probable error of the mean would be ±16 wave numbers, or ±0.002 volt. This is not a safe assumption, but it is evident that the ionization potential is very well determined.

The authors are deeply indebted to H. D. Babcock for the very valuable observations of the Zeeman effect, which he generously placed at their disposal, to A. S. King for supplying a complete series of his original negatives of arc and furnace spectra, and to Miss Charlotte E. Moore for measuring many new lines on King's spectrograms, for a very large amount of painstaking care and labor in checking the tables and calculations—and for the discovery, at the last moment, of the interesting terms x^6P°, w^6D°, and x^6F°. We wish also to thank Jerome K. Strauss for pure-metal electrodes, which greatly facilitated the description of vanadium spectra.

IV. REFERENCES

[1] M. A. Catalán, Trans. Roy. Soc. [A], **223,** 127 (1922).
[2] W. F. Meggers, J. Wash. Acad. Sci. **13,** 317 (1923).
[3] O. Laporte, Naturwiss. **11,** 779 (1923); Phys. Z. 24, 510 (1923).
[4] A. Landé, Z. Phys. **15,** 189 (1923).
[5] W. F. Meggers, J. Wash. Acad. Sci. **14,** 151 (1924).

73059—36——13

[6] K. Bechert and L. A. Sommer, Z. Phys. **31,** 145 (1925).
[7] A. Hund, Linienspektren und periodisches System der Elemente (J. Springer, Berlin, 1927).
[8] R. F. Bacher and S. Goudsmit, Atomic Energy States, p. 486 (McGraw-Hill Book Co., New York, 1932).
[9] H. N. Russell, Astrophys. J. **66,** 283 (1927).
[10] C. E. Moore, Term Designations for Excitation Potentials, p. 15 (University Observatory, Princeton, 1934).
[11] H. Kayser, Handbuch der Spectroscopie **6,** 750 (S. Hirzel, Leipzig, 1912).
[12] F. Exner and E. Haschek, Die Spektren der Elemente bei Normalem Druck, **2,** 308 (F. Deuticke, Leipzig und Wien, 1911).
[13] C. M. Kilby, Astrophys. J. **30,** 243 (1909).
[14] W. Ludwig, Z. wiss. Phot. **16,** 157 (1917).
[15] C. C. Kiess and W. F. Meggers, BS Sci. Paper **16,** 51 (1920), S372.
[16] K. Burns and F. M. Walters, Jr., Pub. Allegheny Obs. **6,** 159 (1929).
[17] Trans. Int. Astron. Union **3,** 86 (1928).
[18] W. F. G. Ferguson, BS J. Research **8,** 382 (1932), RP423.
[19] A. S. King, Astrophys. J. **41,** 86 (1915); 60, 282 (1924).
[20] H. E. White, Phys. Rev. **40,** 1041 (1932).
[21] H. Kopferman and E. Rasmussen, Z. Phys. **98,** 624 (1936).
[22] R. Frerichs, Ann. Phys. **81,** 807 (1926).
[23] H. N. Russell, Proc. Nat. Acad. Sci. **11,** 314 (1925).
[24] H. D. Babcock, Astrophys. J. **34,** 209 (1911).
[25] H. N. Russell and H. D. Babcock, Zeeman Verhandelingen, p. 286 (Martinus Nijhoff, The Hague, 1935).
[26] A. G. Shenstone and H. A. Blair, Phil. Mag. **8,** 764 (1929). See also H. N. Russell, Phys. Rev. **36,** 1590 (1930).
[27] H. Gieseler and W. Grotrian, Z. Phys. **25,** 342 (1924).
[28] A. S. King, Astrophys. J. **60,** 282 (1924).
[29] Revision of Rowland's Preliminary Table (Carnegie Inst. Washington, 1928); C. E. Moore, Atomic Lines in the Sun-spot Spectrum (University Observatory, Princeton, 1933).
[30] H. Kayser, Tabelle der Schwingungszahlen (S. Hirzel, Leipzig, 1925).
[31] H. D. Babcock, Phys. Rev. **46,** 382 (1934).
[32] W. F. Meggers and C. G. Peters, BS Sci. Paper **14,** 697 (1918); S327.
[33] H. N. Russell, A. G. Shenstone, and L. Turner, Phys. Rev. **33,** 900 (1929).
[34] C. C. Kiess and W. F. Meggers, BS J. Research **1,** 641 (1928), RP23.
[35] R. F. Bacher and S. Goudsmit, Atomic Energy States (McGraw-Hill Book Co., New York, 1932). A number of unpublished terms of Cr II have been kindly communicated by C. C. Kiess.

WASHINGTON, March 20, 1936.